Syntheses of Polycyclic Aromatic Compounds with Heteroatom Junctions via Tandem Hetero-Friedel–Crafts Reactions

Sigma Hashimoto

Department of Energy and Hydrocarbon Chemistry
Graduate School of Engineering
Kyoto University

2013

Table of Contents

General Introduction

Fused polycyclic aromatic and heteroaromatic compounds

Polycyclic aromatic compounds are an important class of materials for organic electronics, dyes, sensors, and liquid crystal displays.[1] Among them, ladder-type π-conjugated molecules with fully ring-fused polycyclic skeletons have been the subjects of extensive research.[2] For example, their rigid π-conjugated frameworks with no conformational disorder can provide attractive photophysical properties such as intense photoluminescence. In addition, their planar frameworks are suitable for achieving dense molecular packing in the condensed phase, which can induce desirable electronic properties such as high carrier mobility. Therefore, in the past few decades, significant effort has been devoted to developing various intriguing ladder-type π-conjugated molecules.

The introduction of heteroatoms in the fused-ring system has been one major approach to modifying the physical and chemical properties of ladder-type polycyclic aromatic compounds.[3] These compounds also form π-stacking arrangements in the solid states and show relatively high charge carrier mobilities in comparison to their all-carbon parent congeners. These properties make polycyclic heteroaromatic compounds promising candidates for organic electronic materials (Figure 1).[4] In particular, in 2005, Ong and co-workers reported that functionalized indolo[3,2-*b*]carbazole **1** exhibited a high mobility that is suitable for organic thin-film transistor (OTFT) applications.[4a] Yamaguchi and co-workers synthesized benzoannulated fused oligoselenophene **2** and its derivatives and used the compounds as air-stable organic semiconductors for high-quality organic field-effect transistors (OFET).[4b] They explained that the high mobility of the compound is due to its considerable Se-Se orbital interactions. Takimiya and co-worker developed organic semiconductors based on dinaphtho[2,3-*b*:2′,3′-*f*]thiopheno[3,2-*b*]thiophene **3** and its analogs.[4c] The extended π-framework of these molecules contributes to effective molecular overlap, which can lead to high carrier mobility in the thin-film transistor. Nakamura and co-workers synthesized bis(carbazolyl)benzodifuran **4**, which exhibits high, well-balanced carrier mobilities for holes and electrons, both greater than 10^{-3} cm^2 V^{-1} s^{-1}.[4d]

---

[1] Reviews: (a) Fabian, J.; Nakazumi, H.; Matsuoka, M. *Chem. Rev.* **1992,** *92*, 1197–1226. (b) Scherf, U. *J. Mater. Chem.* **1999,** *9*, 1853–1864. (c) Mitschke, U.; Bäuerle, P. *J. Mater. Chem.* **2000,** *10*,

[2] Anthony, J. E. *Chem. Rev.* **2006,** *106*, 5028–5048.

[3] Fukazawa, A.; Yamaguchi, S. *Chem. Asian J.* **2009,** *4*, 1386–1400.

[4] (a) Wu, Y.; Li, Y.; Gardner, S.; Ong, B. S. *J. Am. Chem. Soc.* **2005,** *127*, 614–618. (b) Yamada, K.; Okamoto, T.; Kudoh, K.; Wakamiya, A.; Yamaguchi, S.; Takeya, J. *Appl. Phys. Lett.* **2007,** *90*, 072102-1–3. (c) Yamamoto, T.; Takimiya, K. *J. Am. Chem. Soc.* **2007,** *129*, 2224–2225. (d) Tsuji, H.; Mitsui, C.; Sato, Y.; Nakamura, E. *Adv. Mater.* **2009,** *21*, 3776–3779.

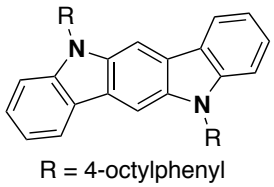

R = 4-octylphenyl

1

Organic Thin Film Transistors (OTFTs)

mobility (hole) 0.01–0.02 $cm^2\ V^{-1}\ s^{-1}$
on/off ratio 10^5–10^6 (at 25 ºC)

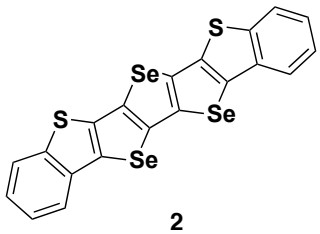

2

Organic Field Effect Transistors (OFETs)

mobility (hole) 1.1 $cm^2\ V^{-1}\ s^{-1}$
(at 25 ºC, single crystal)

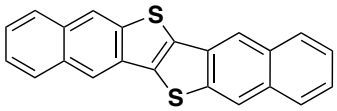

3

Organic Field Effect Transistors (OFETs)

mobility (hole) 0.7–1.9 $cm^2\ V^{-1}\ s^{-1}$
on/off ratio 10^6–10^7 (at 25 ºC)

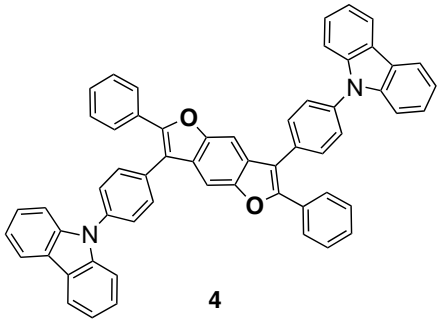

4

Ambipolar Material

mobilities (by TOF)
hole 3.7×10^{-3} $cm^2\ V^{-1}\ s^{-1}$
electron 4.4×10^{-3} $cm^2\ V^{-1}\ s^{-1}$

Figure 1. Ladder-type polycyclic heteroaromatic compounds as organic electronic materials.

One of the key factors responsible for high electronic performance is the solid-state packing structure. In general, strong electronic interactions between the π-electron-rich frameworks of adjacent molecules lead to high carrier mobilities. One promising arrangement for achieving strong electronic interactions is a cofacial π-stacking structure. One-dimensionally extended ladder-type compounds have strong interactions; however, in most cases they are only along one or two stacking axes. Therefore, compounds with a multidimensionally extended π-conjugated plane are desirable for obtaining good omnidirectional intermolecular interaction (Figure 2).

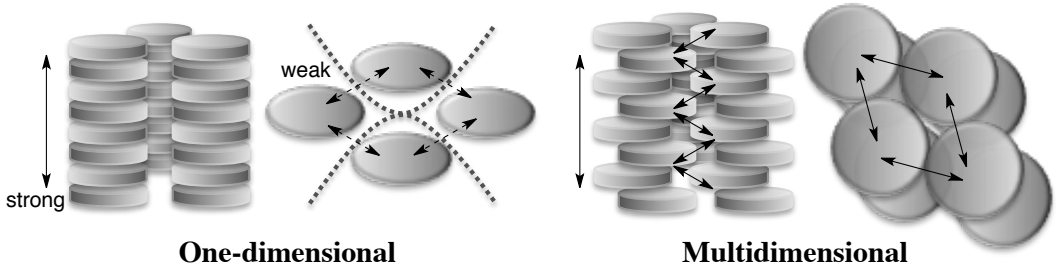

One-dimensional **Multidimensional**

Figure 2. Multidimensionally extended π-conjugated plane for enhancing intermolecular interactions.

General Introduction

Multidimensionally extended, fully fused polycyclic aromatic compounds such as hexabenzocoronenes have also been extensively studied.[5] However, despite numerous theoretical investigations [6] suggesting that such hetero-π-conjugated molecules could be fascinating substructures of heteroatom-embedded nanocarbons,[7] only a few multidimensional polycyclic aromatic compounds incorporating heteroatoms have been synthesized to date.[8,9] Recently, some researchers have succeeded in particularly difficult syntheses of this class of compounds (Figure 3). Müllen and co-workers synthesized fused hexapyrrolohexaazacoronene derivative **5** by performing cyclodehydrogenation of hexapyrrolylbenzene and subsequent neutralization.[8b] In 2012, Yamaguchi and co-workers reported the synthesis of a new planarized triarylborane **6**, in which a tri-coordinated B atom is embedded in the electron-donating polycyclic π-skeleton.[8e] The rigid and cyclic π-skeleton around the B atom of **6** retards a particular decomposition process that proceeds through the reaction with Lewis bases. They also succeeded in the bottom-up organic synthesis of a stable "B-doped nanographene" **7** as a single closed-shell compound.[8g] These compounds show unique optical and electrical properties, but their overall yields are mostly low because of the multistep synthesis. Since practical applications require large-scale supplies of functional materials, the development of facile and scalable methods for constructing π-conjugated skeletons with heteroatom ring junctions has been eagerly anticipated.

---

[5] (a) Watson, M. D.; Fechtenkötter, A.; Müllen, K. *Chem. Rev.* **2001,** *101*, 1267–1300. (b) Wu, J.; Pisula, W.; Müllen, K. *Chem. Rev.* **2007,** *107*, 718–747.

[6] (a) Casanovas, J.; Ricart, J. M.; Rubio, J.; Illas, F.; Jimènez-Mateos, J. M. *J. Am. Chem. Soc.* **1996,** *118*, 8071–8076. (b) Kurita, N.; Endo, M. *Carbon* **2002,** *40*, 253–260. (c) Tran, F.; Alameddine, B.; Jenny, T. A.; Wesolowski, T. A. *J. Phys. Chem. A* **2004,** *108*, 9155–9160. (d) Hasegawa, T.; Suzuki, T.; Mukai, S. R.; Tamon, H. *Carbon* **2004,** *42*, 2195–2200. (e) Mandumpal, J.; Gemming, S.; Seifert, G. *Chem. Phys. Lett.* **2007,** *447*, 115–120.

[7] Reviews: (a) Kawaguchi, M. *Adv. Mater.* **1997,** *9*, 615–625. (b) Terrones, M.; Jorio, A.; Endo, M.; Rao, A. M.; Kim, Y. A.; Hayashi, T.; Terrones, H.; Charlier, J.-C.; Dresselhaus, G.; Dresselhaus, M. S. *Mater. Today* **2004,** *7*, 30–45. (c) Vostrowsky, O.; Hirsch, A. *Chem. Rev.* **2006,** *106*, 5191–5207.

[8] (a) Leupin, W.; Wirz, J. *J. Am. Chem. Soc.* **1980,** *102*, 6068–6075. (b) Wu, D.; Zhi, L.; Bodwell, G. J.; Cui, G.; Tsao, N.; Müllen, K. *Angew. Chem., Int. Ed.* **2007,** *46*, 5417–5420. (c) Takase, M.; Enkelmann, V.; Sebastiani, D.; Baumgarten, M.; Müllen, K. *Angew. Chem., Int. Ed.* **2007,** *46*, 5524–5527. (d) Wharton, S. I.; Henry, J. B.; MacNab, H.; Mount, A. R. *Chem. Eur. J.* **2009,** *15*, 5482–5490. (e) Saito, S.; Matsuo, K.; Yamaguchi, S. *J. Am. Chem. Soc.* **2012,** *134*, 9130–9133. (f) Chen, L.; Puniredd, S. R.; Tan, Y.-Z.; Baumgarten, M.; Zschieschang, U.; Enkelmann, V.; Pisula, W.; Feng, X.; Klauk, H.; Müllen, K. *J. Am. Chem. Soc.* **2012,** *134*, 17869–17872. (g) Dou, C.; Saito, S.; Matsuo, K.; Hisaki, I.; Yamaguchi, S. *Angew. Chem., Int. Ed.* **2012,** *51*, 12206–12210.

[9] The substitution of B–N fragments for C–C fragments in aromatic hydrocarbons has been investigated extensively: Bosdet, M. J. D.; Piers, W. E. *Can. J. Chem.* **2008,** *86*, 8–29, Campbell, P. G.; Marwitz, A. J. V.; Liu, S.-Y. *Angew. Chem., Int. Ed.* **2012,** *51*, 6074–6092, and references cited therein.

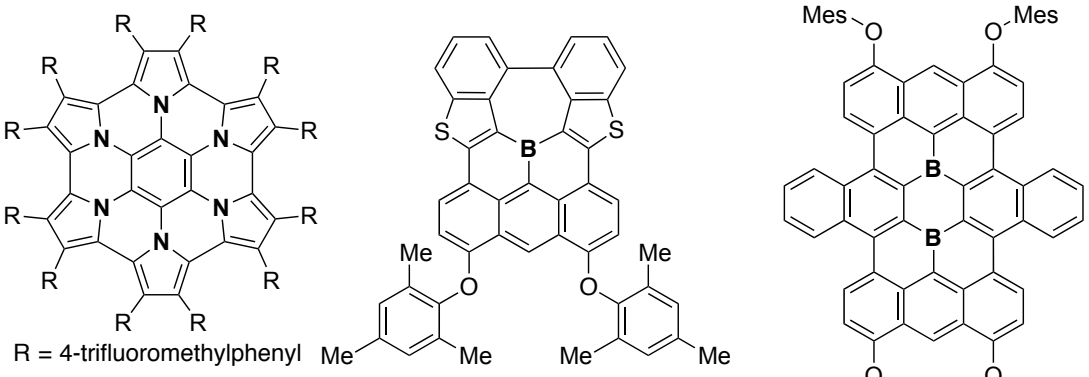

5
3–4 steps
overall ~30% yield
(from pyrrole)

6
8 steps
overall 2–3% yield
(from 1,3-dibromobenzene)

7
5 steps
overall 6–7% yield
(from 2,4,6-trimethylphenol)

Figure 3. Multidimensional polycyclic aromatic compounds incorporating heteroatom junctions.

Hetero-Friedel–Crafts reactions as a method for forming aromatic carbon–heteroatom bonds

The Friedel–Crafts reaction is a typical electrophilic substitution reaction occurring in the aromatic nucleus. As such, it is a powerful tool for introducing carbon substituents to aromatic rings.[10,11] Similarly, the *hetero-Friedel–Crafts reaction*, which introduces heteroatom substituents instead of carbon substituents (Scheme 1), is useful for incorporating heteroatoms into π-conjugated frameworks (Chart 1).[12] However, to the best of our knowledge, there are only a few applications of such a methodology to the construction of multidimensional polycyclic aromatic compounds incorporating heteroatoms (Chart 2). The following sections introduce various hetero-Friedel–Crafts reactions classified by element.

Scheme 1. Hetero-Friedel–Crafts reaction

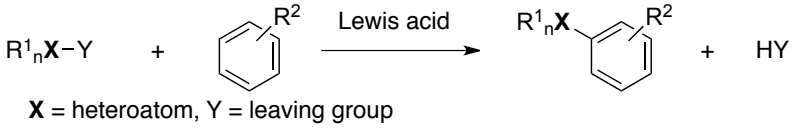

[10] (a) Friedel, C.; Crafts, J. M. *Compt. Rend.* **1877,** *84*, 1392. (b) Friedel, C.; Crafts, J. M. *J. Chem. Soc.* **1877,** *32*, 725–791.
[11] Reviews: (a) Gore, P. H. *Chem. Rev.* **1955,** *55*, 229–281. (b) Olah, G. A. *Friedel–Crafts and Related Reactions*; Wiley: New York, **1963**. (c) Groves, J. K. *Chem. Soc. Rev.* **1972,** *1*, 73–97. (d) Eyley, S. C. *Comp. Org. Syn.* **1991,** *2*, 707–731. (e) Heaney, H. *Comp. Org. Syn.* **1991,** *2*, 733–752. (f) Rueping, M.; Nachtsheim, B. J. *Beilstein J. Org. Chem.* **2010,** *6*, 6-1–24.
[12] Olah, G. A. *Friedel–Crafts Chemistry*; Wiley: New York, **1973**.

Chart 1. Incorporation of a heteroatom into a ladder-type π-conjugated framework in the hetero-Friedel–Crafts reaction

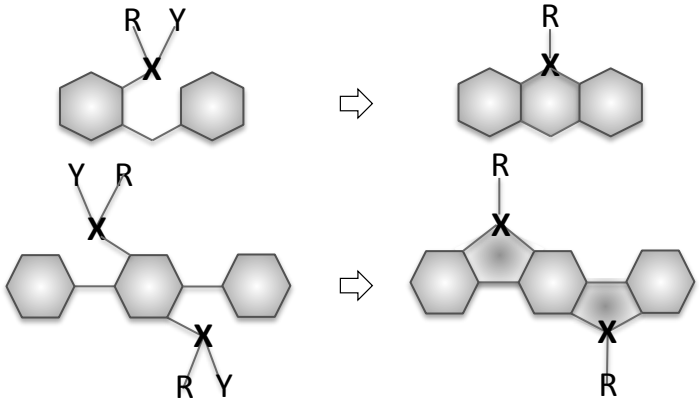

Chart 2. Incorporation of a heteroatom into a multidimensional π-conjugated framework in the hetero-Friedel–Crafts reaction

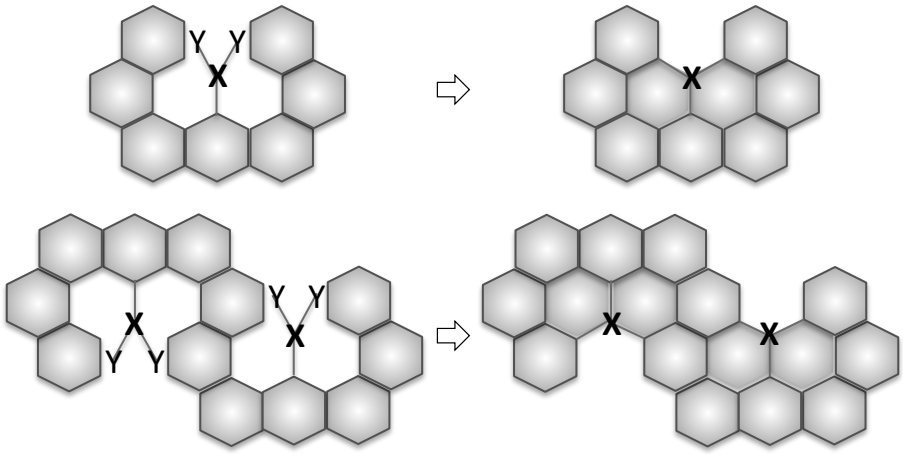

Sulfur

The Friedel–Crafts sulfinylation of aromatic compounds forms diaryl or alkyl aryl sulfoxides. In 1926, the first synthesis of phenyl *p*-tolyl sulfoxide from benzene and *p*-toluenesulfinyl chloride was reported (eq. 1).[13] More than 30 years later, Douglas et al. reported the synthesis of methyl phenyl sulfoxide from the reaction of benzene with methanesulfinyl chloride in the presence of anhydrous aluminum chloride (eq. 2).[14]

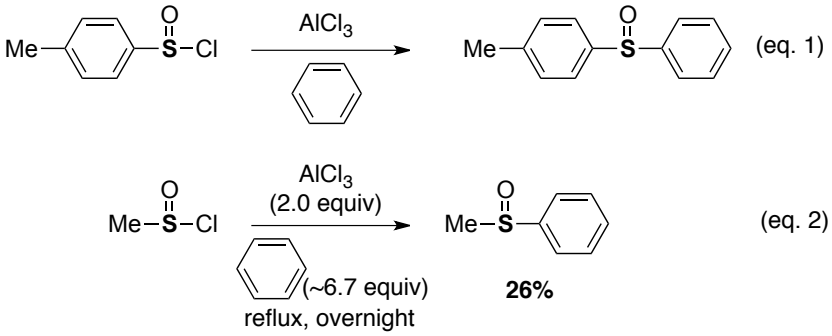

Yuste and co-workers reported that the Friedel–Crafts reaction of methyl alkyl- and arylsulfinates with aromatic systems activated by electron-donating substituents provides alkyl aryl and diaryl sulfoxides under mild conditions in moderate to good yields (eq. 3).[15] They suggested that a Wheland intermediate having a trigonal bipyramidal structure provided the very high regioselectivity in these sulfinylation reactions.

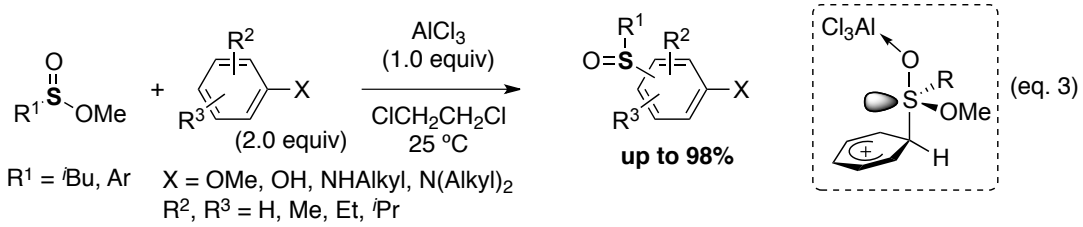

Gupta reported the synthesis of aromatic *N*,*N*-dialkylsulfonamides *via* the reaction of dialkylsulfamyl chlorides with aromatic hydrocarbons in the presence of aluminum chloride (eq. 4).[16] They also prepared the same products by reacting a novel sulfamyl chloride–aluminum chloride complex with hydrocarbons (eq. 5).

---

[13] Schöberl, A.; Wagner, A. *Houben-Weyl*, Vol. IX, 4th ed.; Müller, E., Ed.; Thieme: Stuttgart, **1955**, p. 217.
[14] Douglas, J. B.; Farah, B. S. *J. Org. Chem.* **1958,** *23*, 805–807.
[15] Yuste, F.; Linares, A. H.; Mastranzo, V. M.; Ortiz, B.; Sánchez-Obregón, R.; Fraile, A.; Ruano, J. L. G. *J. Org. Chem.* **2011,** *76*, 4635–4644.
[16] Gupta, S. K. *Synthesis* **1977,** 39–41.

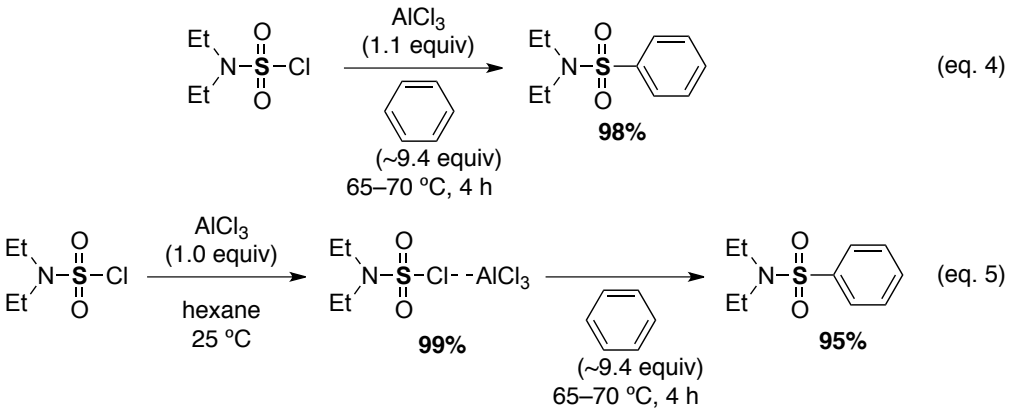

Phosphorus and Arsenic

The reaction of phosphorus trichloride (PCl_3) with benzene under Friedel–Crafts conditions has been widely studied. However, only phenyldichlorophosphine and diphenylchlorophosphine have been obtained as products, and no conditions that yielded triphenylphosphine were found, probably owing to an unfavorable disproportionation equilibrium.[17] Phosphorus oxychloride ($POCl_3$) also fails to give triphenylphosphine oxide (eq. 6). On the other hand, in 1964, Maier found that phosphorus sulfochloride ($PSCl_3$) yields triphenylphosphine sulfide upon reaction with benzene and excess aluminum chloride (eq. 7).[18]

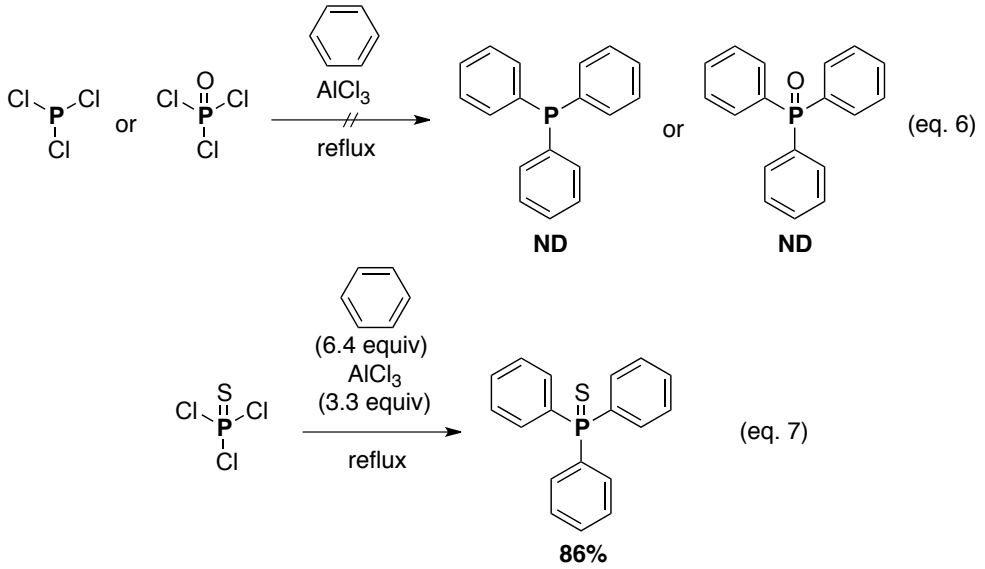

Olah and co-workers simplified this method to prepare triphenylphosphine sulfide in 71% yield directly from benzene by reacting it with sulfur, phosphorus trichloride, and aluminum chloride (eq. 8).[19] Thus, sulfidation will be essential for the phospha-Friedel–Crafts reaction of diaryl phosphorus chlorides.

---

[17] Kosoiapoff, G. M. *Friedel–Crafts and Related Reactions*, Vol. IV, Olah, G. A., Ed.; Wiley: New York, **1965,** pp. 213–226.
[18] Maier, L. *Helv. Chim. Acta* **1964,** *47*, 120–132.
[19] Olah, G. A.; Hehemann, D. *J. Org. Chem.* **1977,** *42*, 2190.

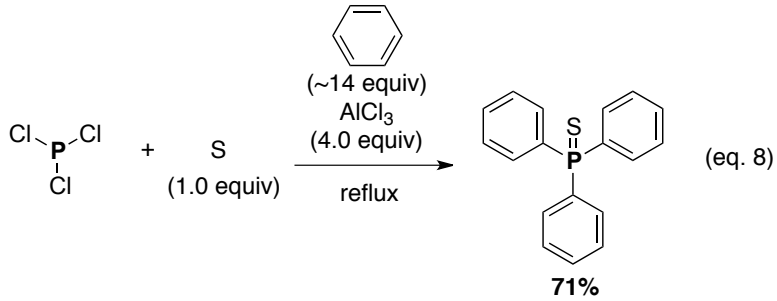

(eq. 8)

Wehmschulte and co-workers synthesized unsymmetrical 9-phosphafluorenes using an $AlCl_3$-catalyzed Friedel–Crafts ring-closure reaction, but this method suffers from difficult workup procedures.[20] Alternatively, they also obtained the same products in close to quantitative yields by performing simple thermolysis of *m*-terphenyldichlorophosphines (eq. 9) and -arsines (eq. 10). The reaction temperatures were about 250 °C for the phosphine and 140 °C for the arsine, and the reactions were complete within 5 min.

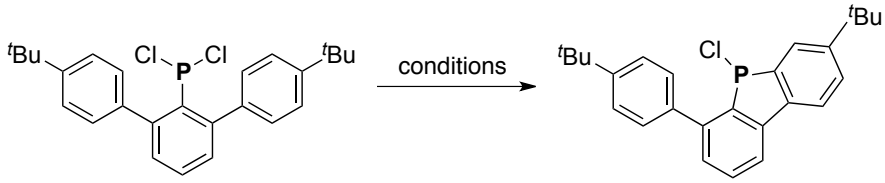

(eq. 9)

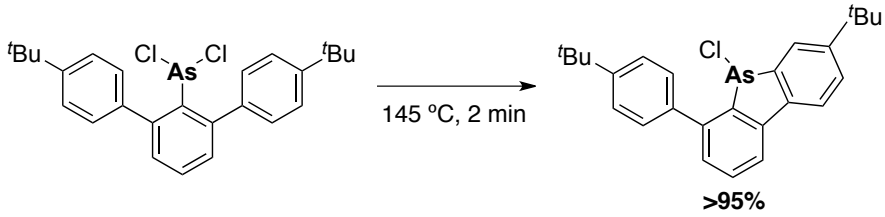

(eq. 10)

They also reported that the reaction temperature could be further reduced to room temperature if iodo precursors were employed (eq. 11).[21] According to their quantum mechanical calculations, iodide substituents reduce the activation barrier by ca. 8 kcal/mol compared to chloride substituents.

[20] Diaz, A. A.; Young, J. D.; Khan, M. A.; Wehmschulte, R. J. *Inorg. Chem.* **2006,** *45*, 5568–5575.
[21] Diaz, A. A.; Buster, B.; Schomisch, D.; Khan, M. A.; Baum, J. C.; Wehmschulte, R. J. *Inorg. Chem.* **2008,** *47*, 2858–2863.

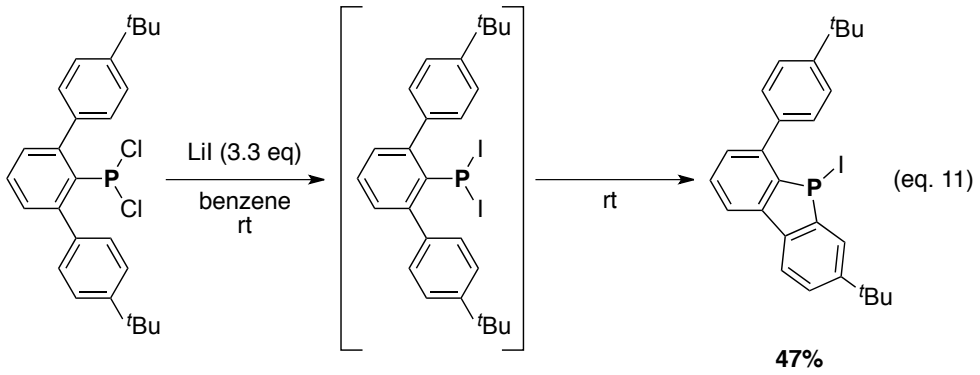

Silicon

Electrophilic silylation of aromatic compounds such as benzene and toluene under typical Friedel–Crafts alkylation conditions using halosilanes and a Lewis acid catalyst has never been observed, although this is possible for highly activated aromatics (ferrocene, pyrrole, etc.). The difficulty of this reaction is probably due to the great ease with which any arylsilane formed under the reaction conditions undergoes protodesilylation.[22] In 1989, Olah and co-workers reported the direct silylation of benzene and toluene with a series of chlorotrialkylsilanes under Friedel–Crafts reaction conditions in the presence of Hunig bases (hindered tertiary amines) as proton acceptors (eq. 12).[23] Their strategy for achieving silylation of benzene or toluene was to slow down the rate of protodesilylation by trapping the proton eliminated in the silylation reaction with a suitable hindered base (eq. 13).

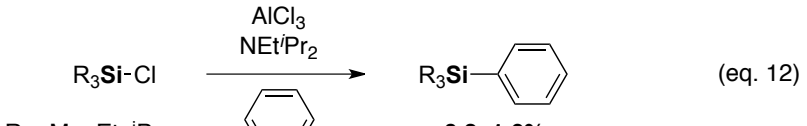

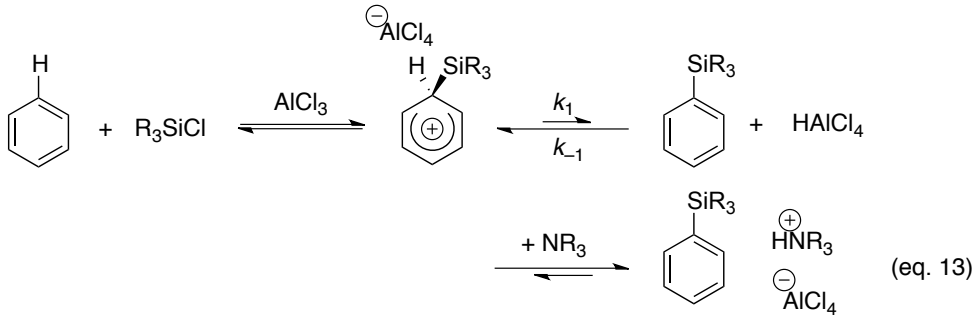

Recently, Kobayashi and co-workers developed an intramolecular sila-Friedel–Crafts reaction and applied it to the synthesis of dibenzosilole derivatives (eq. 14).[24] This reaction proceeds under mild conditions to afford the target in relatively high yield, indicating its versatility as a synthetic method. The synthesis of

[22] (a) Bott, R. W.; Eaborn, C.; Greasley, P. M. *J. Chem. Soc.* **1964,** 4804–4806. (b) Szele, I. *Helv. Chim. Acta* **1981,** *64*, 2733–2737.
[23] Olah, G. A.; Bach, T.; Surya Prakash, G. K. *J. Org. Chem.* **1989,** *54*, 3770–3771.
[24] Furukawa, S.; Kobayashi, J.; Kawashima, T. *J. Am. Chem. Soc.* **2009,** *131*, 14192–14193.

trisilasumanene, a silicon analog of sumanene, was also achieved using this reaction (eq. 15).

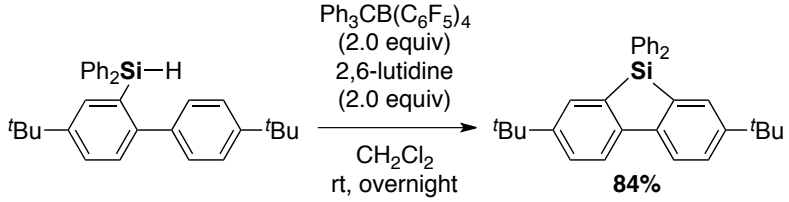

(eq. 14)

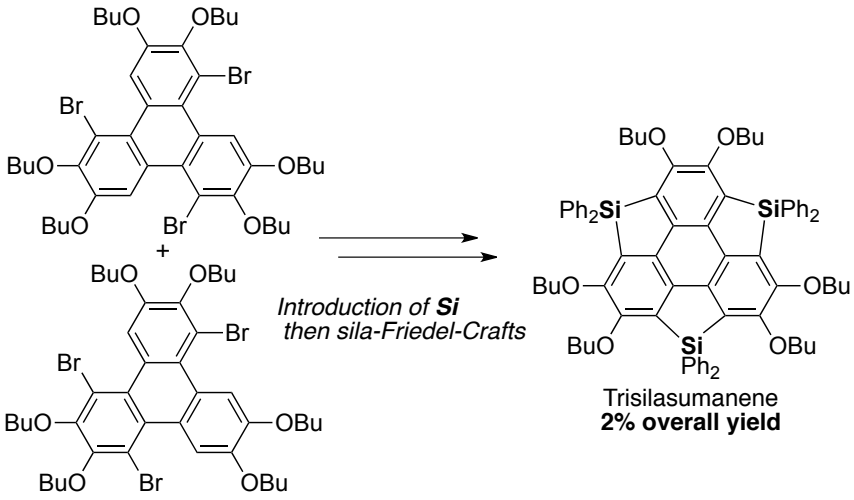

(eq. 15)

Boron

The direct electrophilic borylation of aromatic compounds dates back to as early as 1948,[25] when the borylation of benzene with diborane at high temperature was reported. Muetterties and Lappert independently reported a boron analog of the Friedel–Crafts reaction in which BX_3 (X = Cl, Br) activated by AlX_3 is used for the borylation of alkyl aromatics (eq. 16).[26] In both cases, the removal of the Brønsted acid byproduct of the electrophilic aromatic substitution (either as gaseous HBr or as H_2 from the reaction of HX with Al) was essential for preventing protodeboronation.

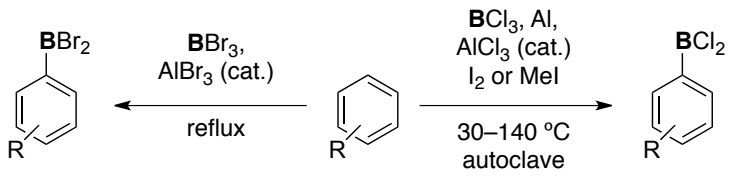

(eq. 16)

Dewar and co-workers reported that upon heating with aluminum chloride, 2-diphenylylaminoboron dichloride prepared from 2-aminodiphenyl and boron trichloride gives 10-chloro-9-aza-10-boraphenanthrene in moderate yield (eq. 17).[27]

---

[25] Hurd, D. T. *J. Am. Chem. Soc.* **1948,** *70*, 2053–2055.
[26] (a) Muetterties, E. L. *J. Am. Chem. Soc.* **1959,** *81*, 2597. (b) Bujwid, Z. J.; Gerrard, W.; Lappert, M. F. *Chem. Ind.* **1959,** 1091–1092.
[27] Dewar, M. J. S.; Kubba, V. P.; Petit, R. *J. Chem. Soc.* **1958,** 3073–3076.

They also succeeded in synthesizing bis-borazaro compounds using this intramolecular Friedel–Crafts cyclization (eq. 18).[28]

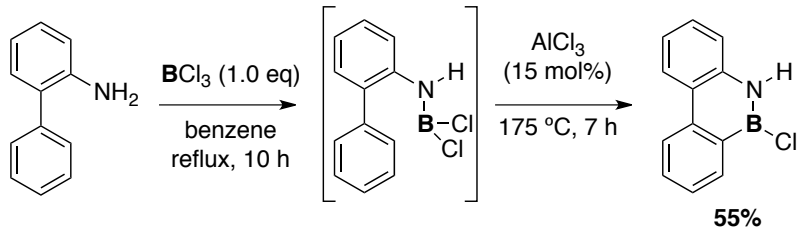

(eq. 17)

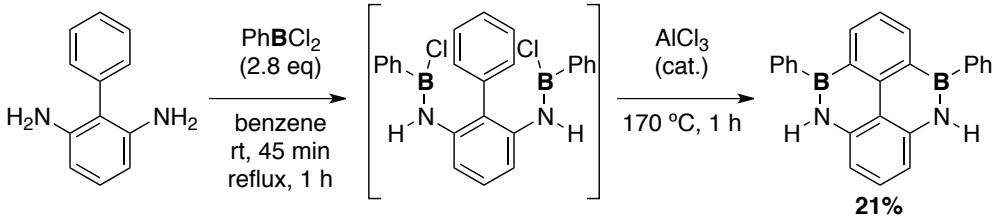

(eq. 18)

Recently, Ingleson and co-workers reported an electrophilic borylation of aromatic compounds *via* catecholatoborenium cations (eq. 19).[29] Subsequent one-pot transesterification provides the synthetically useful pinacol boronate esters.

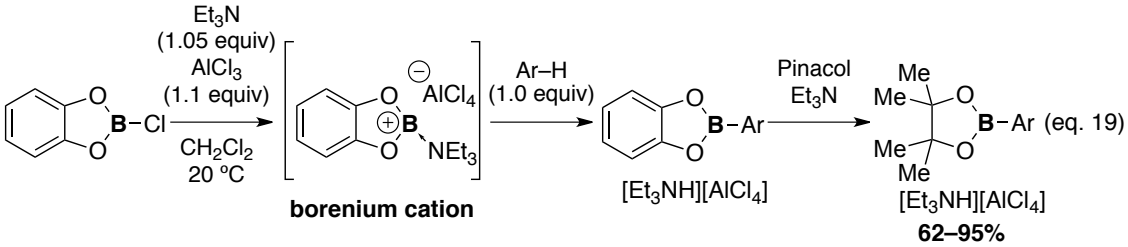

(eq. 19)

As described above, a number of hetero-Friedel–Crafts reactions have been developed so far. However, only a few synthetic applications of this reaction for synthesizing multidimensional polycyclic aromatic compounds have been reported. This author envisioned that the development of a tandem intramolecular hetero-Friedel–Crafts reaction could provide facile access to multidimensional π-conjugated frameworks with ring-junction heteroatoms, as shown in Chart 2.

[28] Chissick, S. S.; Dewar, M. J. S.; Maitlis, P. M. *Tetrahedron Lett.* **1960,** *1*, 8–10.
[29] Grosso, A. D.; Singleton, P. J.; Muryn, C. A.; Ingleson, M. J. *Angew. Chem., Int. Ed.* **2011,** *50*, 2102–2106.

Outline of this thesis

This thesis is composed of Chapters 1–5 in addition to this general introduction. In Chapter 1, the synthesis of 4b-aza-12b-boradibenzochrysene derivatives *via* the tandem bora-Friedel–Crafts reaction is described. The compound adopts a twisted conformation that results in a tight stacking array in the solid state. Time-resolved microwave conductivity measurements prove that the intrinsic hole mobility (0.07 $cm^2 V^{-1} s^{-1}$) is comparable to that of rubrene (0.05 $cm^2 V^{-1} s^{-1}$), one of the most commonly used organic semiconductors, indicating that the replacement of the ring-fusing CC units of PAHs with the isoelectronic BN unit generates potential candidates for organic electronic materials. In Chapter 2, the synthesis and physical properties of azaboradibenzo[6]helicene, a new semiconductor material of helical chirality, are described. Unprecedented carrier inversion was observed between amorphous films of the racemate (p-type semiconductor) and those of a single enantiomer (n-type semiconductor). This carrier inversion is explained in terms of the different molecular packings in their crystal structures. Chapter 3 describes the synthesis of 14b^1-aza-14b-borabenzo[*p*]indeno[1,2,3,4-*defg*] chrysene *via* a tandem bora-Friedel–Crafts reaction and a subsequent cyclization reaction. The rigid planar structure gave rise to a tight single-dimensional stacking array, and an electronic coupling calculation based on the crystal structure suggests its potential as a good p-type semiconductor material. In photophysical measurements, the compound exhibited relatively high quantum yield. This chapter also includes discussion of the synthesis of BN-fused polycyclic aromatic compounds containing heterocyclic five-membered rings. Chapter 4 contains discussion of triaryl phosphine derivatives containing curved π-conjugated frameworks with a phosphorus ring junction synthesized *via* a tandem phospha-Friedel–Crafts reaction. Their rigid molecular frameworks enable these unprecedented phosphine compounds to hold extended π-conjugation spread over the whole molecule. Finally, Chapter 5 describes studies on the reaction mechanism of the bora-Friedel–Crafts reaction. Based on NMR experiments and DFT calculations, a reaction pathway without generation of four-fold coordinated species is suggested. Then, the feasibility and generality of the method are demonstrated by extending it to sila- and germa-Friedel–Crafts reactions.

Chapter 1

Synthesis of BN-fused Polycyclic Aromatic Compounds *via* a Tandem Bora-Friedel–Crafts Reaction

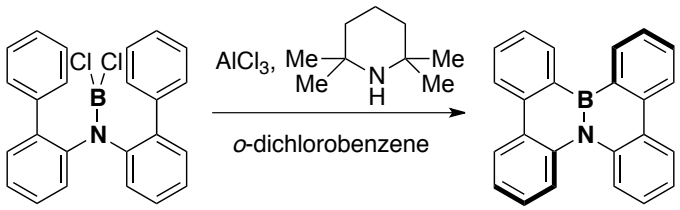

4b-aza-12b-boradibenzo[*g*,*p*]chrysene

"Tandem bora-Friedel–Crafts reaction"

Abstract: A tandem intramolecular bora-Friedel–Crafts reaction has been developed as a framework for the general synthesis of BN-fused polycyclic aromatic compounds including, as an illustrative example, 4b-aza-12b-boradibenzo[*g*,*p*]chrysene. This compound adopts a twisted conformation that results in a tight and offset face-to-face stacking array in the solid state. Time-resolved microwave conductivity measurements prove that the intrinsic hole mobility of the compound (0.07 $cm^2\ V^{-1}\ s^{-1}$) is comparable to that of rubrene (0.05 $cm^2\ V^{-1}\ s^{-1}$), one of the most commonly used organic semiconductors, indicating that BN-substituted polycyclic aromatic compounds are potential organic electronic materials.

Chapter 1

1-1. Introduction

Polycyclic aromatic compounds are an important class of materials that are used to produce organic electronics, dyes, sensors, and liquid crystal displays.[1] Replacement of the C–C units in polycyclic aromatic compounds with isoelectronic B–N units affords novel hetero-π-conjugated molecules that are structurally similar to their all-carbon analogs but exhibit substantially different optical and electronic properties because of the local dipole moment and/or polarized frontier orbitals.[2] Following the pioneering work of Dewar,[3] intensive efforts have been devoted to the synthesis of BN-substituted aromatic compounds. In particular, Piers,[4] Ashe,[5] and Liu[6] have carried out extensive research in this direction in recent years.[7] However, because of the lack of a suitable methodology, construction of polycyclic frameworks with B–N units requires multiple steps,[4] and hence, BN-substituted polycyclic aromatic compounds have not yet been studied in detail.

---

[1] Reviews: (a) Fabian, J.; Nakazumi, H.; Matsuoka, M. *Chem. Rev.* **1992,** *92*, 1197–1226. (b) Scherf, U. *J. Mater. Chem.* **1999,** *9*, 1853–1864. (c) Mitschke, U.; Bäuerle, P. *J. Mater. Chem.* **2000,** *10*, 1471–1507. (d) Watson, M. D.; Fechtenkötter, A.; Müllen, K. *Chem. Rev.* **2001,** *101*, 1267–1300. (e) Bendikov, M.; Wudl, F.; Perepichka, D. F. *Chem. Rev.* **2004,** *104*, 4891–4946. (f) Klauk, H. *Organic Electronics*; Wiley-VCH: Weinheim, **2006**. (g) Anthony, J. E. *Chem. Rev.* **2006,** *106*, 5028–5048. (h) Sergeyev, S.; Pisula, W.; Geerts, Y. H. *Chem. Soc. Rev.* **2007,** *36*, 1902–1929.

[2] Reviews: (a) Liu, Z.; Marder, T. B. *Angew. Chem., Int. Ed.* **2008,** *47*, 242–244. (b) Bosdet, M. J. D.; Piers, W. E. *Can. J. Chem.* **2009,** *87*, 8–29. (c) Ashe, A. J., III *Organometallics* **2009,** *28*, 4236–4248.

[3] (a) Dewar, M. J. S.; Kubba, V. P.; Pettit, R. *J. Chem. Soc.* **1958,** 3073–3076. (b) Dewar, M. J. S.; Kaneko, C.; Bhattacharjee, M. K. *J. Am. Chem. Soc.* **1962,** *84*, 4884–4887. (c) Culling, G. C.; Dewar, M. J. S.; Marr, P. A. *J. Am. Chem. Soc.* **1964,** *86*, 1125–1127. (d) Davies, K. M.; Dewar, M. J. S.; Rona, P. *J. Am. Chem. Soc.* **1967,** *89*, 6294–6297.

[4] (a) Emslie, D. J. H.; Piers, W. E.; Parvez, M. *Angew. Chem., Int. Ed.* **2003,** *42*, 1252–1255. (b) Jaska, C. A.; Emslie, D. J. H.; Bosdet, M. J. D.; Piers, W. E.; Sorensen, T. S.; Parvez, M. *J. Am. Chem. Soc.* **2006,** *128*, 10885–10896. (c) Bosdet, M. J. D.; Jaska, C. A.; Piers, W. E.; Sorensen, T. S.; Parvez, M. *Org. Lett.* **2007,** *9*, 1395–1398. (d) Bosdet, M. J. D.; Piers, W. E.; Sorensen, T. S.; Parvez, M. *Angew. Chem., Int. Ed.* **2007,** *46*, 4940–4943. (e) Bosdet, M. J. D.; Piers, W. E.; Sorensen, T. S.; Parvez, M. *Can. J. Chem.* **2010,** *88*, 426–433.

[5] (a) Ashe, A. J., III; Fang, X. *Org. Lett.* **2000,** *2*, 2089–2091. (b) Ashe, A. J., III; Fang, X.; Kampf, J. W. *Organometallics* **2001,** *20*, 5413–5418. (c) Pan, J.; Kampf, J. W.; Ashe, A. J., III *Organometallics* **2004,** *23*, 5626–5629. (d) Fang, X.; Yang, H.; Kampf, J. W.; Banaszak Holl, M. M.; Ashe, A. J., III *Organometallics* **2006,** *25*, 513–518. (e) Pan, J.; Kampf, J. W.; Ashe, A. J., III *Org. Lett.* **2007**, *9*, 679–681.

[6] (a) Lamm, A. N.; Liu, S.-Y. *Mol. BioSyst.* **2009,** *5*, 1303–1305. (b) Marwitz, A. J. V.; Jenkins, H. T.; Zakharov, L. N.; Liu, S.-Y. *Angew. Chem., Int. Ed.* **2010,** *49*, 7444–7447. (c) Abbey, E. R.; Zakharov, L. N.; Liu, S.-Y. *J. Am. Chem. Soc.* **2011,** *133*, 11508–11511.

[7] Recent examples concerning aromatic compounds with boron and nitrogen substituents: (a) Proñ, A.; Zhou, G.; Norouzi-Arasi, H.; Baumgarten, M.; Müllen, K. *Org. Lett.* **2009,** *11*, 3550–3553. (b) Sachdev, H.; Zahn, N.; Huch, V. *Z. Anorg. Allg. Chem.* **2009,** *635*, 2112–2119. (c) Agou, T.; Sekine, M.; Kobayashi, J.; Kawashima, T. *Chem. Eur. J.* **2009**, *15*, 5056–5062. (d) Wakamiya, A.; Mori, K.; Araki, T.; Yamaguchi, S. *J. Am. Chem. Soc.* **2009,** *131*, 10850–10851. (e) Lorbach, A.; Bolte, M.; Lerner, H.-W.; Wagner, M. *Chem. Commun.* **2010,** 3592–3594. (f) Li, H.; Jäkle, F. *Macromol. Rapid. Commun.* **2010,** *31*, 915–920. (g) Taniguchi, T.; Yamaguchi, S. *Organometallics* **2010,** *29*, 5732–5735.

This author has envisioned that a tandem intramolecular bora-Friedel–Crafts reaction [8] would be an efficient means of constructing extended π-conjugated frameworks with BN ring fusion (Scheme 1). Molecules with such frameworks are not only attractive functional materials but also potential starting compounds for the controlled synthesis of BN-embedded nanocarbon materials[9] through surface-assisted coupling[10] or amplification of sheet growth.

Scheme 1. Tandem intramolecular bora-Friedel–Crafts reaction for the synthesis of BN-fused polycyclic aromatic compounds

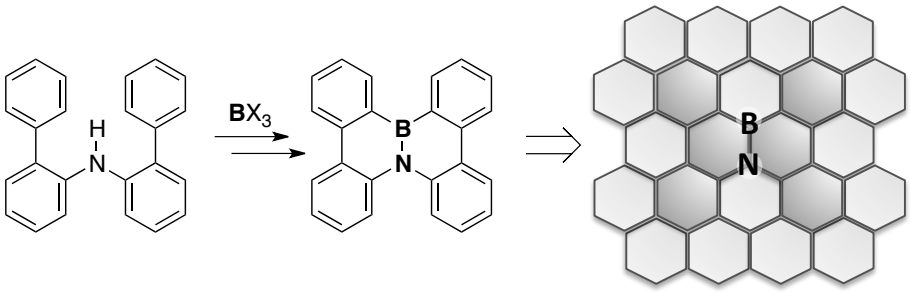

BN-embedded nanocarbon

[8] Nontandem reactions: (a) Genaev, A. M.; Nagy, S. M.; Salnikov, G. E.; Shubin, V. G. *Chem. Commun*. **2000,** 1587–1588. (b) Vries, T. S. D.; Prokofjevs, A.; Harvey, J. N.; Vedejs, E. *J. Am. Chem. Soc*. **2009,** *131*, 14679–14687. See also reference 3. Tandem phospha-Friedel–Crafts reaction: (c) Hatakeyama, T.; Hashimoto, S.; Nakamura, M. *Org. Lett*. **2011,** *13*, 2130–2133.

[9] (a) Kawaguchi, M. *Adv. Mater*. **1997,** *9*, 615–625. (b) Wang, W. L.; Bai, X. D.; Liu, K. H.; Xu, Z.; Golberg, D.; Bando, Y.; Wang, E. G. *J. Am. Chem. Soc*. **2006,** *128*, 6530–6531. (c) Kim, S. Y.; Park, J.; Choi, H. C.; Ahn, J. P.; Hou, J. Q.; Kang, H. S. *J. Am. Chem. Soc*. **2007,** *129*, 1705–1716. (d) Caretti, I.; Torres, R.; Gago, R.; Landa-Cánovas, A. R.; Jiménez, I. *Chem. Mater*. **2010,** *22*, 1949–1951.

[10] Cai, J.; Ruffieux, P.; Jaafar, R.; Bieri, M.; Braun, T.; Blankenburg, S.; Mouth, M.; Seitsonen, A. P.; Saleh, M.; Feng, X.; Müllen, K.; Fasel, R. *Nature* **2010,** *466*, 470–473.

Chapter 1

In this chapter, the development of bora-Friedel–Crafts reaction through careful screening of the conditions is described, along with a comparison of the chemical and physical properties of 4b-aza-12b-boradibenzo[*g*,*p*]chrysene **1** with those of its isoelectronic carbon analog, dibenzo[*g*,*p*]chrysene **2**. In addition, synthesis of extended π-conjugated compounds **3** and **4** with two ring-fusing BN units is described.

Chart 1. Dibenzochrysene derivatives and more extended π-conjugated molecules

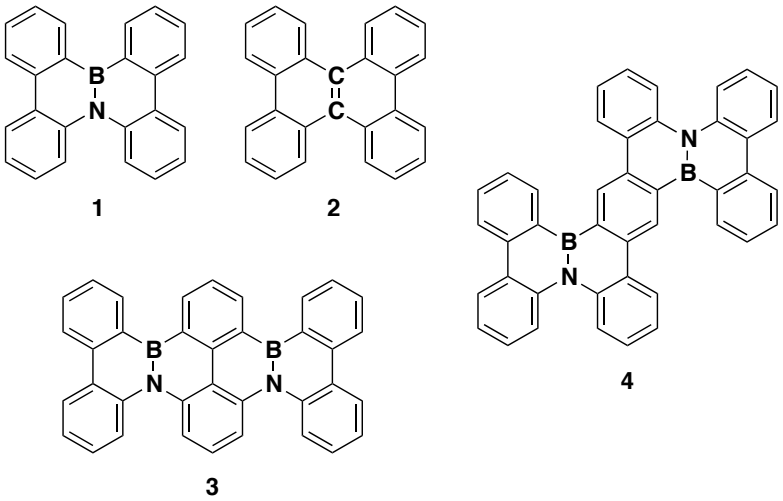

1-2. Results and Discussion

1-2-1. Optimization of the reaction conditions

The synthetic route to **1** *via* the tandem intramolecular bora-Friedel–Crafts reaction is described in Scheme 2. Dichloroboraneamine **6**, prepared *in situ* from bis(biphenyl-2-yl)amine **5**, was treated with a variety of Lewis acids and base additives in *o*-dichlorobenzene (ODCB) at 150 °C for 12 h.

Scheme 2. Synthesis of **1** *via* bora-Friedel–Crafts reaction

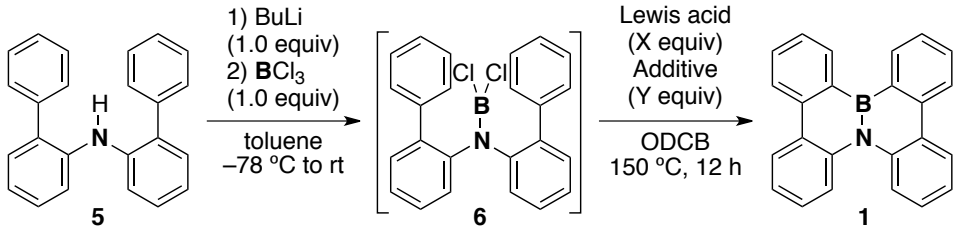

Table 1 summarizes the optimization of the bora-Friedel–Crafts reaction. During the initial screening of Lewis acids such as $AlCl_3$, $AlBr_3$, $GaCl_3$, and $Zn(OTf)_2$ (entries 1–4), the target compound **1** was not obtained and the starting amine **5** was recovered. After extensive screening, compound **1** was found to be obtained in 30% yield when a mixture of $AlCl_3$ (4.0 equiv) and NEt^iPr_2 (1.5 equiv) was used (entry 7). However, reactions with 0.5, 1.0, and 2.0 equiv of NEt^iPr_2 did not give the desired product (entries 5–8). Screening of the base additives (entries 9–14) indicated that the optimum product yield (67%) was achieved when 1.5 equiv of 2,2,6,6-tetramethylpiperidine (TMP) was used (entry 9). Thus, the $AlCl_3$/TMP stoichiometry plays an important role in enhancing the product yield (entries 15–19). The sluggish conversion in the presence of low and high concentrations of the base is possibly due to the decomposition of the product and the deactivation of $AlCl_3$, respectively. The other Lewis acids considered were not as effective as $AlCl_3$ (entries 20–24). Boron sources other than BCl_3, such as $BF_3{\cdot}Et_2O$, BBr_3, and $B(OMe)_3$, did not afford the target compound **1** even under the optimized conditions.

Table 1. Screening of Lewis acids and Brønsted bases

Entry[a]	Lewis acid (X equiv)	Additive (Y equiv)	Yield[b] (%) of **1**
1	$AlCl_3$ (4.0)	none	0
2	$AlBr_3$ (4.0)	none	0
3	$GaCl_3$ (4.0)	none	0
4	$Zn(OTf)_2$ (4.0)	none	0
5	$AlCl_3$ (4.0)	NEt^iPr_2 (0.5)	0
6	$AlCl_3$ (4.0)	NEt^iPr_2 (1.0)	0
7	$AlCl_3$ (4.0)	NEt^iPr_2 (1.5)	30
8	$AlCl_3$ (4.0)	NEt^iPr_2 (2.0)	0
9[c]	**$AlCl_3$ (4.0)**	**2,2,6,6-tetramethylpiperidine (1.5)**	**67**[d]
10	$AlCl_3$ (4.0)	1,2,2,6,6-pentamethylpiperidine (1.5)	27
11	$AlCl_3$ (4.0)	2,4,6-collidine (1.5)	27
12	$AlCl_3$ (4.0)	proton sponge (1.5)	<1
13	$AlCl_3$ (4.0)	NCy_2Me (1.5)	15
14	$AlCl_3$ (4.0)	$^iBu_3N$ (1.5)	16
15	$AlCl_3$ (4.0)	2,2,6,6-tetramethylpiperidine (1.0)	0
16	$AlCl_3$ (4.0)	2,2,6,6-tetramethylpiperidine (2.0)	42
17	$AlCl_3$ (3.0)	2,2,6,6-tetramethylpiperidine (1.5)	0
18	$AlCl_3$ (5.0)	2,2,6,6-tetramethylpiperidine (1.5)	34
19	$AlCl_3$ (6.0)	2,2,6,6-tetramethylpiperidine (2.25)	28
20	$AlBr_3$ (4.0)	NEt^iPr_2 (1.5)	30
21	$AlBr_3$ (4.0)	2,2,6,6-tetramethylpiperidine (1.5)	36
22	$GaCl_3$ (4.0)	NEt^iPr_2 (1.5)	38
23	$GaCl_3$ (4.0)	2,2,6,6-tetramethylpiperidine (1.5)	6
24	$Zn(OTf)_2$ (4.0)	NEt^iPr_2 (1.5)	0

[a]Reactions were carried out on a 0.6 mmol scale. [b]The yield was determined from ^1H NMR measurements using 1,1,2,2-tetrachloroethane as the internal standard. [c]The reaction was carried out on a 15 mmol scale. [d]Isolated yield.

1-2-2. X-ray single crystal structures

The structure of **1** has been determined using X-ray crystallography (Figure 1a). The B–N bond length [1.426(3) Å] was found to be shorter than that in typical BN aromatic compounds (1.45–1.47 Å), which confirms the double bond character (1.37–1.40 Å).[3–5] On the other hand, the B–C1, B–C2, N–C3, and N–C4 lengths in **1** are 1.535(3), 1.534(3), 1.442(3), and 1.448(3) Å, respectively, indicating that these are single bonds. The aforementioned observations reveal the low aromaticity of the BNC_4 rings and are consistent with the results of a nucleus-independent chemical shift (NICS) analysis discussed below. Because of the steric repulsion between the hydrogen atoms at the *ortho* position to the heteroatoms (dihedral angle: C5–C7–C6–C8, 38.87°), **1** adopts a twisted conformation and hence has a unique packing structure (Figure 1b). That is, the molecules are arranged in an offset face-to-face stacking array with a π-π distance of 3.3–3.6 Å; in this arrangement, the local dipole moments of the B–N bonds also offset each other. Each array includes an enantiomer with a left- or right-handed helical structure [*M*-helix (shown in pink) or *P*-helix (shown in blue), respectively] containing CH–π interactions (3.0–3.4 Å).

To investigate the effect of replacing the B–N unit with C–C, the structure of the isoelectronic carbon analog, dibenzo[*g*,*p*]chrysene **2**, was also determined using X-ray crystallography (Figure 1c, d). The central C1–C2 bond is highly olefinic [1.3882(16) Å] and much shorter than the four radial C–C bonds [1.4608(19)–1.4657(18) Å], indicating a large degree of bond alternation and low aromaticity of the central rings, as observed in **1**. The molecular arrangement of **2** in the solid state is almost identical to that of **1**, and surprisingly, the lattice constants are also nearly equal to those of **1**.

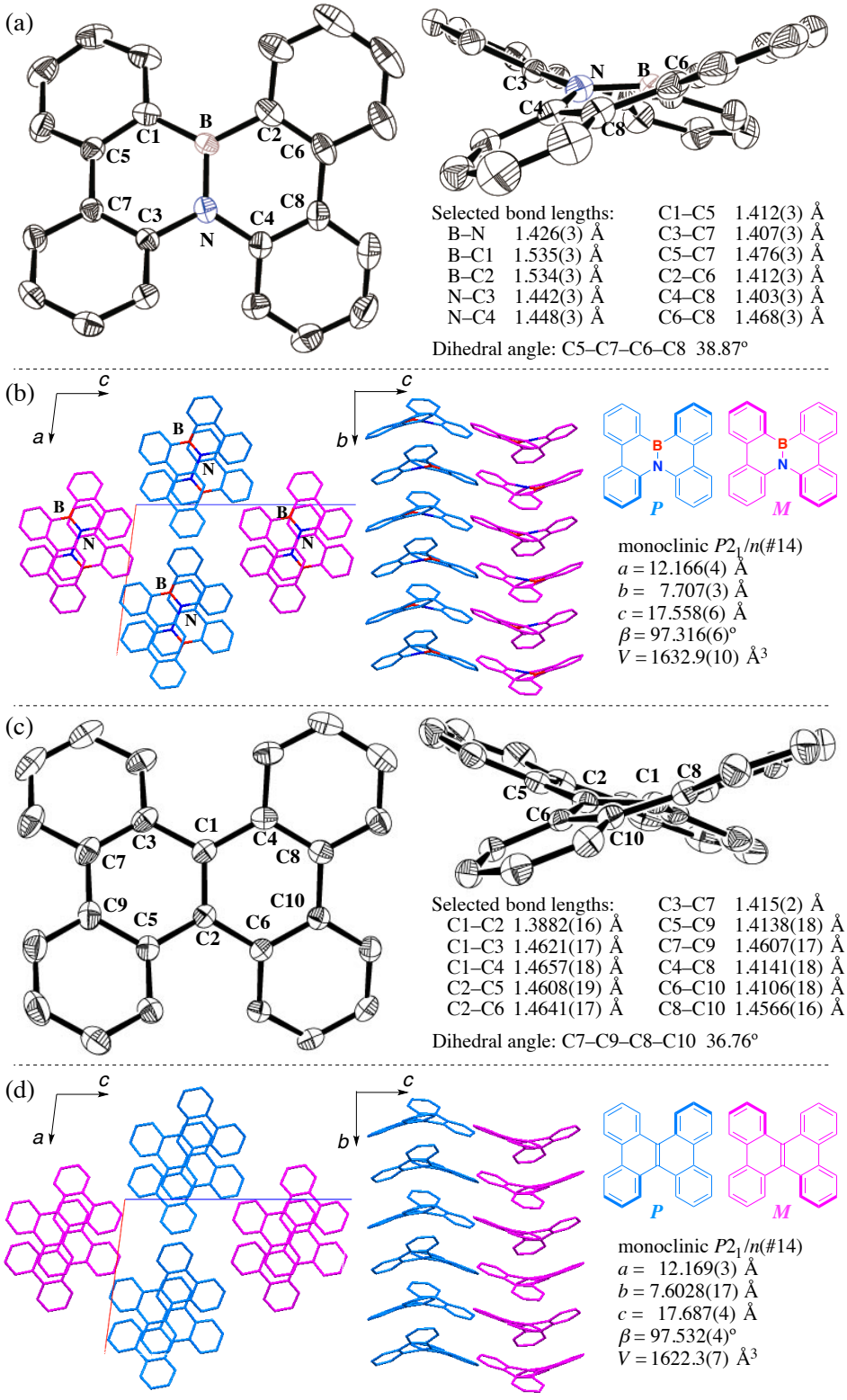

Figure 1. ORTEP drawings and packing structures of **1** (a, b) and **2** (c, d). Thermal ellipsoids are shown at 50% probability and H atoms have been omitted for clarity. The *P*-enantiomer is shown in blue and *M*-enantiomer is shown in pink.

1-2-3. Chemical and physical properties of BN-fused compound 1: Comparison with the isoelectronic carbon analog 2

The introduction of the BN unit causes only a subtle change in the melting point (**1**, 227 °C; **2**, 229 °C), but the solubility in polar organic solvents is significantly improved (solubility in Et_2O and AcOEt: **1**, 4.4 and 7.7 mg/mL; **2**, 2.5 and 5.0 mg/mL), probably because of its enhanced dipole moment.

In the UV-visible absorption spectrum, **1** has a relatively strong absorption band with a maximum at 340 nm ($\log\varepsilon$ = 4.06) corresponding to a π-π^* transition (Figure 2), whereas **2** has an absorption maximum at 351 nm ($\log\varepsilon$ = 4.21). BN replacement leads to a small blue shift in the UV-visible absorbance, because the low aromaticity of the BNC_4 rings (*vide infra*) could weaken the delocalization of the π-electrons in the dibenzochrysene framework.

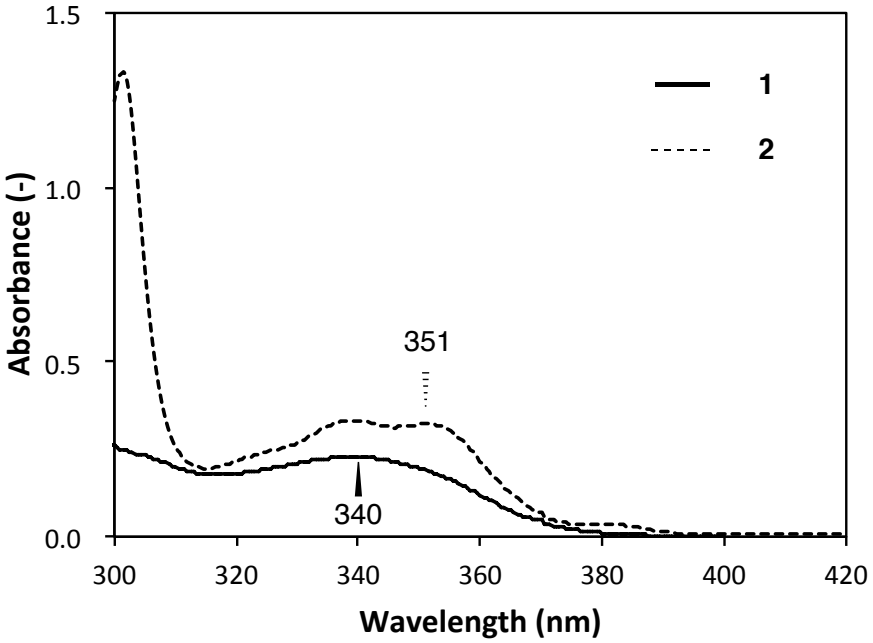

Figure 2. UV-visible absorption spectra of **1** (solid line) and **2** (dotted line) in 2.0×10^{-5} M CH_2Cl_2.

Redox potentials were determined by performing cyclic voltammetry (CV) measurements in THF (E_{red}) or CH_2Cl_2 (E_{ox}) with 0.10 M n-$Bu_4N^+PF_6^-$ or n-$Bu_4N^+BPh_4^-$. The reversible oxidation and reduction waves with peak potentials at +0.76 V (+0.89 V) and –2.77 V (–2.65 V) *vs*. Fc/Fc^+, respectively, are observed for **1** (**2**) (Figure 3). BN replacement leads to a negative shift in the redox potential, which could partially account for its improved hole mobility.

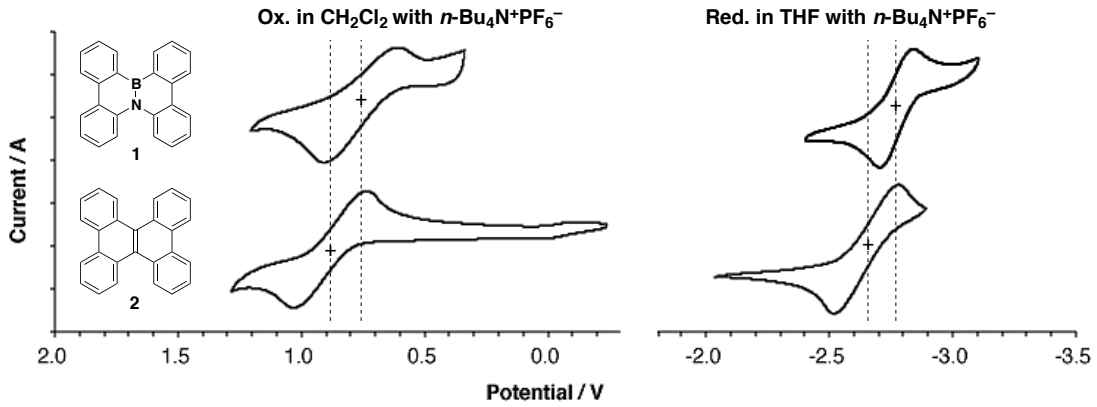

Figure 3. Cyclic voltammograms of **1** and **2**.

The aromaticities of the six-membered rings in **1** and **2** were evaluated by performing a NICS analysis using the B3LYP hybrid functional with the 6-31G(d) basis set (Figure 4). Interestingly, the BNC_4 rings in **1** have low aromaticity, as suggested by their low NICS(1) value (–2.9; *cf.* 10a-aza-10b-borapyrene: –9.5[4d]), whereas the corresponding C_6 rings in **2** have moderate aromaticity (–6.5). On the other hand, BN replacement does not significantly affect the aromaticity of the surrounding C_6 rings in **1** (–10.2 and –10.6; *cf.* benzene: –11.2[11]). Despite the low aromaticity of the central BNC_4 rings, DFT calculations show that the π-conjugation in **1** extends over the entire molecule, and reasonable orbital distribution is observed.

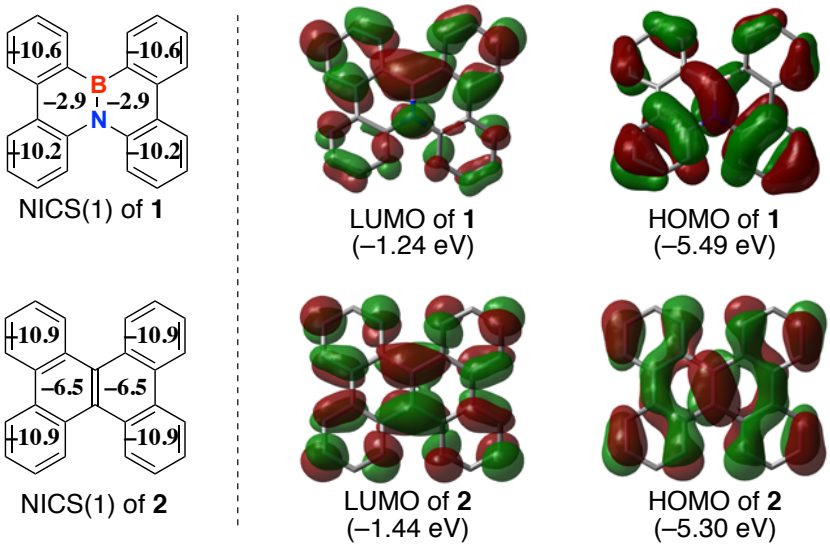

Figure 4. NICS(1) values of **1** and **2** (left) and the Kohn–Sham LUMO and HOMO of **1** and **2** (right) calculated at the B3LYP/6-31G(d) level.

[11] Moran, D.; Stahl, F.; Bettinger, H. F.; Schaefer, H. F., III; Schleyer, P. V. R. *J. Am. Chem. Soc.* **2003,** *125*, 6746–6752.

1-2-4. Evaluation of charge transport properties

The time-resolved microwave conductivity (TRMC) technique is known to be a facile method for measuring the charge carrier mobility.[12] Because it allows for the observation of the nanometer-scale oscillating motion of the charge carriers, this method is insusceptible to extrinsic factors (impurities, defect sites, etc.), as opposed to conventional direct-current methods such as the time of flight (TOF) and field-effect transistor (FET) techniques. As shown in Figure 5, TRMC measurements confirmed that **1** has a high intrinsic hole mobility (0.07 $cm^2\ V^{-1}\ s^{-1}$) that rivals that of rubrene (0.05 $cm^2\ V^{-1}\ s^{-1}$), one of the most popular organic semiconductors.[12d] Interestingly, the hole mobility of **2** is only one-tenth of that of **1** (0.007 $cm^2\ V^{-1}\ s^{-1}$). The transient conductivity of **1** is not quenched even in a SF_6 environment, suggesting that the major charge carriers in **1** are positive charges (holes). The pseudo-first-order decay kinetics (Figure 5a) also indicate that the mobile holes are trapped rapidly by impurities or structural defects at the interfaces rather than through bulk recombination with negative charges *via* second-order reactions in the polycrystalline phases.

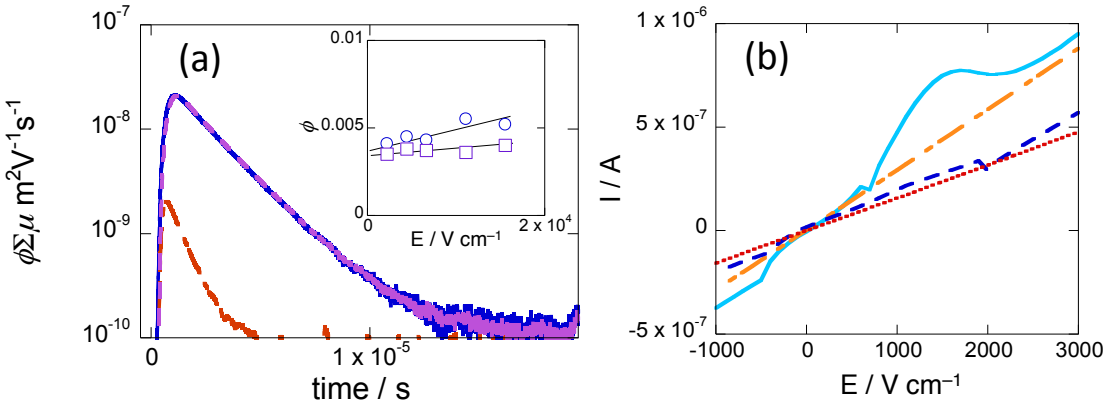

Figure 5. (a) Transient conductivity monitored for the polycrystalline phase of **1** in Ar (blue) and SF_6 (violet) environments. Identical traces were observed for both atmospheres. The kinetic trace for the transient conductivity was also observed for **2** (orange). Excitation was carried out at 355 nm using 13 mJ cm^{-2} pulses for all transients. The inset shows the dependence of ϕ on the applied electric field strength between interdigitated Au electrodes with a 5 μm gap. The values of ϕ were determined by performing photocurrent integration for thin films of **1** (120 nm thick) and **2** (80 nm thick) under illumination at 355 nm and 22 mJ cm^{-2}. The photocurrent under 355 nm illumination was also traced using identical samples; the I-V traces are illustrated in (b). Blue dashed and red dotted lines are the traces for **1** (dark and illuminated, respectively), and turquoise solid and orange dot-dashed lines are the traces for **2** (dark and illuminated, respectively).

---

[12] (a) Grozema, F. C.; Siebbeles, L. D. A.; Warman, J. M.; Seki, S.; Tagawa, S.; Scherf, U. *Adv. Mater.* **2002,** *14*, 228–231. (b) Acharya, A.; Seki, S.; Saeki, A.; Koizumi, Y.; Tagawa, S. *Chem. Phys. Lett.* **2005,** *404*, 35–39. (c) Acharya, A.; Seki, S.; Koizumi, Y.; Saeki, A.; Tagawa, S. *J. Phys. Chem. B* **2005,** *109*, 20174–20179. (d) Saeki, A.; Seki, S.; Takenobu, T.; Iwasa, Y.; Tagawa, S. *Adv. Mater.* **2008,** *20*, 920–923.

To provide detailed insight into the hole mobility, the electronic coupling V (meV) between neighboring molecules was calculated from the X-ray crystal structures of **1** and **2** (Figure 6).[13] These electronic coupling V and reorganization energy λ calculations were performed using the PW91 or B3LYP hybrid functional with the DZP basis set of the ADF2010 program. The electronic hopping rate W is proportional to V^2 according to the Marcus-Hush equation.[13c] Although the molecular packing is virtually the same in these compounds, the electronic coupling varies significantly. The V values along the *a*-axis in **1** [6.1 and 2.4 meV, (Figure 6a)] are ten times larger than the corresponding values in **2** [0.6 and 0.3 meV, (Figure 6c)], while those along the *b*- and *c*-axes are comparable to the corresponding values in **2** (Figures 6a–d). It is supposed that the partial localization of the frontier orbitals induced by the BN replacement increases the electronic coupling along the *a*-axis in **1**, leading to an improvement in the total hole mobility. To evaluate this hypothesis, a single-point calculation for side-by-side molecules was performed for each crystal packing. An example in which adjacent HOMOs overlap along the *a*-axis in **1** and **2** is shown in Figure 7. The frontier orbitals of **2** have a node at the position of the overlap, whereas the partially localized orbitals of **1** overlap efficiently with the same phase. Therefore, the V value of **1** would be larger than that of **2** (6.1 *vs*. 0.6 meV). The reorganization energies λ of **1** and **2** are 0.21541 and 0.20413 eV, respectively.[12,13] Such a small difference is unlikely to be a dominant factor affecting the different hole mobilities of these compounds.

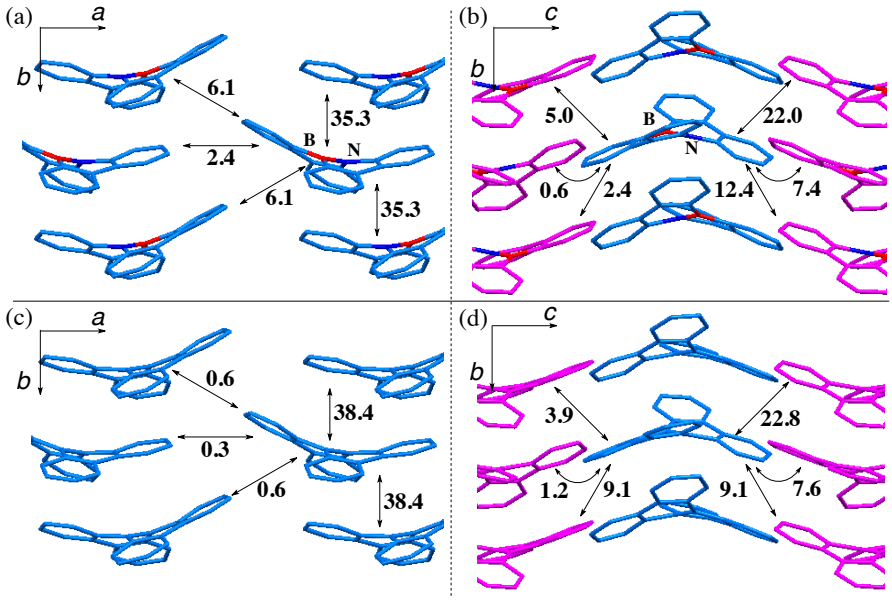

Figure 6. Electronic coupling V (meV) between neighboring molecules in the X-ray crystal structures of **1** (a, b) and **2** (c, d).

[13] (a) Velde, G. T.; Bickelhaupt, F. M.; Baerends, E. J.; Fonseca Guerra, C.; Gisbergen, S. J. A. V.; Snijders J. G.; Ziegler, T. *J. Comput. Chem.* **2001,** *22*, 931–967. (b) Senthilkumar, K.; Grozema, F. C.; Bickelhaupt, F. M.; Siebbeles, L. D. A. *J. Chem. Phys.* **2003,** *119*, 9809–9817. (c) Wen, S.-H.; Li, A.; Song, J.; Deng, W.-Q.; Han, K.-L.; Goddard, W. A., III *J. Phys. Chem. B* **2009,** *113*, 8813–8819.

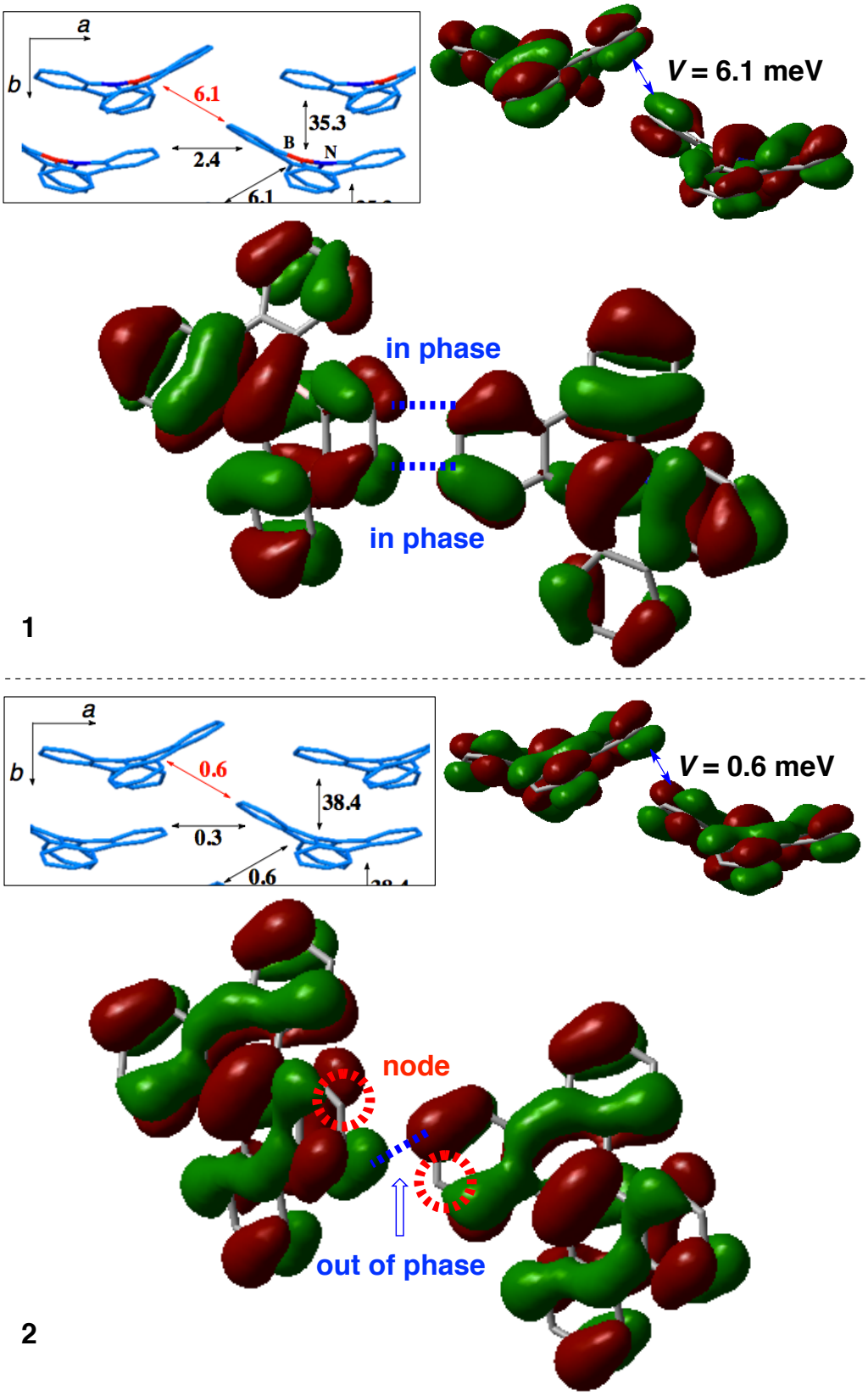

Figure 7. Overlapping adjacent HOMOs of **1** and **2**.

1-2-5. Extension of π-conjugated framework

In a further application of the present synthetic strategy, an extended π-conjugated molecule containing two fused BN rings was synthesized in two steps from commercially available sources (Scheme 3). *N*,*N*′-bis(biphenyl-2-yl) biphenyl-2,6-diamine **9**, which was prepared from 2,6-dichlorobiphenyl **7** and 2-aminobiphenyl **8** in 87% yield, was used for the synthesis of 8b,11b-diaza-19b,22b-diborahexabenzo[*a*,*c*,*fg*,*j*,*l*,*op*]tetracene **3**.[14] The introduction of boron substituents in **9** and subsequent tandem bora-Friedel–Crafts reaction afforded **3** in 40% yield. Moreover, the diagonally extended π-conjugated compound **4** was also prepared from 2,2″-dichloro-1,1′:4′,1″-terphenyl **10** and 2-aminobiphenyl **8** in a similar fashion (Scheme 4).

Scheme 3. Two-step synthesis of **3**

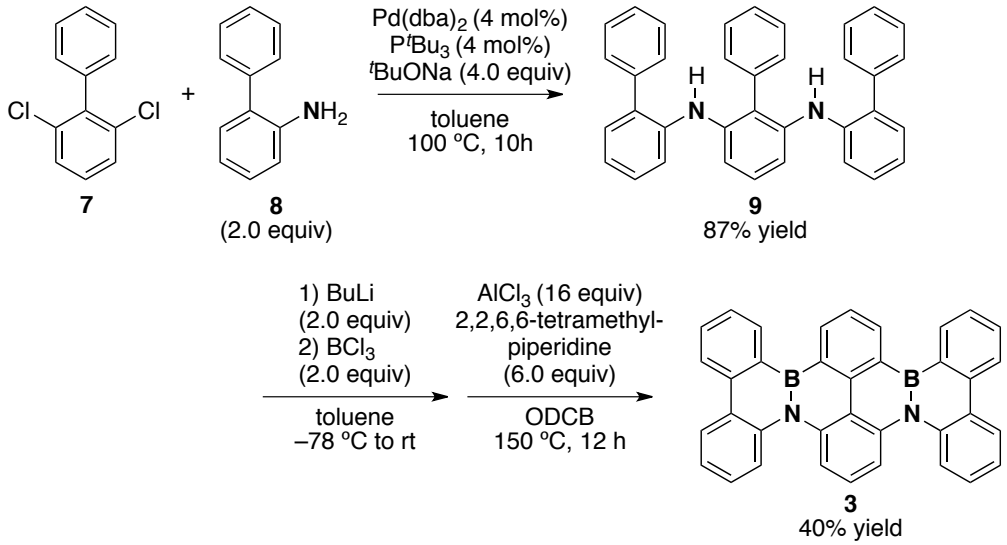

[14] The isoelectronic carbon analog has been investigated: Mochida, K.; Kawasumi, K.; Segawa, Y.; Itami, K. *J. Am. Chem. Soc.* **2011,** *133*, 10716–10719.

Scheme 4. Two-step synthesis of **4**

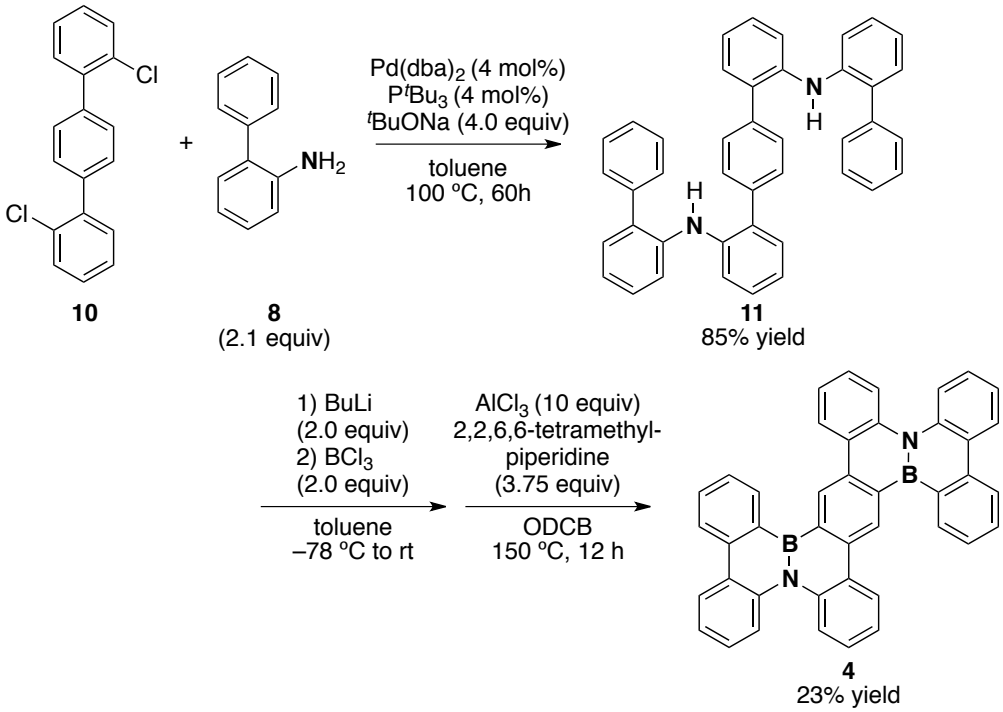

In the CV experiments, compound **3** showed an irreversible oxidation wave and a reversible reduction wave with peak potentials at +0.10 and –1.57 V, respectively (*vs*. Fc/Fc^{+}). While the electrochemical HOMO-LUMO gap (1.67 eV) in **3** is smaller than that in pentacene [2.09 eV, (E_{ox} = 0.22 V, E_{red} = –1.87 V)],[15] no obvious decomposition was observed even at the melting point (358 °C) in the ambient atmosphere. Despite its polycyclic aromatic structure, **3** is fairly soluble in organic solvents such as chlorobenzene (6.7 mg/mL) and *o*-dichlorobenzene (8.6 mg/mL), probably because of its flexible molecular framework and dipole moment. These advantageous physical properties of **3** make it suitable for use in organic electronics.

[15] Sakamoto, Y.; Suzuki, T.; Kobayashi, M.; Gao, Y.; Fukai, Y.; Inoue, Y.; Sato, F.; Tokito, S. *J. Am. Chem. Soc.* **2004,** *126*, 8138–8140.

1-3. Conclusions

This author has developed a tandem intramolecular bora-Friedel–Crafts reaction to synthesize BN-fused polycyclic aromatic compounds that adopt twisted geometries. TRMC measurements confirm that the replacement of the C–C units in dibenzo[*g*,*p*]chrysene with isoelectronic B–N units dramatically enhances its hole mobility because of the strong electronic coupling between neighboring molecules in the solid state. The strategy is simple and practical, and it can also be employed for the extension of π-conjugated frameworks. Thus, it forms the basis for pioneering research in materials science and will spur further development of bottom-up approaches toward BN-embedded nanocarbon materials.

1-4. Experimental Section

General. All the reactions dealing with air- or moisture-sensitive compounds were carried out in a dry reaction vessel under a positive pressure of argon. Air- and moisture-sensitive liquids and solutions were transferred *via* a syringe or a stainless steel cannula. Organic solutions were concentrated by rotary evaporation at *ca*. 30–400 mmHg. Gel permeation chromatography was performed on a JAIGEL-1H and 2H (20 mm i.d.) with an LC-9204 (Japan Analytical Industry Co., Ltd.).

Instrumentation. Proton nuclear magnetic resonance (^{1}H NMR) and carbon nuclear magnetic resonance (^{13}C NMR) spectra were recorded on JEOL ECS400 (392 MHz) or BRUKER AVANCE III (600 MHz) NMR spectrometers. Proton chemical shift values are reported in parts per million (ppm, δ scale) downfield from tetramethylsilane, and are referenced to the tetramethylsilane (δ 0). ^{13}C NMR spectra were recorded at 98.5 or 151 MHz: carbon chemical shift values are reported in parts per million (ppm, δ scale) downfield from tetramethylsilane, and are referenced to the carbon resonance of $CDCl_3$ (δ 77.0) and tetramethylsilane (δ 0). ^{11}B NMR spectra were recorded at 193 MHz: boron chemical shift values are reported in parts per million (ppm, δ scale) and are referenced to the external standard boron signal of $BF_3{\cdot}Et_2O$ (δ 0). Data are presented as: chemical shift, multiplicity (s = singlet, d = doublet, t = triplet, q = quartet, quint = quintet, sext = sextet, sept = septet, m = multiplet and/or multiplet resonances, br = broad), coupling constant in hertz (Hz), signal area integration in natural numbers, and assignment (*italic*). IR spectra were recorded on an ATR-FTIR spectrometer (FT/IR-Spectrum One, PerkinElmer). Characteristic IR absorptions are reported in cm^{-1}. Melting points were recorded on a Yanaco MP-500V. High-resolution mass spectra (HRMS) were obtained using the electron impact (EI) method with JEOL JMS-700, JMS-SX102A. Cyclic voltammetry was conducted on a BAS Electrochemical Analyzer ALS 620C using a three-electrode cell with a glassy carbon working electrode, a platinum wire counter electrode, and an $Ag/AgNO_3$ reference electrode. Purity of isolated compounds was determined by GC analysis on Shimadzu GC-17A instrument equipped with an FID detector and a capillary column, InertCap 1MS (GL Sciences Inc., 30 m × 0.25 mm i.d., 0.25 μm film thickness) and/or ^{1}H NMR analyses.

Solvent. Anhydrous tetrahydrofuran (THF) and toluene were purchased from Wako Pure Chemical Industries, Ltd. (Wako) and dried over Molecular Sieves 4A and degassed before use. Water content of the solvent was determined with a Karl Fischer Moisture Titrator (MKC-610, Kyoto Electronics Company) to be less than 15 ppm.

Materials. Dibenzo[*g*,*p*]chrysene was purchased from Tokyo Chemical Industry Co., Ltd. and was used after sublimation. Other materials were purchased from Wako, Tokyo Chemical Industry Co., Ltd., Aldrich Inc., Hokko Chemical Industry Co., Ltd., and

other commercial suppliers, and were used after appropriate purification, unless otherwise noted. Florisil® (100–200 mesh) and Celite® were purchased from Wako. Aryl halides and aryl amines were purified by distillation or recrystallization to be over 99.5% pure by GC analysis.

Synthesis of 4b-aza-12b-boradibenzo[*g*,*p*]chrysene (1)

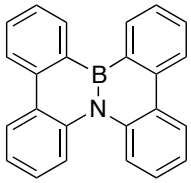

A solution of butyllithium in hexane (9.35 mL, 1.60 M, 15 mmol) was added slowly to a solution of **5** (4.82 g, 15.0 mmol) in toluene (80 mL) at –78 ºC under argon. After 1 h, the reaction mixture stirred at 0 ºC for 1 h. A solution of boron trichloride in heptane (15.0 mL, 1.0 M, 15 mmol) was added at –78 ºC. After stirring at room temperature for 8 h, solvent was removed *in vacuo*, and the reaction mixture was added to a solution of aluminum trichloride (8.00 g, 60 mmol) and 2,2,6,6-tetramethylpiperidine (3.18 g, 22.5 mmol) in *o*-dichlorobenzene (100 mL) at 0 ºC. After stirring at 150 ºC for 12 h, 1,4-diazabicyclo[2.2.2]octane (6.73 g, 60 mmol) was added. The reaction mixture was filtered with a pad of Celite®. After the solvent was removed *in vacuo*, the crude product was purified by GPC (eluent: toluene) to obtain the title compound (3.31 g, 67% yield) as white-yellow powder. IR (neat): cm^{-1} 3056 (Ar-H), 1598, 1575, 1485, 1445, 1430, 1319, 1300, 1286, 1259, 1238, 1166, 1134, 1049, 935, 744, 723, 624, 587, 558; mp: 226.5–227.3 ºC; ^{1}H NMR (CS_2/CD_2Cl_2=2/1, 600 MHz) δ 7.26–7.34 (m, 4H, NCCHC*H*C*H*), 7.55 (td, *J* = 1.2, 7.2 Hz, 2H, BCCHC*H*), 7.71 (td, *J* = 1.2, 7.2 Hz, 2H, BCCCHC*H*), 8.04 (dd, *J* = 1.8, 7.8 Hz, 2H, NCC*H*), 8.28 (dd, *J* = 1.8, 7.8 Hz, 2H, NCCC*H*), 8.33 (d, *J* = 7.8 Hz, 2H, BCCC*H*), 8.62 (dd, *J* = 1.2, 7.2 Hz, 2H, BCC*H*); ^{13}C NMR (CS_2/CD_2Cl_2=2/1, 151 MHz) δ 121.3 (2C), 123.1 (2C), 123.2 (2C), 125.6 (2C), 126.9 (4C), 127.6 (2C), 131.1 (2C), 132.6 (br, 2C, *C*B*C*), 135.6 (2C), 137.1 (2C), 138.8 (2C); ^{11}B NMR (CS_2/CD_2Cl_2=2/1, 193 MHz) δ 35.6; HRMS(EI) *m*/*z* $[M]^+$ calcd for $C_{24}H_{16}NB$ 329.1376; observed 329.1380; Anal. calcd for $C_{24}H_{16}NB$ C, 87.56; H, 4.90; N, 4.25. found C, 87.79; H, 5.14; N, 4.31.

Synthesis of 8b,19b-diaza-11b,12b-diborahexabenzo[*a*,*c*,*fg*,*j*,*l*,*op*]tetracene (3)

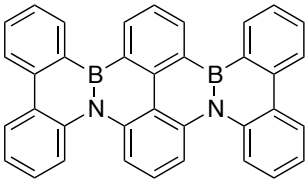

A solution of butyllithium in hexane (2.50 mL, 1.60 M, 4.0 mmol) was added slowly to a solution of **9** (0.977 g, 2.0 mmol) in toluene (20 mL) at –78 ºC under argon. After 1 h, the solution was allowed to warm to 0 ºC and stirred for 1 h, and then a solution of

boron trichloride in heptane (5.00 mL, 1.00 M, 5.0 mmol) was added to reaction mixture at –78 ºC. After stirring at room temperature for 8 h, solvent was removed *in vacuo*, and the reaction mixture was added to a solution of aluminum trichloride (2.67 g, 20.0 mmol) and 2,2,6,6-tetramethylpiperidine (1.06 g, 7.5 mmol) in *o*-dichlorobenzene (25 mL) at 0 ºC. After stirring at 150 ºC for 12 h, 1,4-diazabicyclo[2.2.2]octane (2.24 g, 20.0 mmol) was added. The reaction mixture was filtered with a pad of Celite®. After the solvent was removed *in vacuo*, the crude product was purified by GPC (eluent: toluene) to obtain the title compound (0.323 g, 32% yield) as white-yellow powder. IR (neat): cm^{-1} 3058 (Ar-H), 2922, 1590, 1484, 1429, 1293, 1239, 1137, 1066, 1043, 820, 792, 743, 725, 677, 647, 615, 578, 558, 527; mp: 357.2–358.2 ºC; ^{1}H NMR (CS_2/CD_2Cl_2=2/1, 600 MHz) δ 7.31–7.34 (m, 4H, NCCC*H*C*H*), 7.55 (t, *J* = 8.4 Hz, 1H, NCCHC*H*CHCN), 7.61 (td, *J* = 1.2, 7.2 Hz, 2H, BCCHC*H*CHCH), 7.78 (td, *J* = 1.2, 7.2 Hz, 2H, BCCHCHC*H*CH), 7.91 (t, *J* = 7.2 Hz, 1H, BCCHC*H*CHCB), 8.05 (d, *J* = 8.4 Hz, 2H, NCC*H*CHC*H*CN), 8.11–8.13 (m, 2H, NCC*H*CHCHCH), 8.32–8.35 (m, 2H, NCCC*H*), 8.40 (d, *J* = 7.2 Hz, 2H, BCCC*H*), 8.71 (d, *J* = 7.2 Hz, 2H, BCC*H*CHCHCH), 8.96 (d, *J* = 7.2 Hz, 2H, BCC*H*CHC*H*CB); ^{13}C NMR (CS_2/CD_2Cl_2=2/1, 151 MHz) δ 114.3 (2C), 119.2, 121.8 (2C), 123.1 (2C), 123.4 (2C), 125.7, 125.8 (2C), 126.2, 126.7 (2C), 127.1 (2C), 128.1 (2C), 130.5 (br, 2C, CB*C*C*C*BC), 131.4 (2C), 133.0 (br, 2C, *C*BCCCB*C*), 135.8 (2C), 137.5 (4C), 137.6 (2C), 138.9, 139.0 (2C); ^{11}B NMR (CS_2/CD_2Cl_2=2/1, 193 MHz) δ 36.5; Anal. calcd for $C_{36}H_{22}N_2B_2$ C, 85.76; H, 4.40; N, 5.56. found C, 85.85; H, 4.24; N, 5.66.

Synthesis of 4b,17b-diaza-9b,22b-diboratetrabenzo[*a*,*c*,*f*,*m*]phenanthro[9,10-*k*] tetraphene (4)

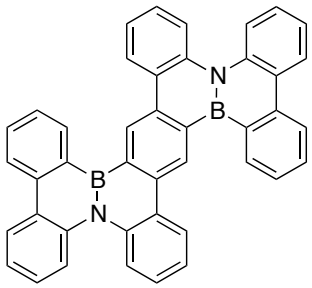

A solution of butyllithium in hexane (0.62 mL, 1.63 M, 1.0 mmol) was added slowly to a solution of **11** (0.977 g, 2.0 mmol) in toluene (20 mL) at –78 ºC under argon. After 1 h, the solution was allowed to warm to 0 ºC and stirred for 1 h, and then a solution of boron trichloride in heptane (1.00 mL, 1.00 M, 1.0 mmol) was added to reaction mixture at –78 ºC. After stirring at room temperature for 8 h, solvent was removed *in vacuo*, and the reaction mixture was added to a solution of aluminum trichloride (2.13 g, 16.0 mmol) and 2,2,6,6-tetramethylpiperidine (1.06 g, 7.5 mmol) in *o*-dichlorobenzene (20 mL) at 0 ºC. After stirring at 150 ºC for 12 h, 1,4-diazabicyclo[2.2.2]octane (1.79 g, 16.0 mmol) was added. The reaction mixture was filtered with a pad of Celite®. After the solvent was removed *in vacuo*, the crude product was purified by GPC (eluent:

toluene) to obtain the title compound (0.133 g, 23% yield) as white-yellow powder. IR (neat): cm^{-1} 3056 (Ar-H), 1600, 1574, 1487, 1432, 1390, 1309, 1292, 1264, 1164, 1051, 942, 893, 865, 745, 725, 701, 678, 663, 618, 558, 527, 499, 471; mp: 411.6–412.5 ºC; ^{1}H NMR (*o*-dichlorobenzene-d_4 at 100 ºC, 600 MHz) δ 7.25–7.31 (m, 8H), 7.66 (t, *J* = 7.2 Hz, 2H, BCCHC*H*), 7.73 (td, *J* = 1.2, 7.2 Hz, 2H, BCCHCHC*H*), 8.05–8.67 (m, 2H), 8.10 [d, *J* = 7.8 Hz, 2H, NCC*H*(edge)], 8.30 [dd, *J* = 1.8, 7.2 Hz, 2H, NCCC*H*(edge)], 8.36 (d, *J* = 7.8 Hz, 2H, BCCC*H*CH), 8.58 [t, *J* = 4.2 Hz, 2H, NCCC*H*(center)], 8.96 (d, *J* = 7.2 Hz, 2H, BCC*H*CH), 9.70 (s, 2H, BCC*H*C); ^{13}C NMR (*o*-dichlorobenzene-d_4 at 100 ºC, 151 MHz) δ 121.1 (2C), 122.2 (2C), 123.0 (4C), 123.3 (2C), 125.4 (2C), 125.6 (2C), 126.6 (2C), 126.8 (2C), 127.6 (2C), 127.9 (2C), 130.0 (2C), 131.0 (2C), 132.3 (broad, 2C), 134.8 (broad, 2C), 135.4 (2C), 136.8 (2C), 137.1 (2C), 137.2 (2C), 139.1 (2C); ^{11}B NMR (CS_2/C_6D_6=2/1, 126 MHz) δ 35.7; HRMS(FAB) *m/z* $[M]^+$ calcd for $C_{42}H_{24}N_2B_2$ 580.2282; observed 580.2296.

Crystallographic data collection and structure determination. Crystals of **1** and **2** were mounted on a Rigaku Saturn CCD diffractometer for data collection using graphite-monochromated Mo Kα radiation (λ = 0.71070 Å). Crystal data and data statistics are summarized in Figure 8. The structures were solved by direct methods with (SIR2008) [16] and refined by full-matrix least-squares techniques against F^2 (SHELXL-97)[17]. The non-hydrogen atoms were refined anisotropically. Hydrogen atoms were placed at calculated positions (C–H = 0.95 Å) and kept fixed. In the subsequent refinement, the function $\sum w(F_o^2 - F_c^2)^2$ was minimized, where $|F_o|$ and $|F_c|$ are the observed and calculated structure factor amplitudes, respectively. The agreement indices are defined as $R1 = \sum(||F_o| - |F_c||)/\sum|F_o|$ and $wR2 = [\sum w(F_o^2 - F_c^2)^2 / \sum(wF_o^4)]^{1/2}$. All calculations were performed by using Crystal Structure 4.0, and illustrations were drawn by using ORTEP–3.

[16] Burla, M. C.; Caliandro, R.; Camalli, M.; Carrozzini, B.; Cascarano, G. L.; de Caro, L.; Giacovazzo, C.; Polidori, G.; Siliqi, D.; Spagna, R. *J. Appl. Cryst.* **2007,** *40*, 609-613.
[17] Sheldrick, G. M. Program for the Solution of Crystal Structures; University of Göttingen, Germany, 1997.

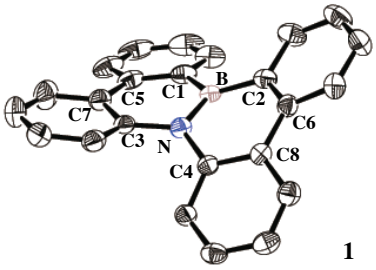

1

Selected bond lengths

B–N	1.426(3) Å	C1–B–C2	127.17(16)°
B–C1	1.535(3) Å	C1–B–N	116.23(16)°
B–C2	1.534(3) Å	C2–B–N	116.51(17)°
N–C3	1.442(3) Å	C3–N–C4	120.97(14)°
N–C4	1.448(3) Å	C3–N–B	120.01(16)°
		C4–N–B	119.00(15)°

Dihedral angle
C5–C7–C6–C8 38.87°

Formula	$C_{24}H_{16}BN$
Formula Weight	329.21
Temperature, K	173
Wavelength, Å	0.71070
Crystal System	Monoclinic
Space Group	$P\,2_1/n$ (No. 14)
a, Å	12.166(4)
b, Å	7.707(3)
c, Å	17.558(6)
α, deg	90
β, deg	97.316(6)
γ, deg	90
Volume, Å	1632.9(10)
Z	4
$Density_{calcd}$, g·cm^{-3}	1.339

Abs. Coefficient, cm^{-1}	0.076
F(000)	688.00
Crystal Size, mm^3	0.3, 0.15, 0.15
$2\theta_{min}$, $2\theta_{max}$, deg	6.1, 51.0
Index Ranges	–14≤h≤14
	–9≤k≤9
	–21≤l≤17
Reflections (unique)	3034
Reflections (I>2.0σ(I))	2232
Parameters	299
GOF on F^2	1.078
$R1$ (I>2.0σ(I))	0.0543
R, w$R2$ (all data)	0.0805, 0.1372
Largest diff peak and hole, e, Å^{-3}	0.23, –0.24

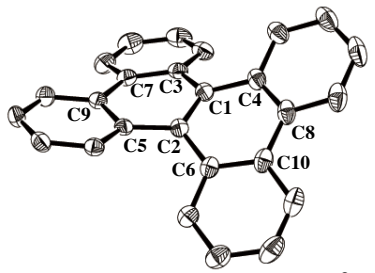

2

Selected bond lengths

C1–C2	1.3882(16) Å	C3–C1–C4	123.38(10)°
C1–C3	1.4621(17) Å	C2–C1–C3	118.46(11)°
C1–C4	1.4657(18) Å	C2–C1–C4	118.12(11)°
C2–C5	1.4608(19) Å	C5–C2–C6	122.32(10)°
C2–C6	1.4641(17) Å	C5–C2–C1	118.84(11)°
		C6–C2–C1	118.82(12)°

Dihedral angle
C7–C9–C8–C10 36.76°

Formula	$C_{26}H_{16}$
Formula Weight	328.41
Temperature, K	173
Wavelength, Å	0.71070
Crystal System	Monoclinic
Space Group	$P\,2_1/n$ (No. 14)
a, Å	12.169(3)
b, Å	7.6028(17)
c, Å	17.687(4)
α, deg	90
β, deg	97.532(4)
γ, deg	90
Volume, Å	1622.3(7)
Z	4
$Density_{calcd}$, g·cm^{-3}	1.345

Abs. Coefficient, cm^{-1}	0.076
F(000)	688.00
Crystal Size, mm^3	0.2, 0.2, 0.2
$2\theta_{min}$, $2\theta_{max}$, deg	6.1, 51.5
Index Ranges	–14≤h≤13
	–9≤k≤9
	–21≤l≤19
Reflections (unique)	3056
Reflections (I>2.0σ(I))	2367
Parameters	299
GOF on F^2	1.007
$R1$ (I>2.0σ(I))	0.0395
R, w$R2$ (all data)	0.0566, 0.0953
Largest diff peak and hole, e, Å^{-3}	0.160, –0.170

Figure 8. X-ray crystal structures of **1** and **2** (left), and crystal data and structure refinement (right). Thermal ellipsoids are shown at 50% probability and H atoms have been omitted for clarity.

Time-resolved microwave conductivity (TRMC) method. Nanosecond laser pulses from a Nd:YAG laser [Spectra Physics, INDY−HG, third harmonic generation (THG), 355 nm] with FWHM of 3-5 ns were used as excitation sources. The photon density of the laser was set at 1.8×10^{15} – 2.3×10^{16} photons cm^{-2}. A microwave frequency of 8.6–9.4 GHz was used for the TRMC measurement with a power of 3.0 mW in the microwave cavity, low enough to suppress the local heating of the materials loaded. The reflected microwave from the cavity was picked up by a diode (rise time < 1 ns), and monitored by a Tektronix TDS3032B digital oscilloscope. All the experiments were carried out at 25 ºC. Microcrystals of the samples were mounted on a quartz substrate in random orientation. The transient change in the reflected microwave power ($\Delta P_r(t) / P_r$) was converted directly into the transient photoconductivity ($\Delta\sigma$) as follows:[12]

$$\langle \Delta\sigma \rangle = \frac{1}{A}\frac{\Delta P_r}{P_r} \qquad (1)$$

$$\Delta\sigma = e \sum \mu \phi N \qquad (2)$$

where A, e, ϕ, N, and $\Sigma\mu$ are a sensitivity factor, elementary charge of electron, photo carrier generation yield (quantum efficiency), the number of absorbed photons per unit volume, and sum of mobilities for negative and positive carriers, respectively. The number of photons absorbed by the sample was estimated based on the power loss of incident laser pulses averaged over 200 shots. The values of ϕ in the compounds were determined by conventional photo-current measurement in a vacuum chamber (< 10^{-5} Pa) using an inter-digitated Au electrodes on a quartz substrate with 5 mm gap under excitation at 355 nm with the photon density of 4.1×10^{16} photons/cm^2. Samples were deposited onto the substrates in a vacuum chamber (~ 10^{-6} Pa) at 80 ~ 12 nm thick. Transient current was predominantly observed under the applied bias of 0 – 2 V (~ 0 – 4.0×10^3 V cm^{-1}), and monitored by a Keithley 2612 source meter. The other details of the set of apparatus were described elsewhere.[18]

[18] (a) Seki, S.; Yoshida, Y.; Tagawa, S.; Asai, K.; Ishigure, K.; Furukawa, K.; Fujiki, M.; Matsumoto, N. *Philos. Mag. B* **1999,** *79*, 1631–1645. (b) Sato, S.; Seki, S.; Honsho, Y.; Wang, L.; Nikawa, H.; Luo, G.; Lu, J.; Haranaka, M.; Tsuchiya, T.; Nagase, S.; Akasaka, T. *J. Am. Chem. Soc.* **2011,** *133*, 2766–2771.

Computational studies. Molecular orbital calculations and nucleus-independent chemical shift (NICS) calculations were performed with Gaussian 03[19] and 09[20] packages. The DFT method was employed using the B3LYP hybrid functional.[21] Structures were optimized with the 6-31G(d) basis set.[22] Nucleus independent chemical shifts (NICS) were evaluated by using the gauge invariant atomic orbital[23] (GIAO) approach at the GIAO-B3LYP/6-31G(d) level. The reorganization energy calculations were performed using the B3LYP hybrid functional with the DZP basis set[24] in the ADF program.[25] The electronic coupling calculations of dimers were performed by the local density functional VWN in the conjunction with the PW91[26] gradient corrections with the DZP basis set, as implemented in the ADF program according to the literature.[13]

---

[19] Gaussian 03, Revision E.01, Frisch, M. J.; Trucks, G. W.; Schlegel, H. B.; Scuseria, G. E.; Robb, M. A.; Cheeseman, J. R.; Montgomery, Jr., J. A.; Vreven, T.; Kudin, K. N.; Burant, J. C.; Millam, J. M.; Iyengar, S. S.; Tomasi, J.; Barone, V.; Mennucci, B.; Cossi, M.; Scalmani, G.; Rega, N.; Petersson, G. A.; Nakatsuji, H.; Hada, M.; Ehara, M.; Toyota, K.; Fukuda, R.; Hasegawa, J.; Ishida, M.; Nakajima, T.; Honda, Y.; Kitao, O.; Nakai, H.; Klene, M.; Li, X.; Knox, J. E.; Hratchian, H. P.; Cross, J. B.; Bakken, V.; Adamo, C.; Jaramillo, J.; Gomperts, R.; Stratmann, R. E.; Yazyev, O.; Austin, A. J.; Cammi, R.; Pomelli, C.; Ochterski, J. W.; Ayala, P. Y.; Morokuma, K.; Voth, G. A.; Salvador, P.; Dannenberg, J. J.; Zakrzewski, V. G.; Dapprich, S.; Daniels, A. D.; Strain, M. C.; Farkas, O.; Malick, D. K.; Rabuck, A. D.; Raghavachari, K.; Foresman, J. B.; Ortiz, J. V.; Cui, Q.; Baboul, A. G.; Clifford, S.; Cioslowski, J.; Stefanov, B. B.; Liu, G.; Liashenko, A.; Piskorz, P.; Komaromi, I.; Martin, R. L.; Fox, D. J.; Keith, T.; Al-Laham, M. A.; Peng, C. Y.; Nanayakkara, A.; Challacombe, M.; Gill, P. M. W.; Johnson, B.; Chen, W.; Wong, M. W.; Gonzalez, C. and Pople, J. A. Gaussian, Inc., Wallingford CT, 2004.

[20] Gaussian 09, Revision B.01, Frisch, M. J.; Trucks, G. W.; Schlegel, H. B.; Scuseria, G. E.; Robb, M. A.; Cheeseman, J. R.; Scalmani, G.; Barone, V.; Mennucci, B.; Petersson, G. A.; Nakatsuji, H.; Caricato, M.; Li, X.; Hratchian, H. P.; Izmaylov, A. F.; Bloino, J.; Zheng, G.; Sonnenberg, J. L.; Hada, M.; Ehara, M.; Toyota, K.; Fukuda, R.; Hasegawa, J.; Ishida, M.; Nakajima, T.; Honda, Y.; Kitao, O.; Nakai, H.; Vreven, T.; Montgomery, Jr., J. A.; Peralta, J. E.; Ogliaro, F.; Bearpark, M.; Heyd, J. J.; Brothers, E.; Kudin, K. N.; Staroverov, V. N.; Kobayashi, R.; Normand, J.; Raghavachari, K.; Rendell, A.; Burant, J. C.; Iyengar, S. S.; Tomasi, J.; Cossi, M.; Rega, N.; Millam, N. J.; Klene, M.; Knox, J. E.; Cross, J. B.; Bakken, V.; Adamo, C.; Jaramillo, J.; Gomperts, R.; Stratmann, R. E.; Yazyev, O.; Austin, A. J.; Cammi, R.; Pomelli, C.; Ochterski, J. W.; Martin, R. L.; Morokuma, K.; Zakrzewski, V. G.; Voth, G. A.; Salvador, P.; Dannenberg, J. J.; Dapprich, S.; Daniels, A. D.; Farkas, Ö.; Foresman, J. B.; Ortiz, J. V.; Cioslowski, J.; Fox, D. J. Gaussian, Inc., Wallingford CT, 2009.

[21] (a) Becke, A. D. *J. Chem. Phys.* **1993,** *98*, 5648–5652. (b) Lee, C.; Yang, W.; Parr, R. G. *Phys. Rev. B* **1988,** *37*, 785–789.

[22] Hehre, W. J.; Radom, L.; Schleyer, P. v. R.; Pople, J. A. *Ab Initio Molecular Orbital Theory*; John Wiley & Sons: New York, **1986** and references cited therein.

[23] (a) Dichtfield, R. *Mol. Phys.* **1974,** *27*, 789–807. (b) Wolinski, K.; Hinton, J. F.; Pulay, P. *J. Am. Chem. Soc.* **1990,** *112*, 8251–8260.

[24] van Lenthe, E.; Baerends, E. J. *J. Comput. Chem.* **2003,** *24*, 1142–1156.

[25] ADF2010, SCM, Theoretical Chemistry, Vrije Universiteit, Amsterdam, The Netherlands.

[26] Perdew, J. P.; Chevary, J. A.; Vosko, S. H.; Jackson, K. A.; Pederson, M. R.; Sing, D. J.; Fiolhais, C. *Phys. Rev. B* **1992,** *46*, 6671–6687.

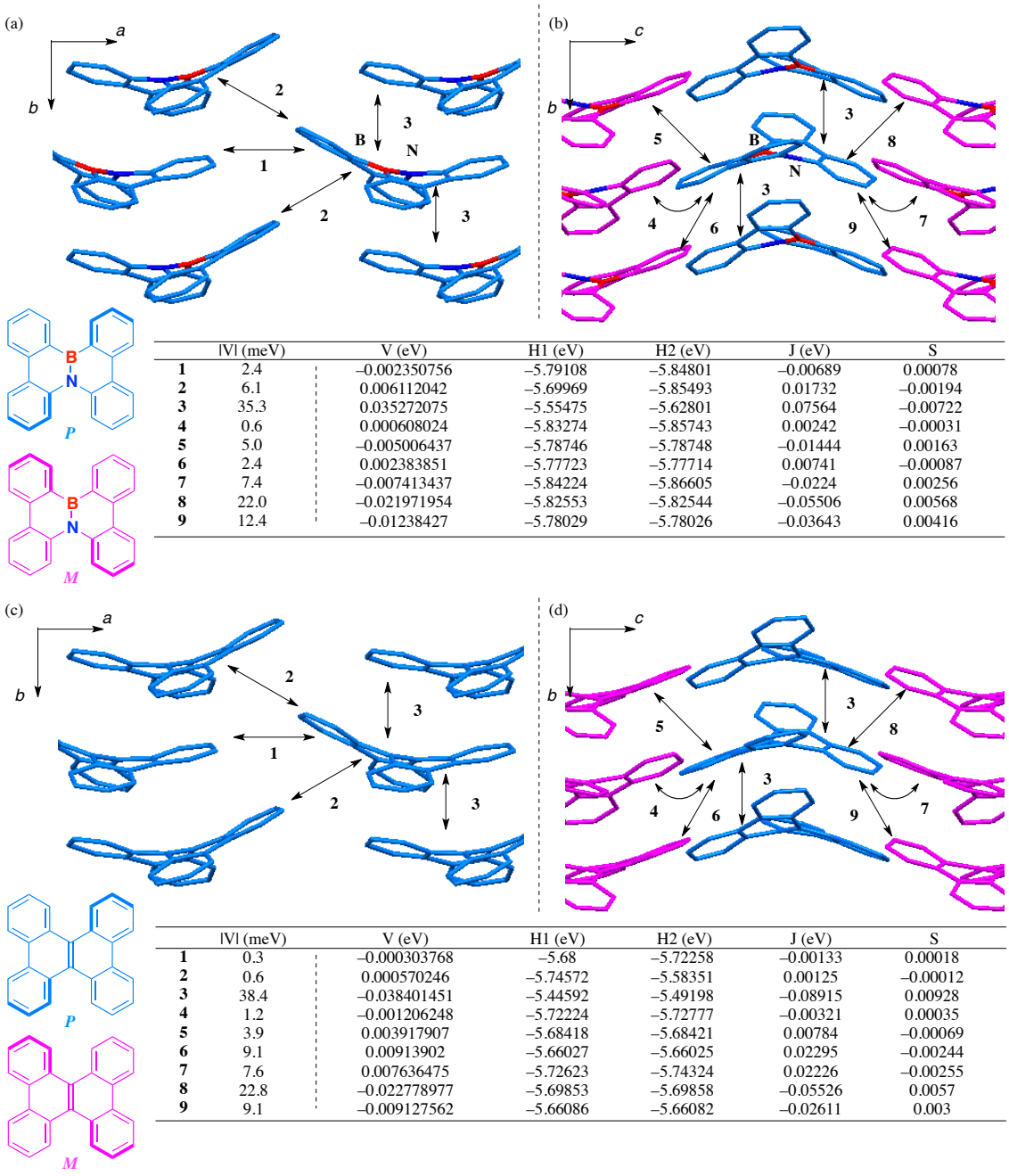

	|V| (meV)	V (eV)	H1 (eV)	H2 (eV)	J (eV)	S
1	2.4	–0.002350756	–5.79108	–5.84801	–0.00689	0.00078
2	6.1	0.006112042	–5.69969	–5.85493	0.01732	–0.00194
3	35.3	0.035272075	–5.55475	–5.62801	0.07564	–0.00722
4	0.6	0.000608024	–5.83274	–5.85743	0.00242	–0.00031
5	5.0	–0.005006437	–5.78746	–5.78748	–0.01444	0.00163
6	2.4	0.002383851	–5.77723	–5.77714	0.00741	–0.00087
7	7.4	–0.007413437	–5.84224	–5.86605	–0.0224	0.00256
8	22.0	–0.021971954	–5.82553	–5.82544	–0.05506	0.00568
9	12.4	–0.01238427	–5.78029	–5.78026	–0.03643	0.00416

	|V| (meV)	V (eV)	H1 (eV)	H2 (eV)	J (eV)	S
1	0.3	–0.000303768	–5.68	–5.72258	–0.00133	0.00018
2	0.6	0.000570246	–5.74572	–5.58351	0.00125	–0.00012
3	38.4	–0.038401451	–5.44592	–5.49198	–0.08915	0.00928
4	1.2	–0.001206248	–5.72224	–5.72777	–0.00321	0.00035
5	3.9	0.003917907	–5.68418	–5.68421	0.00784	–0.00069
6	9.1	0.00913902	–5.66027	–5.66025	0.02295	–0.00244
7	7.6	0.007636475	–5.72623	–5.74324	0.02226	–0.00255
8	22.8	–0.022778977	–5.69853	–5.69858	–0.05526	0.0057
9	9.1	–0.009127562	–5.66086	–5.66082	–0.02611	0.003

Figure 9. Electron couplings *V* (meV) between neighboring molecules in the X-ray crystal structures of **1** (a, b) and **2** (c, d) at the PW91/DZP level on ADF2010 program. H atoms have been omitted for clarity. The *P*-enantiomer is shown in blue and *M*-enantiomer is shown in pink. *V* (eV) = [J – 0.5S(H1 + H2)]/(1 – S^2), J (eV): charge transfer integral, H1 and H2 (eV): site energies, S: overlap integral.

	1	**2**
E	–321.82132	–323.88293
E*	–321.69273	–323.75055
E+	–314.54316	–316.78809
E+*	–314.45634	–316.71635
λ	0.21541	0.20413

Figure 10. Cohesive energies (eV) for neutral energy in neutral geometry (E), neutral energy in cation geometry (E*), cation energy in neutral geometry (E+), cation energy in cation geometry (E+*), and reorganization energies λ (eV) of **1** and **2** at the B3LYP/DZP level on ADF2010 program. λ = (E*–E)+(E+*–E+).

Cartesian coordinates

Cartesian coordinates for reorganization energy

1 (neutral geometry)

Center Number			Atomic Number	Atomic Type	Coordinates X	Y	Z
1	7	0	0.000026	-0.634416	0.000127		
2	5	0	-0.000010	0.801018	0.000331		
3	6	0	-1.357792	1.462781	-0.307026		
4	6	0	-2.520136	0.661902	-0.257730		
5	6	0	-2.418498	-0.686961	0.303873		
6	6	0	-1.161584	-1.317696	0.416104		
7	6	0	1.161397	-1.317716	-0.416184		
8	6	0	2.418356	-0.686846	-0.304620		
9	6	0	2.520173	0.661991	0.256916		
10	6	0	1.357765	1.462726	0.307430		
11	6	0	-1.459522	2.757571	-0.836771		
12	6	0	-3.729418	1.174938	-0.741740		
13	6	0	-3.539796	-1.361890	0.804706		
14	6	0	-1.064826	-2.555181	1.061119		
15	6	0	1.064659	-2.555696	-1.060310		
16	6	0	3.539528	-1.361854	-0.805593		
17	6	0	3.729714	1.175015	0.740362		
18	6	0	1.459635	2.757214	0.837889		
19	6	0	-2.663661	3.259786	-1.293946		
20	6	0	-3.802578	2.459556	-1.246001		
21	6	0	-3.441957	-2.603566	1.397916		
22	6	0	-2.190040	-3.196621	1.537431		
23	6	0	2.189834	-3.197346	-1.536435		
24	6	0	3.441700	-2.603953	-1.397940		
25	6	0	3.802975	2.459301	1.245391		
26	6	0	2.663950	3.259338	1.294603		
27	1	0	-0.572058	3.365108	-0.929492		
28	1	0	-4.614147	0.557976	-0.758205		
29	1	0	-4.503322	-0.879323	0.763502		
30	1	0	-0.093017	-2.997902	1.212390		
31	1	0	0.092936	-2.998712	-1.211130		
32	1	0	4.502993	-0.879095	-0.765197		
33	1	0	4.614670	0.558337	0.755708		
34	1	0	0.572086	3.364476	0.931694		
35	1	0	-2.715869	4.256708	-1.707520		
36	1	0	-4.744141	2.833738	-1.622570		
37	1	0	-4.326120	-3.091635	1.781044		
38	1	0	-2.087402	-4.145488	2.043954		
39	1	0	2.087102	-4.146607	-2.042205		
40	1	0	4.325797	-3.092018	-1.781238		
41	1	0	4.744750	2.833433	1.621466		
42	1	0	2.716340	4.256077	1.708595		

1 (cation geometry)

Center Number			Atomic Number	Atomic Type	Coordinates X	Y	Z
1	7	0	0.000111	-0.653423	-0.000348		
2	5	0	-0.000195	0.830046	-0.000216		
3	6	0	-1.343667	1.459578	-0.359702		
4	6	0	-2.505119	0.662520	-0.266070		
5	6	0	-2.396175	-0.658311	0.359243		
6	6	0	-1.131630	-1.309940	0.453654		
7	6	0	1.132066	-1.309427	-0.454283		
8	6	0	2.396430	-0.657372	-0.359525		
9	6	0	2.504766	0.663414	0.265887		
10	6	0	1.342997	1.460020	0.359570		
11	6	0	-1.439871	2.733398	-0.929193		
12	6	0	-3.714816	1.152403	-0.755182		

13	6	0	-3.496701	-1.323018	0.892031
14	6	0	-1.015331	-2.556438	1.101263
15	6	0	1.016445	-2.556050	-1.101808
16	6	0	3.497355	-1.321835	-0.891836
17	6	0	3.714205	1.153676	0.755290
18	6	0	1.438589	2.733623	0.929597
19	6	0	-2.653038	3.217160	-1.398901
20	6	0	-3.786415	2.421775	-1.313811
21	6	0	-3.377625	-2.566203	1.493428
22	6	0	-2.128371	-3.179900	1.608782
23	6	0	2.129887	-3.179431	-1.608437
24	6	0	3.378939	-2.565314	-1.492747
25	6	0	3.785352	2.423156	1.313699
26	6	0	2.651607	3.217979	1.399072
27	1	0	-0.551914	3.336038	-1.048937
28	1	0	-4.604617	0.542996	-0.734835
29	1	0	-4.464422	-0.848191	0.870695
30	1	0	-0.035421	-2.982964	1.251304
31	1	0	0.036785	-2.983253	-1.251584
32	1	0	4.465000	-0.846893	-0.869879
33	1	0	4.604258	0.544649	0.734935
34	1	0	0.550435	3.336055	1.049002
35	1	0	-2.708325	4.196874	-1.850356
36	1	0	-4.730059	2.781083	-1.698345
37	1	0	-4.253812	-3.043304	1.908017
38	1	0	-2.029397	-4.120089	2.130593
39	1	0	2.031521	-4.120160	-2.129393
40	1	0	4.255516	-3.042512	-1.906411
41	1	0	4.728841	2.782820	1.698263
42	1	0	2.706554	4.197802	1.850322

13	6	0	-2.390297	3.256749	-1.346210
14	6	0	-3.633112	1.305839	-0.713269
15	6	0	-1.228081	-2.660864	0.909042
16	6	0	-3.606532	2.580292	-1.234793
17	6	0	-3.632762	-1.306210	0.713598
18	6	0	-2.389488	-3.257084	1.345853
19	6	0	1.228418	-2.660846	-0.908839
20	6	0	3.606130	-2.580387	-1.234941
21	6	0	3.632889	-1.305731	-0.713962
22	6	0	2.389907	3.256760	1.346558
23	6	0	2.389911	-3.256989	-1.345544
24	6	0	-3.605830	-2.580735	1.234913
25	6	0	3.632979	1.306214	0.712993
26	6	0	3.606242	2.580546	1.234759
27	1	0	-0.288981	3.164641	-1.066561
28	1	0	0.288544	3.164374	1.067088
29	1	0	-2.351448	4.234708	-1.804282
30	1	0	-4.567963	0.768402	-0.695658
31	1	0	-0.288266	-3.164801	1.065246
32	1	0	-4.518956	3.037532	-1.589800
33	1	0	-4.567725	-0.768977	0.696175
34	1	0	-2.350395	-4.235172	1.803631
35	1	0	0.288692	-3.165056	-1.064635
36	1	0	4.518491	-3.037903	-1.589725
37	1	0	4.567823	-0.768442	-0.696537
38	1	0	2.350977	4.234632	1.804788
39	1	0	2.351010	-4.235338	-1.802774
40	1	0	-4.518109	-3.038202	1.589977
41	1	0	4.567889	0.768888	0.695284
42	1	0	4.518626	3.037840	1.589755

2 (neutral geometry)

Center Number	Atomic Number	Atomic Type	Coordinates X	Y	Z
1	6	0	-2.464189	0.677636	-0.258575
2	6	0	-1.236069	1.376803	-0.332156
3	6	0	1.235887	1.376918	0.332160
4	6	0	0.000044	-0.692135	-0.000059
5	6	0	-1.228690	2.660779	-0.909579
6	6	0	-0.000053	0.692495	-0.000019
7	6	0	-2.464036	-0.677711	0.258816
8	6	0	2.464107	0.677947	0.258293
9	6	0	-1.235807	-1.376664	0.332173
10	6	0	1.228342	2.660722	0.909915
11	6	0	2.464098	-0.677362	-0.259165
12	6	0	1.235958	-1.376505	-0.332287

2 (cation geometry)

Center Number	Atomic Number	Atomic Type	Coordinates X	Y	Z
1	6	0	-2.441873	-0.668284	0.294118
2	6	0	-1.212808	-1.373311	0.380666
3	6	0	1.213613	-1.372691	-0.381139
4	6	0	-0.000188	0.710950	-0.000405
5	6	0	-1.187211	-2.644801	0.989638
6	6	0	0.000177	-0.713222	-0.000408
7	6	0	-2.441640	0.665284	-0.297984
8	6	0	2.442260	-0.666946	-0.294510
9	6	0	-1.212915	1.371009	-0.381454
10	6	0	1.188869	-2.644397	-0.989682
11	6	0	2.441245	0.666657	0.297491
12	6	0	1.212123	1.371678	0.380865

13	6	0	-2.345537	-3.223844	1.460475
14	6	0	-3.594961	-1.275139	0.780285
15	6	0	-1.186947	2.645098	-0.984749
16	6	0	-3.553596	-2.541827	1.345500
17	6	0	-3.594230	1.272935	-0.784296
18	6	0	-2.344737	3.224705	-1.456200
19	6	0	1.185307	2.645558	0.984542
20	6	0	3.550789	2.542855	1.346433
21	6	0	3.593407	1.274813	0.784199
22	6	0	2.347633	-3.222912	-1.460100
23	6	0	2.342622	3.225504	1.456780
24	6	0	-3.552463	2.541211	-1.346084
25	6	0	3.595818	-1.273347	-0.780102
26	6	0	3.555286	-2.540191	-1.345010
27	1	0	-0.241113	-3.136117	1.151907
28	1	0	0.243108	-3.136382	-1.151922
29	1	0	-2.308412	-4.187154	1.947254
30	1	0	-4.535275	-0.747788	0.756810
31	1	0	-0.240962	3.138777	-1.140928
32	1	0	-4.462062	-2.982962	1.729693
33	1	0	-4.534665	0.745744	-0.762328
34	1	0	-2.307563	4.190145	-1.938768
35	1	0	0.238942	3.138300	1.141336
36	1	0	4.458522	2.985012	1.731131
37	1	0	4.533970	0.747807	0.763052
38	1	0	2.311194	-4.186460	-1.946457
39	1	0	2.304654	4.190368	1.940434
40	1	0	-4.460663	2.983326	-1.729702
41	1	0	4.535938	-0.745657	-0.756145
42	1	0	4.464128	-2.981029	-1.728585

Cartesian coordinates at stationary points

1

E(RB3LYP) = –1003.87184967 hartree

Center Number	Atomic Number	Atomic Type	Coordinates X	Y	Z
1	5	0	0.006012	0.733139	-0.074722
2	7	0	0.009964	-0.697388	0.139328
3	6	0	-3.574417	-2.546158	1.436569
4	6	0	-3.614044	-1.374252	0.695816
5	6	0	-2.335281	-3.104980	1.763977
6	6	0	-1.164337	-2.503235	1.324295
7	6	0	-1.194351	-1.340088	0.531067
8	6	0	-2.445602	-0.737854	0.231354
9	6	0	-2.505569	0.538330	-0.496643
10	6	0	1.218323	-1.419937	-0.048325
11	6	0	-3.691666	0.993103	-1.105057
12	6	0	-1.331909	1.334763	-0.572647
13	6	0	-3.731827	2.215500	-1.763840
14	6	0	1.195404	-2.764359	-0.466797
15	6	0	-2.581177	3.008179	-1.847656
16	6	0	2.370041	-3.461914	-0.712021
17	6	0	-1.401016	2.562256	-1.264587
18	6	0	3.605820	-2.824966	-0.563278
19	6	0	3.638321	-1.487549	-0.197586
20	6	0	2.465958	-0.749542	0.061340
21	6	0	2.518295	0.684036	0.384094
22	6	0	3.701233	1.303238	0.832291
23	6	0	3.734161	2.665161	1.104492
24	6	0	2.579315	3.441528	0.952942
25	6	0	1.402176	2.838120	0.526428
26	6	0	1.340317	1.461487	0.224136
27	1	0	-4.496597	-3.003250	1.783646
28	1	0	-4.575516	-0.911438	0.501007
29	1	0	-2.278214	-3.996246	2.382751
30	1	0	-0.208878	-2.919403	1.619507
31	1	0	-4.584671	0.376511	-1.090668
32	1	0	-4.656433	2.544327	-2.231369
33	1	0	0.242477	-3.253830	-0.626694
34	1	0	-2.605972	3.954926	-2.380585
35	1	0	2.318390	-4.495453	-1.043243
36	1	0	-0.501266	3.158188	-1.378967
37	1	0	4.530746	-3.358505	-0.762115
38	1	0	4.597046	-0.982651	-0.147232
39	1	0	4.597366	0.714371	0.998764
40	1	0	4.656433	3.121506	1.454987
41	1	0	2.598465	4.502884	1.185318
42	1	0	0.499207	3.436646	0.461670
43	0	0	-1.243561	-0.028183	-0.040390
44	0	0	-1.311493	0.388596	0.865936
45	0	0	-1.175583	-0.444977	-0.946700
46	0	0	1.259796	0.001953	0.114334
47	0	0	1.193298	-0.131760	1.102890
48	0	0	1.326294	0.135666	-0.874344
49	0	0	-2.540497	1.775375	-1.175079
50	0	0	-2.796051	2.235214	-0.324707
51	0	0	-2.285049	1.315400	-2.025497
52	0	0	2.545883	2.065613	0.670700
53	0	0	2.291779	1.873428	1.618637
54	0	0	2.800049	2.257767	-0.277069

55	0	0	-2.388031	-1.934433	0.997177
56	0	0	-2.352081	-1.383606	1.831024
57	0	0	-2.423965	-2.485245	0.163422
58	0	0	2.415634	-2.118027	-0.321091
59	0	0	2.453796	-2.400742	0.637238
60	0	0	2.377487	-1.835297	-1.279495

2

E(RB3LYP) = –1000.42954691 hartree

Center Number	Atomic Number	Atomic Type	Coordinates X	Y	Z
1	6	0	0.000000	0.697144	-0.048752
2	6	0	0.000000	-0.697144	0.048752
3	1	0	-2.234100	-4.181015	2.176651
4	6	0	-2.305756	-3.212189	1.689941
5	1	0	-0.221451	-3.137253	1.257446
6	6	0	-1.172119	-2.630280	1.148773
7	6	0	-3.592896	-1.272095	1.076126
8	6	0	-1.213791	-1.359375	0.523117
9	6	0	-3.532974	-2.535324	1.638718
10	6	0	-2.451767	-0.654739	0.520248
11	1	0	-4.425491	-2.982208	2.067963
12	1	0	-4.650253	0.795059	-0.217575
13	1	0	-4.533981	-0.733383	1.099762
14	6	0	-1.272964	1.376083	-0.284256
15	6	0	-1.334229	2.647110	-0.908035
16	6	0	-2.497025	0.687988	-0.044922
17	6	0	-2.542297	3.244751	-1.224243
18	1	0	-0.414963	3.141525	-1.196304
19	1	0	-2.551727	4.213165	-1.716965
20	6	0	-3.746231	2.584213	-0.939529
21	1	0	-4.698105	3.043488	-1.191589
22	6	0	-3.714783	1.321182	-0.374191
23	6	0	1.272964	1.402237	0.089981
24	6	0	3.746231	2.689804	0.570755
25	6	0	2.497025	0.687531	-0.051270
26	6	0	1.334244	2.747726	0.530807
27	6	0	2.542297	3.383545	0.760773
28	6	0	3.714798	1.360397	0.186707
29	1	0	0.414963	3.277451	0.747467
30	1	0	2.551712	4.411102	1.113937
31	1	0	4.650238	0.817612	0.104828
32	1	0	4.698120	3.179688	0.756439
33	6	0	1.213791	-1.418945	-0.328842
34	6	0	3.532974	-2.738693	-1.269943
35	6	0	1.172134	-2.764557	-0.771545
36	6	0	2.451767	-0.720779	-0.424057
37	6	0	3.592911	-1.409485	-0.888641
38	6	0	2.305756	-3.416107	-1.226471
39	1	0	0.221451	-3.281723	-0.808609
40	1	0	4.533966	-0.879288	-0.987015
41	1	0	2.234085	-4.443253	-1.573624
42	1	0	4.425507	-3.240967	-1.632813
43	0	0	-1.239258	0.008316	0.119034
44	0	0	-1.146536	0.328059	1.061994
45	0	0	-1.331980	-0.311407	-0.823926
46	0	0	1.239258	-0.008316	-0.119034
47	0	0	1.331979	-0.193713	0.859247
48	0	0	1.146537	0.177061	-1.097315
49	0	0	-2.517914	1.976868	-0.629181
50	0	0	-2.547045	2.402184	0.275394
51	0	0	-2.488794	1.551592	-1.533776
52	0	0	2.517914	2.045197	0.347961
53	0	0	2.488798	1.749934	1.302920
54	0	0	2.547051	2.340480	-0.607018
55	0	0	-2.378204	-1.943985	1.099472
56	0	0	-2.171788	-1.520279	1.981444
57	0	0	-2.584641	-2.367722	0.217530
58	0	0	2.378220	-2.078079	-0.818253
59	0	0	2.584650	-2.374959	0.114093
60	0	0	2.171790	-1.781230	-1.750588

3

E(RB3LYP) = –1544.44868597 hartree

Center Number	Atomic Number	Atomic Type	Coordinates X	Y	Z
1	5	0	-2.536026	0.629532	0.008957
2	7	0	-2.442719	-0.758300	0.405350
3	6	0	-5.856506	-2.539932	2.180923
4	6	0	-5.994705	-1.498749	1.275223
5	6	0	-4.574417	-2.982040	2.520355
6	6	0	-3.460419	-2.404205	1.927063
7	6	0	-3.591125	-1.384171	0.965042
8	6	0	-4.886108	-0.888916	0.654877
9	6	0	-5.051117	0.269562	-0.236130
10	6	0	-1.217224	-1.455643	0.237915
11	6	0	-6.287521	0.583420	-0.832230
12	6	0	-3.927704	1.103928	-0.477112
13	6	0	-6.425629	1.708679	-1.635544
14	6	0	-1.205124	-2.846954	0.070328
15	6	0	-5.326431	2.540680	-1.877975
16	6	0	0.000351	-3.521667	-0.078430

17	6	0	-4.096436	2.229752	-1.309800	56	1	0	5.429428	2.943390	3.418625
18	6	0	1.205627	-2.831894	-0.119858	57	1	0	7.388031	1.548248	2.761810
19	6	0	1.217636	-1.431473	-0.067581	58	1	0	7.144028	-0.206802	1.067856
20	5	0	2.536316	0.592285	0.484665	59	1	0	2.471634	-2.374527	-2.232178
21	7	0	2.443024	-0.716476	-0.123962	60	1	0	4.439240	-3.234695	-3.418625
22	6	0	0.000153	-0.719635	0.142090	61	1	0	6.735229	-2.560150	-2.682907
23	6	0	0.000153	0.729523	0.256180	62	1	0	6.987793	-0.963165	-0.834396
24	6	0	1.223831	1.407318	0.504379	63	0	0	-3.739136	-0.171371	0.220154
25	6	0	1.193024	2.810013	0.593140	64	0	0	-3.776123	0.363556	1.064224
26	6	0	0.000046	3.521300	0.475983	65	0	0	-3.702103	-0.706360	-0.623871
27	6	0	-1.192825	2.837082	0.248900	66	0	0	-1.236526	-0.022766	0.194565
28	6	0	3.927933	0.984665	1.039200	67	0	0	-1.226563	-0.021194	1.194534
29	6	0	-1.223618	1.437820	0.117020	68	0	0	-1.246506	-0.024368	-0.805344
30	6	0	4.096527	1.966431	2.037796	69	0	0	1.236847	-0.023056	0.199280
31	6	0	5.326431	2.184555	2.647583	70	0	0	1.246857	-0.181061	1.186676
32	6	0	6.425735	1.400742	2.278229	71	0	0	1.226852	0.134903	-0.788055
33	6	0	6.287735	0.414856	1.308700	72	0	0	3.739410	-0.165802	0.150925
34	6	0	5.051346	0.198257	0.670837	73	0	0	3.702271	-0.826263	0.900864
35	6	0	4.886429	-0.806519	-0.390564	74	0	0	3.776566	0.494614	-0.599000
36	6	0	3.591507	-1.247131	-0.774582	75	0	0	-5.185791	1.405991	-1.061478
37	6	0	3.460922	-2.104111	-1.884247	76	0	0	-5.425827	1.956894	-0.262146
38	6	0	4.574936	-2.582108	-2.560608	77	0	0	-4.945755	0.855103	-1.860764
39	6	0	5.857025	-2.198563	-2.155945	78	0	0	0.000092	2.123856	0.365921
40	6	0	5.995132	-1.311813	-1.098480	79	0	0	-0.149994	2.042267	1.351227
41	1	0	-6.734619	-2.979584	2.644821	80	0	0	0.150192	2.205429	-0.619324
42	1	0	-6.987411	-1.113083	1.069046	81	0	0	5.185944	1.191574	1.663712
43	1	0	-4.438629	-3.760849	3.265762	82	0	0	4.945816	0.522461	2.367004
44	1	0	-2.471130	-2.725723	2.228271	83	0	0	5.426071	1.860703	0.960403
45	1	0	-7.143845	-0.068451	-0.691452	84	0	0	-4.727188	-1.949661	1.587250
46	1	0	-7.388031	1.930038	-2.090042	85	0	0	-4.679947	-1.274429	2.323318
47	1	0	-2.135818	-3.398956	0.057266	86	0	0	-4.774460	-2.624893	0.851166
48	1	0	-5.429428	3.410721	-2.520798	87	0	0	0.000229	-2.134552	0.030716
49	1	0	0.000351	-4.604828	-0.163712	88	0	0	0.102234	-2.199280	1.023407
50	1	0	-3.236725	2.849182	-1.544922	89	0	0	-0.101761	-2.069839	-0.961914
51	1	0	2.136429	-3.379013	-0.193329	90	0	0	4.727646	-1.708374	-1.477402
52	1	0	2.121048	3.356232	0.731613	91	0	0	4.774780	-2.490448	-0.855988
53	1	0	0.000046	4.604828	0.561279	92	0	0	4.680542	-0.926300	-2.098816
54	1	0	-2.120926	3.398148	0.197678	---					
55	1	0	3.236832	2.541504	2.366623						

Chapter 2

Synthesis of BN-fused Helical π-Conjugated Molecules

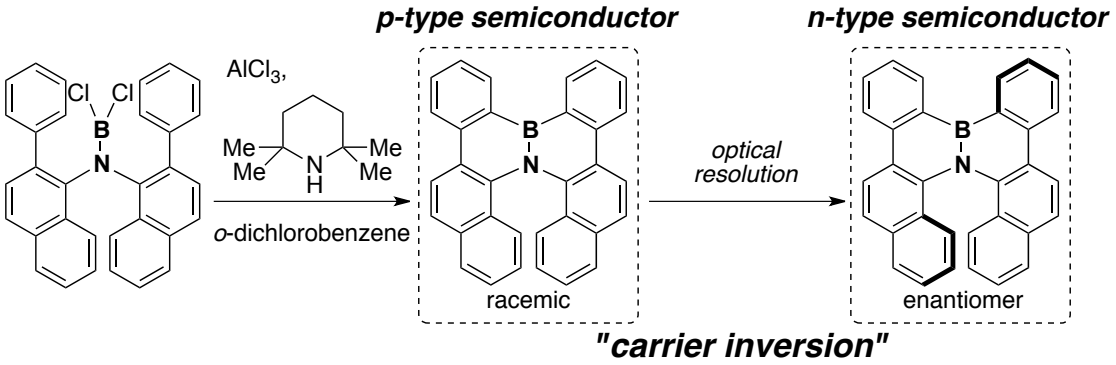

Abstract: Azaboradibenzo[6]helicene, a new semiconductor material possessing helical chirality, has been synthesized *via* a tandem bora-Friedel–Crafts reaction. The solution- and solid-phase structures of azaboradibenzo[6]helicene were characterized and its optical isomers were resolved. Thin films were prepared from the racemate and a single enantiomer, and investigated for their electronic properties. Unprecedented carrier inversion was observed between the racemate (displaying p-type semiconductivity) and the single enantiomer (displaying n-type semiconductivity), which can be explained by changes in the molecular packing induced by helical homochirality.

Chapter 2

2-1. Introduction

Helicenes, nonplanar screw-shaped polycyclic aromatic compounds consisting of *ortho*-fused aromatic rings, have attracted considerable attention because of their inherent chirality.[1] Recently, the self-assembly of helicenes *via* unique π–π stacking interactions in solution, as well as in crystals, has been studied extensively because these aggregates display intriguing properties such as liquid crystallinity,[2] nonlinear optical susceptibility,[3] and circularly polarized luminescence.[4] So far, however, the electrical properties (such as charge mobility) of these aggregates have not been thoroughly investigated, even though the π–π stacking interactions are expected to facilitate charge transport. This author envisioned that the tandem intramolecular bora-Friedel–Crafts reaction described in Chapter 1 would be an efficient method for the construction of helical π-conjugated frameworks containing a B–N ring fusion (Scheme 1).

Scheme 1. Synthesis of helical BN-fused polycyclic aromatic compounds *via* a tandem intramolecular bora-Friedel–Crafts reaction

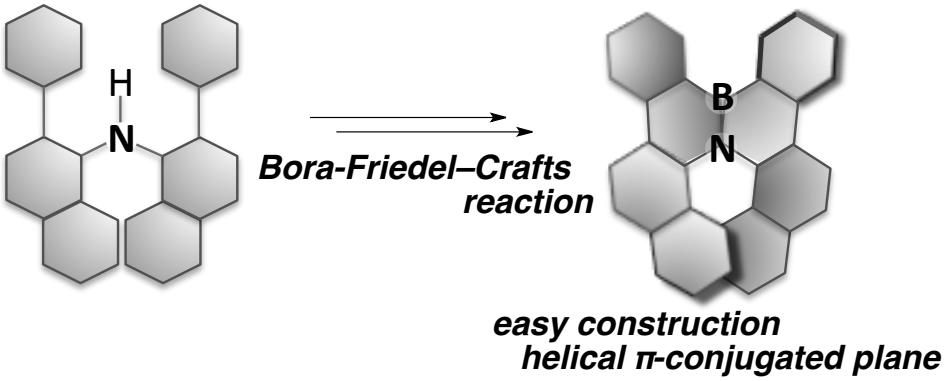

This chapter describes the synthesis of azaboradibenzo[6]helicene **1** *via* a tandem bora-Friedel–Crafts reaction. Determination of the solution- and solid-phase

---

[1] Recent reviews: (a) Starý, I.; Stará, I. G.; Alexandrová, Z.; Sehnal, P.; Teplý, F.; Šaman, D.; Rulíšek L. *Pure Appl. Chem.* **2006,** *78*, 495–499. (b) Collins, S. K.; Vachon, M. P. *Org. Biomol. Chem.* **2006,** *4*, 2518–2524. (c) Rajca, A.; Rajca, S.; Pink, M.; Miyasaka, M. *Synlett* **2007,** 1799–1822. (d) Amemiya, R.; Yamaguchi, M. *Chem. Rec.* **2008,** *8*, 116–127. (e) Dumitrascu, F.; Dumitrescu, D. G.; Aron, I. *ARKIVOC* **2010,** 1–32. (f) Jørgensen, K. B. *Molecules* **2010,** *15*, 4334–4358. (g) Shen, Y.; Chen, C.-F. *Chem. Rev.* **2012,** *112*, 1463–1535.

[2] (a) Nuckolls, C.; Katz, T. J. *J. Am. Chem. Soc.* **1998,** *120*, 9541–9544. (b) Vyklický, L.; Eichhorn, S. H.; Katz, T. J. *Chem. Mater.* **2003,** *15,* 3594-3601. (c) Shcherbina, M. A.; Zeng, X.-b. Tadjiev, T.; Ungar, G.; Eichhorn, S. H.; Phillips, K. E. S.; Katz, T. J. *Angew. Chem., Int. Ed.* **2009,** *48*, 7837–7840.

[3] (a) Verbiest, T.; Elshocht, S. V.; Kauranen, M.; Hellemans, L.; Snauwaert, J.; Nuckolls, C.; Katz, T. J.; Persoons, A. *Science* **1998,** *282,* 913–915. (b) Verbiest, T.; Elshocht, S. V.; Persoons, A.; Nuckolls, C.; Phillips, K. E.; Katz, T. J. *Langmuir* **2001,** *17,* 4685–4687. (c) Verbiest, T.; Sioncke, S.; Persoons, A.; Vyklický, L.; Katz, T. J. *Angew. Chem., Int. Ed.* **2002,** *41*, 3882–3884.

[4] (a) Field, J. E.; Muller, G.; Riehl, J. P.; Venkataraman, D. *J. Am. Chem. Soc.* **2003,** *125*, 11808–11809. (b) Kaseyama, T.; Furumi, S.; Zhang, X.; Tanaka, K.; Takeuchi, M. *Angew. Chem., Int. Ed.* **2011,** *50*, 3684–3687.

structures of **1**, and chiral separation of each axial optical isomer are also discussed. In addition, investigation of the electronic properties of thin films fabricated from a racemic mixture and a single enantiomer of **1** are described. Charge mobility measurements of the thin films based on the time-of-flight (TOF) method suggest that the racemate and one of the enantiomers of **1** are p-type and n-type semiconductors, respectively. This unprecedented carrier inversion might be caused by changes in the packing structure of the respective hetero- and homochiral crystals of **1**, as suggested by calculation of the electronic coupling.[5]

Chart 1. Azaboradibenzo[6]helicene

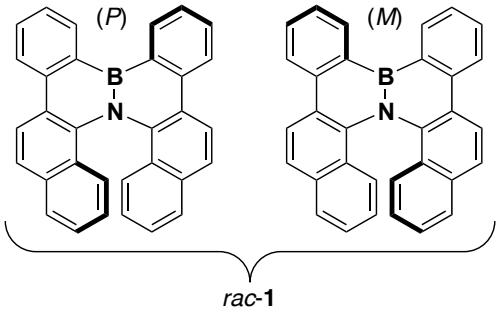

2-2. Results and Discussion

2-2-1. Synthesis and optical resolution of the BN-fused helicene

Scheme 1 summarizes the synthesis of **1**. Coupling of 1-bromo-2-phenylnaphthalene **2**, which was prepared in two steps from commercially available 1-bromonaphthalen-2-ol, with lithium amide in the presence of tris(dibenzylideneacetone)dipalladium(0) [$Pd_2(dba)_3$] and 2-dicyclohexylphosphino -2′,6′-dimethoxybiphenyl (SPhos) gave diarylamine **3** in 74% yield. Borylation of **3** by treatment with BuLi and BCl_3, and the subsequent tandem bora-Friedel–Crafts reaction with $AlCl_3$ and 2,2,6,6-tetramethylpiperidine afforded the racemate of **1** (*rac*-**1**) in 68% yield.

[5] (a) Fonseca Guerra, C.; Snijders, J. G.; te Velde, G.; Baerends, E. J. *Theor. Chem. Acc.* **1998,** *99*, 391–403. (b) te Velde, G.; Bickelhaupt, F. M.; Baerends, E. J.; Fonseca Guerra, C.; van Gisbergen, S. J. A.; Snijders J. G.; Ziegler, T. *J. Comput. Chem.* **2001,** *22*, 931–967. (c) Senthilkumar, K.; Grozema, F. C.; Bickelhaupt, F. M.; Siebbeles, L. D. A. *J. Chem. Phys.* **2003,** *119*, 9809–9817. (d) Wen, S.-H.; Li, A.; Song, J.; Deng, W.-Q.; Han, K.-L.; Goddard, W. A., III *J. Phys. Chem. B* **2009,** *113*, 8813–8819.

Scheme 2. Synthesis of azaboradibenzo[6]helicene **1**

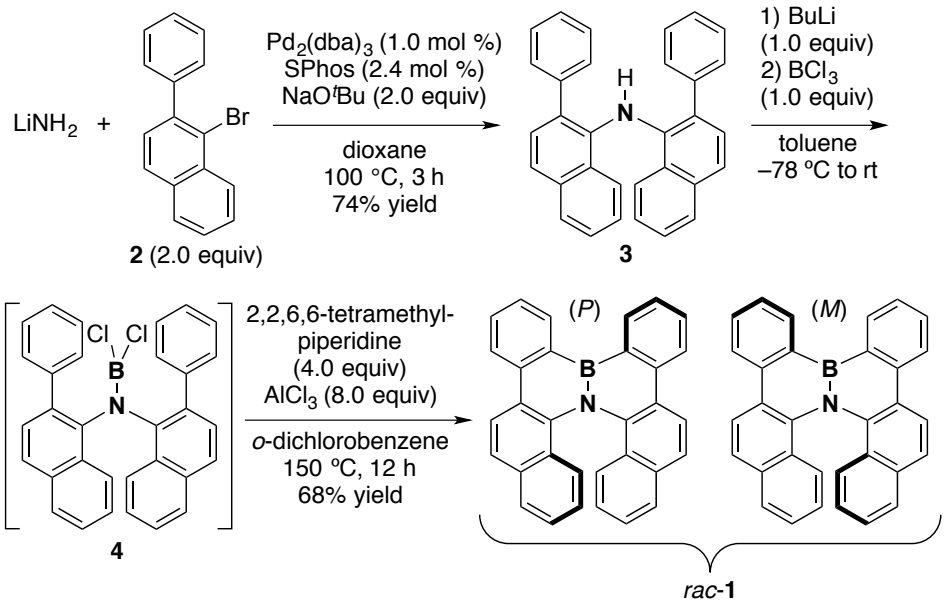

Optical resolution of *rac*-**1** into enantiopure (*P*)-**1** and (*M*)-**1** was carried out by chiral HPLC on a DAICEL CHIRALPAK® IA-3 column (eluent: *n*-hexane/CH_2Cl_2) (Figure 1). The absolute configuration of enantiopure **1** in each fraction was determined by X-ray crystallographic analysis of the dibromo derivative of fraction **A**. Dibromination of **1** selectively occurred at the *para* position of the aniline moiety in the presence of 2 equivalents of *N*-bromosuccinimide (Scheme 3).

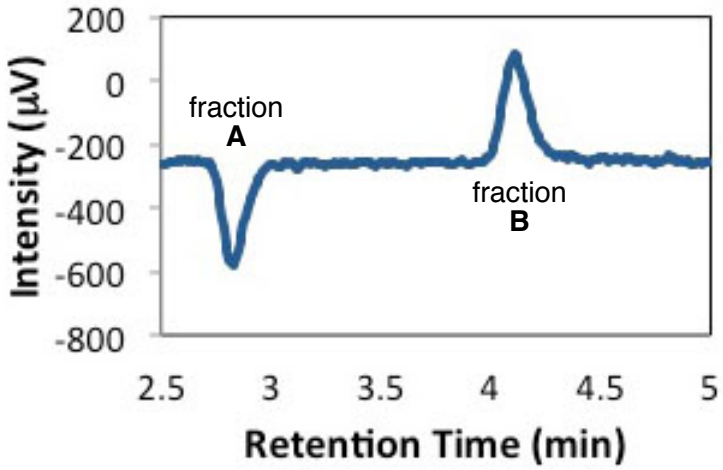

Figure 1. Chiral HPLC chromatogram of *rac*-**1** [CHIRALPAK® IA-3 column, 4.6 mm I.D., 150 mm L, 25 °C, 268 nm (CD), 1 mL/min, hexane/CH_2Cl_2 = 7:3].

Scheme 3. Dibromination of enantiopure **1** and determination of the absolute configuration

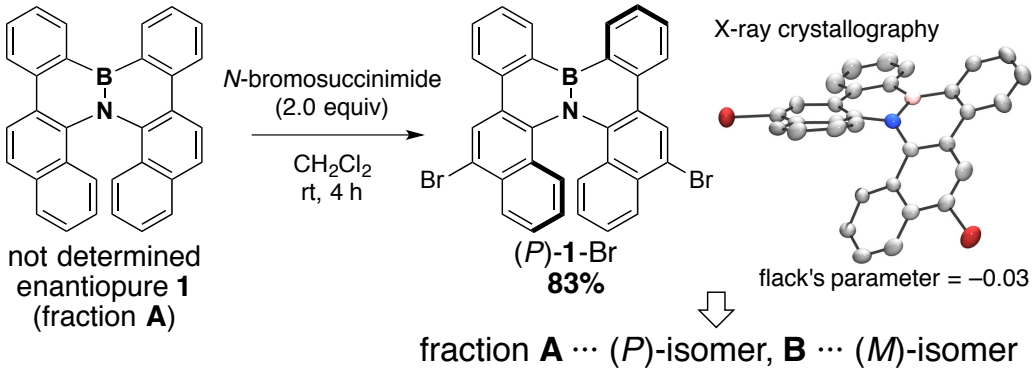

2-2-2. Optical characterization of the racemate and single enantiomer

The UV-visible absorption spectrum of *rac*-**1** has a relatively strong absorption band with a maximum (λ_{ab}) at 373 nm corresponding to a π–π^* transition. In the fluorescence spectrum, *rac*-**1** exhibits a cyan fluorescence at 447 nm (Figure 2). The CD spectrum shows positive cotton effects at 287 nm and 329 nm, and a negative cotton effect at 380 nm for (*P*)-**1**. This trend is inverted relative to that of the known (*P*)-[6]helicene.[6] The spectra of the two antipodes of **1** are almost exact mirror images, which are expected to correspond to enantiomers (Figure 3).

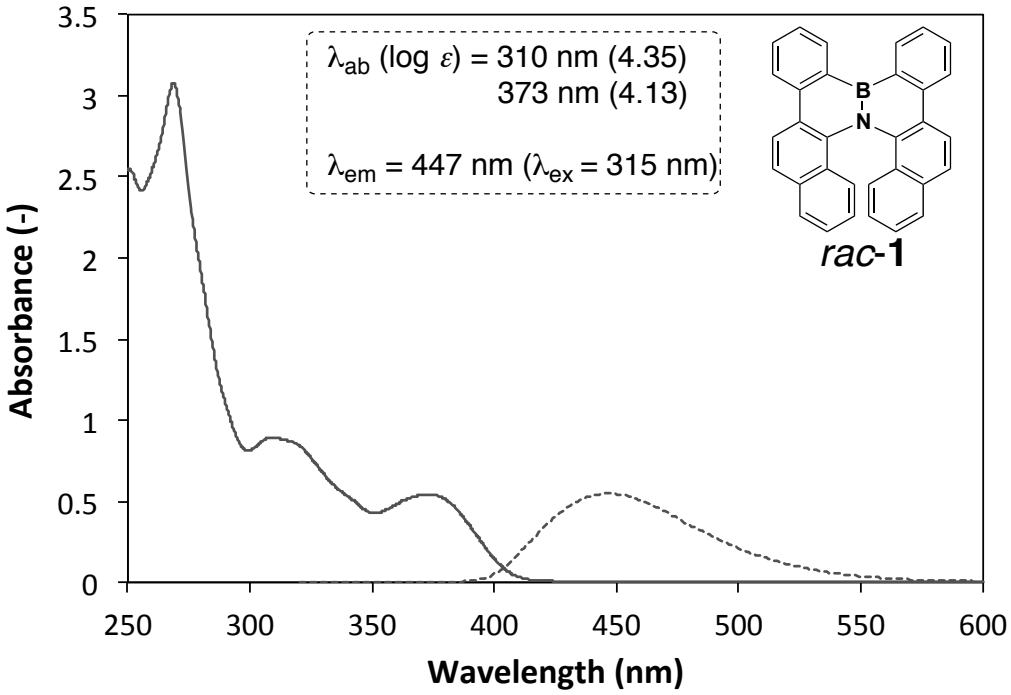

Figure 2. UV-visible absorption (solid line) and fluorescence (dotted line, excited at 315 nm) spectra of *rac*-**1** in dichloromethane solution (4.0×10^{-5} M).

[6] Nakai, Y.; Mori, T.; Inoue, Y. *J. Phys. Chem. A* **2012,** *116*, 7372–7385.

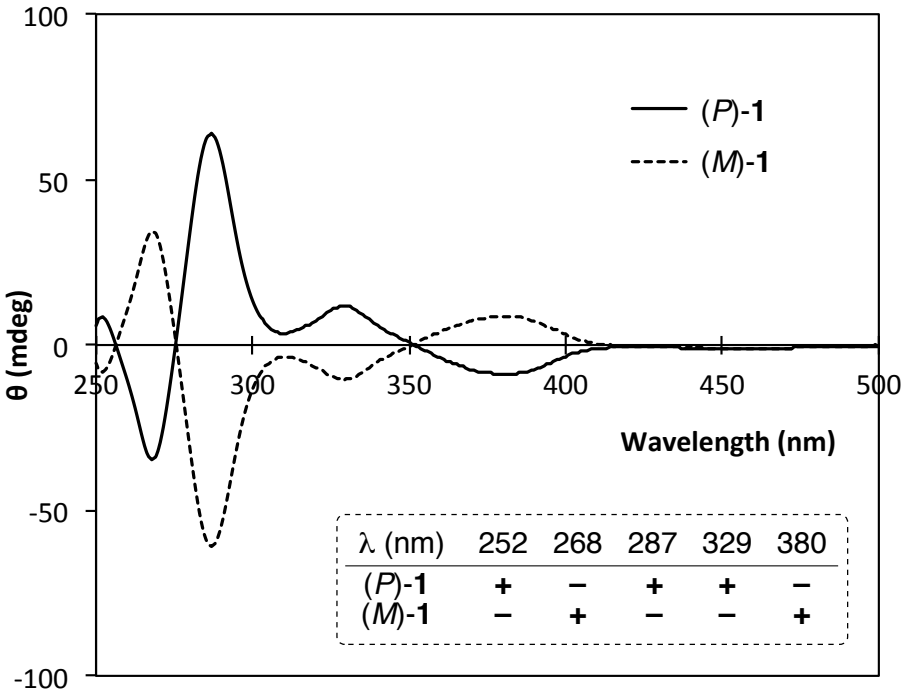

Figure 3. CD spectra of (*P*)-**1** (solid line) and (*M*)-**1** (dotted line) in dichloromethane solution (4.0×10^{-5} M).

2-2-3. Molecular packing of the single crystal

The helical structure of *rac*-**1** was determined to be C_2 symmetric by X-ray crystallography (Figure 4a). The B–N bond length [1.448(3) Å] is similar to that in typical BN aromatics (1.45–1.47 Å).[7] Furthermore, the B–C1(C1′) and N–C2(C2′) lengths are 1.5527(19) and 1.425(2), respectively, indicating that they are single bonds. These observations, together with the highly distorted BNC_4 ring structure [B–N–C4(C4′)–C3(C3′) dihedral angle = 21.66°], reveal the low aromaticity of the BNC_4 rings, which is consistent with the relatively positive nucleus-independent chemical shift [NICS(1)] value of –1.8 (Figure 4b). This value is more positive than reported for other BN-substituted aromatic compounds (–4.6 and –6.3).[8] In contrast, the surrounding C_6 rings are nearly planar and show large NICS(1) values. Notably, molecular orbital (MO) calculations indicated that the π-conjugation is spread over the entire molecule despite the large distortion induced by the BNC_4 rings (Figure 4c).

---

[7] Reviews: (a) Liu, Z.; Marder, T. B. *Angew. Chem., Int. Ed.* **2008,** *47*, 242–244. (b) Bosdet, M. J. D.; Piers, W. E. *Can. J. Chem.* **2009,** *87*, 8–29. (c) Ashe, A. J., III *Organometallics* **2009,** *28*, 4236–4248. (d) Campbell, P. G.; Marwitz, A. J. V.; Liu, S.-Y. *Angew. Chem., Int. Ed.* **2012,** *51*, 6074–6092.

[8] Bosdet, M. J. D.; Jaska, C. A.; Piers, W. E.; Sorensen, T. S.; Parvez, M. *Org. Lett.* **2007,** *9*, 1395–1398.

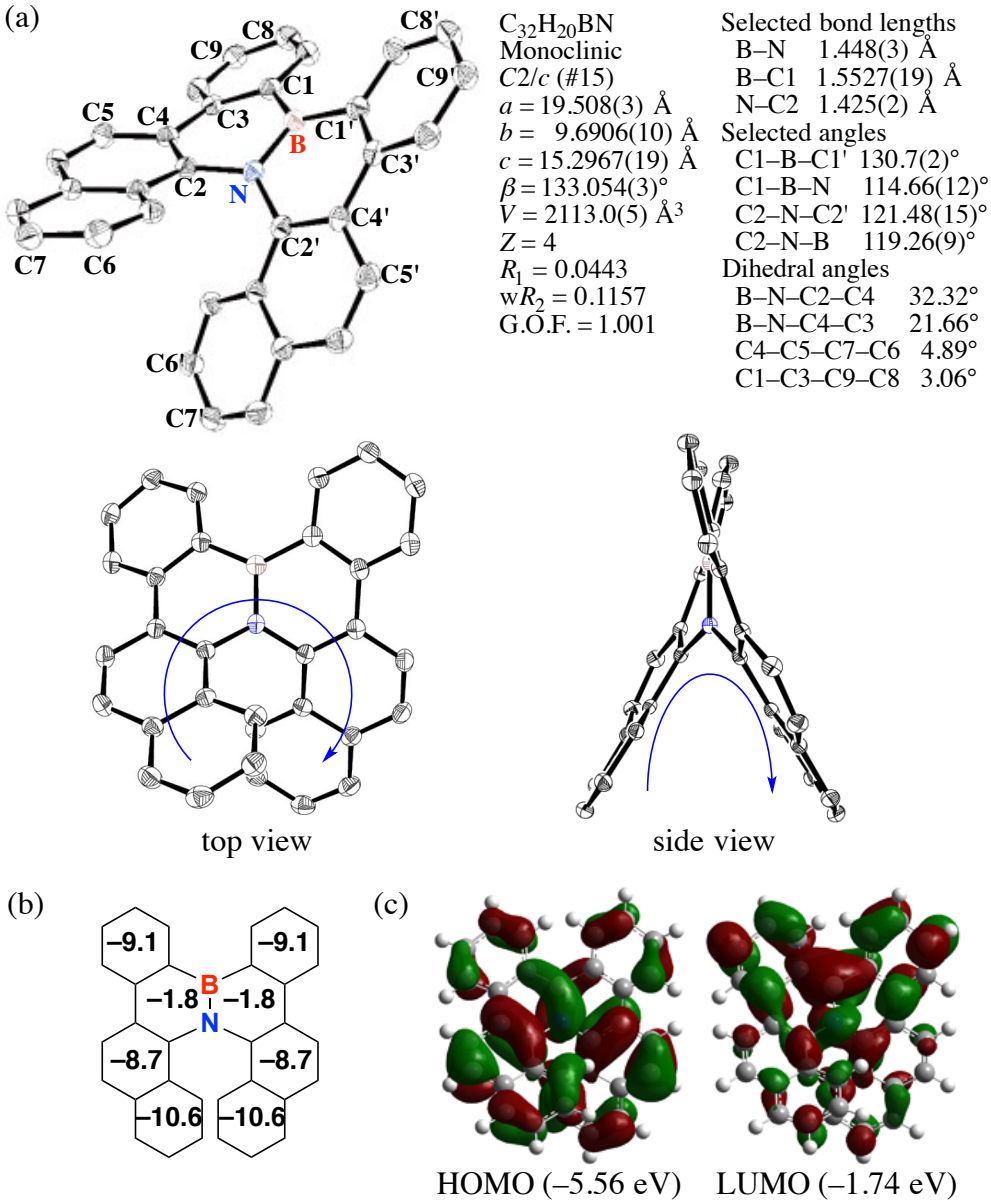

$C_{32}H_{20}BN$
Monoclinic
*C*2/*c* (#15)
a = 19.508(3) Å
b = 9.6906(10) Å
c = 15.2967(19) Å
β = 133.054(3)°
V = 2113.0(5) Å^3
Z = 4
R_1 = 0.0443
wR_2 = 0.1157
G.O.F. = 1.001

Selected bond lengths
B–N 1.448(3) Å
B–C1 1.5527(19) Å
N–C2 1.425(2) Å
Selected angles
C1–B–C1' 130.7(2)°
C1–B–N 114.66(12)°
C2–N–C2' 121.48(15)°
C2–N–B 119.26(9)°
Dihedral angles
B–N–C2–C4 32.32°
B–N–C4–C3 21.66°
C4–C5–C7–C6 4.89°
C1–C3–C9–C8 3.06°

Figure 4. (a) ORTEP drawing of *rac*-**1** obtained by X-ray crystal analysis. Thermal ellipsoids are shown at 50% probability and H atoms have been omitted for clarity. (b) NICS(1) values, and (c) the Kohn–Sham highest occupied MO (HOMO) and lowest unoccupied MO (LUMO) of (*P*)-**1**. DFT calculations, including NICS analysis, were performed at the B3LYP/6-311+G(d,p)//B3LYP/6-31G(d) level.

The unique packing structure of the heterochiral crystal is shown in Figure 5. The molecules are stacked in a head-to-tail array with a CH–π distance of 2.9–3.3 Å. Each array is formed from a single enantiomer, resulting in alternating right-handed (*P*-helical, shown in blue) and left-handed (*M*-helical, shown in pink) configurations, which are arranged in a face-to-face fashion (π–π distance = 3.4–3.6 Å), while the local dipole moments of the B–N bonds cancel each other.

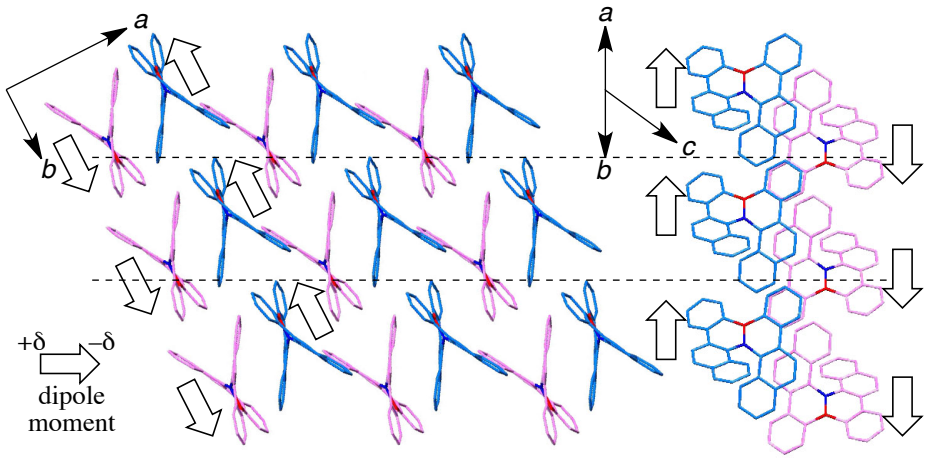

Figure 5. Packing structure of *rac*-**1** obtained by X-ray crystal analysis. H atoms have been omitted for clarity. The *P* enantiomer is shown in blue and the *M* enantiomer is shown in pink.

The molecular structure of (*P*)-**1** in the homochiral crystal (Figure 6a) is C_2 symmetric and the bond lengths and angles are almost identical to those found in the heterochiral crystal (Figure 4a). On the other hand, the packing structure of the homochiral crystal differs significantly from that of the heterochiral crystal and has a one-dimensional columnar alignment along the *c*-axis (Figure 6b).[9] Interestingly, the molecules in neighboring columns are parallel to each other and show a rotation of 120° with each layer (Figure 6c). As a result, the local dipole moments, which run perpendicular to the *c*-axis, are offset at every third layer.

[9] One-dimensional columnar alignment of helicenes: (a) Murguly, E.; McDonald, R.; Branda, N. R. *Org. Lett.* **2000,** *2,* 3169–3172. (b) Caronna, T.; Sinisi, R.; Catellani, M.; Malpezzi, L.; Meille, S. V.; Mele, A. *Chem. Commun.* **2000,** 1139–1140. (c) Miyasaka, M.; Rajca, A.; Pink, M.; Rajca, S. *J. Am. Chem. Soc.* **2005,** *127,* 13806–13807. (d) Nakano, K.; Oyama, H.; Nishimura, Y.; Nakasako, S.; Nozaki, K. *Angew. Chem., Int. Ed.* **2012,** *51,* 695–699.

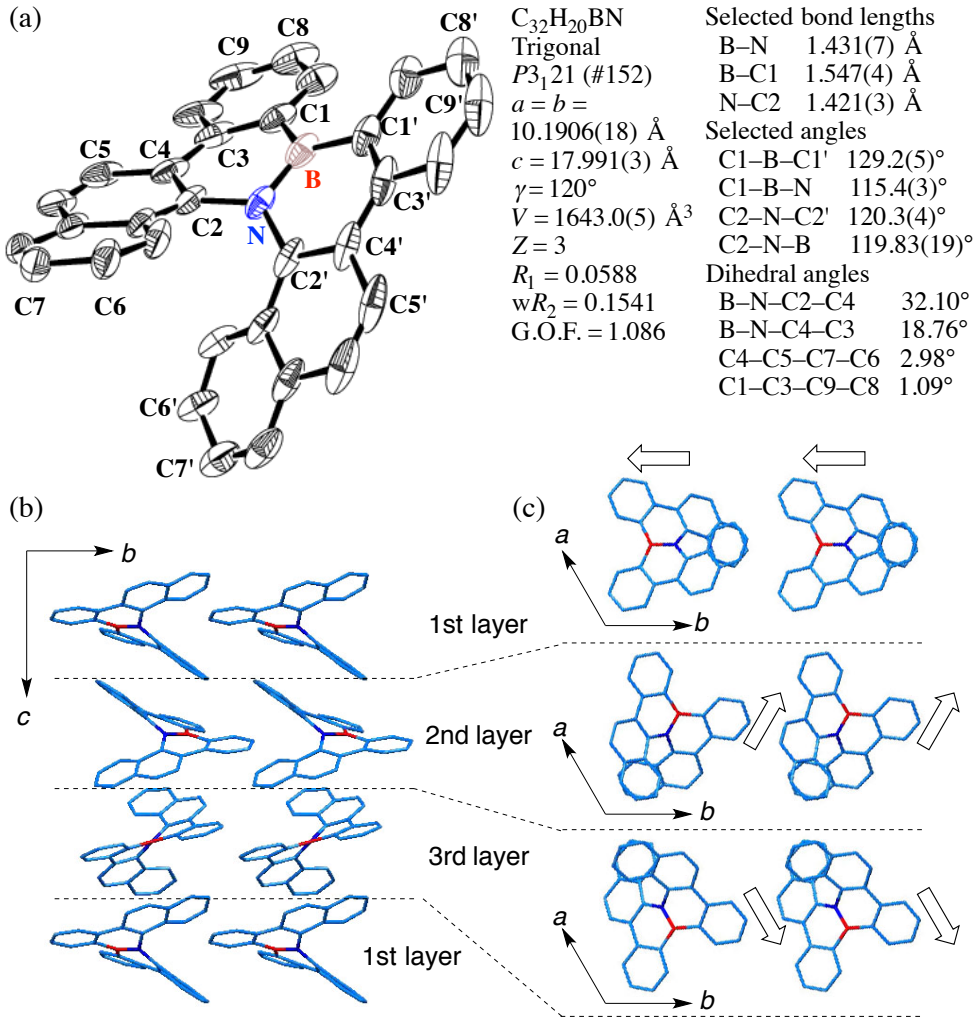

$C_{32}H_{20}BN$	
Trigonal	
$P3_121$ (#152)	
$a = b =$ 10.1906(18) Å	
$c = 17.991(3)$ Å	
$\gamma = 120°$	
$V = 1643.0(5)$ Å^3	
$Z = 3$	
$R_1 = 0.0588$	
$wR_2 = 0.1541$	
G.O.F. = 1.086	

Selected bond lengths	
B–N	1.431(7) Å
B–C1	1.547(4) Å
N–C2	1.421(3) Å
Selected angles	
C1–B–C1'	129.2(5)°
C1–B–N	115.4(3)°
C2–N–C2'	120.3(4)°
C2–N–B	119.83(19)°
Dihedral angles	
B–N–C2–C4	32.10°
B–N–C4–C3	18.76°
C4–C5–C7–C6	2.98°
C1–C3–C9–C8	1.09°

Figure 6. (a) ORTEP drawing and (b, c) packing structures of (*P*)-**1**. Thermal ellipsoids are shown at 30% probability and H atoms have been omitted for clarity.

2-2-4. Evaluation of carrier-transport properties

Since the enantiopurity of (*P*)-**1** did not decrease upon heating (even at 275 °C), films of *rac*-**1** and (*P*)-**1** with thicknesses of 8.2 and 6.7 μm, respectively, were prepared by vacuum-deposition under 5.0×10^{-3} Pa for use in TOF measurements.[8] Additionally, the calculated racemization barrier is 43.2 kcal mol^{-1} [Figure 7, $\Delta G^{\ddagger}$ at the B3LYP/6-31G(d) level], which is consistent with the experimental results and is considerably higher than that of [6]helicene (35.2 kcal mol^{-1}).[10]

[10] Grimme, S.; Peyerimhoff, S. D. *Chem. Phys.* **1996,** *204*, 411–417.

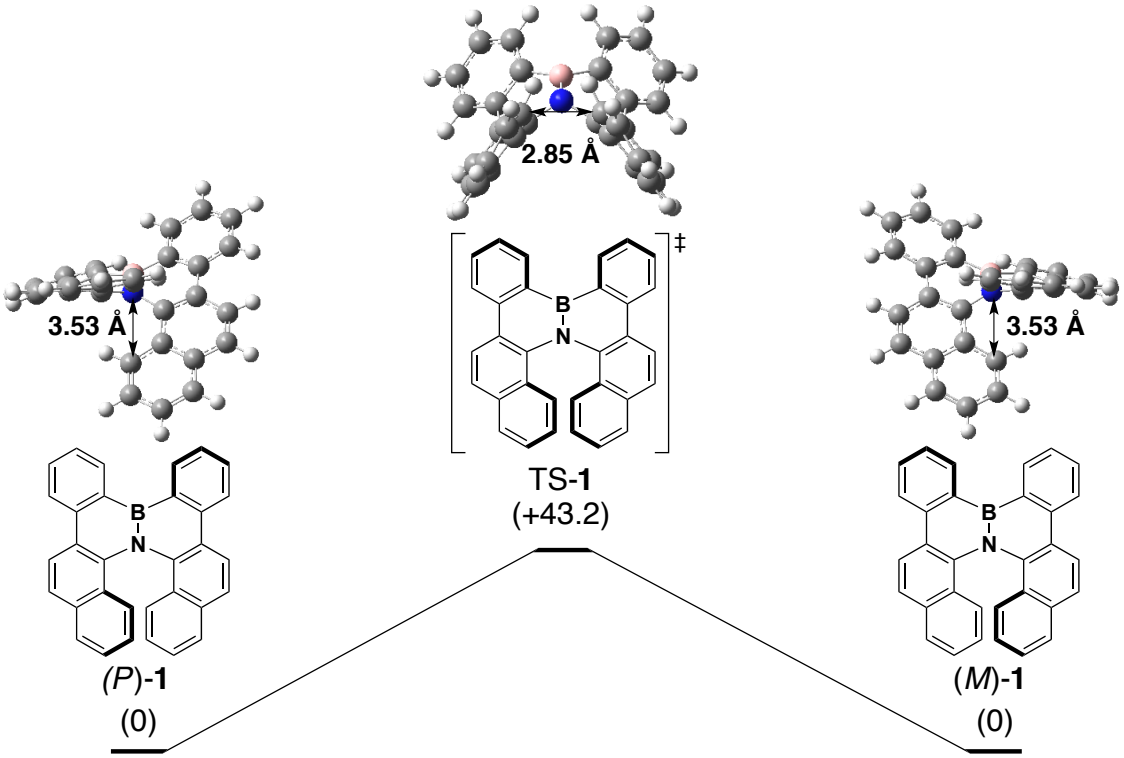

Figure 7. Energy diagram for the isomerization pathway from (*P*)-**1** to (*M*)-**1**. Gibbs free energies relative to (*P*)-**1** [$\Delta G^{\ddagger}$, B3LYP/6-31G(d)] are given in kcal mol^{-1}.

The carrier-transport properties of the films were then evaluated at room temperature and electric fields of 5.0×10^5 (*rac*-**1**) and 5.2×10^5 V cm^{-1} [(*P*)-**1**], respectively. It was found that *rac*-**1** showed high hole mobility ($\mu_h = 4.6 \times 10^{-4}$ cm^2 V^{-1} s^{-1}), but no transient photocurrent was detected in electron mobility measurements (Table 1). Interestingly, enantiopure (*P*)-**1** showed higher electron mobility ($\mu_e = 4.5 \times 10^{-3}$ cm^2 V^{-1} s^{-1}) than hole mobility ($\mu_h = 7.9 \times 10^{-4}$ cm^2 V^{-1} s^{-1}). Since the corresponding physical properties of the vacuum-deposited films, such as ionization potential (I_p) and electron affinity (E_a), were almost identical, the carrier inversion must be caused by the distinct orientation of (*P*)-**1** in the homochiral film.

Table 1. Electronic properties of amorphous films of *rac*-**1** and (*P*)-**1**

	μ_h[a]	μ_e[b]	I_p[c]	E_a[d]
rac-**1**	4.6×10^{-4}	—[e]	5.54	2.55
(*P*)-**1**	7.9×10^{-4}	4.5×10^{-3}	5.55	2.55

[a]Hole-transport ability (cm^2 V^{-1} s^{-1}). [b]Electron-transport ability (cm^2 V^{-1} s^{-1}). [c]Ionization potential (eV) measured by photoelectron spectroscopy in air (PESA) using an AC-1 system (RIKEN KEIKI Co., Ltd.). [d]Electron affinity (eV) estimated from the ionization potentials and UV-visible absorption edge wavelengths. [e]Transient photocurrent was not detected.

To provide detailed insight into the carrier-transport properties, the electronic coupling, V (meV),[5] between neighboring molecules in different stacks was calculated from the X-ray crystal structures of *rac*-**1** and (*P*)-**1** (Figure 8). In the heterochiral crystal of *rac*-**1** (Figure 8a), the (*P*)- and (*M*)-enantiomers were arranged in a tightly offset face-to-face stacking array. The maximum coupling between the HOMOs of neighboring molecules (42.0 meV) was six times larger than that of the corresponding LUMOs (7.2 meV). In contrast, in the homochiral crystal of (*P*)-**1** (Figure 8b), the maximum coupling of the HOMOs (30.1 meV) was only two-fifths of that of the LUMOs (73.2 meV). Because the electron-hopping rate (W) is proportional to V^2 on the basis of the Marcus–Hush theory,[5] these values are in good agreement with the carrier mobility determined by the TOF method. These results are suggestive of the possibility that the molecular orientation in the amorphous films might be similar to that in the crystal.[11]

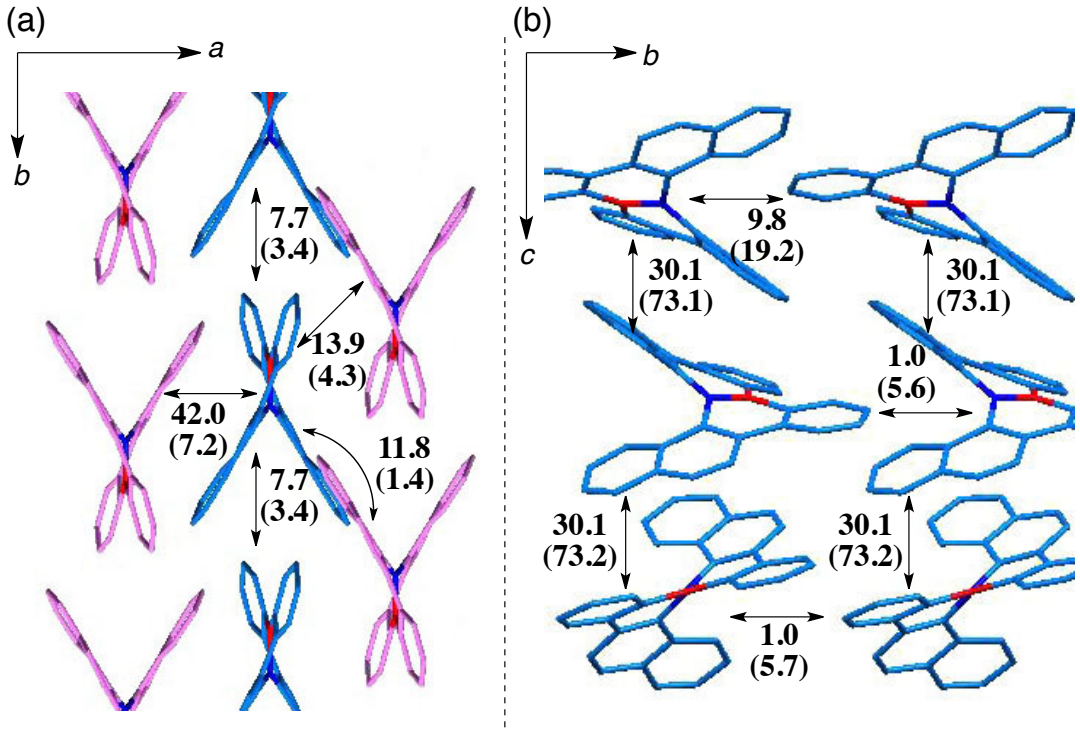

Figure 8. Electronic coupling, V (in meV), between HOMOs of neighboring molecules in the X-ray crystal structures of (a) *rac*-**1** (*P* in blue, *M* in pink) and (b) (*P*)-**1**. The electronic coupling between LUMOs is shown in parentheses.

[11] Molecular orientation in vacuum-deposited amorphous film: Yokoyama, D. *J. Mater. Chem.* **2011,** *21,* 19187–19202 and citations therein.

2-3. Conclusions

In this chapter, the synthesis of azaboradibenzo[6]helicene **1** *via* a tandem bora-Friedel–Crafts reaction was described. In addition, the determination of the structures of **1** in solution and in the solid phase, and chiral separation of each axial optical isomer were detailed. Finally, electronic properties of thin films fabricated with a racemic mixture and a single enantiomer were investigated. Charge mobility measurements by the TOF method suggest that the racemate and single enantiomer of **1** are good p-type and n-type semiconductors, respectively. The unprecedented carrier inversion might be caused by changes in the packing structures of hetero- and homochiral crystals of **1**, as suggested by electronic coupling calculations. The results indicate that these chiral organic semiconductors have potential use in electronic applications such as bipolar junction transistors and morphology-controlled bulk-heterojunction solar cells.

2-4. Experimental Section

General. All the reactions dealing with air- or moisture-sensitive compounds were carried out in a dry reaction vessel under a positive pressure of argon. Air- and moisture-sensitive liquids and solutions were transferred *via* a syringe or a stainless steel cannula. Analytical thin-layer chromatography (TLC) was performed on glass plates coated with 0.25 mm 230–400 mesh silica gel containing a fluorescent indicator (Merck, #1.05715.0009). TLC plates were visualized by exposure to ultraviolet light (254 nm) and/or by immersion in an acidic staining solution of *p*-anisaldehyde followed by heating on a hot plate. Organic solutions were concentrated by rotary evaporation at *ca*. 30–400 mmHg. Flash column chromatography was performed on Merck silica gel 60 (spherical, neutral, 140–325 mesh) as described by Still et al.[12] Gel permeation chromatography was performed on a JAIGEL-1H and 2H (20 mm i.d.) with an LC-9204 (Japan Analytical Industry Co., Ltd.).

Instrumentation. Proton nuclear magnetic resonance (^{1}H NMR) and carbon nuclear magnetic resonance (^{13}C NMR) spectra were recorded on JEOL ECS400 (392 MHz) NMR spectrometers. Proton chemical shift values are reported in parts per million (ppm, δ scale) downfield from tetramethylsilane, and are referenced to the tetramethylsilane (δ 0). ^{13}C NMR spectra were recorded at 98.5 MHz: carbon chemical shift values are reported in parts per million (ppm, δ scale) downfield from tetramethylsilane, and are referenced to the carbon resonance of $CDCl_3$ (δ 77.0) and tetramethylsilane (δ 0). ^{11}B NMR spectra were recorded at 131 MHz: boron chemical shift values are reported in parts per million (ppm, δ scale) and are referenced to the external standard boron signal of $BF_3{\cdot}Et_2O$ (δ 0). Data are presented as: chemical shift, multiplicity (s = singlet, d = doublet, t = triplet, q = quartet, quint = quintet, sext = sextet, sept = septet, m = multiplet and/or multiplet resonances, br = broad), coupling constant in hertz (Hz), signal area integration in natural numbers, and assignment (*italic*). IR spectra were recorded on an ATR-FTIR spectrometer (FT/IR-Spectrum One, PerkinElmer). Characteristic IR absorptions are reported in cm^{-1}. Melting points were recorded on a Yanaco MP-500V. High-resolution mass spectra (HRMS) were obtained using the electron impact (EI) method with JEOL JMS-700, JMS-SX102A. UV-visible absorption spectra were measured by JASCO Ubest V-570. Fluorescence spectra were measured by HORIBA Scientific FluoroMax-4. Circular dichroism (CD) spectra were recorded on a JASCO J-820 spectropolarimeter. Purity of isolated compounds was determined by GC analysis on Shimadzu GC-2010 Plus instrument equipped with an FID detector and a capillary column, ZB-1MS (Phenomenex, 10 m × 0.10 mm i.d., 0.10 μm film thickness) and/or ^{1}H NMR analyses.

[12] Still, W. C.; Kahn, M.; Mitra, A. *J. Org. Chem.* **1978,** *43*, 2923–2925.

Solvent. *o*-Dichlorobenzene and anhydrous toluene were purchased from Wako Pure Chemical Industries, Ltd. (Wako) and dried over Molecular Sieves 4A and degassed before use. Water content of the solvent was determined with a Karl Fischer Moisture Titrator (MKC-610, Kyoto Electronics Company) to be less than 15 ppm.

Materials. Materials were purchased from Wako, Tokyo Chemical Industry Co., Ltd., Aldrich Inc., Hokko Chemical Industry Co., Ltd., and other commercial suppliers, and were used after appropriate purification, unless otherwise noted. Florisil® (100–200 mesh) and Celite® were purchased from Wako. Aryl halides and aryl amines were purified by distillation or recrystallization to be over 99.5% pure by GC analysis. Arylmagnesium bromides (ArMgBr) were prepared from the corresponding aryl bromides and magnesium (turnings) using a standard method and titrated before use.

Synthesis of 1-bromo-2-phenylnaphthalene (2)

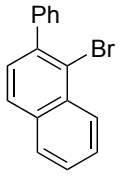

Pyridine (14.0 mL, 0.174 mol) was added to a mixture of 1-bromonaphthalen-2-ol (33.5 g, 0.150 mol) in dichloromethane (190 mL) at –15 °C with an ice/methanol cooling bath under argon. Triflic anhydride (28.0 mL, 0.166 mol) was added gradually to the reaction mixture. Upon completion of the addition, the reaction mixture was stirred for 30 min at –15 °C, and then allowed to warm to room temperature. After stirring at room temperature for 2 h, water (110 mL) was added to the mixture at –15 °C and the resulting two-phase mixture was stirred for 10 min. The layers were separated and the organic (lower) layer was washed with 1 N hydrochloric acid, water and brine (100 mL each). The final organic layer was filtered with a pad of silica gel. The filtrate was concentrated to give 1-bromonaphthalen-2-yl trifluoromethanesulfonate (52.9 g, 99% yield, 98% pure on GC analysis) as a yellow solid. IR(neat): cm^{-1} 3067 (Ar-H), 1590, 1504, 1424, 1408, 1354, 1325, 1245, 1218, 1208, 1185, 1155, 1130, 978, 932, 872, 830, 813, 769, 756, 705, 658; mp: 29.9–31.6 °C; ^{1}H NMR (392 MHz, $CDCl_3$) δ 7.44 (d, J = 9.0 Hz, 1H, OCC*H*), 7.62 (ddd, J = 1.6, 6.7, 7.4 Hz, 1H, OCCHCHCCHC*H*), 7.70 (ddd, J = 1.6, 6.7, 7.4 Hz, 1H, OCCCCHC*H*), 7.90 [m(overlap), 2H, C*H*CHCHC*H*], 8.32 (d, J = 9.0 Hz, 1H, OCCHC*H*); ^{13}C NMR (98.5 MHz, $CDCl_3$) δ 116.2, 118.7 (d, $J_{C\text{-}F}$ = 320 Hz), 119.9, 127.7, 127.8, 128.3, 128.8, 129.7, 132.6, 133.0, 145.0; HRMS (FAB) *m/z* $[M]^+$ calcd for $C_{11}H_6BrF_3O_3S$ 353.9173; observed 353.9172. A solution of phenylmagnesium bromide in diethyl ether (170 mL, 1.00 M, 0.170 mol) was added to a mixture of 1-bromonaphthalen-2-yl trifluoromethanesulfonate (35.5 g, 0.100 mol) and lithium bromide (8.68 g, 0.100 mol) at 0 °C under argon. Then dichloro[1,3-bis(diphenylphosphino)propane]palladium(II) (1.77 g, 3.00 mmol) was added to the reaction mixture. After stirring at 0 °C for 18 h, saturated ammonium

chloride aqueous solution (200 mL) and water (300 mL) was added at 0 °C. After the organic layer was separated, the aqueous layer was extracted with ethyl acetate (300 mL × 3). The combined organic layers were dried by magnesium sulfate. After filtration, the solvent was removed *in vacuo*, hexane (2.0 L) was added to the crude product, and then filtered with a pad of silica gel. After removal of the solvent *in vacuo*, the crude product was purified by GPC (eluent: $CHCl_3$) to obtain the titled compound (27.2 g, 96% yield, 99% pure on GC analysis) as a white solid. Analytical data for the titled compound have been reported.[13]

Synthesis of bis(2-phenylnaphthalen-1-yl)amine (3)

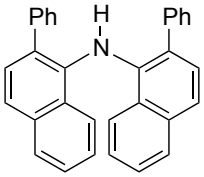

Compound **2** (19.8 g, 70.0 mmol) was added to a mixture of lithium amide (0.804 g, 35.0 mmol), tris(dibenzylideneacetone)dipalladium(0)-chloroform adduct (0.362 g, 0.350 mmol), 2-dicyclohexylphosphino-2′,6′-dimethoxybiphenyl (0.345 g, 0.840 mmol) and sodium *tert*-butoxide (6.73 g, 70.0 mmol) in dioxane (35 mL) at 0 °C under argon. After stirring at 100 °C for 3 h, the reaction mixture was cooled to room temperature, and then toluene (200 mL) was added. The reaction mixture was filtered with a pad of Florisil® and silica gel. After removal of the solvent *in vacuo*, hexane (200 mL) was added. The reaction mixture was filtered with a pad of silica gel. After the solvent was removed *in vacuo*, the title compound was obtained (10.9 g, 74% yield, >99% pure on GC analysis) as a pink solid. IR(neat): cm^{-1} 3392 (N-H), 3052 (Ar-H), 1596, 1561, 1494, 1475, 1440, 1423, 1382, 1347, 1312, 1281, 1162, 1115, 1074, 1030, 957, 919, 861, 815, 806, 761, 740, 701, 671; mp: 137.7–138.8 °C; ^{1}H NMR (392 MHz, $CDCl_3$) δ 6.76 (s, 1H, N*H*), 7.09–7.19 (m, 12H), 7.24 (ddd, *J* = 1.3, 7.4, 8.5 Hz, 2H, NCCCHC*H*CH), 7.37 (ddd, *J* = 1.3, 7.4, 8.1 Hz, 2H, NCCCHCHC*H*), 7.39 (d, *J* = 8.5 Hz, 2H, NCCCHC*H*C), 7.72 (d, *J* = 8.1 Hz, 2H, NCCCHCHCHC*H*), 7.84 (d, *J* = 8.5 Hz, 2H, NCCC*H*CHCH); ^{13}C NMR (98.5 MHz, $CDCl_3$) δ 121.9 (2C), 123.4 (2C), 125.3 (2C), 125.6 (2C), 126.5 (2C), 127.4 (2C), 127.9 (4C), 128.1 (2C), 128.5 (2C), 128.8 (6C), 134.0 (2C), 137.0 (2C), 140.1 (2C); HRMS (EI) *m/z* $[M]^+$ calcd for $C_{32}H_{23}N$ 421.1834; observed 421.1830.

[13] Isogai, Y.; Menggenbateer, F.; Khan, N.; Asao, N. *Tetrahedron* **2009,** *65*, 9575–9582.

Synthesis of 16c-aza-8a-boradibenzo[*i*,*l*]hexahelicene (*rac*-1)

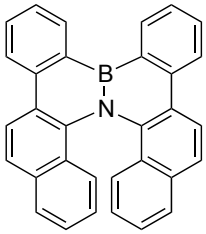

A solution of butyllithium in hexane (8.75 mL, 1.60 M, 14.0 mmol) was added slowly to a solution of **3** (5.91 g, 14.0 mmol) in toluene (70 mL) at –78 °C under argon. After 5 min, the reaction mixture was allowed to warm to 0 °C and stirred for 2.5 h. To the reaction mixture was added trichloroborane in heptane (14.0 mL, 1.00 M, 14.0 mmol) at –78 °C. After 30 min, the reaction mixture was allowed to warm to room temperature and stirred overnight. After removal of the solvent *in vacuo*, *o*-dichlorobenzene (84.0 mL) was added. The reaction mixture was added to a mixture of aluminum trichloride (14.9 g, 0.112 mol) and 2,2,6,6-tetramethylpiperidine (9.53 mL, 56.0 mmol) in *o*-dichlorobenzene (86.0 mL) at 0 °C. After stirring at 150 °C for 12 h, 1,4-diazabicyclo[2.2.2]octane (12.6 g, 0.112 mol) was added. The reaction mixture was filtered with a pad of Celite®. After removal of the solvent *in vacuo*, the crude product was washed with hexane (300 mL) by using a sonicator two times, and purified by GPC (eluent: toluene) to obtain the titled compound (4.27 g, 68% yield, 99% pure on GC analysis) as a white-yellow powder. *rac*-**1** can be separated into enantiopure (*P*)-**1** and (*M*)-**1** by HPLC with a DAICEL CHIRALPAK® IA-3 column (4.6 mm × 150 mm) [t_R = 2.8 min for (*P*)-**1** and 4.1 min for (*M*)-**1** (flow rate: 1.0 mL/min; solvent: hexane/CH_2Cl_2 = 70/30)]. IR(neat): cm^{-1} 3061 (Ar-H), 1599, 1568, 1509, 1479, 1463, 1443, 1424, 1367, 1342, 1316, 1290, 1247, 1157, 1144, 1098, 1024, 952, 942, 932, 889, 872, 856, 813, 787, 756, 731, 683; mp: 309.2–310.0 °C (*rac*-**1**), 332.1–333.2 °C [(*P*)-**1**]; sublimation temp: 180 °C (*rac*-**1**, 4.4 × 10^{-3} Pa), 210 °C [(*P*)-**1**, 5.0 × 10^{-3} Pa]; ^{1}H NMR (392 MHz, $CDCl_3$) δ 6.68 (ddd, *J* = 1.3, 6.7, 7.2 Hz, 2H, NCCCHC*H*CH), 7.12 (ddd, *J* = 1.3, 6.7, 7.2 Hz, 2H, NCCCHCHC*H*), 7.17 (d, *J* = 8.1 Hz, 2H, NCCC*H*CHCH), 7.67 (ddd, 0.9, 7.6, 8.0 Hz, 2H, BCCHC*H*), 7.70 (d, *J* = 8.1 Hz, 2H, NCCCHCHCHC*H*), 7.80 (d, *J* = 8.5 Hz, 2H, NCCCHC*H*C), 7.87 (ddd, *J* = 0.9, 7.6, 8.1 Hz, 2H, BCCHCHC*H*), 8.49 (d, *J* = 8.5 Hz, 2H, NCCC*H*CHC), 8.61 (d, *J* = 8.1 Hz, 2H, BCCC*H*), 8.85 (d, *J* = 8.0 Hz, 2H, BCC*H*); ^{13}C NMR (98.5 MHz, $CDCl_3$) δ 122.6 (2C), 122.7 (2C), 123.4 (2C), 124.1 (2C), 124.3 (2C), 124.4 (2C), 125.6 (2C), 126.4 (2C), 126.8 (2C), 127.9 (2C), 131.3 (2C), 133.0 (2C), 133.6 (br, 2C, *CBC)*, 135.5 (2C), 136.1 (2C), 139.6 (2C); ^{11}B NMR (131 MHz, $CDCl_3$) δ 37.8; HRMS (EI) *m/z* $[M]^+$ calcd for $C_{32}H_{20}BN$ 429.1694; observed 429.1698.; Anal. calcd for $C_{32}H_{20}BN$ C, 89.52; H, 4.79; N, 3.26. found C, 89.40; H, 4.64; N, 3.21.

Synthesis of 5,12-dibromo-16c-aza-8a-boradibenzo[*i*,*l*]hexahelicene [(*P*)-**1**-Br]

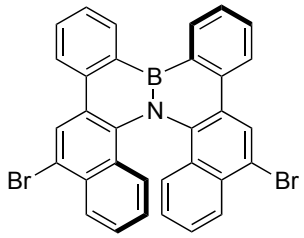

N-Bromosuccinimide (8.9 mg, 0.050 mmol) was added to a solution of (*P*)-**1** (21.5 mg, 0.050 mmol) in dichloromethane (1.0 mL). After the mixture was stirred for 2 h at room temperature, *N*-bromosuccinimide (8.9 mg, 0.050 mmol) was added and stirred for 2 h. Subsequently the solvent was removed *in vacuo*, the crude product was purified by GPC (eluent: toluene) to obtain the title compound (24.3 mg, 83% yield, 98% pure on GC analysis) as a white yellow powder. IR(neat): cm^{-1} 3058 (Ar-H), 1596, 1475, 1401, 1357, 1312, 1292, 1138, 942, 914, 901, 864, 785, 753, 729, 687, 653, 637, 626; mp: 179.0–179.9 °C; ^{1}H NMR (392 MHz, $CDCl_3$) δ 6.76 (ddd, J = 1.3, 7.2, 8.5 Hz, 2H, NCCCHC*H*), 7.16–7.25 (m, 4H), 7.69 (t, J = 7.2 Hz, 2H, BCCHC*H*), 7.88 (ddd, J = 1.3, 7.2, 8.1 Hz, 2H, BCCHCHC*H*), 8.11 (d, J = 8.1 Hz, 2H, BrCCC*H*), 8.52 (d, J = 8.1 Hz, 2H, BCCC*H*), 8.77 (s, 2H, BrCC*H*), 8.81 (d, J = 7.2 Hz, 2H, BCC*H*); ^{13}C NMR (98.5 MHz, $CDCl_3$) δ 118.2 (2C), 123.4 (2C), 123.5 (2C), 124.2 (2C), 125.4 (2C), 126.7 (2C), 127.0 (2C), 127.3 (4C), 127.5 (2C), 130.8 (2C), 131.7 (2C), 133.3 (br, 2C, *C*B*C*), 135.6 (2C), 135.7 (2C), 138.4 (2C); ^{11}B NMR (131 MHz, $CDCl_3$) δ 36.7; HRMS (EI) m/z $[M]^+$ calcd for $C_{32}H_{18}Br_2NB$ 586.9887; observed 586.9885.

Crystallographic data collection and structure determination. Crystals of *rac*-**1**, (*P*)-**1** and (*P*)-**1**-Br were mounted on a Rigaku Saturn CCD diffractometer for data collection using graphite-monochromated Mo Kα radiation (λ = 0.71070 Å). Crystal data and data statistics are summarized in Figure 9. The structures were solved by direct methods with SIR2008 [14] or SIR2004 [15] and refined by full-matrix least-squares techniques against F^2 (SHELXL-97) [16]. The non-hydrogen atoms were refined anisotropically. Hydrogen atoms were placed at calculated positions (C–H = 0.95 Å) and kept fixed. In the subsequent refinement, the function $\sum w(F_o^2 - F_c^2)^2$ was minimized, where $|F_o|$ and $|F_c|$ are the observed and calculated structure factor amplitudes, respectively. The agreement indices are defined as $R_1 = \sum(||F_o| - |F_c||)/\sum|F_o|$ and $wR_2 = [\sum w(F_o^2 - F_c^2)^2 / \sum(wF_o^4)]^{1/2}$. All calculations were performed by using Crystal Structure 4.0 or Yadokari-XG 2009 and illustrations were drawn by using ORTEP–3.

---

[14] Burla, M. C.; Caliandro, R.; Camalli, M.; Carrozzini, B.; Cascarano, G. L.; De Caro, L.; Giacovazzo, C.; Polidori, G.; Siliqi, D.; Spagna, R. *J. Appl. Cryst.* **2007,** *40*, 609–613.

[15] Burla, M. C.; Caliandro, R.; Camalli, M.; Carrozzini, B.; Cascarano, G. L.; De Caro, L.; Giacovazzo, C.; Polidori, G.; Spagna, R. *J. Appl. Cryst.* **2005,** *38*, 381–388.

[16] Sheldrick, G. M. Program for the Solution of Crystal Structures; University of Göttingen, Germany, 1997.

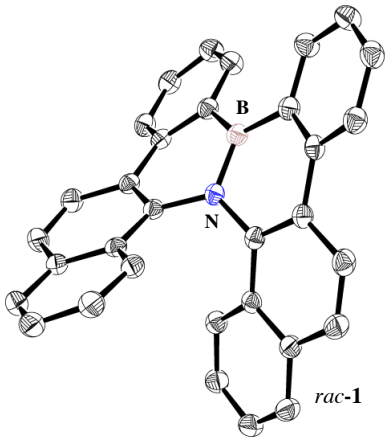

rac-**1**

Formula	$C_{32}H_{20}BN$
Formula Weight	429.33
Temperature, K	173
Wavelength, Å	0.71070
Crystal System	Monoclinic
Space Group	*C*2/*c* (No. 15)
a, Å	19.508(3)
b, Å	9.6906(10)
c, Å	15.2967(19)
α, deg	90
β, deg	133.054(3)
γ, deg	90
Volume, Å	2113.0(5)
Z	4
$Density_{calcd}$, g·cm^{-3}	1.349

Abs. Coefficient, cm^{-1}	0.077
F(000)	896.00
Crystal Size, mm^3	0.1, 0.1, 0.1
$2\theta_{min}$, $2\theta_{max}$, deg	6.0, 51.0
Index Ranges	–23≤h≤21
	–11≤k≤11
	–18≤l≤18
Reflections (unique)	1963
Reflections (I>2.0σ(I))	1456
Parameters	155
GOF on F^2	1.001
R_1 (I>2.0σ(I))	0.0443
R, wR_2 (all data)	0.0638, 0.1157
Largest diff peak and hole, e, Å^{-3}	0.20, –0.20

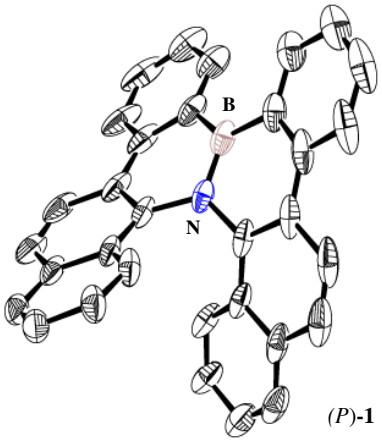

(*P*)-**1**

Formula	$C_{32}H_{20}BN$
Formula Weight	429.30
Temperature, K	273*
Wavelength, Å	0.71070
Crystal System	Trigonal
Space Group	$P3_121$ (No. 152)
a, Å	10.240(3)
b, Å	10.240(3)
c, Å	18.097(6)
α, deg	90
β, deg	90
γ, deg	120
Volume, Å	1643.3(10)
Z	3
$Density_{calcd}$, g·cm^{-3}	1.301

Abs. Coefficient, cm^{-1}	0.074
F(000)	672.00
Crystal Size, mm^3	0.2, 0.2, 0.2
$2\theta_{min}$, $2\theta_{max}$, deg	6.4, 51.0
Index Ranges	–12≤h≤12
	–12≤k≤11
	–21≤l≤20
Reflections (unique)	2051
Reflections (I>2.0σ(I))	1417
Parameters	155
GOF on F^2	1.097
R_1 (I>2.0σ(I))	0.0792
R, wR_2 (all data)	0.1158, 0.1728
Largest diff peak and hole, e, Å^{-3}	0.10, –0.11

*A phase transition occured at low temperature

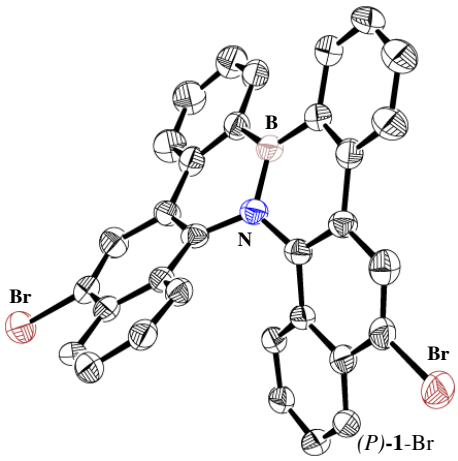

(*P*)-**1**-Br

Formula	$C_{32}H_{18}BNBr_2$
Formula Weight	630.19
Temperature, K	173
Wavelength, Å	0.71070
Crystal System	Orthorhombic
Space Group	$P222_1$ (No. 17)
a, Å	9.696(3)
b, Å	12.111(4)
c, Å	23.872(7)
α, deg	90
β, deg	90
γ, deg	90
Volume, Å	2803.3(15)
Z	4
$Density_{calcd}$, g·cm^{-3}	1.493

Abs. Coefficient, cm^{-1}	2.917
F(000)	1268.0
Crystal Size, mm^3	0.1, 0.1, 0.05
$2\theta_{min}$, $2\theta_{max}$, deg	6.1, 51.0
Index Ranges	–11≤h≤10
	–14≤k≤14
	–28≤l≤28
Reflections (unique)	5227
Reflections (I>2.0σ(I))	4186
Parameters	354
GOF on F^2	1.073
R_1 (I>2.0σ(I))	0.0510
R, wR_2 (all data)	0.0650, 0.1278
Flack's parameter	–0.033(14)
Largest diff peak and hole, e, Å^{-3}	0.46, –0.52

Figure 9. X-ray crystal structures of *rac*-**1**, (*P*)-**1** and (*P*)-**1**-Br (left), and crystal data and structure refinement (right). Thermal ellipsoids are shown at 50% [*rac*-**1**, (*P*)-**1**-Br] or 30% [(*P*)-**1**] probability and H atoms have been omitted for clarity.

Charge mobility measurement by time of flight (TOF) method. Purchased glasses (Nippon Sheet Glass Co. Ltd.) were used as a transparent substrate. These glasses were cleaned in a detergent solution for 5 minutes and then in distilled water for 10 minutes by ultrasonication. After predrying by a jet spin washer, they were dried finally for 5 minutes in 150 °C oven. Aluminum and 16c-aza-8a-boradibenzo[*i*,*l*]hexahelicene (**1**) were vacuum deposited sequentially on the glasses to fabricate a photocell with an Al/**1**/Al structure. The pressure of the vacuum system was 5.0×10^{-3} Pa during deposition. Firstly, to fabricate the under translucent electrode, a 10 nm aluminum electrode layer was deposited at a rate of 0.1–0.5 nm/s through a 2.0 mm metal shadow mask on the cleaned glasses. Then 6.0–10 μm thin films of **1** were evaporated at a rate of 3.0–10 nm/s on the Al layer through a larger metal shadow mask than 2.0 mm. Finally, 50 nm aluminum top electrode layer was deposited at a rate of 0.1–0.5 nm/s through a 2.0 mm shadow mask, resulting in a active area of 4.0 mm^2. The thickness of every layer was controlled with a calibrated quartz crystal microbalance during deposition. TOF measurements were performed using a commercial TOF-401 system (Sumitomo Heavy Industries Advanced Machinery Co., Ltd.) at room temperature under various electric fields. First, a dye laser (USHO, Pulsed Dye Laser KEC-160) with a wavelength of 365 nm was used to form the carriers by illuminating from the glass side. Voltage pulses and transient current were recorded by a digitizing oscilloscope (Tektronix TDS 3052B). The normalized light intensity versus frequency curve was used to determine the transit time and mobility. The details of the TOF analysis can be found in page 69–70 of "Organic Electroluminescence Materials and Displays" (CMC Co., Ltd.).

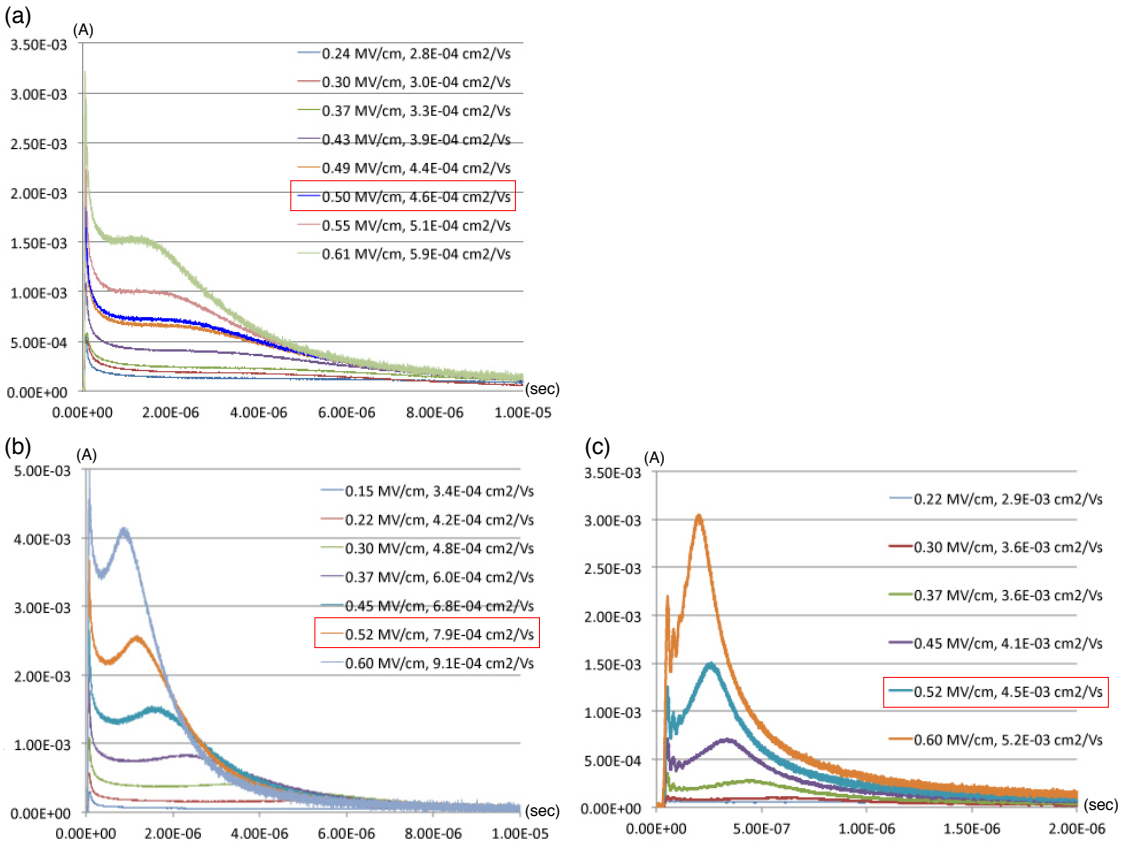

Figure 10. Transient photocurrent of (a) *rac*-**1** (hole), (b) *(P)*-**1** (hole), and (c) *(P)*-**1** (electron).

Ionization potential measurement by photoelectron spectroscopy in air (PESA). Glass structures coated with indium-tin-oxide (ITO) were cleaned in a detergent solution for 5 minutes and then in distilled water 10 minutes by ultrasonication. After predrying by a jet spin washer, they were dried finally for 5 minutes in 150 °C oven. A 60–80 nm thin films of *rac*-**1** and (*P*)-**1** were vacuum deposited at a rate of 0.5–1.0 nm/s on the cleaned glasses. The pressure of the vacuum system was 5.0×10^{-3} Pa, and the film thickness was controlled with a calibrated quartz crystal microbalance during deposition. Ionization potential (IP) of the thin films were measured by photoelectron spectroscopy in air (PSAE) using an AC-1 (RIKEN KEIKI Co., Ltd.) system at room temperature. Electron affinities were estimated from the ionization potentials and UV-visible absorption edge wavelengths of the thin films prepared side by side.

Computational studies. Molecular orbital calculations and nucleus-independent chemical shift (NICS) calculations were performed with Gaussian 09[17] packages. The DFT method was employed using the B3LYP hybrid functional.[18] Structures were optimized with the 6-31G(d) basis set.[19] Nucleus independent chemical shifts (NICS) were evaluated by using the gauge invariant atomic orbital[20] (GIAO) approach at the GIAO-B3LYP/6-311+G(d,p) level. The reorganization energy calculations were performed using the B3LYP hybrid functional with the DZP basis set[21] in the ADF program.[22] The electronic coupling calculations of dimers were performed by the local density functional VWN in the conjunction with the PW91[23] gradient corrections with the DZP basis set, as implemented in the ADF program according to the literature.[5]

---

[17] Gaussian 09, Revision B.01, Frisch, M. J.; Trucks, G. W.; Schlegel, H. B.; Scuseria, G. E.; Robb, M. A.; Cheeseman, J. R.; Scalmani, G.; Barone, V.; Mennucci, B.; Petersson, G. A.; Nakatsuji, H.; Caricato, M.; Li, X.; Hratchian, H. P.; Izmaylov, A. F.; Bloino, J.; Zheng, G.; Sonnenberg, J. L.; Hada, M.; Ehara, M.; Toyota, K.; Fukuda, R.; Hasegawa, J.; Ishida, M.; Nakajima, T.; Honda, Y.; Kitao, O.; Nakai, H.; Vreven, T.; Montgomery, Jr., J. A.; Peralta, J. E.; Ogliaro, F.; Bearpark, M.; Heyd, J. J.; Brothers, E.; Kudin, K. N.; Staroverov, V. N.; Kobayashi, R.; Normand, J.; Raghavachari, K.; Rendell, A.; Burant, J. C.; Iyengar, S. S.; Tomasi, J.; Cossi, M.; Rega, N.; Millam, N. J.; Klene, M.; Knox, J. E.; Cross, J. B.; Bakken, V.; Adamo, C.; Jaramillo, J.; Gomperts, R.; Stratmann, R. E.; Yazyev, O.; Austin, A. J.; Cammi, R.; Pomelli, C.; Ochterski, J. W.; Martin, R. L.; Morokuma, K.; Zakrzewski, V. G.; Voth, G. A.; Salvador, P.; Dannenberg, J. J.; Dapprich, S.; Daniels, A. D.; Farkas, Ö.; Foresman, J. B.; Ortiz, J. V.; Cioslowski, J.; Fox, D. J. Gaussian, Inc., Wallingford CT, 2009.

[18] (a) Becke, A. D. *J. Chem. Phys.* **1993,** *98*, 5648–5652. (b) Lee, C.; Yang, W.; Parr, R. G. *Phys. Rev. B* **1988,** *37*, 785–789.

[19] Hehre, W. J.; Radom, L.; Schleyer, P. v. R.; Pople, J. A. *Ab Initio Molecular Orbital Theory*; John Wiley & Sons: New York, **1986** and references cited therein.

[20] (a) Dichtfield, R. *Mol. Phys.* **1974,** *27*, 789–807. (b) Wolinski, K.; Hinton, J. F.; Pulay, P. *J. Am. Chem. Soc.* **1990,** *112*, 8251–8260.

[21] van Lenthe, E.; Baerends, E. J. *J. Comput. Chem.* **2003,** *24*, 1142–1156.

[22] ADF2010, SCM, Theoretical Chemistry, Vrije Universiteit, Amsterdam, The Netherlands.

[23] Perdew, J. P.; Chevary, J. A.; Vosko, S. H.; Jackson, K. A.; Pederson, M. R.; Sing, D. J.; Fiolhais, C. *Phys. Rev. B* **1992,** *46*, 6671–6687.

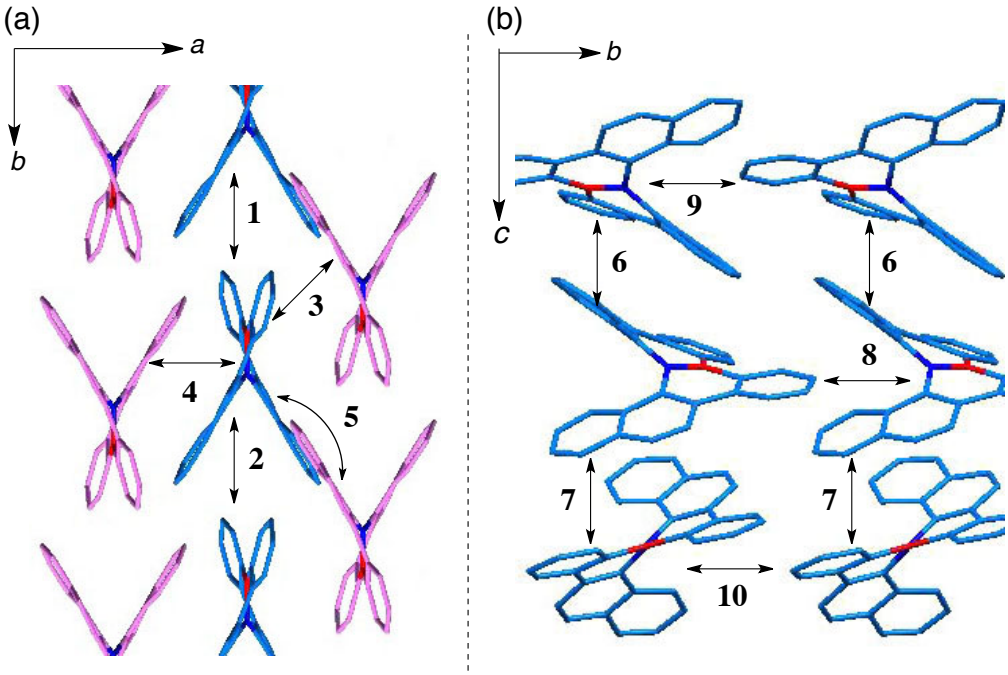

Electron couplings V (meV) between HOMOs of neighboring molecules

	|V| (meV)	V (eV)	H1 (eV)	H2 (eV)	J (eV)	S
1	7.7	0.007656739	-5.48909	-5.51842	0.01982	-0.00221
2	7.7	0.007656739	-5.51842	-5.48909	0.01982	-0.00221
3	13.9	0.013859982	-5.47693	-5.47686	0.03396	-0.00367
4	42	-0.041952101	-5.35567	-5.35566	-0.0894	0.00886
5	11.8	0.011754524	-5.52237	-5.52237	0.03042	-0.00338
6	30.1	0.030082597	-5.34375	-5.34399	0.06316	-0.00619
7	30.1	-0.030072535	-5.34398	-5.34378	-0.06315	0.00619
8	1.0	0.001047774	-5.56279	-5.54834	0.00327	-0.0004
9	9.8	0.009842044	-5.52712	-5.54843	0.02568	-0.00286
10	1.0	0.001007762	-5.56288	-5.54831	0.00323	-0.0004

Electron couplings V (meV) between LUMOs of neighboring molecules

	|V| (meV)	V (eV)	H1 (eV)	H2 (eV)	J (eV)	S
1	3.4	0.003426833	-2.75576	-2.79058	0.0062	-0.001
2	3.4	0.003426833	-2.79058	-2.75576	0.0062	-0.001
3	4.3	-0.00428792	-2.72346	-2.7234	-0.00023	-0.00149
4	7.2	0.007153884	-2.70812	-2.70813	0.00886	-0.00063
5	1.4	0.001368556	-2.80412	-2.80413	0.00235	-0.00035
6	73.1	-0.073136621	-2.57352	-2.57244	-0.10755	0.01338
7	73.2	0.073156825	-2.57244	-2.57349	0.10757	-0.01338
8	5.6	-0.005605295	-2.79743	-2.77966	-0.00884	0.00116
9	19.7	0.019711493	-2.75786	-2.77758	0.03164	-0.00431
10	5.7	-0.005665348	-2.7972	-2.7798	-0.0089	0.00116

Figure 11. Electron couplings *V* (meV) of neighboring molecules in the X-ray crystal structures of *rac*-**1** (a) and *(P)*-**1** (b) at the PW91/DZP level on ADF2010 program. H atoms have been omitted for clarity. The *P* enantiomer is shown in blue and the *M* enantiomer is shown in pink. *V* (eV) = [J – 0.5S(H1 + H2)]/(1 – S^2), J (eV): charge transfer integral, H1 and H2 (eV): site energies, S: overlap integral.

Cartesian coordinates

(*P*)-**1**

Center Number	Atomic Number	Atomic Type	Coordinates X	Y	Z
1	5	0	-1.796902	-0.000032	-0.000121
2	7	0	-0.345854	-0.000040	0.000032
3	6	0	-0.278296	2.429467	0.047357
4	6	0	1.532265	1.169304	1.155989
5	6	0	2.218707	2.401072	1.410859
6	6	0	0.323497	1.199682	0.363298
7	6	0	0.426180	3.631495	0.351407
8	6	0	-1.626052	2.480971	-0.539086
9	6	0	1.648275	3.622900	0.963862
10	6	0	2.051312	-0.007705	1.763780
11	6	0	3.916982	1.226903	2.701435
12	6	0	-2.453115	1.328401	-0.442105
13	6	0	-3.438986	3.685385	-1.629267
14	6	0	3.206268	0.020778	2.516173
15	6	0	3.421494	2.392960	2.164001
16	6	0	-4.263801	2.559037	-1.531201
17	6	0	-3.765455	1.397345	-0.952484
18	6	0	-2.136223	3.644854	-1.146816
19	1	0	-0.033120	4.582613	0.107259
20	1	0	2.167929	4.554530	1.172227
21	1	0	1.523529	-0.945886	1.656907
22	1	0	4.834592	1.235184	3.283297
23	1	0	-3.809630	4.593380	-2.098172
24	1	0	3.567441	-0.895490	2.975006
25	1	0	3.933363	3.338439	2.327333
26	1	0	-5.277484	2.586620	-1.921704
27	1	0	-4.391090	0.510673	-0.930205
28	1	0	-1.508427	4.521401	-1.268060
29	6	0	-0.278348	-2.429523	-0.047405
30	6	0	1.532236	-1.169365	-1.155987
31	6	0	2.218632	-2.401146	-1.410937
32	6	0	0.323494	-1.199749	-0.363283
33	6	0	0.426073	-3.631573	-0.351559
34	6	0	-1.626146	-2.480971	0.539040
35	6	0	1.648161	-3.622984	-0.964037
36	6	0	2.051327	0.007669	-1.763680
37	6	0	3.917018	-1.226916	-2.701325
38	6	0	-2.453213	-1.328400	0.441966
39	6	0	-3.439061	-3.685205	1.629462
40	6	0	3.206329	-0.020779	-2.516007
41	6	0	3.421447	-2.393003	-2.164040
42	6	0	-4.263887	-2.558901	1.531210
43	6	0	-3.765533	-1.397270	0.952361
44	6	0	-2.136288	-3.644747	1.146995
45	1	0	-0.033313	-4.582667	-0.107516
46	1	0	2.167788	-4.554601	-1.172522
47	1	0	1.523509	0.945845	-1.656797
48	1	0	4.834679	-1.235165	-3.283100
49	1	0	-3.809675	-4.593122	2.098544
50	1	0	3.567567	0.895526	-2.974715
51	1	0	3.933280	-3.338497	-2.327416
52	1	0	-5.277564	-2.586426	1.921732
53	1	0	-4.391153	-0.510592	0.929988
54	1	0	-1.508478	-4.521246	1.268458

TS-**1**

Center Number	Atomic Number	Atomic Type	Coordinates X	Y	Z
1	5	0	-1.654750	0.000664	-0.776700
2	7	0	-0.223387	0.000278	-0.547077
3	6	0	-0.475844	-2.095010	0.710586
4	6	0	1.719902	-1.650966	-0.208579
5	6	0	2.313756	-2.532804	0.756783
6	6	0	0.354524	-1.228195	-0.018069
7	6	0	0.131374	-2.968631	1.663462
8	6	0	-1.897671	-2.218901	0.351895
9	6	0	1.489127	-3.096307	1.766789
10	6	0	2.446051	-1.427858	-1.406701
11	6	0	4.375134	-2.605420	-0.533702
12	6	0	-2.430000	-1.340662	-0.627724
13	6	0	-3.935075	-3.548646	0.275573
14	6	0	3.730344	-1.901833	-1.573821
15	6	0	3.667665	-2.926710	0.604074
16	6	0	-4.438403	-2.729720	-0.741875
17	6	0	-3.696244	-1.634192	-1.166618
18	6	0	-2.679458	-3.299299	0.812378
19	1	0	-0.508089	-3.519324	2.344387
20	1	0	1.934100	-3.720750	2.536899
21	1	0	1.937522	-0.959246	-2.237122
22	1	0	5.400949	-2.941704	-0.656743
23	1	0	-4.514054	-4.396576	0.632317
24	1	0	4.242631	-1.744010	-2.519008
25	1	0	4.115222	-3.547547	1.376554
26	1	0	-5.406019	-2.942411	-1.188377

27	1	0	-4.109742	-1.001271	-1.944075
28	1	0	-2.288421	-3.983776	1.556949
29	6	0	-0.474028	2.096155	0.710028
30	6	0	1.720780	1.650604	-0.210877
31	6	0	2.315864	2.533144	0.753067
32	6	0	0.355378	1.228727	-0.018965
33	6	0	0.134481	2.970399	1.661530
34	6	0	-1.896316	2.219996	0.353104
35	6	0	1.492365	3.097913	1.763262
36	6	0	2.446124	1.425290	-1.409055
37	6	0	4.376569	2.602551	-0.538652
38	6	0	-2.429742	1.341976	-0.626140
39	6	0	-3.934259	3.549158	0.280155
40	6	0	3.730798	1.897781	-1.577369
41	6	0	3.669900	2.926047	0.598998
42	6	0	-4.438832	2.730389	-0.736797
43	6	0	-3.696959	1.635231	-1.162938
44	6	0	-2.677827	3.299964	0.815093
45	1	0	-0.504030	3.521799	2.342757
46	1	0	1.938271	3.722951	2.532350
47	1	0	1.936726	0.956003	-2.238576
48	1	0	5.402582	2.937866	-0.662677
49	1	0	-4.513001	4.396751	0.638083
50	1	0	4.242531	1.738084	-2.522541
51	1	0	4.118322	3.547589	1.370409
52	1	0	-5.407221	2.942837	-1.181737
53	1	0	-4.111603	1.002206	-1.939671
54	1	0	-2.286075	3.984225	1.559473

(*M*)-**1**

Center Number		Atomic Number	Atomic Type	Coordinates X	Y	Z
1	5	0	1.796830	0.000138	-0.000039	
2	7	0	0.345762	-0.000017	0.000098	
3	6	0	0.278524	-2.429516	-0.047317	
4	6	0	-1.532132	-1.169550	-1.155983	
5	6	0	-2.218353	-2.401418	-1.411005	
6	6	0	-0.323425	-1.199811	-0.363242	
7	6	0	-0.425645	-3.631658	-0.351655	
8	6	0	1.626286	-2.480800	0.539228	
9	6	0	-1.647708	-3.623211	-0.964201	
10	6	0	-2.051358	0.007427	-1.763679	
11	6	0	-3.916849	-1.227382	-2.701436	
12	6	0	2.453254	-1.328172	0.442028	
13	6	0	3.439287	-3.684797	1.629778	
14	6	0	-3.206318	-0.021157	-2.516060	
15	6	0	-3.421149	-2.393412	-2.164149	
16	6	0	4.264045	-2.558457	1.531333	
17	6	0	3.765610	-1.396924	0.952347	
18	6	0	2.136502	-3.644468	1.147323	
19	1	0	0.033913	-4.582698	-0.107724	
20	1	0	-2.167166	-4.554890	-1.172835	
21	1	0	-1.523665	0.945679	-1.656764	
22	1	0	-4.834487	-1.235741	-3.283250	
23	1	0	3.809971	-4.592623	2.098980	
24	1	0	-3.567616	0.895116	-2.974787	
25	1	0	-3.932843	-3.338971	-2.327580	
26	1	0	5.277747	-2.585855	1.921802	
27	1	0	4.391221	-0.510238	0.929840	
28	1	0	1.508721	-4.520975	1.268903	
29	6	0	0.278028	2.429504	0.047178	
30	6	0	-1.532381	1.169271	1.156019	
31	6	0	-2.218885	2.401014	1.410870	
32	6	0	-0.323661	1.199693	0.363245	
33	6	0	-0.426516	3.631497	0.351240	
34	6	0	1.625811	2.481032	-0.539269	
35	6	0	-1.648564	3.622845	0.963785	
36	6	0	-2.051342	-0.007720	1.763903	
37	6	0	-3.917044	1.226837	2.701593	
38	6	0	2.452966	1.328536	-0.442147	
39	6	0	3.438733	3.685435	-1.629518	
40	6	0	-3.206275	0.020733	2.516326	
41	6	0	-3.421626	2.392887	2.164099	
42	6	0	4.263646	2.559184	-1.531210	
43	6	0	3.765344	1.397526	-0.952398	
44	6	0	2.135936	3.644872	-1.147151	
45	1	0	0.032689	4.582640	0.107049	
46	1	0	-2.168239	4.554460	1.172176	
47	1	0	-1.523472	-0.945871	1.657102	
48	1	0	-4.834635	1.235074	3.283483	
49	1	0	3.809339	4.593390	-2.098534	
50	1	0	-3.567395	-0.895547	2.975177	
51	1	0	-3.933500	3.338370	2.327400	
52	1	0	5.277362	2.586818	-1.921625	
53	1	0	4.391034	0.510896	-0.929945	
54	1	0	1.508092	4.521347	-1.268609	

Chapter 3

Synthesis of BN-fused Polycyclic Aromatic Compounds Containing Five-membered Heterocyclic Ring

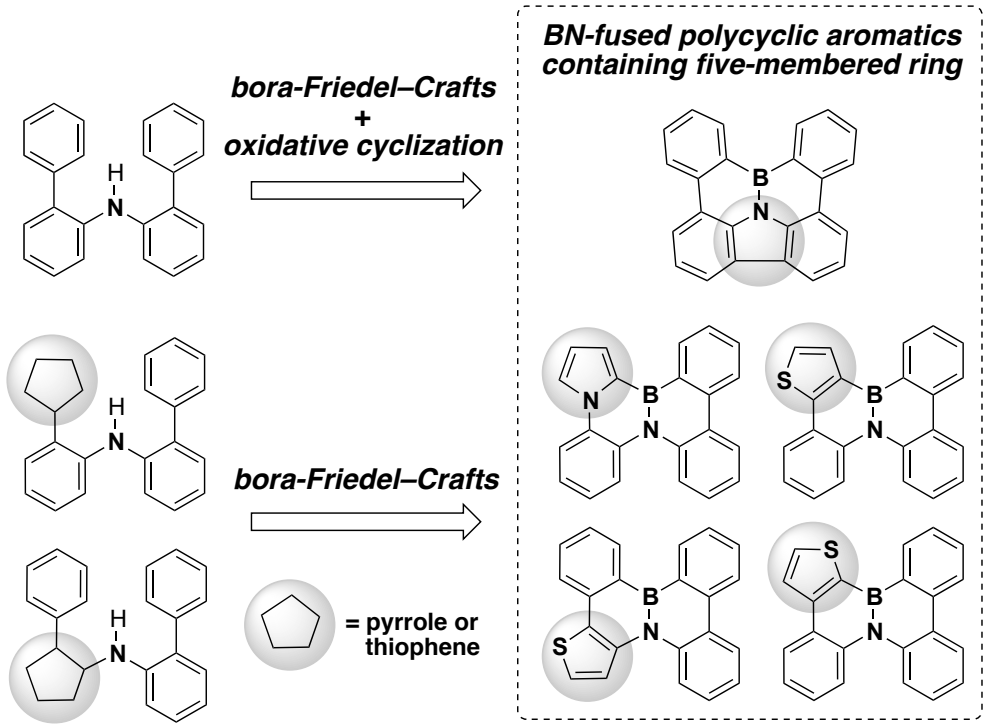

Abstract: 14b[1]-Aza-14b-borabenzo[*p*]indeno[1,2,3,4-*defg*]chrysene has been synthesized from bis(biphenyl-2-yl)amine *via* intramolecular oxidative cyclization and tandem bora-Friedel–Crafts reaction. Further, BN-fused polycyclic aromatic compounds including a thiophene or pyrrole ring have been synthesized *via* the bora-Friedel–Crafts reaction from the corresponding diarylamines. As compared with 4b-aza-12b-boradibenzo[*g*,*p*]chrysene, the benzoindenochrysene derivative shows a higher quantum yield, and the pyrrole-fused derivative shows higher charge mobility, as suggested by electron coupling calculations. The proposed synthetic methodologies can provide facile access to various BN-fused polycyclic aromatic compounds containing a five-membered heterocyclic ring.

Chapter 3

3-1. Introduction

Polycyclic heteroaromatic compounds, in which one or more carbocyclic rings are replaced by a five-membered heterocyclic rings, constitute one of the most important classes of small-molecule semiconducting materials.[1] In particular, one-dimensionally extended ladder-type heteroaromatic compounds including sulfur or nitrogen atoms have been extensively studied.[2,3,4] The planar π-conjugated system of these compounds increases the effective conjugation length,[5] and their rigid structure can suppress conformational disorder and hence decrease the reorganization energy, thus enhancing the intrinsic charge mobility. On the other hand, in polycyclic heteroaromatic compounds containing two-dimensionally extended π-conjugation systems, effective charge transport is expected because the large π-conjugated framework induces a solid-state packing arrangement that in turn may facilitate multichannel interactions.[6] However, because of the lack of a suitable synthetic

---

[1] (a) Anthony, J. E. *Chem. Rev.* **2006,** *106*, 5028–5048. (b) Wang, C.; Dong, H.; Hu, W.; Liu, Y.; Zhu, D. *Chem. Rev.* **2012,** *112*, 2208–2267.

[2] Sulfur: Review; (a) Takimiya, K.; Shinamura, S.; Osaka, I.; Miyazaki, E. *Adv. Mater.* **2011,** *23*, 4347–4370. Selected examples; (b) Laquindanum, J. G.; Katz, H. E.; Lovinger, A. J. *J. Am. Chem. Soc.* **1998,** *120*, 664–672. (c) Xiao, K.; Liu, Y.; Qi, T.; Zhang, W.; Wang, F.; Gao, J.; Qiu, W.; Ma, Y.; Cui, G.; Chen, S.; Zhan, X.; Yu, G.; Qin, J.; Hu, W.; Zhu, D. *J. Am. Chem. Soc.* **2005,** *127*, 13281–13286. (d) Wex, B.; Kaafarani, B. R.; Schroeder, R.; Majewski, L. A.; Burckel, P.; Grell, M.; Neckers, D. C. *J. Mater. Chem.* **2006,** *16*, 1121–1124. (e) Tang, M. L.; Okamoto, T.; Bao, Z. N. *J. Am. Chem. Soc.* **2006,** *128*, 16002–16003. (f) Valiyev, F.; Hu, W. S.; Chen, H. Y.; Kuo, M. Y.; Chao, I.; Tao, Y. T. *Chem. Mater.* **2007,** *19*, 3018–3026. (g) Gao, J.; Li, R.; Li, L.; Meng, Q.; Jiang, H.; Li, H.; Hu, W. *Adv. Mater.* **2007,** *19*, 3008–3011. (h) Yamada, K.; Okamoto, T.; Kudoh, K.; Wakamiya, A.; Yamaguchi, S.; Takeya, J. *Appl. Phys. Lett.* **2007,** *90*, 072102-1–3. (i) Chen, Y.; Chang, H.; Tian, H.; Bao, C.; Li, W.; Yan, D.; Geng, Y.; Wang, F. *Org. Electron.* **2012,** *13*, 3268–3275. (j) Huang, J.; Luo, H.; Wang, L.; Guo, Y.; Zhang, W.; Chen, H.; Zhu, M.; Liu, Y.; Yu, G. *Org. Lett.* **2012,** *14*, 3300–3303.

[3] Nitrogen: Reviews; (a) Bunz, U. H. F. *Chem. Eur. J.* **2009,** *15*, 6780–6789. (b) Richards, G. J.; Hill, J. P.; Mori, T.; Ariga, K. *Org. Biomol. Chem.* **2011,** *9*, 5005–5017. Selected examples; (c) Miao, Q.; Nguyen, T.-Q.; Someya, T.; Blanchet, G. B.; Nuckolls, C. *J. Am. Chem. Soc.* **2003,** *125*, 10284–10287. (d) Wakim, S.; Bouchard, J.; Simard, M.; Drolet, N.; Tao, Y.; Leclerc, M. *Chem. Mater.* **2004,** *16*, 4386–4388. (e) Ma, Y.; Sun, Y.; Liu, Y.; Gao, J.; Chen, S.; Sun, X.; Qiu, W.; Yu, G.; Cui, G.; Hu, W.; Zhu, D. *J. Mater. Chem.* **2005,** *15*, 4894–4898. (f) Wu, Y.; Li, Y.; Gardner, S.; Ong, B. S. *J. Am. Chem. Soc.* **2005,** *127*, 614–618. (g) Kawaguchi, K.; Nakano, K.; Nozaki, K. *J. Org. Chem.* **2007,** *72*, 5119–5128. (h) Ahmed, E.; Briseno, A. L.; Xia, Y.; Jenekhe, S. A. *J. Am. Chem. Soc.* **2008,** *130*, 1118–1119. (i) Pho, T. V.; Yuen, J. D.; Kurzman, J. A.; Smith, B. G.; Miao, M.; Walker, W. T. Seshadri, R.; Wudl, F. *J. Am. Chem. Soc.* **2012,** *134*, 18185–18188.

[4] S,N-hybridized: (a) Qi, T.; Guo, Y.; Liu, Y.; Xi, H.; Zhang, H.; Gao, X.; Liu, Y.; Lu, K.; Du, C.; Yu, G.; Zhu, D. *Chem. Commun.* **2008,** 6227–6229. (b) Gao, P.; Cho, D.; Yang, X.; Enkelmann, V.; Baumgarten, M.; Müllen, K. *Chem. Eur. J.* **2010,** *16*, 5119–5128. (c) Wu, J.-S.; Cheng, Y.-J.; Lin, T.-Y.; Shih, P.-I.; Hsu, C.-S. *Adv. Funct. Mater.* **2012,** *22*, 1711–1722. (d) Kato, S.-i.; Furuya, T.; Kobayashi, A.; Nitani, M.; Ie, Y.; Aso, Y.; Yoshihara, T.; Tobita, S.; Nakamura, Y. *J. Org. Chem.* **2012,** *77*, 7595–7606.

[5] (a) Patil, S. A.; Scherf, U.; Kadashchuk, A. *Adv. Funct. Mater.* **2003,** *13*, 609–614. (b) Mishra, A. K.; Graf, M.; Grasse, F.; Jacob, J.; List, E. J. W.; Müllen, K. *Chem. Mater.* **2006,** *18*, 2879–2885.

[6] (a) Sun, Y. M.; Tan, L.; Jiang, S. D.; Qian, H. L.; Wang, Z. H.; Yan, D. W.; Di, C. G.; Wang, Y.; Wu, W. P.; Yu, G.; Yan, S. K.; Wang, C. R.; Hu, W. P.; Liu, Y. Q.; Zhu, D. B. *J. Am. Chem. Soc.*

methodology, two-dimensional polycyclic heteroaromatic compounds have not been studied in detail. Because the synthetic method of BN-fused two-dimensional polycyclic aromatic compounds has been established by using tandem bora-Friedel–Crafts reaction in Chapter 1, this author envisioned that two strategies for construction of BN-fused two-dimensional polycyclic aromatic compounds including heterocyclic five-membered ring would worth studying for the synthesis of two-dimensionally extended polycyclic heteroaromatic compounds: 1) formation of a five-membered ring *via* intramolecular oxidative cyclization of BN-fused polycyclic aromatic compounds and 2) introduction of a five-membered heteroaromatic ring and subsequent bora-Friedel–Crafts reaction (Scheme 1). This chapter describes the syntheses of 14b[1]-aza-14b-borabenzo[*p*]indeno[1,2,3,4-*defg*]chrysene **1** and BN-fused polycyclic aromatic compounds including nitrogen (**2**) or sulfur (**3**, **4**, **5**) heterocycles.

Scheme 1. Synthesis of BN-fused polycyclic aromatic compounds including a five-membered heterocyclic ring

1) Formation of a five-membered ring *via* intramolecular oxidative cyclization of BN-fused polycyclic aromatic compounds

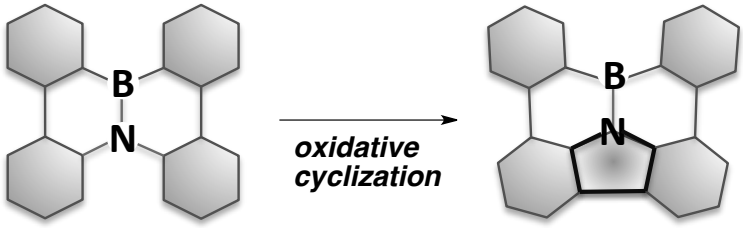

2) Introduction of a five-membered heteroaromatic ring and subsequent bora-Friedel–Crafts reaction

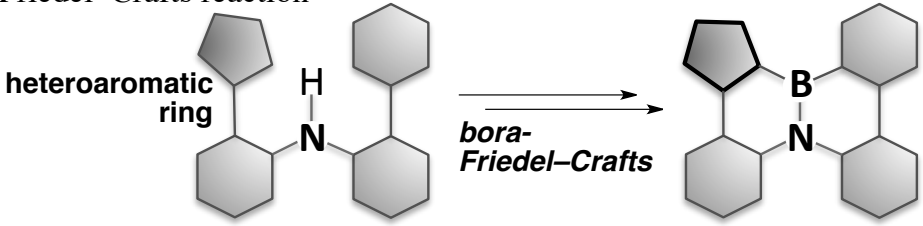

Chart 1. BN-fused polycyclic aromatic compounds including a five-membered heterocyclic ring

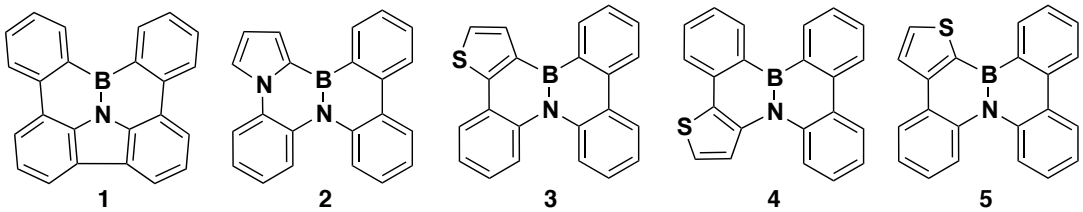

2007, *129*, 1882–1883. (b) Wang, J.-Y.; Zhou, Y.; Yan, J.; Ding, L.; Ma, Y.; Cao, Y.; Wang, J.; Pei, J. *Chem. Mater*. **2009,** *21*, 2595–2597.

3-2. Results and Discussion

3-2-1. Development of oxidative cyclization and screening of reaction conditions

To investigate the feasibility of intramolecular oxidative cyclization,[7] 4b-aza-12b-boradibenzo[*g*,*p*]chrysene **6** was treated with various Lewis acids (Table 1). The target compound, 14b[1]-aza-14b-borabenzo[*p*]indeno[1,2,3,4-*defg*]chrysene **1**, was obtained in 40% yield when 2 equiv of $AlCl_3$ was used (entry 1). However, reactions with $FeCl_3$, CoF_3, $MoCl_5$, and $SbCl_5$ did not afford the desired product (entries 2–5). The yield increased when the reaction was carried out using 0.25 equiv of *N*,*N*-diisopropylethylamine (NEt^iPr_2); however, the reaction was terminated upon the addition of excess (0.50 equiv) NEt^iPr_2 (entries 6–7). This result suggested that the reaction would proceed only under acidic conditions.

Table 1. Oxidative cyclization of BN-fused precursor **6**

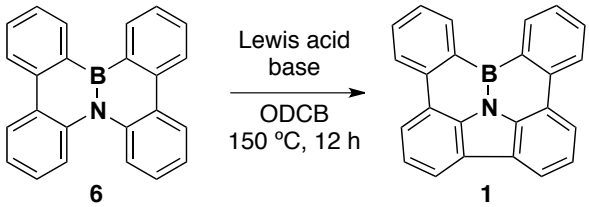

6 **1**

entry[a]	Lewis acid (equiv)	base (equiv)	yield[b] of **1**(%)
1	$AlCl_3$ (2.0)	none	40
2	$FeCl_3$ (2.0)	none	ND
3	CoF_3 (2.0)	none	ND
4	$MoCl_5$ (2.0)	none	ND
5	$SbCl_5$ (2.0)	none	ND
6	$AlCl_3$ (2.0)	NEt^iPr_2 (0.25)	70
7	$AlCl_3$ (2.0)	NEt^iPr_2 (0.50)	ND

[a] Reactions were carried out on a 0.1 mmol scale. [b] The yield was determined by ^1H NMR.

The desired compound **1** was also obtained in a cascade manner, albeit in very low (5%) yield, when aminoboron dichloride **8**, which was prepared *in situ* from bis(biphenyl-2-yl)amine **7**, was treated with $AlCl_3$ in *o*-dichlorobenzene at 150 °C for 12 h (Scheme 2). Compound **6** was not obtained because of the possible decomposition under acidic conditions (see Chapter 1). Table 2 summarizes the results of screening for the one-pot synthesis of **1**. A mixture of $AlCl_3$ (4 equiv) and NEt^iPr_2 (1 equiv) afforded **1** in moderate yield (39%, entry 3), but the product yield decreased when using 0.5, 1.5, and 2.0 equiv of NEt^iPr_2 (entries 2, 4, 5), indicating that the $AlCl_3$/NEt^iPr_2 stoichiometry plays an important role in enhancing the product yield and promoting the bora-Friedel–Crafts reaction. However, 2,2,6,6-tetramethylpiperidine was not as effective as NEt^iPr_2 in the reaction (entries 6–8).

[7] Formation of carbazole moiety *via* oxidative cyclization: (a) El-Zohry, M. F. *Indian J. Chem. B* **1993,** *32*, 275–280. (b) Fox, M. A.; Dulay, M. T.; Krosley, K. *J. Am. Chem. Soc.* **1994,** *116*, 10992–10999. (c) Yamamoto, M.; Matsubara, S. *Chem. Lett.* **2007,** *36*, 172–173.

Scheme 2. One-pot synthesis of **1** from diarylamine **7**

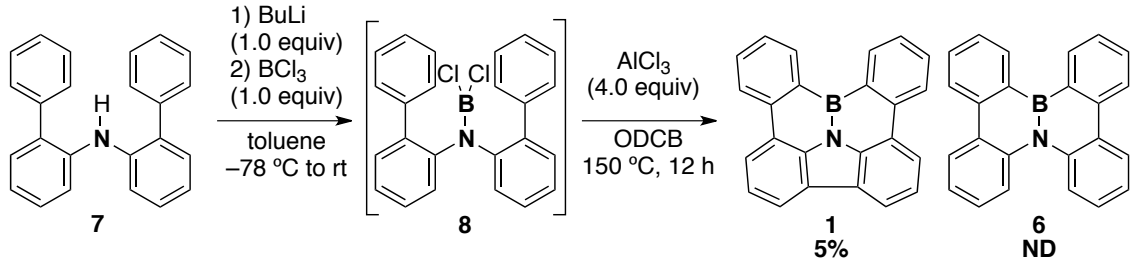

Table 2. Screening additives for one-pot synthesis

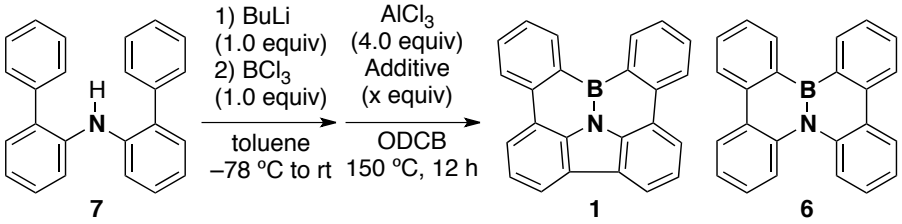

entry[a]	additive (equiv)	yield[b] (%) **1**	**6**
1	none	5	ND
2	NEt^iPr_2 (0.5)	19	ND
3	NEt^iPr_2 (1.0)	**39**	ND
4	NEt^iPr_2 (1.5)	10	30
5	NEt^iPr_2 (2.0)	ND	ND
6	2,2,6,6-tetramethylpiperidine (0.5)	9	ND
7	2,2,6,6-tetramethylpiperidine (1.0)	13	ND
8	2,2,6,6-tetramethylpiperidine (1.5)	ND	64

[a] Reactions were carried out on a 0.6 mmol scale. [b] The yield was determined by ^{1}H NMR.

The treatment of dibenzo[*g*,*p*]chrysene **9** with $AlCl_3$ did not give the cyclized product **10** or **11** (Scheme 3), implying that replacement of the C–C unit by a B–N unit would play an important role in the cyclization. That is, the introduction of a B–N moiety to various PAH frameworks would enable the stepwise construction of a carbazole substructure in BN-fused aromatic compounds.

Scheme 3. Cyclization of dibenzo[*g*,*p*]chrysene **9**

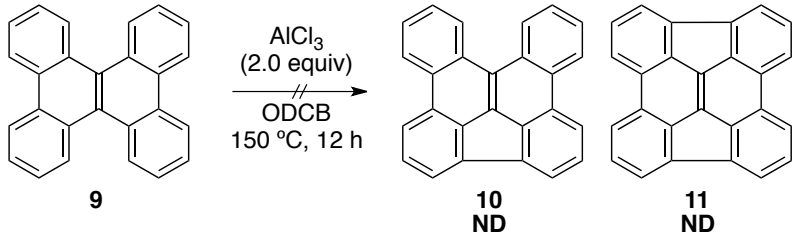

3-2-2. Molecular and electronic structures of 1

The highly planar structure of **1** was confirmed by X-ray crystallography (Figure 1). The B–N bond length [1.409(2) Å] in **1** was shorter than that in typical BN aromatic compounds (1.45–1.47 Å), confirming the double-bond character. Moreover, the B–C1, B–C2, C5–C7, and C6–C8 lengths in **1** were 1.584(3), 1.575(3), 1.473(2), and 1.473(2) Å, respectively, indicating that these are single bonds. The N–C3, N–C4, C3–C7, and C4–C8 lengths, on the other hand, were 1.392(2), 1.392(2), 1.391(1), and 1.393(2) Å, respectively, indicating that these are one-and-a-half bonds. These observations suggested that the carbazole moiety in **1** is isolated from the π-conjugated system.

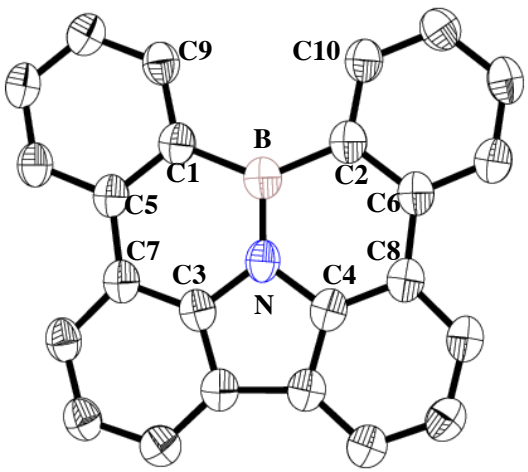

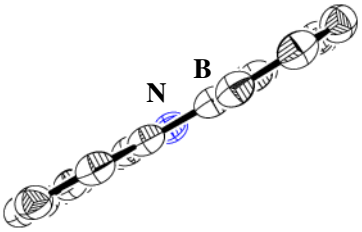

Selected bond lengths:			
B–N	1.409(2) Å	C1–C5	1.435(2) Å
B–C1	1.584(3) Å	C3–C7	1.391(2) Å
B–C2	1.575(3) Å	C5–C7	1.473(2) Å
N–C3	1.392(2) Å	C2–C6	1.436(2) Å
N–C4	1.392(2) Å	C4–C8	1.393(2) Å
		C6–C8	1.473(2) Å

Dihedral angles: C5–C7–C6–C8 0.83°
C9–C1–C2–C10 1.79°

Figure 1. ORTEP drawing of **1**. Thermal ellipsoids are shown at 50% probability. H atoms have been omitted for clarity.

The aromaticities of the five- and six-membered rings in **1** and **6** were evaluated by a nucleus-independent chemical shift (NICS) analysis (Figure 2). Because of the formation of the highly aromatic carbazole ring, the BNC_4 rings in **1** have less aromaticity than those of **6** [–2.3 *vs*. –2.9 in NICS(1)].

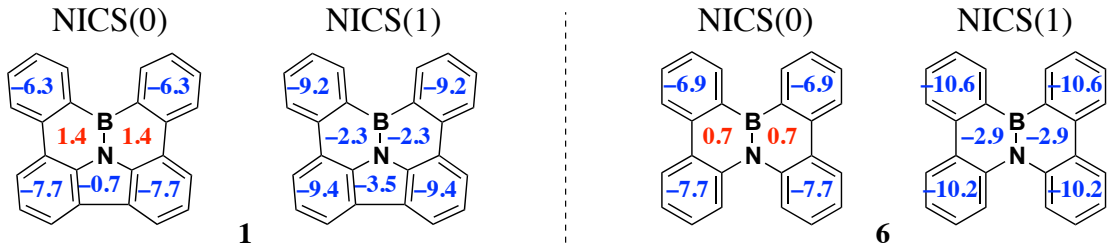

Figure 2. NICS values calculated at the B3LYP/6–311+G(d) level.

Because of the weak steric repulsion between the hydrogen atoms at the *ortho* position to boron, **1** adopts a slightly twisted structure (C9–C1–C2–C10 dihedral angle = 1.79°) and hence has an axis of helical chirality, which allows for the formation of

racemic co-crystals. The molecules are arranged in a herringbone stacking array with a π–π distance of 3.4–3.6 Å and a CH–π distance of 2.7–3.0 Å (Figure 3a). In this arrangement, the local dipole moments of the B–N bonds partially offset each other despite the alternate arrangement in **6**, because the dipole moment of **1** is smaller than that of **6** according to the calculated values at the B3LYP/6-31G(d) level (Figures 3b–c, 0.06 *vs*. 0.37 Debye).

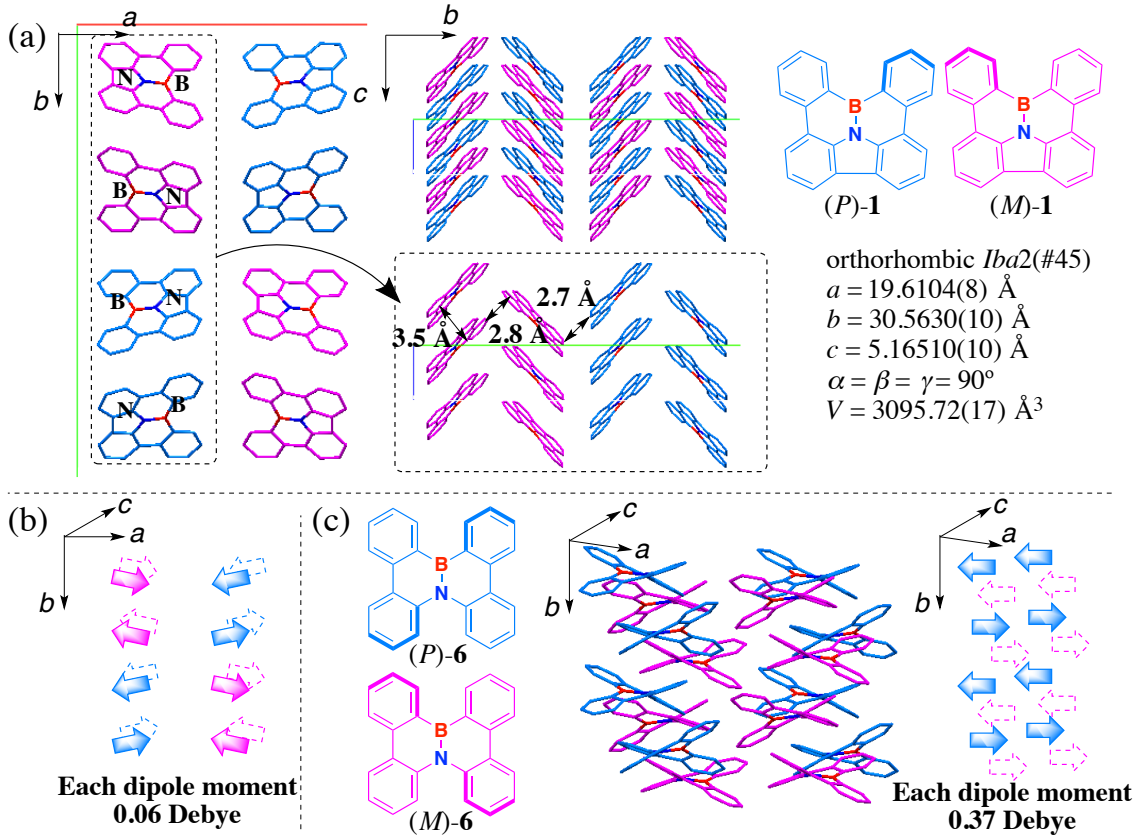

Figure 3. (a) Packing structure of **1**. (b, c) Molecular orientations of **1** and **6** defined by individual dipole moments. H atoms have been omitted for clarity. The *P*-enantiomer is shown in blue, and the *M*-enantiomer is shown in pink.

3-2-3. Photochemical properties of 1

To reveal the photochemical properties of **1**, UV-visible absorption and photoluminescence spectra were measured in dichloromethane solution (Figure 4). Compound **1** exhibited a relatively strong absorption band with a maximum (λ_{abs}) at 370 nm (corresponding to a π–π^* transition) and a shoulder at 352 nm. The photoluminescence emission demonstrated a first maximum at 372 nm and vibronic fine structures at 390 and 409 nm. The small Stokes shift of ca. 0.02 eV indicated that the geometry of the excited state of **1** is similar to that of the ground state, probably because of the rigid geometry as well as the small dipole moment (0.06 Debye).

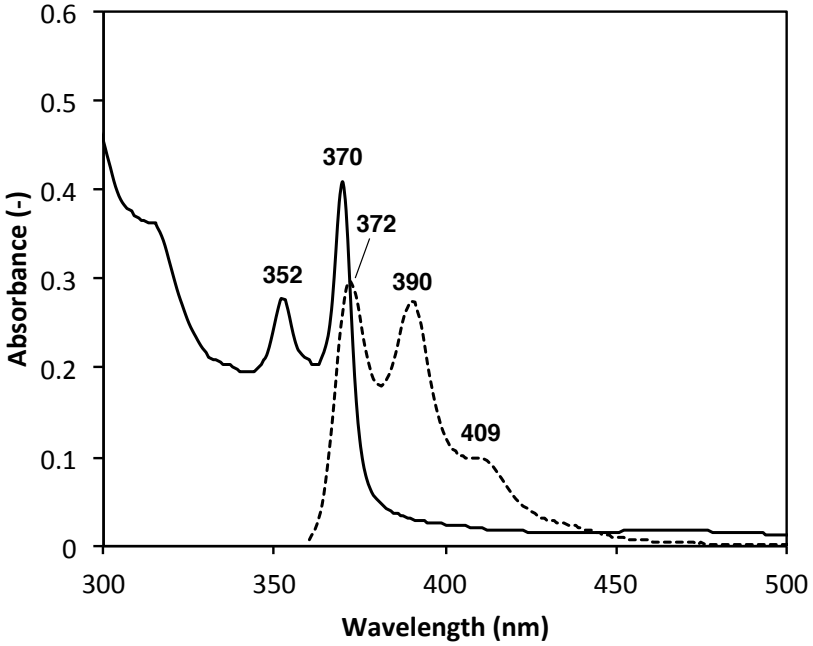

Figure 4. UV-visible absorption (solid line) and fluorescence (dotted line, excited at 350 nm) spectra of **1** in CH_2Cl_2 solution (2.0×10^{-5} M).

Table 3 summarizes the photophysical data of **1** and its precursor **6**. Because of the extended effective conjugation length, the longest absorption maximum for **1** is longer than that of **6**. In contrast, the Stokes shift of **1** is smaller than that of **6** (2 nm *vs*. 70 nm), which is due to the flexibility and relatively large dipole moment (0.37 Debye) of the latter. It is noteworthy that the quantum yield of **1** (Φ_f = 0.35) exceeds that of **6** (Φ_f = 0.10). Thus, the aforementioned cyclization-based transformation may be an efficient means of inducing photoluminescence in BN-fused polycyclic aromatic compounds.

Table 3. Summary of photophysical data for **1** and **6**

Compound	λ_{ab}[a] (nm)	log ε ($M^{-1}cm^{-1}$)	λ_{em}[b] (nm)	Φ_f[c]	$HOMO_{calc}$[d] (eV)	$LUMO_{calc}$[d] (eV)
1	370	4.38	372	0.35	–5.73	–1.64
6	340	4.06	410	0.10	–5.49	–1.24

[a] Only the longest absorption maxima are shown. [b] Emission maxima upon excitation at 350 nm (**1**) and 340 nm (**6**). [c] Absolute fluorescence quantum yields determined by a calibrated integrating sphere system with ≤ 3% error. [d] Calculated at the B3LYP/6-31G(d) level.

3-2-4. Evaluation of charge transport properties on the basis of calculated electronic coupling elements

The electronic coupling V (meV) between neighboring molecules was calculated from the X-ray crystal structure of **1** by using the PW91 hybrid functional with the DZP basis set of the ADF2010 program (Figure 5). The V values between lowest-unoccupied molecular orbitals (LUMOs) were relatively larger than the corresponding values between the highest-occupied molecular orbitals (HOMOs). Notably, there was a significant difference between the values along the *c*-axis for different isomers (15.7 *vs*. 0.5 meV, Figure 5b).

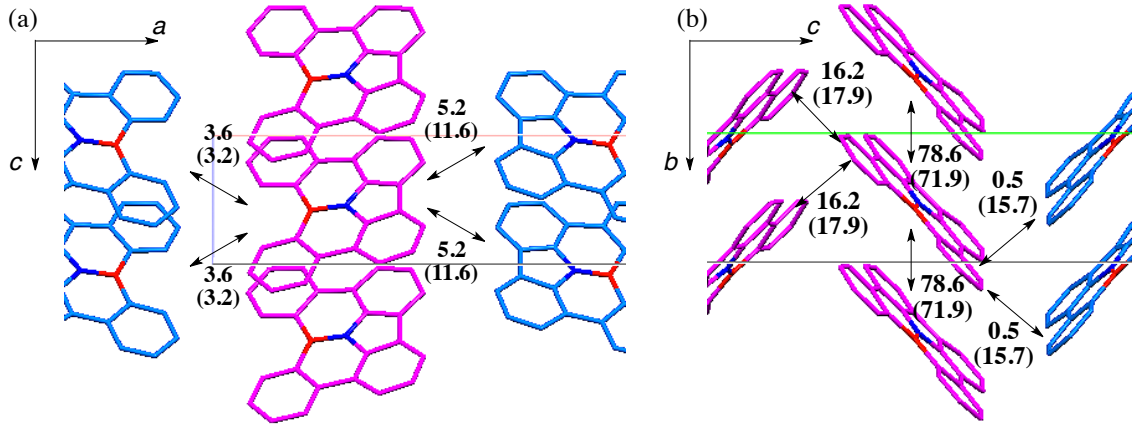

Figure 5. Electronic coupling, V (in meV), between HOMOs of neighboring molecules in the X-ray crystal structure of **1** (*P* in blue, *M* in pink). The electronic coupling between the LUMOs is shown in parentheses.

To understand this difference better, a single-point calculation for adjacent molecules was performed. The overlapping adjacent HOMOs and LUMOs along the *c*-axis are visualized in Figure 6. The HOMOs overlap in the antibonding position (Figure 6a), whereas the LUMOs show efficient same-phase overlap (Figure 6b), and this feature results in different V values in the two cases. Thus, **1** is a potential candidate for an electron transport material.

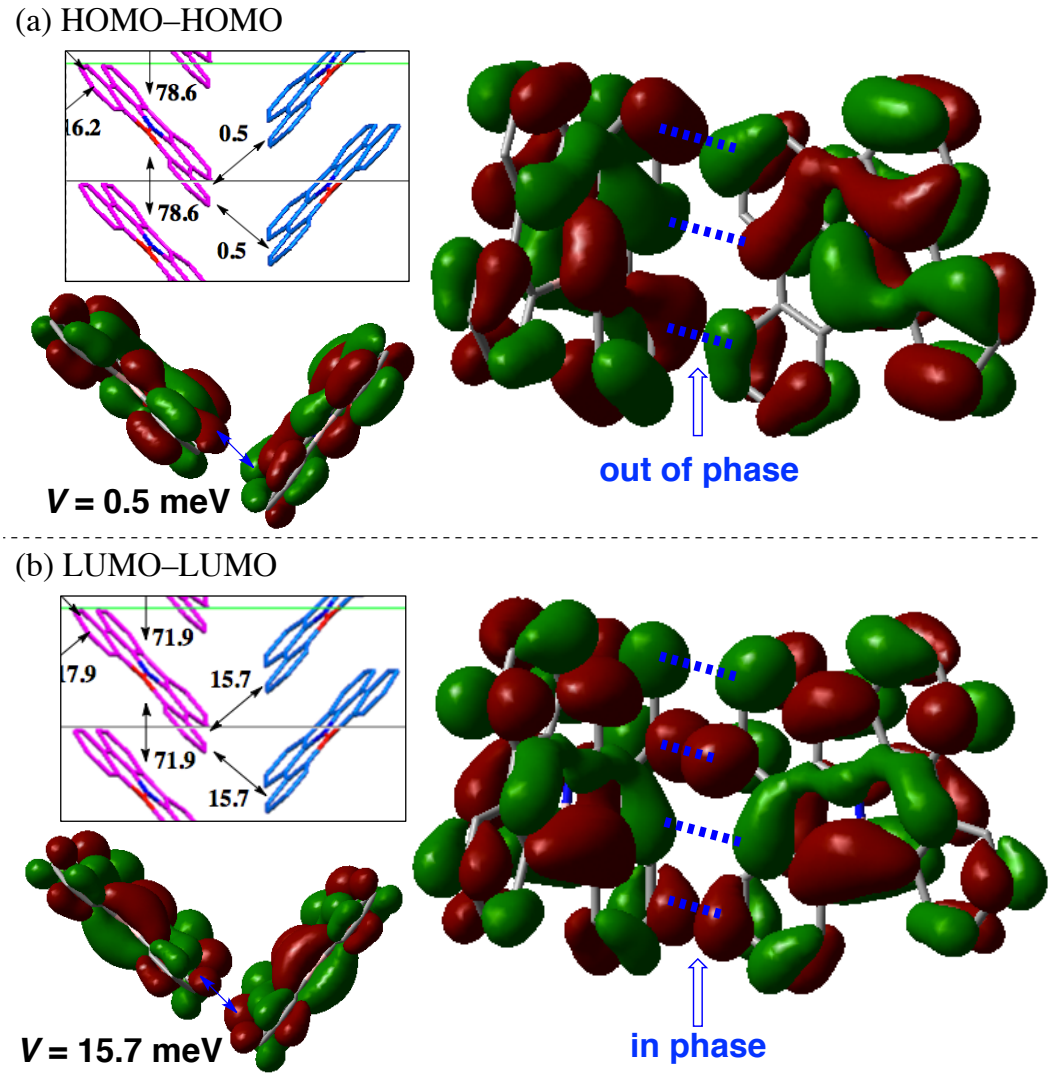

Figure 6. Overlapping adjacent HOMOs and LUMOs of **1**.

3-2-5. Synthesis of BN-fused polycyclic aromatic compounds including a pyrrole ring

Compound **2**, which includes a pyrrole ring, was designed with the aim of investigating non-planar BN-fused polycyclic aromatic compounds having a five-membered heterocyclic ring. Borylation of diaryl amine **12** by treatment with BuLi and BCl_3 and subsequent tandem bora-Friedel–Crafts reaction with $AlCl_3$ and 2,2,6,6-tetramethylpiperidine afforded **2** in very low (4%) yield (Scheme 4), although the starting amine **12** was consumed. The poor yield could be attributed to the formation of oligomeric by-products resulting from dimerization or other side reactions, which were initiated by electrophilic attack on the pyrrole ring under the harsh reaction conditions adopted.

Scheme 4. Synthesis of **2** *via* bora-Friedel–Crafts reaction

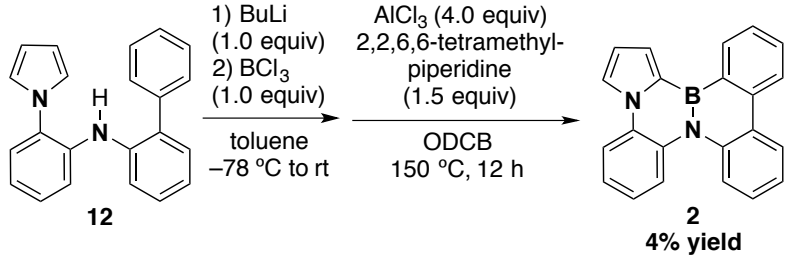

The structure of **2** was determined using X-ray crystallography; its molecular structure is shown in Figure 7. The B–N length [1.441(2) Å] in **2** was similar to that in typical BN aromatic compounds (1.45–1.47 Å).[3–5] On the other hand, the B–C1, B–C2, N1–C3, and N1–C4 lengths were 1.527(2), 1.536(2), 1.429(2), and 1.4218(19) Å, respectively, indicating that these are single bonds. Because of steric repulsion between the hydrogen atoms at the *ortho* position to the heteroatoms (C5–C1–C2–C6 dihedral angle = 32.41°), **2** adopts a twisted conformation, similar to **6**,[8] and hence has a similar packing structure (Figure 7b). In this arrangement, the pyrrole rings are located on the opposite faces of adjacent molecules so that the local dipole moments offset each other.

[8] X-ray crystal structure and parameters of **6** are mentioned in chapter 1-2-2.

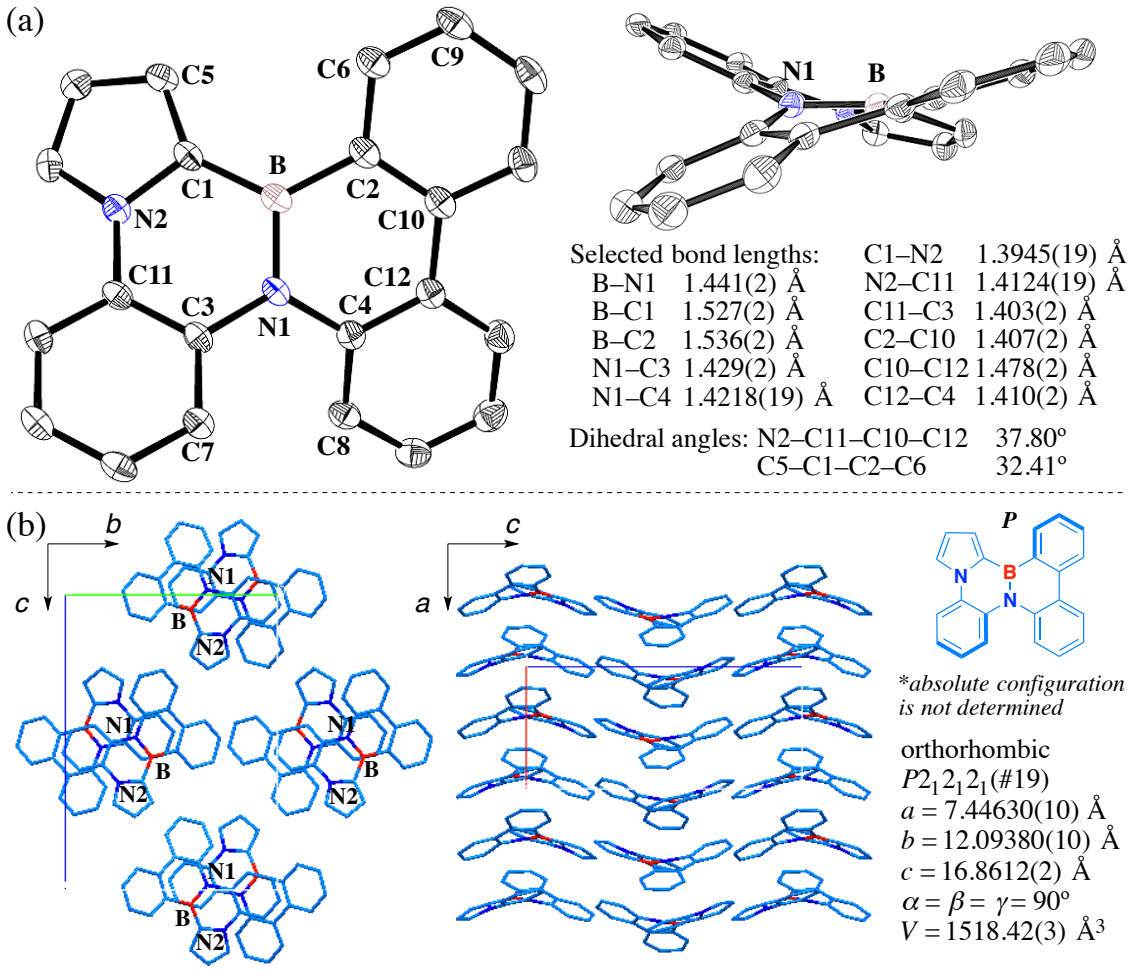

Figure 7. ORTEP drawing and packing structure of (*P*)-**2** (absolute configuration is not determined). Thermal ellipsoids are shown at 50% probability and H atoms have been omitted for clarity.

The electronic coupling *V* (meV) was calculated from the X-ray crystal structure of **2** (Figures 8a–b). Although the molecular packing is virtually the same in **2** and **6**, the electronic coupling varies significantly. The *V* values between the HOMOs along the *c*-axis in **2** [11.1, 2.0, and 13.0 meV, (Figure 8b)] are larger than the corresponding values in **6** [2.4, 0.6, and 5.0 meV, (Figure 8d)], while those along the *a*- and *b*-axes are comparable to each other (Figures 8a–d).

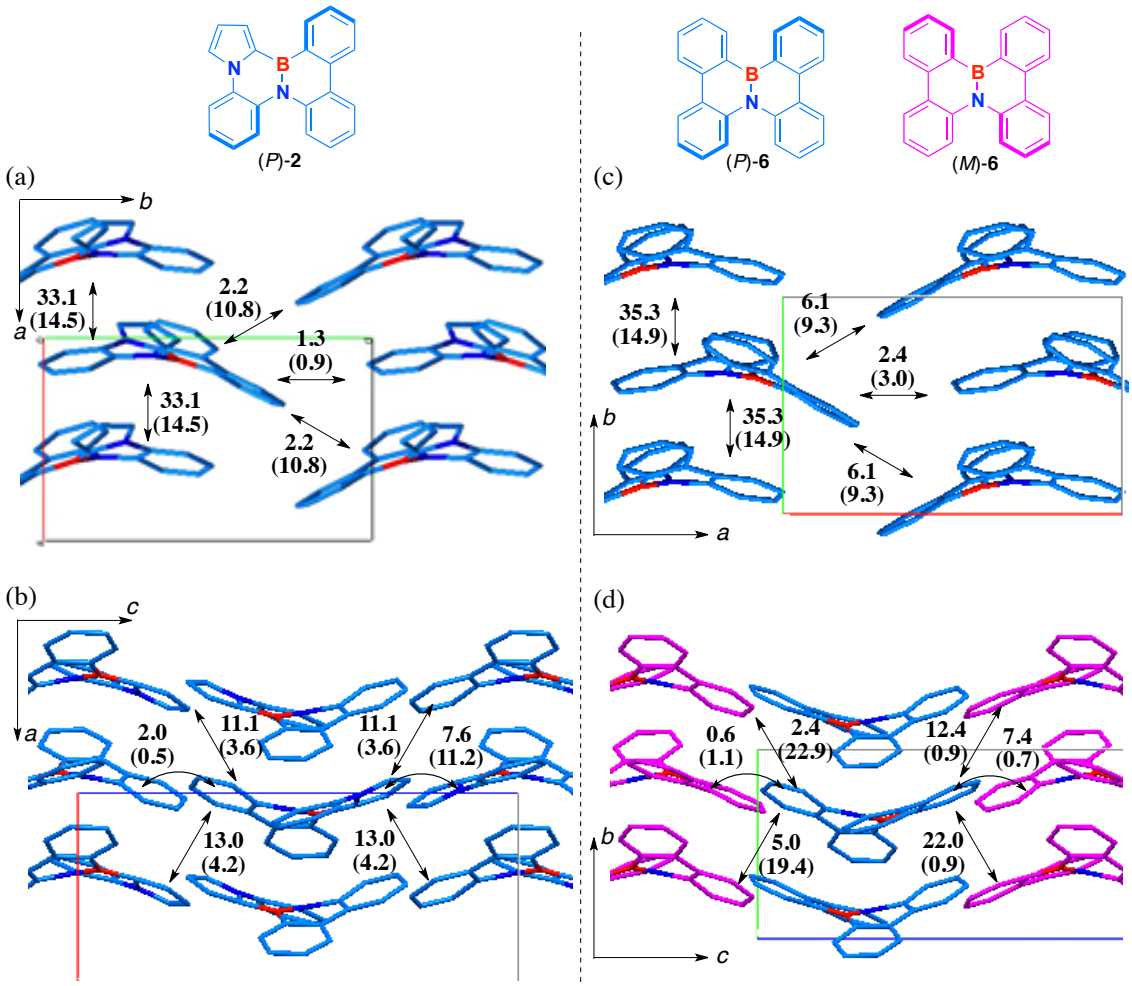

Figure 8. Electronic coupling, *V* (in meV) between HOMOs of neighboring molecules in the X-ray crystal structures of (a, b) **2** and (c, d) **6** (*P* in blue, *M* in pink). The electronic coupling between LUMOs is shown in parentheses.

The Kohn–Sham frontier orbitals and overlapping adjacent HOMOs of **2** and **6** are visualized in Figure 9. The orbitals of **2** are more polarized than those of **6** because of the introduction of the electron-rich pyrrole ring (Figures 9a–b), and hence, the HOMOs of **2** can show efficient same-phase overlap (Figure 9c); however, the HOMOs of **6** overlap in the antibonding position (Figure 9d). Thus, **2** is a potential candidate for a hole transport material.

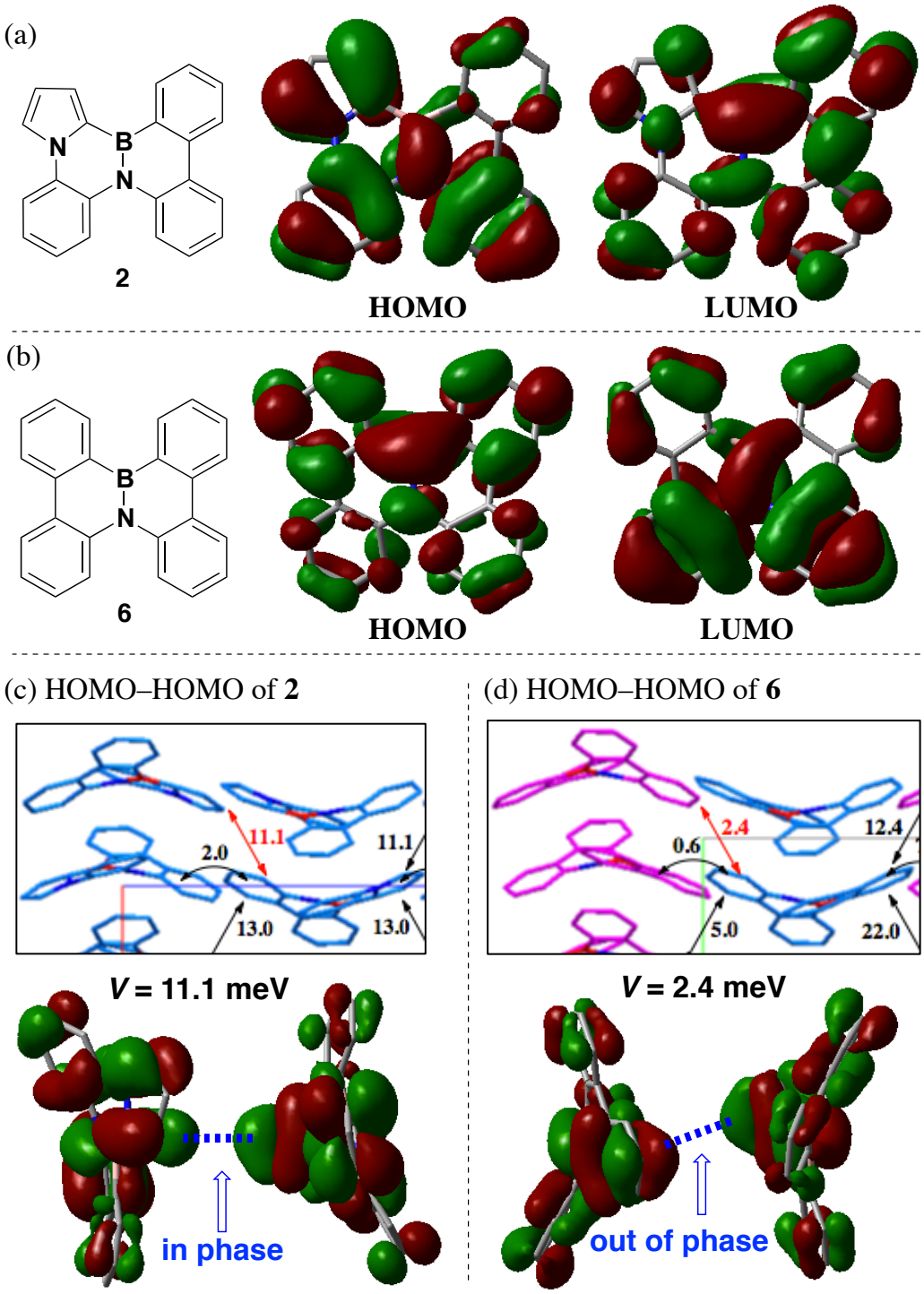

Figure 9. The Kohn–Sham HOMO and LUMO of (a) **2** and (b) **6**, and overlapping adjacent HOMOs of (c) **2** and (d) **6** calculated at the B3LYP/6-31G(d) level.

3-2-6. Synthesis of BN-fused polycyclic aromatic compounds including a thiophene ring

In a further application for the introduction of another heterocyclic unit, BN-fused polycyclic aromatic compounds including a thiophene ring (**3**, **4**, and **5**) were synthesized *via* the bora-Friedel–Crafts reaction (Scheme 5). Borylation of diaryl amines (**13** and **15**) by treatment with BuLi and BCl_3 and subsequent tandem bora-Friedel–Crafts reaction with $AlCl_3$ and 2,2,6,6-tetramethylpiperidine afforded **3** and **4** in 19% and 5% yields, respectively. In the same manner, **17** gave BN-fused product **5** in 8% yield, while another conceivable cyclization product **19** was not generated under these conditions. The product yields were relatively lower in the case of the substrate with a thiophene ring than in the case of substrates without a thiophene moiety. Because the starting amines (**13**, **15**, **17**) were not recovered from the corresponding crude products, the low yield could be attributed to the formation of unidentified higher-molecular-weight by-products generated by oligomerization following the decomposition of the thiophene ring *via* desulfurization.[9]

Scheme 5. Synthesis of **3**–**5** *via* bora-Friedel–Crafts reaction

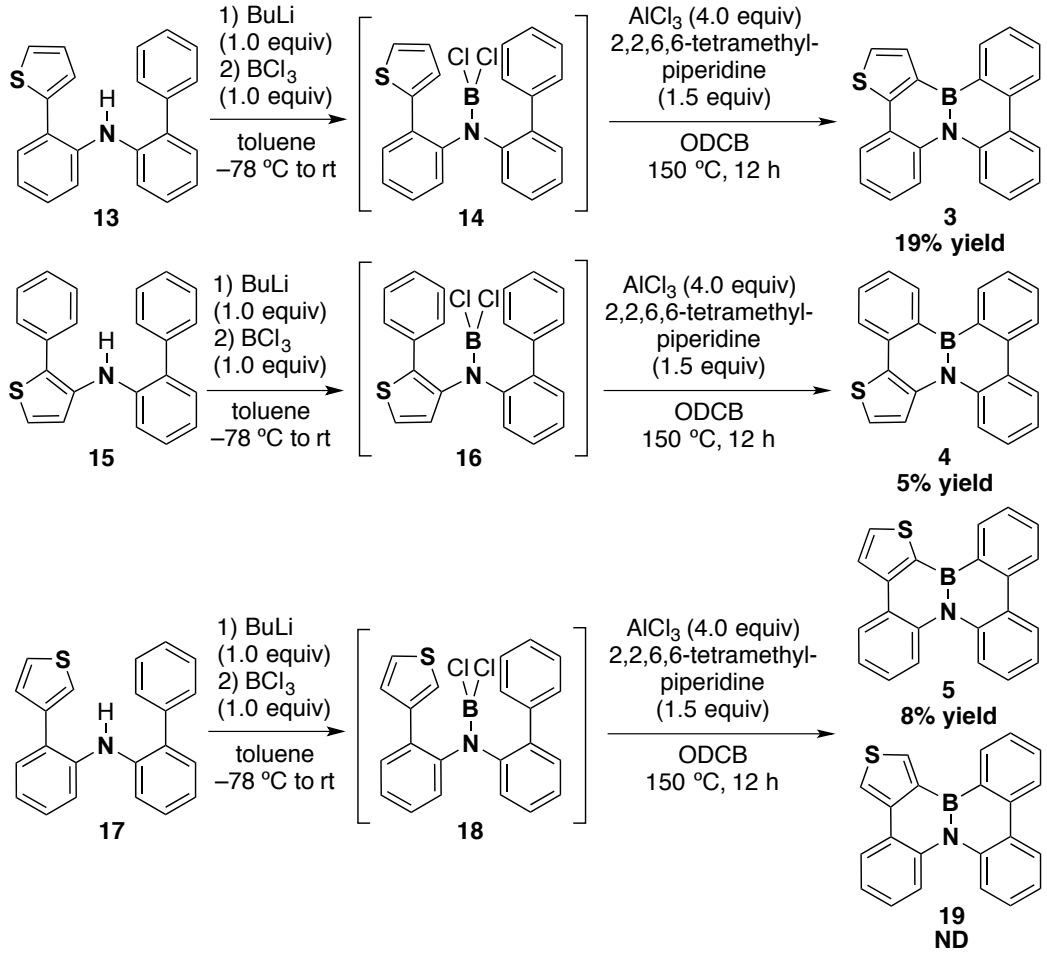

[9] Miki, Y.; Sugimoto, Y.; Yamadaya, S. *Sekiyu Gakkaishi* **1992,** *35*, 332–338.

3-2-7. Regioselectivity at thiophene ring in bora-Friedel–Crafts reaction

To gain a detailed insight into the regioselectivity at the thiophene ring of **18**, the Fukui function [$f(r)$] and molecular orbital values were calculated by the DFT method (Figure 10). Parr and Young reported that sites with the largest Fukui function values show the highest reactivity.[10,11] The condensed Fukui function $f^-(r)$ for nucleophilicity is defined below:

$$f^-(r) = \left(\frac{\partial \rho(r)}{\partial N}\right)_v^- = \rho_N(r) - \rho_{N-1}(r) \qquad \text{(eq. 1)}$$

where $\rho(r)$ is the electronic density (evaluated from natural population analysis), N is the number of electrons, and r is the external potential exerted by the nucleus. A molecule is susceptible to electrophilic attack at the sites where $f^-(r)$ is large. According to the calculation results for **18**, C1 has a larger value of $f^-(r)$ than does C3 (0.277 *vs*. 0.022), and hence, the reaction might occur at the C1 position. This result is in good agreement with the selectivity at other thiophene rings for electrophilic aromatic substitution reactions.[12]

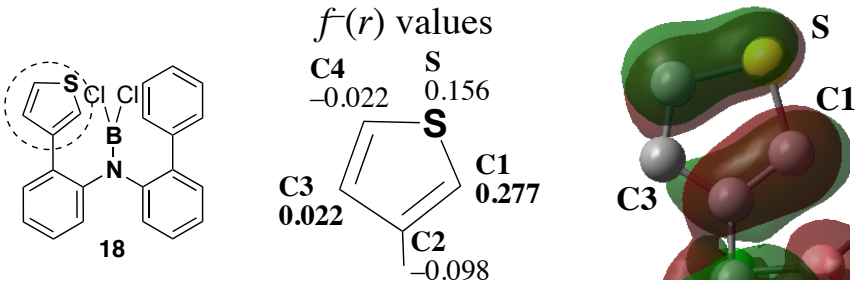

Figure 10. Condensed Fukui function $f^-(r)$ values for nucleophilicity and Kohn–Sham HOMO of **18** calculated at the B3LYP/6-31G(d) level.

---

[10] (a) Parr, R. G.; Yang, W. *J. Am. Chem. Soc.* **1984,** *106*, 4049–4050. (b) Parr, R. G.; Yang, W. *Functional Theory of Atoms and Molecules*, Oxford University Press, New York, **1989**.

[11] Selected examples: (a) Olah, J.; Van Alsenoy, C.; Sannigrahi, A. B. *J. Phys. Chem. A* **2002,** *106*, 3885–3890. (b) Càrdenas, C.; Rabi, N.; Ayers, P. W.; Morell, C.; Jaramillo, P.; Fuentealba, P. *J. Phys. Chem. A* **2009,** *113*, 8660–8667. (c) Mendoza-Huizar, L. H.; Rios-Reyes, C. H. *J. Mex. Chem. Soc.* **2011,** *55*, 142–147. (d) Ghomuri, A.; Mechelleche, S. M. *J. Theor. Comput. Chem.* **2011,** *10*, 435–445.

[12] Belen'kii, L. I.; Suslov, I. A.; Chuvylkin, N. D. *Chem. Heterocycl. Compd.* **2003,** *39*, 36–48.

3-3. Conclusions

In this chapter, the synthesis of highly planar 14b^1-aza-14b-borabenzo[*p*]indeno[1,2,3,4-*defg*]chrysene **1** *via* intramolecular oxidative cyclization of 4b-aza-12b-boradibenzo[*g*,*p*]chrysene **6** is described. Photophysical measurements revealed that the quantum yield of **1** is higher than that of **6**, and electronic coupling calculations suggested that **1** has potential applications as an efficient n-type semiconductor material. The results indicated that the proposed cyclization methodology might be an efficient means of improving physical properties such as quantum yield or charge mobility, relative to those of the cyclization precursors. Further, BN-fused polycyclic aromatic compounds including a five-membered ring were synthesized by the bora-Friedel–Crafts reaction from the corresponding diarylamines containing a heteroaromatic ring instead of the phenyl group. In particular, pyrrole-fused derivative **2** showed crystal packing and twisted geometry similar to **6**, whereas the calculation result suggested that hole mobility may be increased by changes in the electronic polarization. The proposed synthetic methodologies would allow for the easy introduction of five-membered heteroaromatic rings into various BN-fused polycyclic aromatic compounds and aid in the development of optoelectronic functionalized BN-embedded nanocarbon materials.

3-4. Experimental Section

General. All the reactions dealing with air- or moisture-sensitive compounds were carried out in a dry reaction vessel under a positive pressure of argon. Air- and moisture-sensitive liquids and solutions were transferred *via* a syringe or a stainless steel cannula. Organic solutions were concentrated by rotary evaporation at *ca*. 30–400 mmHg. Gel permeation chromatography was performed on a JAIGEL-1H and 2H (20 mm i.d.) with an LC-9204 (Japan Analytical Industry Co., Ltd.).

Instrumentation. Proton nuclear magnetic resonance (^{1}H NMR) and carbon nuclear magnetic resonance (^{13}C NMR) spectra were recorded on JEOL ECS400 (392 MHz) or BRUKER AVANCE III (600 MHz) NMR spectrometers. Proton chemical shift values are reported in parts per million (ppm, δ scale) downfield from tetramethylsilane, and are referenced to the tetramethylsilane (δ 0). ^{13}C NMR spectra were recorded at 98.5 or 151 MHz: carbon chemical shift values are reported in parts per million (ppm, δ scale) downfield from tetramethylsilane, and are referenced to the carbon resonance of CD_2Cl_2 (δ 53.8), C_6D_6 (δ 128.0) and tetramethylsilane (δ 0). ^{11}B NMR spectra were recorded at 131 MHz: boron chemical shift values are reported in parts per million (ppm, δ scale) and are referenced to the external standard boron signal of $BF_3{\cdot}Et_2O$ (δ 0). Data are presented as: chemical shift, multiplicity (s = singlet, d = doublet, t = triplet, q = quartet, quint = quintet, sext = sextet, sept = septet, m = multiplet and/or multiplet resonances, br = broad), coupling constant in hertz (Hz), signal area integration in natural numbers, and assignment (*italic*). IR spectra were recorded on an ATR-FTIR spectrometer (FT/IR-Spectrum One, PerkinElmer). Characteristic IR absorptions are reported in cm^{-1}. Melting points were recorded on a Yanaco MP-500V. High-resolution mass spectra (HRMS) were obtained using the electron impact (EI) method with JEOL JMS-700, JMS-SX102A. UV-visible absorption spectra were measured by JASCO Ubest V-570. Fluorescence spectra were measured by HORIBA Scientific FluoroMax-4. Absolute quantum yields were recorded on a Hamamatsu Photonics C9920-02 Absolute PL Quantum Yield Measurement System. Purity of isolated compounds was determined by GC analysis on Shimadzu GC-2010 Plus instrument equipped with an FID detector and a capillary column, ZB-1MS (Phenomenex, 10 m × 0.10 mm i.d., 0.10 μm film thickness) and/or ^{1}H NMR analyses.

Solvent. *o*-Dichlorobenzene and anhydrous toluene were purchased from Wako Pure Chemical Industries, Ltd. (Wako) and dried over Molecular Sieves 4A and degassed before use. Water content of the solvent was determined with a Karl Fischer Moisture Titrator (MKC-610, Kyoto Electronics Company) to be less than 15 ppm.

Materials. Materials were purchased from Wako, Tokyo Chemical Industry Co., Ltd., Aldrich Inc., Hokko Chemical Industry Co., Ltd., and other commercial suppliers, and

were used after appropriate purification, unless otherwise noted. Florisil® (100–200 mesh) and Celite® were purchased from Wako. Aryl halides and aryl amines were purified by distillation or recrystallization to be over 99.5% pure by GC analysis.

Synthesis of 14b[1]-aza-14b-borabenzo[*p*]indeno[1,2,3,4-*defg*]chrysene (1)

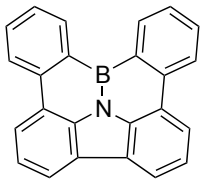

A solution of butyllithium in hexane (1.25 mL, 1.60 M, 2.0 mmol) was added slowly to a solution of **7** (0.643 g, 2.0 mmol) in toluene (10 mL) at –78 ºC under argon. After 1 h, the reaction mixture stirred at 0 ºC for 1 h. A solution of boron trichloride in heptane (2.0 mL, 1.0 M, 2.0 mmol) was added at –78 ºC. After stirring at room temperature for 12 h, solvent was removed *in vacuo*, and the reaction mixture was added to a solution of aluminum trichloride (1.07 g, 8.0 mmol) and NEt^iPr_2 (0.258 g, 2.0 mmol) in *o*-dichlorobenzene (20 mL) at 0 ºC. After stirring at 150 ºC for 12 h, 1,4-diazabicyclo[2.2.2]octane (0.896 g, 8.0 mmol) was added. The reaction mixture was filtered with a pad of Celite®. After the solvent was removed *in vacuo*, the crude product was purified by GPC (eluent: toluene) to obtain the title compound (0.255 g, 39% yield) as white-yellow powder. IR (neat): cm^{-1} 3025 (Ar-H), 1613, 1596, 1545, 1505, 1488, 1464, 1450, 1416, 1351, 1321, 1300, 1281, 1206, 1160, 1144, 1048, 1002, 942, 870, 801, 766, 754, 741, 642, 630, 615, 568; mp: 348.0–349.0 ºC; ^{1}H NMR (CS_2/CD_2Cl_2=2/1, 600 MHz) δ 7.73–7.77 (m, 4H), 7.89 (td, *J* = 1.2, 8.2 Hz, 2H, BCCCHC*H*), 8.26 (dd, *J* = 0.6, 7.8 Hz, 2H, NCCC*H*), 8.48 (dt, *J* = 0.6, 7.8 Hz, 2H, BCCC*H*), 9.23 (dd, *J* = 1.2, 7.8 Hz, 2H, BCC*H*); ^{13}C NMR (CS_2/CD_2Cl_2=2/1, 151 MHz) δ 127.7 (2C), 121.8 (2C), 122.5 (2C), 124.3 (2C), 124.7 (2C), 127.3 (2C), 127.4 (2C), 131.1 (2C), 133.4 (broad, 2C, *C*B*C*), 136.4 (2C), 136.9 (2C), 139.2 (2C); HRMS (EI) *m*/*z* $[M]^+$ calcd for $C_{24}H_{14}NB$ 327.1219; observed 327.1215; Anal. calcd for $C_{24}H_{14}NB$ C, 88.10; H, 4.31; N, 4.28. found C, 88.20; H, 4.57; N, 4.37.

Synthesis of 12b-aza-4b-boradibenzo[*l,k*]pyrrolo[1,2-*f*]phenanthridine (2)

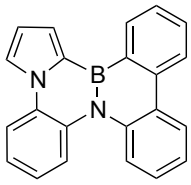

A solution of butyllithium in hexane (1.25 mL, 1.60 M, 2.0 mmol) was added slowly to a solution of **12** (0.621 g, 2.0 mmol) in toluene (10 mL) at –78 ºC under argon. After 1 h, the reaction mixture stirred at 0 ºC for 1 h. A solution of boron trichloride in heptane (2.0 mL, 1.0 M, 2.0 mmol) was added at –78 ºC. After stirring at room temperature for 12 h, solvent was removed *in vacuo*, and the reaction mixture was added to a solution of

aluminum trichloride (1.07 g, 8.0 mmol) and 2,2,6,6-tetramethylpiperidine (0.424 g, 3.0 mmol) in *o*-dichlorobenzene (20 mL) at 0 ºC. After stirring at 150 ºC for 12 h, 1,4-diazabicyclo[2.2.2]octane (0.896 g, 8.0 mmol) was added. The reaction mixture was filtered with a pad of Celite®. After the solvent was removed *in vacuo*, the crude product was purified by GPC (eluent: toluene) to obtain the title compound (0.025 g, 4% yield) as white-yellow powder. IR (neat): cm^{-1} 3058 (Ar-H), 1597, 1576, 1523, 1504, 1486, 1434, 1413, 1349, 1306, 1276, 1247, 1214, 1174, 1135, 1114, 1097, 1052, 1032, 929, 857, 784, 742, 723, 689, 657, 638, 604, 561, 522, 513, 492; mp: 334.2–335.0 ºC; ^{1}H NMR (C_6D_6, 392 MHz) δ 6.72–6.73 (m, 1H, BCNCHCHC*H*), 6.76–6.81 (m, 1H, BCNCCHC*H*), 6.88 (td, *J* = 1.4, 7.2 Hz, 1H, BCNCCCHC*H*), 7.01–7.09 (m, 2H), 7.28 (dd, *J* = 1.3, 8.5 Hz, 1H, BCNCCC*H*), 7.35–7.39 (m, 1H, NCBCCHC*H*), 7.46–7.51 (m, 2H), 7.55 (dd, *J* = 1.3, 8.5 Hz, 1H, BCNC*H*), 7.80 (dd, *J* = 1.3, 8.5 Hz, 1H, BCNCC*H*), 7.86–7.89 (m, 1H, NCBNCC*H*), 8.09–8.13 (m, 2H), 8.71 (dd, *J* = 1.3, 8.5 Hz, 1H, NCBCC*H*); ^{13}C NMR (C_6D_6, 98.5 MHz) δ 113.5, 117.6, 118.1, 120.0, 121.0, 122.6, 122.8, 122.9(2C), 123.9, 125.9, 126.7, 127.0, 127.8, 130.5, 130.6, 131.5, 135.5, 137.6, 139.0; HRMS (EI) *m*/*z* $[M]^+$ calcd for $C_{24}H_{14}NB$ 318.1328; observed 318.1324.

Synthesis of 11b-aza-3b-borabenzo[11,12]chryseno[6,5-*b*]thiophene (3)

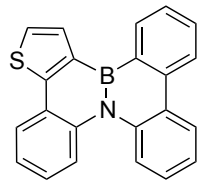

A solution of butyllithium in hexane (1.25 mL, 1.60 M, 2.0 mmol) was added slowly to a solution of **13** (0.655 g, 2.0 mmol) in toluene (10 mL) at –78 ºC under argon. After 1 h, the reaction mixture stirred at 0 ºC for 1 h. A solution of boron trichloride in heptane (2.0 mL, 1.0 M, 2.0 mmol) was added at –78 ºC. After stirring at room temperature for 24 h, solvent was removed *in vacuo*, and the reaction mixture was added to a solution of aluminum trichloride (1.07 g, 8.0 mmol) and 2,2,6,6-tetramethylpiperidine (0.424 g, 3.0 mmol) in *o*-dichlorobenzene (10 mL) at 0 ºC. After stirring at 150 ºC for 12 h, 1,4-diazabicyclo[2.2.2]octane (0.897 g, 8.0 mmol) was added. The reaction mixture was filtered with a pad of Celite®. After the solvent was removed *in vacuo*, the crude product was purified by GPC (eluent: toluene) to obtain the title compound (0.128 g, 19% yield) as white-yellow powder. IR (neat): cm^{-1} 3053 (Ar-H), 1601, 1571, 1514, 1496, 1484, 1452, 1435, 1411, 1330, 1306, 1284, 1237, 1162, 1144, 1110, 1048, 932, 893, 852, 815, 770, 743, 716, 641, 616, 591, 558, 516, 485; mp: 167.0–167.9 ºC; ^{1}H NMR (C_6D_6, 392 MHz) δ 6.92–7.11 (m, 5H), 7.39 (td, *J* = 0.9, 7.6 Hz, 1H, BCCHCHC*H*), 7.50 (td, *J* = 1.8, 7.6 Hz, 1H, BCCCHC*H*), 7.91–8.00 (m, 4H), 8.11–8.16 (m, 2H), 8.63 (dd, *J* = 0.9, 7.6 Hz, 1H, BCC*H*); ^{13}C NMR (C_6D_6, 98.5 MHz) δ 122.1, 122.7, 122.8, 123.2, 123.4, 124.8, 125.0, 126.0, 126.2, 126.5, 126.9, 127.9, 128.1, 131.3, 132.1, 135.4, 137.3, 138.0, 138.7, 151.2; HRMS (EI) *m*/*z* $[M]^+$ calcd for $C_{22}H_{14}NBS$ 335.0940; observed 335.0926.

Synthesis of 3b-aza-11b-borabenzo[11,12]chryseno[6,5-*b*]thiophene (4)

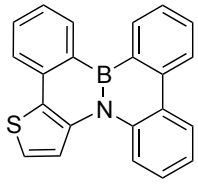

A solution of butyllithium in hexane (1.25 mL, 1.60 M, 2.0 mmol) was added slowly to a solution of **15** (0.655 g, 2.0 mmol) in toluene (10 mL) at –78 ºC under argon. After 1 h, the reaction mixture stirred at 0 ºC for 1 h. A solution of boron trichloride in heptane (2.0 mL, 1.0 M, 2.0 mmol) was added at –78 ºC. After stirring at room temperature for 24 h, solvent was removed *in vacuo*, and the reaction mixture was added to a solution of aluminum trichloride (1.07 g, 8.0 mmol) and 2,2,6,6-tetramethylpiperidine (0.424 g, 3.0 mmol) in *o*-dichlorobenzene (10 mL) at 0 ºC. After stirring at 150 ºC for 12 h, 1,4-diazabicyclo[2.2.2]octane (0.897 g, 8.0 mmol) was added. The reaction mixture was filtered with a pad of Celite®. After the solvent was removed *in vacuo*, the crude product was purified by GPC (eluent: toluene) to obtain the title compound (0.034 g, 5% yield) as white-yellow powder. IR (neat): cm^{-1} 3050 (Ar-H), 1600, 1560, 1484, 1443, 1388, 1322, 1284, 1099, 1053, 1014, 852, 816, 744, 732, 709, 667, 616, 591, 565, 525; mp: 207.2–208.0 ºC; ^{1}H NMR (C_6D_6, 392 MHz) δ 6.76 (d, *J* = 5.8 Hz, 1H, NCC*H*CHS), 7.10–7.21 (m, 2H), 7.30 (td, *J* = 0.9, 7.6 Hz, 1H, SCCCHCHC*H*), 7.35–7.45 (m, 3H), 7.51 (td, *J* = 0.9, 7.6 Hz, 1H, SCCCBCCCHC*H*), 7.90–7.95 (m, 2H), 8.19–8.22 (m, 2H), 8.74 (d, *J* = 7.6 Hz, 2H, BCC*H*); ^{13}C NMR (C_6D_6, 98.5 MHz) δ 120.9, 122.4, 122.5, 123.1, 123.3, 123.4, 125.7, 125.8, 126.9, 127.1, 127.2, 127.9, 130.8, 131.3, 136.3, 136.5, 137.6, 137.8, 138.1, 138.7; ^{11}B NMR (C_6D_6, 131 MHz) δ 34.5; HRMS (EI) *m*/*z* $[M]^+$ calcd for $C_{22}H_{14}NBS$ 335.0940; observed 335.0929.

Synthesis of 11b-aza-3b-borabenzo[11,12]chryseno[5,6-*b*]thiophene (5)

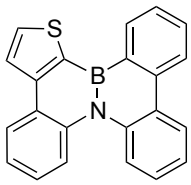

A solution of butyllithium in hexane (1.25 mL, 1.60 M, 2.0 mmol) was added slowly to a solution of **17** (0.655 g, 2.0 mmol) in toluene (10 mL) at –78 ºC under argon. After 1 h, the reaction mixture stirred at 0 ºC for 1 h. A solution of boron trichloride in heptane (2.0 mL, 1.0 M, 2.0 mmol) was added at –78 ºC. After stirring at room temperature for 24 h, solvent was removed *in vacuo*, and the reaction mixture was added to a solution of aluminum trichloride (1.07 g, 8.0 mmol) and 2,2,6,6-tetramethylpiperidine (0.424 g, 3.0 mmol) in *o*-dichlorobenzene (10 mL) at 0 ºC. After stirring at 150 ºC for 12 h, 1,4-diazabicyclo[2.2.2]octane (0.897 g, 8.0 mmol) was added. The reaction mixture was filtered with a pad of Celite®. After the solvent was removed *in vacuo*, the crude product was purified by GPC (eluent: toluene) to obtain the title compound (0.054 g, 8% yield)

as white-yellow powder. IR (neat): cm^{-1} 3054 (Ar-H), 1601, 1571, 1514, 1485, 1435, 1329, 1306, 1284, 1251, 1161, 1110, 1049, 932, 893, 875, 815, 742, 717, 609, 591, 559, 515, 485, 466; mp: 164.1–165.1 ºC; ^{1}H NMR (C_6D_6, 392 MHz) δ 7.00–7.05 (m, 2H), 7.07–7.12 (m, 2H), 7.40–7.50 (m, 3H), 7.63 (d, *J* = 4.9 Hz, 1H, BCCC*H*S), 7.94 (dd, *J* = 1.8, 8.1 Hz, 1H, SCHCCNCC*H*), 8.03 (dd, *J* = 1.3, 8.5 Hz, 1H, SCHCCCC*H*), 8.08–8.15 (m, 3H), 8.95 (dd, *J* = 1.4, 7.6 Hz, 1H, BCC*H*CH); ^{13}C NMR (C_6D_6, 98.5 MHz) δ 122.4, 122.7, 122.8, 123.1, 123.4 (2C), 125.5, 125.7, 125.9, 126.0, 126.4, 127.2, 127.9, 131.5, 134.2, 135.5, 138.1, 138.3, 138.7, 147.0; HRMS (EI) *m*/*z* $[M]^+$ calcd for $C_{22}H_{14}NBS$ 335.0940; observed 335.0943.

Crystallographic data collection and structure determination. Crystals of **1** was mounted on a Rigaku Saturn CCD diffractometer for data collection using graphite-monochromated Mo Kα radiation (λ = 0.71070 Å). Synchrotron X-ray microcrystallographic data was recorded for **2** at 100 K on beamline BL38B2 at SPring-8 (λ = 0.75000 Å). Crystal data and data statistics are summarized in Figure 11. The structures were solved by direct methods with SIR2008[13] or SIR2004[14] and refined by full-matrix least-squares techniques against F^2 (SHELXL-97)[15]. The non-hydrogen atoms were refined anisotropically. Hydrogen atoms were placed at calculated positions (C–H = 0.95 Å) and kept fixed. In the subsequent refinement, the function $\sum w(F_o^2 - F_c^2)^2$ was minimized, where $|F_o|$ and $|F_c|$ are the observed and calculated structure factor amplitudes, respectively. The agreement indices are defined as $R_1 = \sum(||F_o| - |F_c||)/\sum|F_o|$ and $wR_2 = [\sum w(F_o^2 - F_c^2)^2 / \sum(wF_o^4)]^{1/2}$. All calculations were performed by using Crystal Structure 4.0 or Yadokari-XG 2009 and illustrations were drawn by using ORTEP–3.

[13] Burla, M. C.; Caliandro, R.; Camalli, M.; Carrozzini, B.; Cascarano, G. L.; De Caro, L.; Giacovazzo, C.; Polidori, G.; Siliqi, D.; Spagna, R. *J. Appl. Cryst.* **2007,** *40*, 609–613.
[14] Burla, M. C.; Caliandro, R.; Camalli, M.; Carrozzini, B.; Cascarano, G. L.; De Caro, L.; Giacovazzo, C.; Polidori, G.; Spagna, R. *J. Appl. Cryst.* **2005,** *38*, 381–388.
[15] Sheldrick, G. M. Program for the Solution of Crystal Structures; University of Göttingen, Germany, 1997.

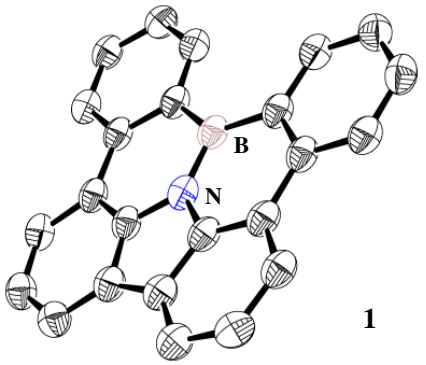

1

Formula	$C_{24}H_{14}BN$	Abs. Coefficient, cm^{-1}	0.080
Formula Weight	327.17	F(000)	1360.00
Temperature, K	103(2)	Crystal Size, mm^3	0.2, 0.2, 0.02
Wavelength, Å	0.71075	$2\theta_{min}$, $2\theta_{max}$, deg	4.9, 51.0
Crystal System	Orthorhombic	Index Ranges	–23≤h≤23
Space Group	*Iba*2 (No. 45)		–36≤k≤36
a, Å	19.6104(8)		–6≤l≤6
b, Å	30.5630(10)	Reflections (unique)	2806
c, Å	5.16510(10)	Reflections (I>2.0σ(I))	2647
α, deg	90	Parameters	235
β, deg	90	GOF on F^2	1.097
γ, deg	90	R_1 (I>2.0σ(I))	0.0355
Volume, Å	3095.72(17)	R, wR_2 (all data)	0.0386, 0.0892
Z	8	Largest diff peak and hole, e, $Å^{-3}$	0.170, –0.131
$Density_{calcd}$, $g{\cdot}cm^{-3}$	1.404		

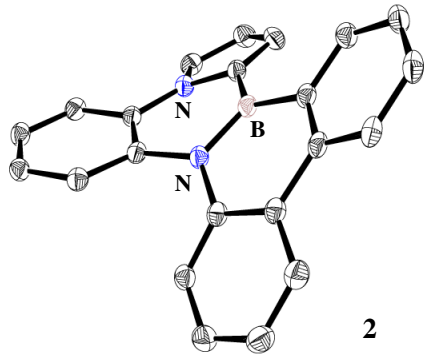

2

Formula	$C_{22}H_{15}BN_2$	Abs. Coefficient, cm^{-1}	0.081
Formula Weight	318.17	F(000)	664.00
Temperature, K	100(2)	Crystal Size, mm^3	0.1, 0.1, 0.05
Wavelength, Å	0.75000	$2\theta_{min}$, $2\theta_{max}$, deg	6.2, 53.0
Crystal System	Orthorhombic	Index Ranges	–8≤h≤8
Space Group	$P2_12_12_1$ (No. 19)		–14≤k≤14
a, Å	7.44630(3)		–20≤l≤20
b, Å	12.09380(2)	Reflections (unique)	2671
c, Å	16.8612(2)	Reflections (I>2.0σ(I))	2580
α, deg	90	Parameters	226
β, deg	90	GOF on F^2	1.096
γ, deg	90	R_1 (I>2.0σ(I))	0.0334
Volume, Å	1518.42(3)	R, wR_2 (all data)	0.0350, 0.0881
Z	4	Largest diff peak and hole, e, $Å^{-3}$	0.152, –0.219
$Density_{calcd}$, $g{\cdot}cm^{-3}$	1.392		

Figure 11. X-ray crystal structures of **1** and **2** (left), and crystal data and structure refinement (right). Thermal ellipsoids are shown at 50% probability and H atoms have been omitted for clarity.

Computational studies. Molecular orbital calculations and nucleus-independent chemical shift (NICS) calculations were performed with Gaussian 09[16] packages. The DFT method was employed using the B3LYP hybrid functional.[17] Structures were optimized with the 6-31G(d) basis set.[18] Nucleus independent chemical shifts (NICS) were evaluated by using the gauge invariant atomic orbital[19] (GIAO) approach at the GIAO-B3LYP/6-31G(d) level. The reorganization energy calculations were performed using the B3LYP hybrid functional with the DZP basis set[20] in the ADF program.[21] The electronic coupling calculations of dimers were performed by the local density functional VWN in the conjunction with the PW91[22] gradient corrections with the DZP basis set, as implemented in the ADF program according to the literature.[5]

---

[16] Gaussian 09, Revision B.01, Frisch, M. J.; Trucks, G. W.; Schlegel, H. B.; Scuseria, G. E.; Robb, M. A.; Cheeseman, J. R.; Scalmani, G.; Barone, V.; Mennucci, B.; Petersson, G. A.; Nakatsuji, H.; Caricato, M.; Li, X.; Hratchian, H. P.; Izmaylov, A. F.; Bloino, J.; Zheng, G.; Sonnenberg, J. L.; Hada, M.; Ehara, M.; Toyota, K.; Fukuda, R.; Hasegawa, J.; Ishida, M.; Nakajima, T.; Honda, Y.; Kitao, O.; Nakai, H.; Vreven, T.; Montgomery, Jr., J. A.; Peralta, J. E.; Ogliaro, F.; Bearpark, M.; Heyd, J. J.; Brothers, E.; Kudin, K. N.; Staroverov, V. N.; Kobayashi, R.; Normand, J.; Raghavachari, K.; Rendell, A.; Burant, J. C.; Iyengar, S. S.; Tomasi, J.; Cossi, M.; Rega, N.; Millam, N. J.; Klene, M.; Knox, J. E.; Cross, J. B.; Bakken, V.; Adamo, C.; Jaramillo, J.; Gomperts, R.; Stratmann, R. E.; Yazyev, O.; Austin, A. J.; Cammi, R.; Pomelli, C.; Ochterski, J. W.; Martin, R. L.; Morokuma, K.; Zakrzewski, V. G.; Voth, G. A.; Salvador, P.; Dannenberg, J. J.; Dapprich, S.; Daniels, A. D.; Farkas, Ö.; Foresman, J. B.; Ortiz, J. V.; Cioslowski, J.; Fox, D. J. Gaussian, Inc., Wallingford CT, 2009.

[17] (a) Becke, A. D. *J. Chem. Phys.* **1993,** *98*, 5648–5652. (b) Lee, C.; Yang, W.; Parr, R. G. *Phys. Rev. B* **1988,** *37*, 785–789.

[18] Hehre, W. J.; Radom, L.; Schleyer, P. v. R.; Pople, J. A. *Ab Initio Molecular Orbital Theory*; John Wiley & Sons: New York, **1986** and references cited therein.

[19] (a) Dichtfield, R. *Mol. Phys.* **1974,** *27*, 789–807. (b) Wolinski, K.; Hinton, J. F.; Pulay, P. *J. Am. Chem. Soc.* **1990,** *112*, 8251–8260.

[20] van Lenthe, E.; Baerends, E. J. *J. Comput. Chem.* **2003,** *24*, 1142–1156.

[21] ADF2010, SCM, Theoretical Chemistry, Vrije Universiteit, Amsterdam, The Netherlands.

[22] Perdew, J. P.; Chevary, J. A.; Vosko, S. H.; Jackson, K. A.; Pederson, M. R.; Sing, D. J.; Fiolhais, C. *Phys. Rev. B* **1992,** *46*, 6671–6687.

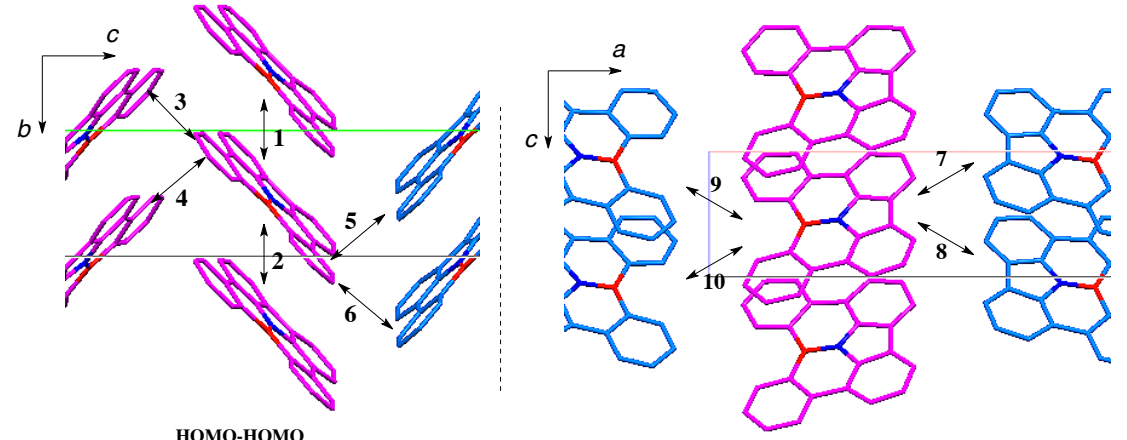

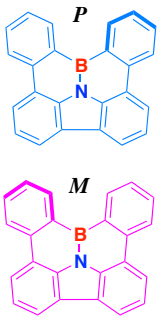

HOMO-HOMO

	|V| (meV)	V (eV)	H1 (eV)	H2 (eV)	J (eV)	S
1	78.6	0.078566446	–5.85032	–5.87874	0.19014	–0.01903
2	78.6	0.078566446	–5.87874	–5.85032	0.19014	–0.01903
3	16.2	0.016244674	–5.86704	–6.14354	0.04543	–0.00486
4	16.2	0.016244699	–6.14353	–5.86704	0.04543	–0.00486
5	0.5	–0.000459686	–6.14249	–5.88896	–0.00058	0.00002
6	0.5	–0.000469683	–5.88924	–6.14246	–0.00059	0.00002
7	5.2	0.005158084	–6.08889	–6.15954	0.00969	–0.00074
8	5.2	0.005148102	–6.1595	–6.08888	0.00968	–0.00074
9	3.6	0.003601065	–6.14085	–6.08517	0.00733	–0.00061
10	3.6	0.003601053	–6.08518	–6.14088	0.00733	–0.00061

LUMO-LUMO

	|V| (meV)	V (eV)	H1 (eV)	H2 (eV)	J (eV)	S
1	71.9	0.071941292	–2.95232	–2.96669	0.11685	–0.01518
2	71.9	0.071941292	–2.96669	–2.95232	0.11685	–0.01518
3	17.9	0.017943264	–2.94957	–3.21355	0.02765	–0.00315
4	17.9	0.017943264	–3.21355	–2.94957	0.02765	–0.00315
5	15.7	0.015720147	–3.23081	–2.96203	0.02439	–0.0028
6	15.7	0.015719937	–2.96229	–3.2307	0.02439	–0.0028
7	11.6	0.011574912	–3.17044	–3.24558	0.01844	–0.00214
8	11.6	0.011574954	–3.24554	–3.17044	0.01844	–0.00214
9	3.2	0.003242387	–3.21183	–3.16155	0.00525	–0.00063
10	3.2	0.003242374	–3.16158	–3.21184	0.00525	–0.00063

Figure 12. Electron couplings *V* (meV) between neighboring molecules in the X-ray crystal structures of **1** at the PW91/DZP level on ADF2010 program. H atoms have been omitted for clarity. The *P*-enantiomer is shown in blue and *M*-enantiomer is shown in pink. *V* (eV) = [J – 0.5S(H1 + H2)]/(1 – S^2), J (eV): charge transfer integral, H1 and H2 (eV): site energies, S: overlap integral.

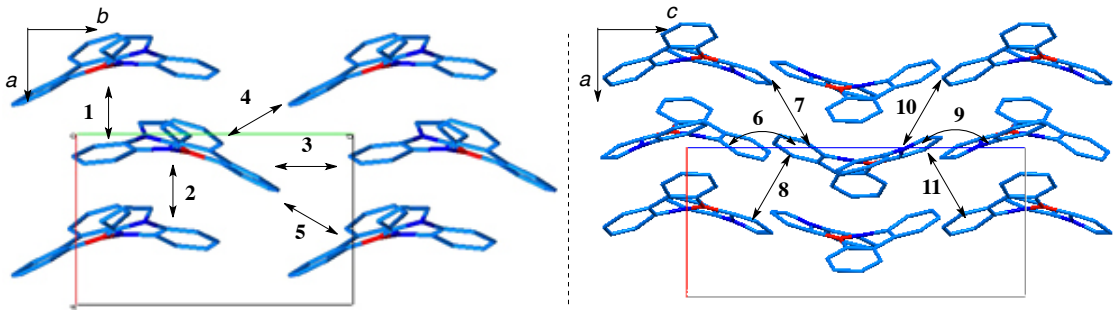

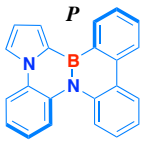

HOMO-HOMO

	|V| (meV)	V (eV)	H1 (eV)	H2 (eV)	J (eV)	S
1	33.1	0.033087388	–5.33847	–5.40637	0.06661	–0.00624
2	33.1	0.03308745	–5.40636	–5.33846	0.06661	–0.00624
3	1.3	–0.001340726	–5.5815	–5.4917	–0.0035	0.00039
4	2.2	0.00221811	–5.56497	–5.40887	0.00562	–0.00062
5	2.2	0.002218048	–5.40903	–5.56501	0.00562	–0.00062
6	2	–0.002033281	–5.57711	–5.56081	–0.00621	0.00075
7	11.1	0.011140131	–5.45924	–5.49884	0.02944	–0.00334
8	13	0.013015244	–5.47715	–5.55605	0.03293	–0.00361
9	7.6	0.007603535	–5.61909	–5.50612	0.02151	–0.0025
10	11.1	0.011140097	–5.49884	–5.45926	0.02944	–0.00334
11	13	0.013005298	–5.55602	–5.47715	0.03292	–0.00361

LUMO-LUMO

	|V| (meV)	V (eV)	H1 (eV)	H2 (eV)	J (eV)	S
1	14.5	–0.014519145	–2.46428	–2.52525	–0.01649	0.00079
2	14.5	–0.014509149	–2.52525	–2.46427	–0.01648	0.00079
3	0.9	0.000909757	–2.66769	–2.55076	0.00211	–0.00046
4	10.8	–0.01078825	–2.62258	–2.41698	–0.01739	0.00262
5	10.8	–0.010788028	–2.41712	–2.62261	–0.01739	0.00262
6	0.5	–0.000462295	–2.64188	–2.61495	–0.00062	0.00006
7	3.6	–0.003582596	–2.52317	–2.57076	–0.00534	0.00069
8	4.2	–0.004168531	–2.52969	–2.60903	–0.00589	0.00067
9	11.2	–0.01117444	–2.65969	–2.55767	–0.01707	0.00226
10	3.6	–0.003582592	–2.57075	–2.52319	–0.00534	0.00069
11	4.2	–0.004168541	–2.60902	–2.52967	–0.00589	0.00067

Figure 13. Electron couplings *V* (meV) between neighboring molecules in the X-ray crystal structures of **2** at the PW91/DZP level on ADF2010 program. H atoms have been omitted for clarity. *V* (eV) = [J – 0.5S(H1 + H2)]/(1 – S^2), J (eV): charge transfer integral, H1 and H2 (eV): site energies, S: overlap integral.

Cartesian coordinates

1

E(RB3LYP) = –1002.69628075 hartree

Center Number	Atomic Number	Atomic Type	Coordinates X	Y	Z
1	6	0	-1.750196	3.566132	-0.063116
2	6	0	-3.079728	3.116513	-0.105982
3	6	0	-0.733306	2.613490	-0.023492
4	6	0	-1.113979	1.252400	-0.029598
5	7	0	0.000004	0.436464	0.000189
6	6	0	-2.415324	0.760097	-0.063169
7	6	0	-2.594865	-0.703052	-0.022713
8	5	0	-0.000017	-0.990218	0.000204
9	6	0	-1.454609	-1.582347	0.036350
10	6	0	-3.412609	1.756850	-0.105093
11	6	0	-3.892673	-1.248736	-0.011955
12	6	0	-1.722330	-2.963696	0.148156
13	6	0	1.114024	1.252357	0.029818
14	6	0	-3.010687	-3.483734	0.166817
15	6	0	0.733409	2.613463	0.023503
16	6	0	-4.104197	-2.617417	0.074609
17	6	0	1.750339	3.566072	0.062946
18	6	0	3.079849	3.116409	0.105882
19	6	0	3.412676	1.756731	0.105152
20	6	0	2.415360	0.760012	0.063316
21	6	0	2.594847	-0.703139	0.022740
22	6	0	3.892637	-1.248848	0.011565
23	6	0	4.104097	-2.617539	-0.075054
24	6	0	3.010541	-3.483828	-0.166888
25	6	0	1.722200	-2.963757	-0.147898
26	6	0	1.454549	-1.582399	-0.036052
27	1	0	-1.532461	4.630482	-0.062382
28	1	0	-3.881710	3.848745	-0.138663
29	1	0	-4.462531	1.483600	-0.134592
30	1	0	-4.752525	-0.588355	-0.063231
31	1	0	-0.896198	-3.657533	0.244677
32	1	0	-3.165097	-4.555727	0.255297
33	1	0	-5.118111	-3.009015	0.082182
34	1	0	1.532650	4.630431	0.061902
35	1	0	3.881858	3.848612	0.138556
36	1	0	4.462582	1.483440	0.134871
37	1	0	4.752527	-0.588488	0.062473
38	1	0	5.118002	-3.009156	-0.083005
39	1	0	3.164899	-4.555833	-0.255321
40	1	0	0.896026	-3.657577	-0.244167

2

E(RB3LYP) = –981.793477931 hartree

Center Number	Atomic Number	Atomic Type	Coordinates X	Y	Z
1	6	0	-1.886511	-2.672392	0.498920
2	6	0	-1.535267	-1.346594	0.174260
3	6	0	-2.535707	-0.342373	0.233689
4	6	0	-3.839018	-0.694782	0.636361
5	6	0	-4.158309	-2.011540	0.944134
6	6	0	-3.181325	-3.011983	0.870951
7	6	0	-0.823380	1.429028	-0.290159
8	6	0	-2.183092	1.031207	-0.163692
9	6	0	-0.528956	2.704273	-0.810139
10	6	0	-1.536485	3.603920	-1.130632
11	6	0	-2.875636	3.243982	-0.957913
12	6	0	-3.178641	1.970544	-0.499010
13	6	0	1.123191	-1.818719	-0.377640
14	6	0	2.628778	0.057760	0.104915
15	6	0	1.528619	0.924704	0.322999
16	6	0	3.922601	0.463622	0.459704
17	6	0	4.148434	1.702863	1.045621
18	6	0	3.064066	2.537019	1.325400
19	6	0	1.776183	2.142688	0.981087
20	6	0	1.285994	-3.119098	-0.849665
21	6	0	2.650044	-3.312909	-1.169865
22	1	0	3.104276	-4.205873	-1.578070
23	1	0	3.214866	3.486969	1.829723
24	1	0	5.158693	1.997547	1.313253
25	1	0	-3.672949	3.936531	-1.211483
26	1	0	-1.273921	4.576836	-1.536949
27	1	0	0.938302	2.779758	1.236009
28	1	0	4.752255	-0.217393	0.305699
29	1	0	-5.169812	-2.259557	1.255801
30	1	0	-4.608038	0.064638	0.732774
31	1	0	-3.430142	-4.039686	1.121613
32	1	0	0.489673	-3.835255	-0.996986
33	1	0	-4.220125	1.675206	-0.434403
34	1	0	0.502625	2.979665	-0.991186
35	1	0	-1.117615	-3.438578	0.491853
36	6	0	3.314141	-2.134871	-0.885900
37	1	0	4.355658	-1.878746	-1.004921
38	7	0	2.396617	-1.228600	-0.413609

39	7	0	0.212747	0.500127	-0.005540
40	5	0	-0.073529	-0.920170	-0.075848

---

18 (neutral geometry)

E(RB3LYP) = –2246.24804726 hartree

Center Number	Atomic Number	Atomic Type	Coordinates X	Y	Z
1	6	0	0.288728	2.296648	-1.397814
2	6	0	0.851082	1.200391	-0.732309
3	6	0	2.253719	1.015782	-0.736259
4	6	0	3.029729	1.935822	-1.465498
5	6	0	2.462637	3.010886	-2.143409
6	6	0	1.081300	3.199221	-2.101145
7	1	0	-0.785232	2.443300	-1.351255
8	1	0	4.108632	1.812587	-1.466973
9	1	0	3.097968	3.704789	-2.686492
10	1	0	0.620298	4.039398	-2.612505
11	6	0	2.965152	-0.077814	-0.026717
12	6	0	2.721304	-0.516800	1.255257
13	1	0	1.965228	-0.176203	1.947500
14	6	0	4.637291	-1.704106	0.219555
15	1	0	5.463589	-2.372166	0.017739
16	16	0	3.823144	-1.755831	1.748746
17	6	0	4.078639	-0.777846	-0.612173
18	1	0	4.417855	-0.607177	-1.627755
19	7	0	-0.031187	0.299203	-0.025964
20	6	0	-0.860482	0.915883	0.983184
21	6	0	-2.267340	0.764748	0.995093
22	6	0	-0.233593	1.706125	1.956864
23	6	0	-2.979216	1.398715	2.030646
24	6	0	-0.965251	2.330522	2.962416
25	1	0	0.843279	1.834598	1.913041
26	6	0	-2.350016	2.169070	3.004162
27	1	0	-4.060815	1.302074	2.041619
28	1	0	-0.454467	2.935826	3.705883
29	1	0	-2.939432	2.651572	3.778662
30	6	0	-3.051487	-0.015519	-0.007596
31	6	0	-4.034779	-0.916247	0.438330
32	6	0	-2.892184	0.155086	-1.392859
33	6	0	-4.830310	-1.619348	-0.464967
34	1	0	-4.157583	-1.080839	1.504992
35	6	0	-3.687846	-0.548790	-2.297428
36	1	0	-2.149425	0.847540	-1.772365
37	6	0	-4.660399	-1.438217	-1.838681
38	1	0	-5.577589	-2.315750	-0.093950
39	1	0	-3.547180	-0.396359	-3.364085
40	1	0	-5.277203	-1.987510	-2.544677
41	5	0	-0.043643	-1.093487	-0.286211
42	17	0	0.577799	-1.751129	-1.815467
43	17	0	-0.674373	-2.253262	0.902030

---

18 (cation geometry)

E(RB3LYP) = –2246.32641654 hartree

Center Number	Atomic Number	Atomic Type	Coordinates X	Y	Z
1	6	0	-0.069440	2.752937	-0.267031
2	6	0	0.653076	1.554979	-0.067954
3	6	0	2.017162	1.514064	-0.534943
4	6	0	2.531280	2.640646	-1.214540
5	6	0	1.788225	3.796615	-1.420553
6	6	0	0.481268	3.851408	-0.927341
7	1	0	-1.089289	2.816771	0.095139
8	1	0	3.563585	2.604504	-1.554001
9	1	0	2.225814	4.646465	-1.939369
10	1	0	-0.121529	4.747890	-1.058131
11	6	0	2.835227	0.362360	-0.262190
12	6	0	2.361607	-0.610149	0.781210
13	1	0	2.456456	-0.157078	1.781114
14	6	0	4.570460	-1.204514	-0.425816
15	1	0	5.469123	-1.683784	-0.796223
16	16	0	3.571590	-2.017751	0.761388
17	6	0	4.051530	-0.001185	-0.860557
18	1	0	4.533294	0.580031	-1.642425
19	7	0	0.059927	0.437034	0.525282
20	6	0	-1.188009	0.642068	1.198298
21	6	0	-2.441495	0.261383	0.665633
22	6	0	-1.142595	1.230183	2.472900
23	6	0	-3.589899	0.466468	1.456662
24	6	0	-2.289552	1.436771	3.232144
25	1	0	-0.167261	1.502811	2.864254
26	6	0	-3.527661	1.043888	2.720791
27	1	0	-4.554473	0.182980	1.043284
28	1	0	-2.215197	1.886282	4.219833
29	1	0	-4.438264	1.192442	3.296970
30	6	0	-2.643111	-0.328353	-0.688989
31	6	0	-3.436549	-1.478167	-0.833187
32	6	0	-2.136007	0.278149	-1.848451
33	6	0	-3.717599	-2.005572	-2.093087

34	1	0	-3.810947	-1.975593	0.057429	40	1	0	-3.427528	-1.798386	-4.222870
35	6	0	-2.421621	-0.245508	-3.108304	41	5	0	0.780687	-0.932882	0.587738
36	1	0	-1.517979	1.165422	-1.764058	42	17	0	0.490031	-1.969731	-0.993360
37	6	0	-3.213555	-1.387819	-3.238520	43	17	0	0.164435	-1.946669	2.085968
38	1	0	-4.321762	-2.906264	-2.177756	---					
39	1	0	-2.014762	0.239582	-3.992459						

Chapter 4

Tandem Phospha-Friedel–Crafts Reaction Producing Curved π-Conjugated Frameworks with a Phosphorus Ring Junction

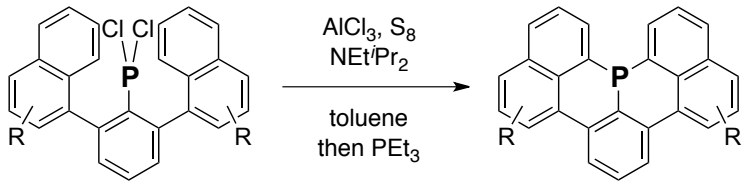

"Tandem phospha-Friedel–Crafts reaction"

Abstract: Triaryl phosphine derivatives containing curved π-conjugated frameworks with a phosphorus ring junction have been synthesized from dichloro(*m*-teraryl)phosphines *via* a tandem phospha-Friedel–Crafts reaction. The rigid molecular frameworks enable these unprecedented phosphine compounds to form extended π-conjugation systems spreading over the whole molecule. This simple and practical strategy is suitable for further extension of π-conjugated frameworks as well as for the introduction of multiple phosphorus atoms.

Chapter 4

4-1. Introduction

Polycyclic aromatic compounds are an important class of materials for organic electronics, dyes, sensors, and liquid crystals.[1] Incorporation of heteroatoms into a π-conjugated skeleton is a promising way to modulate their physical properties and, thus, intensive efforts have been devoted to the construction of new hetero-π-conjugated frameworks.[2] However, because there have not been many suitable synthetic methodologies for producing π-conjugated molecules with heteroatom junctions, the various BN-fused polycyclic aromatic compounds reported previously have been synthesized using the tandem intramolecular bora-Friedel–Crafts reaction described in Chapters 1–3. This author envisioned that this synthetic strategy could be applicable to another heteroatom such as phosphorus and that the development of a tandem phospha-Friedel–Crafts reaction[3] could provide facile access to π-conjugated frameworks with phosphorus ring junctions, as shown in Scheme 1. These triarylphosphines are expected to have unique characteristics because of the phosphorus atom located in the π-conjugated ring-fusion position. To gain insight into these characteristics based on actual measurements, investigations aiming toward the establishment of this synthetic method have been started.

---

[1] Reviews: (a) Fabian, J.; Nakazumi, H.; Matsuoka, M. *Chem. Rev.* **1992,** *92*, 1197–1226. (b) Scherf, U. *J. Mater. Chem.* **1999,** *9*, 1853–1864. (c) Mitschke, U.; Bäuerle, P. *J. Mater. Chem.* **2000,** *10*, 1471–1507. (d) Watson, M. D.; Fechtenkötter, A.; Müllen, K. *Chem. Rev.* **2001,** *101*, 1267–1300. (e) Bendikov, M.; Wudl, F.; Perepichka, D. F. *Chem. Rev.* **2004,** *104*, 4891–4945. (f) Klauk, H. *Organic Electronics*, Wiley-VCH, Weinheim, **2006**. (g) Anthony, J. E. *Chem. Rev.* **2006,** *106*, 5028–5048. (h) Sergeyev, S.; Pisula, W.; Geerts, Y. H. *Chem. Soc. Rev.* **2007,** *36*, 1902–1929. (i) Wu, J.; Pisula, W.; Müllen, K. *Chem. Rev.* **2007,** *107*, 718–747.

[2] Reviews: (a) Yamaguchi, S.; Xu, C.; Okamoto, T. *Pure Appl. Chem.* **2006,** *78*, 721–730. (b) Yamaguchi, S.; Wakamiya, A. *Pure Appl. Chem.* **2006,** *78*, 1413–1324. (c) Baumgartner, T.; Réau, R. *Chem. Rev.* **2006**, *106*, 4681–4727. (d) Loudet, A.; Burgess, K. C*hem. Rev.* **2007,** *107*, 4891–4932. (e) Fukazawa, A.; Yamaguchi, S. *Chem. Asian J.* **2009**, *4*, 1386–1400. (f) Matano, Y.; Imahori, H. *Org. Biomol. Chem.* **2009,** *7*, 1258–1271.

[3] Nontandem reactions have been reported. Phosphorus: (a) Olah, G. A.; Hehemann, D. *J. Org. Chem.* **1977,** *42*, 2190. (b) Wang, Z.-W.; Wang, L.-S. *Green Chem.* **2003,** *5*, 737–739. (c) Diaz, A. A.; Young, J. D.; Khan, M. A.; Wehmschulte, R. J. *Inorg. Chem.* **2006**, *45*, 5568–5575. (d) Diaz, A. A.; Buster, B.; Schomich, D.; Khan, M. A.; Baum, J. C.; Wehmschulte, R. J. *Inorg. Chem.* **2008**, *47*, 2858–2863. Silicon: (e) Olah, G. A.; Bach, T.; Prakash, G. K. S. *J. Org. Chem.* **1989,** *54*, 3770–3771. (f) Furukawa, S.; Kobayashi, J.; Kawashima, T. *J. Am. Chem. Soc.* **2009,** *131*, 14192–14193. Boron: (g) Genaev, A. M.; Nagy, S. M.; Salnikov, G. E.; Shubin, V. G. *Chem. Commun.* **2000,** 1587–1588. (h) Vries, T. S. D.; Prokofjevs, A.; Harvey, J. N.; Vedejs, E. *J. Am. Chem. Soc.* **2009,** *131*, 14679–14687.

Scheme 1. Tandem phospha-Friedel–Crafts reaction producing a π-conjugated framework with a phosphorus ring junction

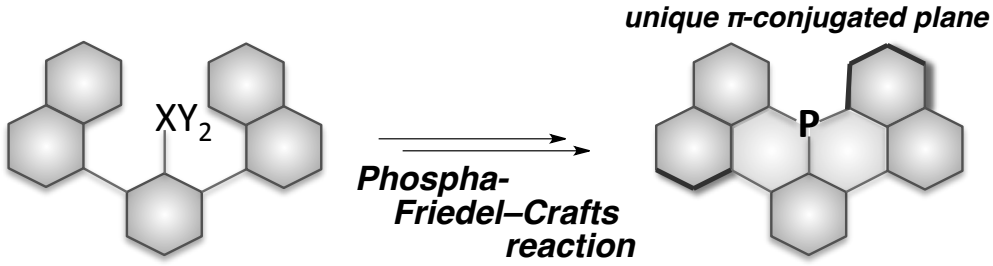

To avoid the undesirable five-membered-ring formation occurring in heterole synthesis,[3c, 3d, 3f-h] careful screening of additives, reaction conditions, and starting substrates has been performed. Ultimately, phosphaperylenes **1** were obtained from the *tandem* phospha-Friedel–Crafts reaction of dichloro(*m*-teraryl)phosphine ($XY_2 = PCl_2$) *via* selective 6,6-ring-closure under particular conditions. In this chapter, the experimental details of the synthesis, crystal structures, and physical properties of the phosphaperylenes **1** and their derivatives are described.

Chart 1. Phosphaperylene derivatives

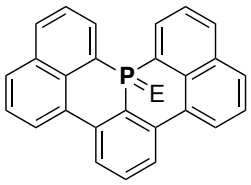

1a (E = none)
2a (E = S), **3a** (E = O)

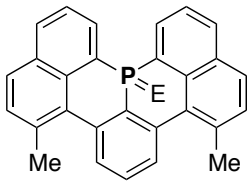

1b (E = none)
2b (E = S), **3b** (E = O)

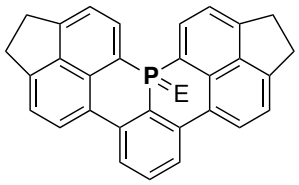

1c (E = none)
2c (E = S), **3c** (E = O)

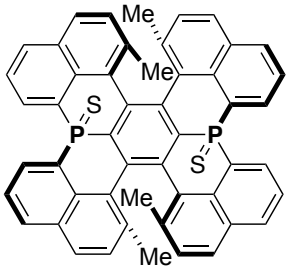

2d

4-2. Results and Discussion

4-2-1. Synthesis of phosphaperylene derivatives *via* a phospha-Friedel–Crafts reaction

The synthetic route to *m*-terarylphosphine dichlorides **5a**–**5c** *via* the phospha-Friedel–Crafts reaction is described in Scheme 2. Selective lithiation at the 2-position of 1,3-dichlorobenzene and subsequent treatment with two equivalents of aryl Grignard reagents gave *m*-teraryl iodides **4a**–**4c** in 32%–79% yields upon iodination quenching.[4] Lithium-halogen exchange of **4a**–**4c** and subsequent trapping of the resulting aryllithiums with trichlorophosphine gave *m*-terarylphosphine dichlorides **5a**–**5c**. After the careful screening of the additives and reaction conditions, the tandem phospha-Friedel–Crafts reaction of **5a**–**5c** was achieved through the combined use of S_8, $AlCl_3$, and NEt^iPr_2. Because the electrophilicity of arylphosphine dichloride is smaller than that of arylthiophosphine dichloride, the reaction did not proceed at all in the absence of S_8. The reaction gave several byproducts in the absence of NEt^iPr_2. Notably, the tandem reaction selectively gave 6,6-ring-closure products, phosphine sulfides **2a**–**2c** (E = S), in 11%–43% yields, and no formation of 5,5- or 5,6-ring-closure products was observed under these reaction conditions. Desulfurization of **2a**–**2c** with triethylphosphine gave the target phosphines, 15b-phosphanaphtho[1,8-*ab*]perylene **1a**, 6,10-dimethyl-15b-phosphanaphtho[1,8-*ab*]perylene **1b**, and 15b-phospha-3,4,12,13-tetrahydroacenaphtho[5,6-*ab*]cyclopenta[*lm*]perylene **1c**, in 75%–80% yields. Similarly, oxidation with H_2O_2 gave the corresponding phosphine oxides **3a**–**3c** in 70%–79% yields.

Scheme 2. Synthesis of **1**–**3**

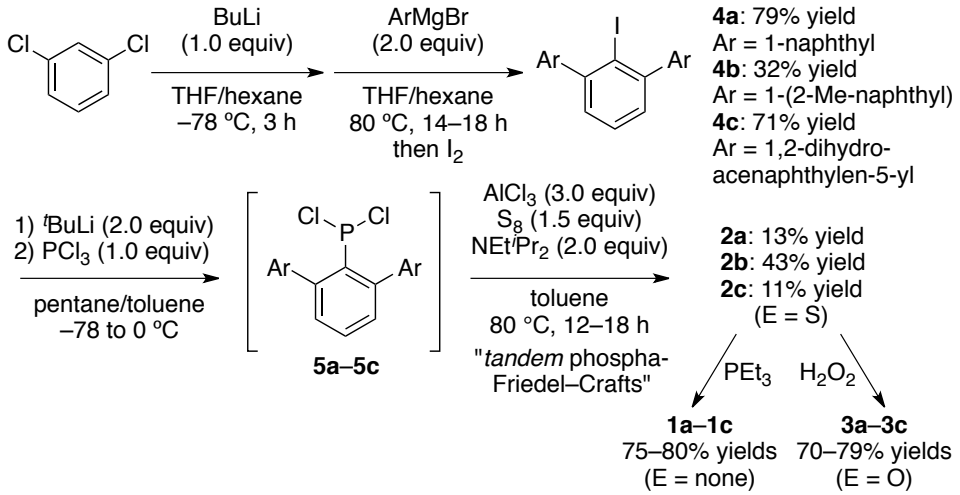

[4] (a) Du, C.-J. F.; Hart, H.; Ng, K.-K. D. *J. Org. Chem.* **1986,** *51*, 3162–3165. (b) Saednya, A.; Hart, H. *Synthesis* **1996,** 1455–1458.

4-2-2. Curved π-conjugated structures

The structures of phosphine sulfides **2a**–**2c** were determined using X-ray crystallography (Figure 1). The phosphorus centers adopt a distorted tetrahedral geometry with C–P–C bond angles of 100.56(12)°–113.31(11)°, 100.92(6)°–114.41(7)°, and 102.4(3)°–114.1(3)°, respectively. Because of the tetrahedral geometry of the phosphorus centers as well as the steric repulsion between the hydrogen atoms at the β-position of the phosphorus atom, **2a** adopts a helical structure (the *M*-enantiomer is shown). On the other hand, **2b** adopts a bowl-shaped structure because of steric repulsion between the methyl groups and the phenyl group. Interestingly, **2c** adopts a planar structure rather than a helical structure. The structure of **1b** was determined by performing Rietveld refinement on the X-ray powder diffraction data. It should be noted that the phosphine **1b** and phosphine oxide **3b** have structures analogous to that of the phosphine sulfide **2b**.

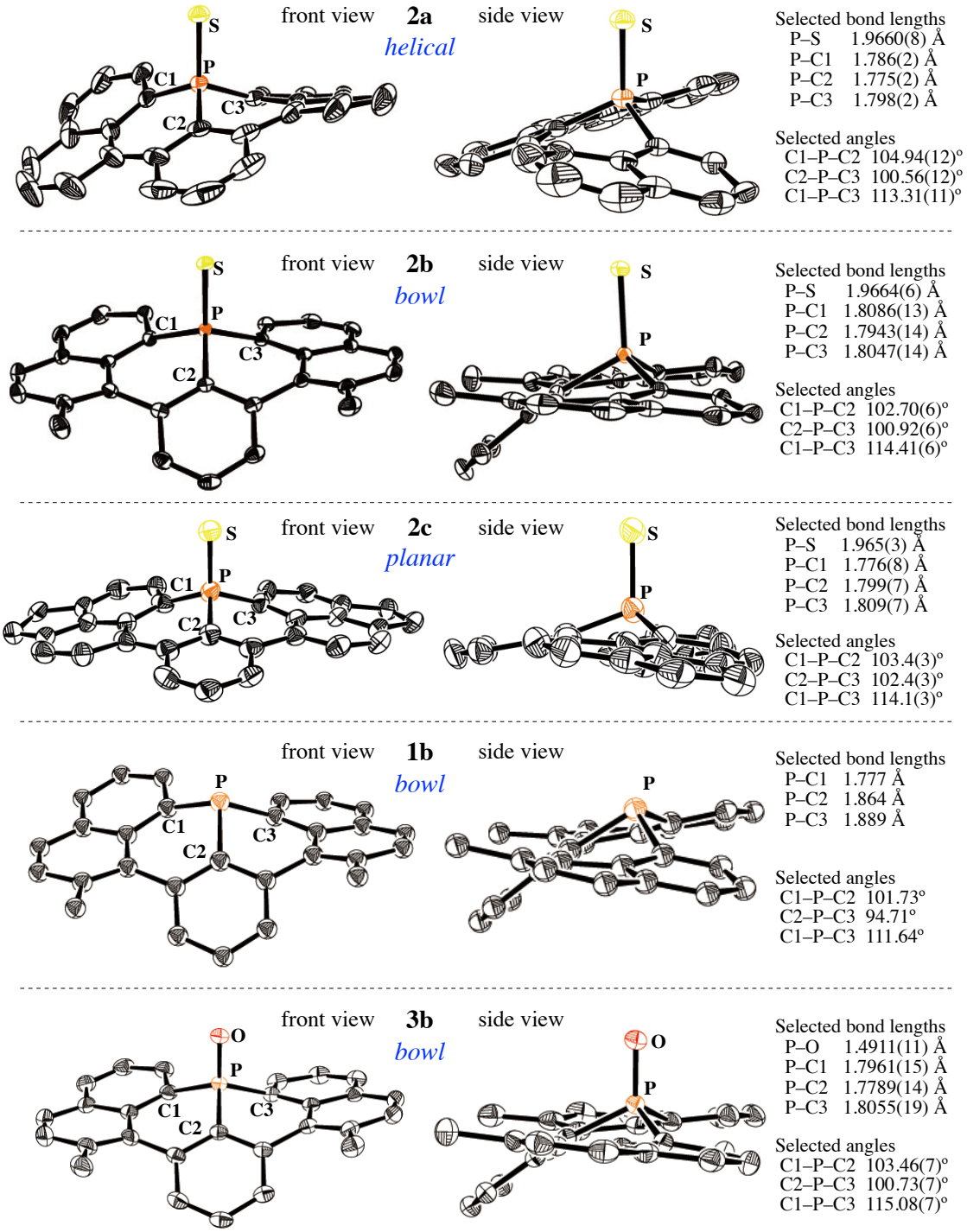

Figure 1. ORTEP drawings of **2a**–**2c**, **1b**, and **3b** (*M*-enantiomers). Thermal ellipsoids show 50% probability and H atoms have been omitted for clarity.

All of these derivatives have helical chirality to some degree and formed racemic crystals; NMR analysis indicates rapid isomerization between enantiomers in the solution phase. The isomerization barrier between the *M*- and *P*-enantiomers of **2a** was estimated to be +1.6 kcal mol^{-1} using DFT calculations ($\Delta G^{\ddagger}$, Figure 2). The present π-conjugated frameworks are thermally stable: none of the derivatives decomposes below 600 K.

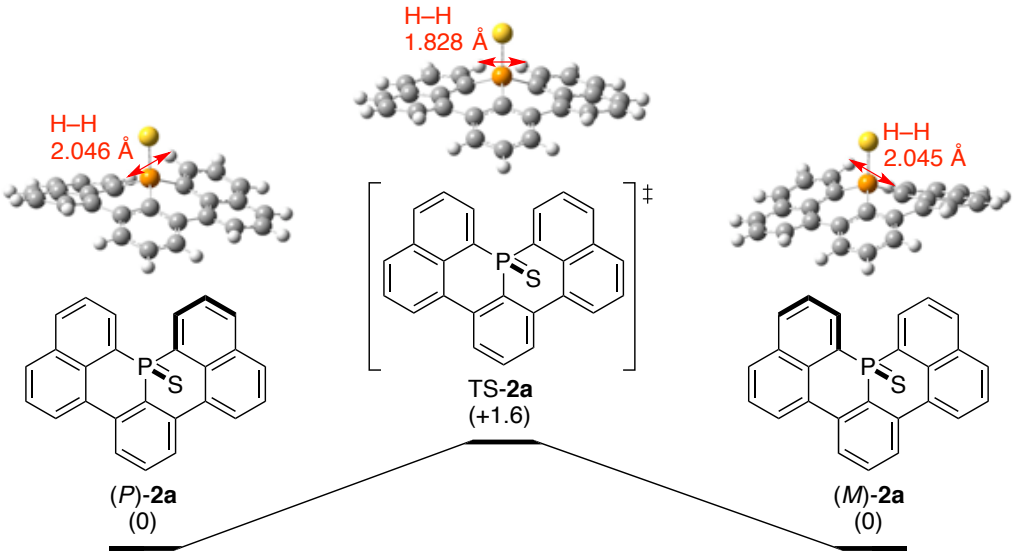

Figure 2. Energy diagram for the isomerization pathway from (*P*)-**2a** to (*M*)-**2a**. Gibbs free energies relative to (*P*)-**2a** [$\Delta G^{\ddagger}$, B3LYP/6-31G(d)] are given in kcal mol^{-1}.

4-2-3. Theoretical studies of phosphaperylene derivatives

To reveal the differences among the electronic state distributions of the phosphines and their derivatives, DFT calculations were performed using the B3LYP hybrid functional. The results of the molecular orbital calculations indicate efficient π-conjugation over the whole molecule despite the molecules' curved structures. In particular, the HOMO and LUMO of **1a**, **2a**, and **3a** are delocalized over the whole molecular surface (Figure 3). The HOMO–LUMO gaps of **1a** (3.60 eV), **2a** (3.47 eV), and **3a** (3.68 eV) are smaller than that of the corresponding carbon analogue (3.92 eV, X = C–H instead of P in Scheme 1) and comparable to that of anthracene (3.59 eV). The HOMO of **1a** consists of the p-orbital of the phosphorus atom and the aromatic π-orbitals. In case of **2a**, the p-orbital of the sulfur atom is mostly localized on the atom. The HOMO and LUMO energies of **2a** and **3a** are lower than those of **1a** (by –0.32 and –0.45 eV, respectively, for **2a** and by –0.51 and –0.43 eV, respectively, for **3a**) because of the electron withdrawing nature of the P=S and P=O groups.

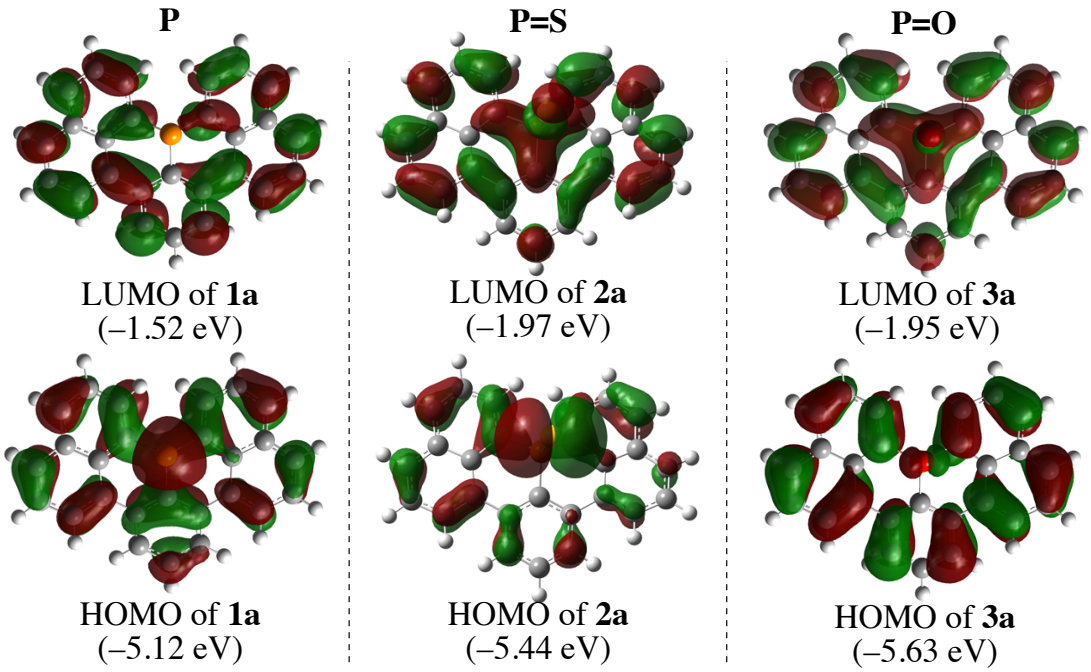

Figure 3. Kohn–Sham HOMOs and LUMOs of **1a**, **2a**, and **3a**.

4-2-4. Photophysical and electrochemical properties

To reveal the photophysical and electrochemical properties of these phosphine derivatives, their UV-visible absorption and fluorescence spectra, absolute fluorescence quantum yields, fluorescence lifetimes, and cyclic voltammograms were measured. Table 1 summarizes the results for phosphines **1a** and **1b** and phosphine oxides **3a**–**3c**. In the UV-visible absorption spectra, the phosphines and phosphine oxides have a strong absorption band with a maximum (λ_{ab}) at 379–412 nm that is assignable to the HOMO–LUMO transition, as shown by the TD-DFT calculations at the B3LYP/6-311+G(d,p) level based on the structures optimized at the B3LYP/6-31G(d) level. The fact that the absorption coefficients of phosphines **1a** and **1b** (log ε = 3.63 and 3.20, respectively) are smaller than those of phosphine oxides **3a** and **3b** (log ε = 4.13 and 4.11, respectively) is consistent with the fact that the oscillator strengths for the HOMO–LUMO transition obtained from the TD-DFT calculations are also smaller. This difference in oscillator strengths can be explained by the substantial contribution of the atomic p-orbital of the phosphorus atom to the HOMO but not to the LUMO, as shown in Figure 3. Phosphine **1a** exhibits strong green fluorescence with two peaks, one at 436 nm and a broader excimer-type emission at 540 nm. Similar excimer-type emission was also observed in the fluorescence spectrum of phosphine **1b**. The intensity of the emission at 505 nm relative to the emission at 428 nm increases in proportion to the concentration of **1b**. This linear correlation suggests that an excimer produces the emission at 505 nm (Figure 4). Phosphine oxides **3a**, **3b**, and **3c** exhibit strong blue and cyan fluorescence with maximums (λ_{em}) at 418, 415, and 468 nm, respectively. In contrast, phosphine sulfide **2b** did not exhibit any significant fluorescent intensity,

potentially because the lone electron pair of the sulfur atom could quench the excited state. The quantum yield of **3b** (Φ_f = 0.83) is larger than that of **3a** (Φ_f = 0.68). Comparable radiative rate constants for **3b** and **3a** (k_r = 3.0 × 10^8 and 4.0 × 10^8 s^{-1}, respectively) and a smaller nonradiative rate constant for **3b** (k_{nr} = 6.2 × 10^9 *vs*. 1.9 × 10^8 s^{-1}) indicate that the methyl substituents make the conformation more rigid and suppress the nonradiative decay process. On the other hand, **3c** shows lower fluorescence efficiency (Φ_f = 0.20) than **3a** as well as a smaller radiative rate constant (k_r = 3.9 × 10^7 s^{-1}) and a comparable nonradiative rate constant (k_{nr} = 1.6 × 10^8 s^{-1}).

Table 1. Photophysical[a] and electrochemical[b] data.

Compd	λ_{ab}[c] (nm)	log ε ($M^{-1}cm^{-1}$)	λ_{em}[d] (nm)	Φ_f[e]	τ_s[f] (ns)	k_r/k_{nr}[g] (10^8 s^{-1})	E_{ox}[h] (V)	E_{red1}[h] (V)	E_{red2}[h] (V)
1a	407	3.63	436 540	–[i]	–	–	+0.38	–2.47	–
1b	400	3.20	428 505	–[i]	–	–	+0.37	–2.57 (–2.53)	–
3a	388	4.13	418	0.68	1.72	4.0/1.9	–	–2.05 (–2.02)	–2.50 (–2.44)
3b	379	4.11	415	0.83	2.74	3.0/0.62	–	–2.17 (–2.14)	–2.59 (–2.50)
3c	412	3.90	468	0.20	5.11	0.39/1.6	–	–2.01 (–1.98)	–2.46 (–2.43)

[a] UV-visible absorption and fluorescence measurements were made in CH_2Cl_2 (0.02 and 0.01 mM, respectively). [b] Redox potentials were determined by performing cyclic voltammetry in MeCN with 0.10 M *n*-$Bu_4N^+PF_6^-$. [c] Only the longest-wavelength absorption maxima are shown. [d] Emission maxima upon excitation at the 360 nm (**3a**–**3c**) and 400 nm (**1a** and **1b**). [e] Absolute fluorescence quantum yields determined using a calibrated integrating sphere system with ≤3% errors. [f] Fluorescence lifetime. [g] The radiative rate constant (k_r) and non-radiative rate constant (k_{nr}) were calculated from Φ_f and τ_s using the formulas $k_r = \Phi_f/\tau_s$ and $k_{nr} = (1 - \Phi_f)/\tau_s$. [h] Oxidation ($E_{ox}$) and reduction ($E_{red1}$, E_{red2}) potentials are given in V versus the ferrocene/ferrocenium couple. For reversible processes, the corresponding half-redox potentials ($E_{1/2}$) are given in parentheses. [i] The Φ_f of **1a** and **1b** have not been determined because partial *in situ* P-oxidation during the measurements introduces errors.

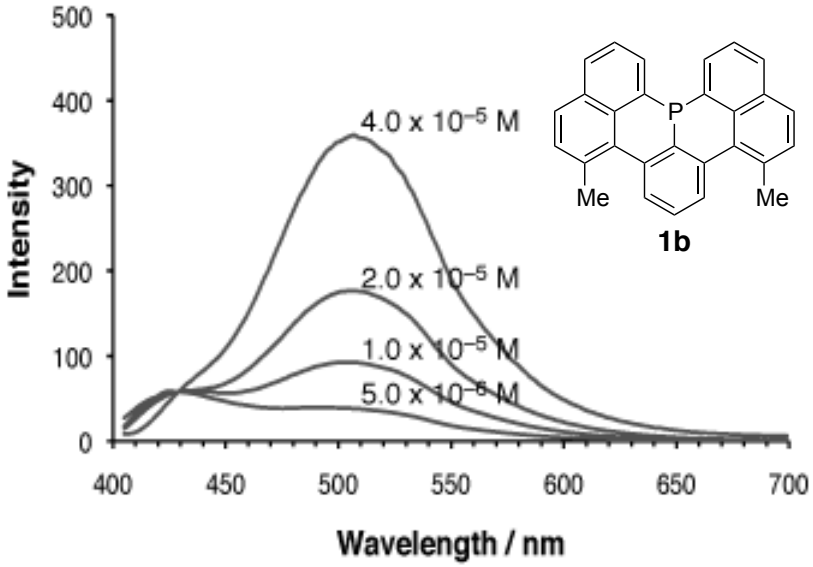

Figure 4. Fluorescence spectra of 0.5, 1.0, 2.0, and 4.0 × 10^{-5} M solutions of **1b** in CH_2Cl_2 normalized at 428 nm.

In the cyclic voltammetry measurements of the redox potential, phosphines **1a** and **1b** show oxidation and reduction waves with peak potentials at +0.38 and –2.47 and at +0.37 and –2.57 V, respectively (vs. ferrocene/ferrocenium). P-oxidation leads to a positive shift in the redox potential: phosphine oxides **3a** and **3b** show no oxidation wave but two reversible reduction waves with peak potentials at –2.05 and –2.50 and at –2.17 and –2.59 V, respectively. The positive shift of the reduction wave from **1a** to **3a** (0.42 V) is consistent with that estimated in the DFT calculations (0.43 eV). The methyl substituents lead to small negative shifts (ΔE = 0.01–0.12 V), albeit with substantial changes in the molecular conformation. Phosphine oxide **3c** also shows two reversible reduction waves with peak potentials at –2.01 and –2.46 V.

4-2-5. Gold complex of 1b: Synthesis, electronic structure, and molecular structure

The ability of **1b** to coordinate with metals has been demonstrated by the efficient formation (97% yield) of a 1:1 complex with AuCl (Figure 5a). The X-ray crystal structure shows a P–Au distance of 2.2343(12) Å (Figure 5b), which is comparable with those of $AuCl(PPh_3)$ and $AuCl(P^tBu_3)$ (2.233 and 2.253 Å, respectively).[5] Molecular orbital calculations indicate efficient conjugation between the atomic orbitals of the gold center and the aromatic π-orbitals of **1b** (Figure 5c). These observations suggest that the novel π-conjugated phosphines could offer potential utility not only as organic electronics materials but also as ligands for transition metal catalysis. The AuCl(**1b**) complex has a unique packing structure owing to the bowl-shaped conformation of **1b**: the complexes are arranged in an offset face-to-face stacking array with a CH–π distance of 2.85 Å (Figure 5d). Each array consists of a one-handed helical enantiomer (*P*, blue; *M*, pink) and adopts a herringbone-like arrangement with partial π-stacking and an interplanar distance of 3.3–3.4 Å (Figure 5e).

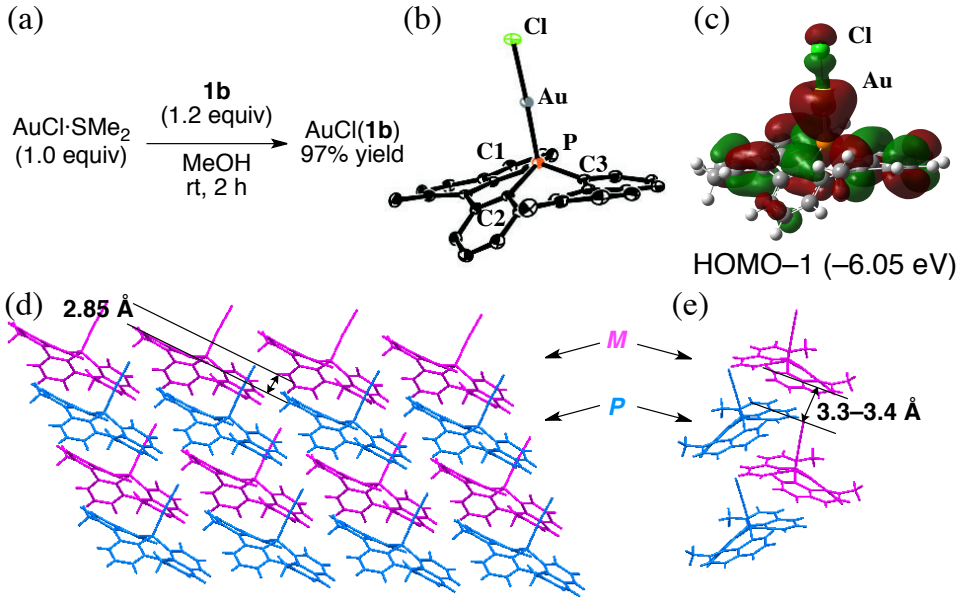

Figure 5. (a) Preparation, (b) ORTEP drawing, (c) Kohn–Sham HOMO–1, and (d) front view and (e) side view of the packing structure (*P*-enantiomer, blue; *M*-enantiomer, pink) of AuCl(**1b**). Selected bond lengths (Å) and angles (deg): Au–Cl = 2.2945(12), Au–P = 2.2343(12), P–C1 = 1.805(6), P–C2 = 1.786(5), P–C3 = 1.815(6), and P–Au–Cl = 175.13(6).

[5] (a) Banditelli, G.; Bandini, A. L.; Minghetti, G.; Bonati, F. *Can. J. Chem.* **1981,** *59*, 1241–1246. (b) Schmidbaur, H.; Brachthäuser, B.; Steigelmann, O.; Beruda, H. *Chem. Ber.* **1992,** *125*, 2705–2710.

4-2-6. Modification of the phospha-Friedel–Crafts reaction: An excess-base–free method

Compound **2b** was also synthesized *via* bis(*N*,*N*-diethylamino)phosphine, as shown in Scheme 3. Lithium-halogen exchange in **4b** and subsequent trapping of the resulting aryllithium with bis(*N*,*N*-diethylamino)chlorophosphine gave *m*-terarylbis(*N*,*N*-diethylamino)phosphine **6b**. After sulfurization of **6b** by S_8, **2b** was obtained *via* the tandem phospha-Friedel–Crafts reaction of **7b** with $AlCl_3$. NEt^iPr_2 is not necessary for this reaction because of the absence of any acidic side product. This method has several advantages over the method shown in Scheme 2: isolation of intermediate **7b** and fine-tuning of the reaction conditions of the phospha-Friedel–Crafts reaction are possible. The lack of acidic side products suppresses undesired side reactions and eliminates the necessity of excess amounts of base additives. These features are practical advantages for the synthesis of molecules containing extended π-conjugation systems or multiple phosphorus atoms, such as the bisphosphine compounds described in the next section.

Scheme 3. Synthesis of **2b** *via* bis(*N*,*N*-diethylamino)phosphine

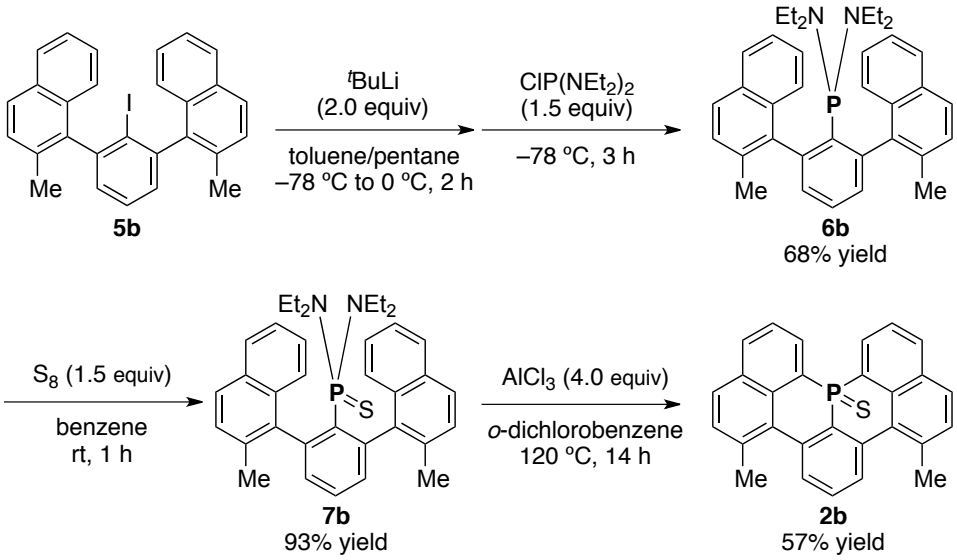

4-2-7. Synthesis of distorted bisphosphine

The synthesis of a double-helical bis(thiophospha)pentacene derivative **2d** demonstrates that multiple phosphorus atoms can be introduced into a π-conjugated framework using this synthetic strategy (Scheme 4). In this synthesis, hexabromobenzene was treated with eight equivalents of aryl Grignard reagents, which gave 2,3,5,6-tetraaryl-1,4-diiodobenzene **4d** in 22% yield upon iodination quenching. Lithium-halogen exchange in **4d** and subsequent trapping of the resulting aryllithium with bis(*N*,*N*-diethylamino)chlorophosphine gave 2,3,5,6-tetraaryl-1,4-bisphophine **6d** in 89% yield. After sulfurization of **6d** by S_8, **2d** was obtained *via* the tandem phospha-Friedel–Crafts reaction of **7d** with $AlCl_3$ in 3% overall yield from

hexabromobenzene. The tandem reaction of the corresponding *p*-phenylenebis(dichlorophosphine) did not give the target compound **2d** with or without NEt^iPr_2.

Scheme 4. Synthesis of **2d**

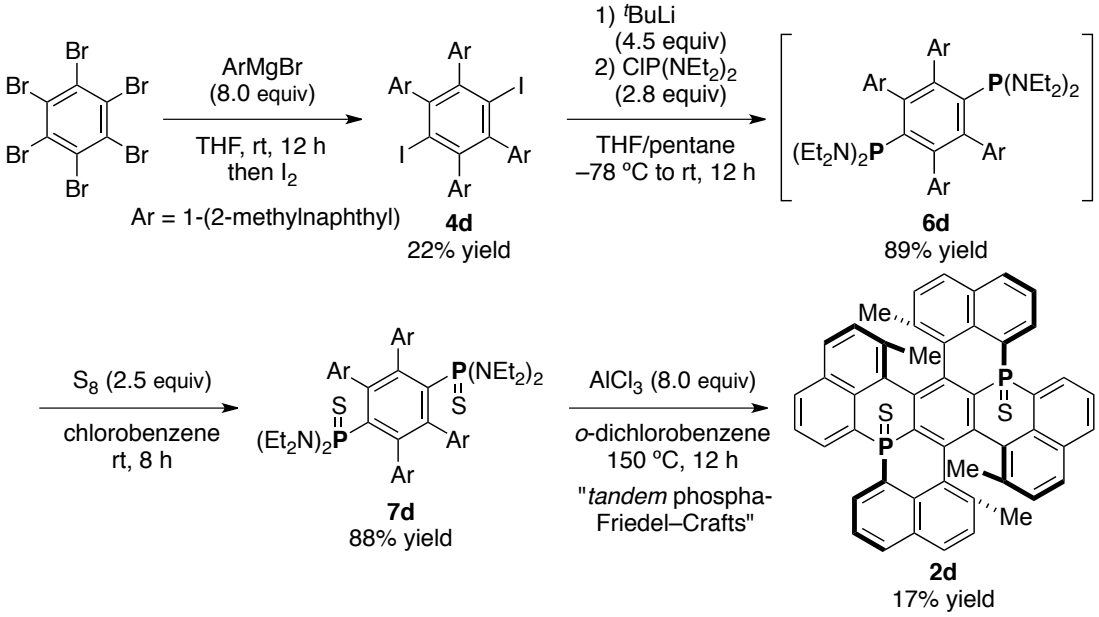

The unexpected double-helical structure[6] of **2d** was confirmed by the X-ray crystallography (Figure 6). The molecule **2d** possesses C_2 symmetry with a *cis* arrangement of the two sulfur atoms (S–S′ distance: 6.402 Å). The two [5]helicene-like fragments of the same helicity (the *M*, *M*′-isomer is shown in Figure 6a) share the central benzene ring and two phosphorus atoms. In the [5]helicene fragment, the torsion angles for each ring are 14.55° for C10–C12–C8–C6, 32.11° for C6–C8–C4–C2, 25.48° for C2–C4–C5′–C2′, 28.14° for C2′–C5′–C9′–C7′, and 11.56° for C7′–C9′–C13′–C11′. Because of the opposite torsion strains introduced by the two independent helicities, the central benzene ring has a large bending angle (23.0°, Figure 6b) that is comparable to that of [1.1]paracyclophane[7] (24.3°), one of the most distorted aromatic compounds. The aromaticities of the six-membered ring in **2d** were evaluated by performing a NICS(0) analysis (Figure 7). The relatively small value of –4.4 in the center of the benzene ring indicates a decrease in aromaticity because of the torsion (planar benzene: –8.0).[8] Despite the highly distorted structure, **2d** was found to be stable even at 600 K under an air atmosphere.

---

[6] Selected papers: (a) Shiraishi, K.; Rajca, A.; Pink, M.; Rajca, S. *J. Am. Chem. Soc.* **2005,** *127*, 9312–9313. (b) Wang, Z.; Shi, J.; Wang, J.; Li, C.; Tian, Z.; Cheng, Y.; Wang, H. *Org. Lett.* **2010,** *12*, 456–459.

[7] Kawai, H.; Suzuki, T.; Ohkita, M.; Tsuji, T. *Angew. Chem., Int. Ed.* **1998,** *37*, 817–819.

[8] Chen, Z.; Wannere, C. S.; Corminboeuf, C.; Puchta, R.; Schleyer, P. v. R. *Chem. Rev.* **2005,** *105*, 3842–3888.

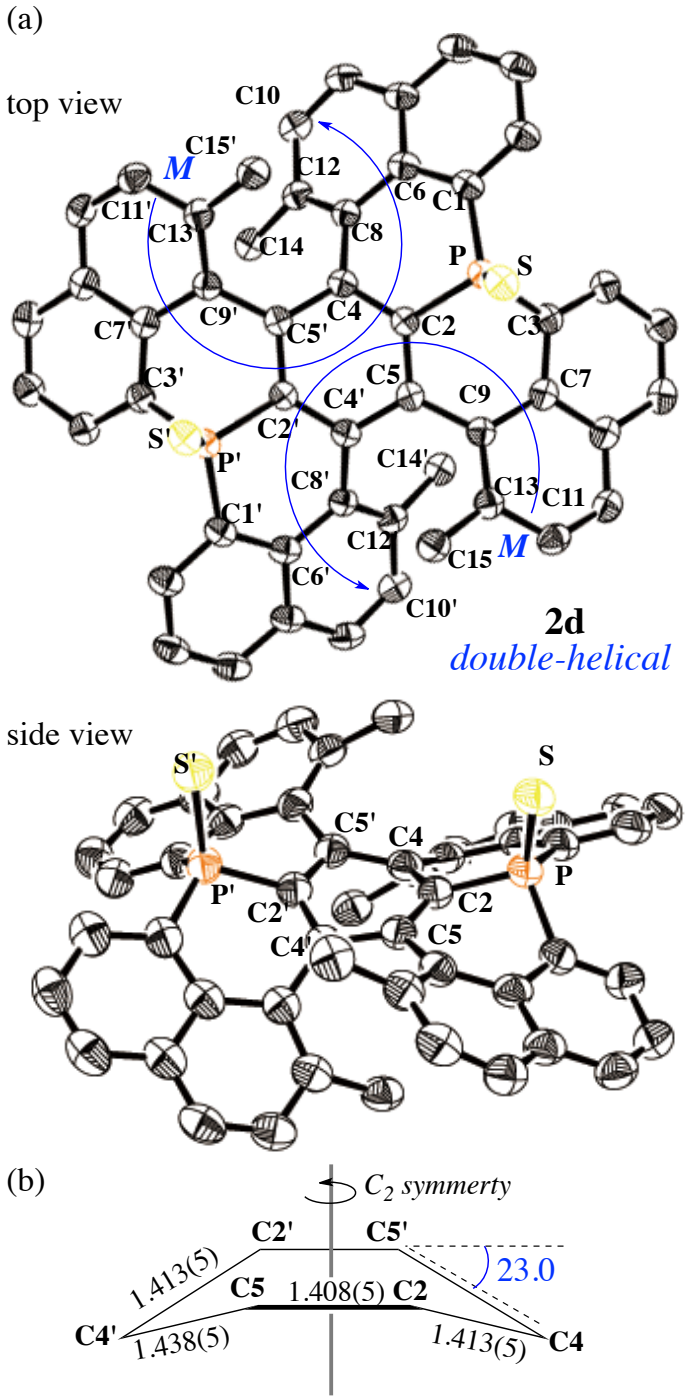

Selected bond lengths
P–S 1.9688(13) Å
P–C1 1.777(4) Å
P–C2 1.777(4) Å
P–C3 1.796(4) Å

Selected distance
S–S' 6.402 Å
P–P' 6.060 Å
C8–C15' 2.947 Å
C14–C9' 2.973 Å

Selected angles
C1–P–C2 105.12(17)°
C2–P–C3 100.24(16)°
C1–P–C3 112.63(13)°

Selected dihedral angles
C10–C12–C8–C6 14.55°
C6–C8–C4–C2 32.11°
C2–C4–C5'–C2' 25.48°
C2'–C5'–C9'–C7' 28.14°
C7'–C9'–C13'–C11' 11.56°

Selected bond lengths
C2–C4 1.413(5) Å
C2–C5 1.408(5) Å
C4'–C5 1.438(5) Å

Selected angles
C4–C2–C5 124.6(3)°
C2–C4–C5' 113.9(3)°
C2–C5–C4' 115.6(3)°

Selected dihedral angles
C4–C2–C5'–C2' 157.11°
C4–C2–C5'–C5 156.95°
C2–C5'–C5–C2' 179.80°

Figure 6. (a) ORTEP drawing of (*M*, *M*′)-**2d** and (b) geometric details of the central benzene ring. Thermal ellipsoids are shown at 50% probability and H atoms have been omitted for clarity.

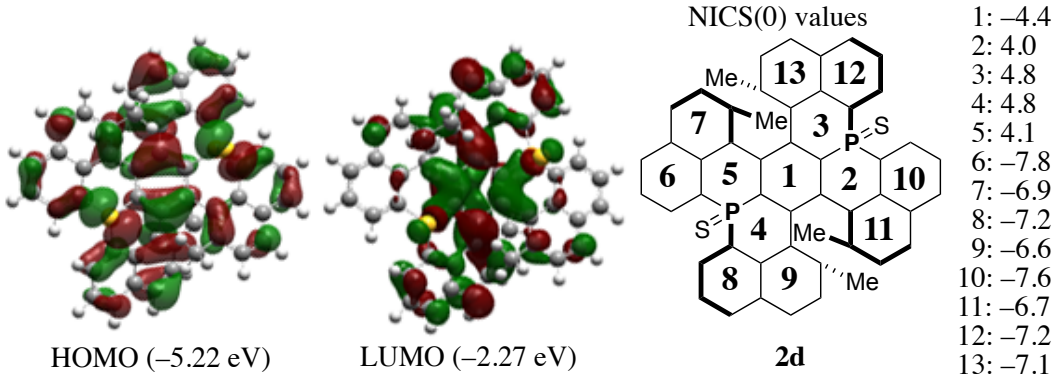

HOMO (–5.22 eV) LUMO (–2.27 eV) **2d**

Figure 7. Kohn–Sham MOs of **2d** calculated at the B3LYP/6-31G(d) level (left) and NICS(0) values calculated at the GIAO/B3LYP/6–311+G(d, p) level (right).

4-3. Conclusions

Novel tandem intramolecular phospha-Friedel–Crafts reactions have been developed, and a series of curved π-conjugated molecules with phosphorus ring junctions have been synthesized based on the newly developed C–P bond formation reaction. In this cyclization reaction, additions of NEt^iPr_2 and sulfur play important roles in improving the selectivity and enhancing the electrophilic reaction activity, respectively. Three types of triarylphosphines containing phosphaperylene frameworks (**1a–c**) and their chalcogenides (**2a–c**, **3a–c**) have been synthesized and characterized. Because of the tetrahedral geometry of the phosphorus centers as well as steric interactions of the substituents, these π-conjugated molecules adopt diverse structures such as helical, bowed, and planar shapes. The rigid molecular frameworks enable these unprecedented phosphine compounds to form π-conjugation systems spread over the whole molecule. Differences between the physical properties of the phosphines and their chalcogenides were also revealed. In particular, the absorption coefficients of the phosphines **1a** were smaller than those of phosphine oxides **3a** because of the substantial contribution of the atomic p-orbital of the phosphorus atom to the HOMO but not to the LUMO. Phosphines (**1a–b**) and phosphine oxides (**3a–c**) exhibit strong fluorescence; however, phosphine sulfide did not exhibit any significant fluorescent intensity, potentially because the lone electron pair of the sulfur atom could quench the excited state.

The double-helical bis(thiophospha)pentacene derivative **2d** has also been synthesized using this synthetic strategy. Although it possesses a distorted structure, thermal decomposition was not observed even at 600 K. The simple and practical synthetic method is suitable for further extension of π-conjugated frameworks as well as the introduction of multiple phosphorus atoms, and it may spur a bottom-up approach to phosphorus-embedded nanocarbons. The synthesized molecules are potentially useful for various applications such as construction of supramolecular metal complexes.

4-4. Experimental Section

General. All the reactions dealing with air- or moisture-sensitive compounds were carried out in a dry reaction vessel under a positive pressure of argon or nitrogen. Air- and moisture-sensitive liquids and solutions were transferred *via* a syringe or a stainless steel cannula. Analytical thin-layer chromatography (TLC) was performed on glass plates coated with 0.25 mm 230–400 mesh silica gel containing a fluorescent indicator (Merck, #1.05715.0009). TLC plates were visualized by exposure to ultraviolet light (254 nm) and/or by immersion in an acidic staining solution of *p*-anisaldehyde followed by heating on a hot plate. Organic solutions were concentrated by rotary evaporation at *ca*. 30–400 mmHg. Flash column chromatography was performed on Merck silica gel 60 (spherical, neutral, 140–325 mesh) as described by Still et al.[9] Gel permeation chromatography was performed on a JAIGEL-1H and 2H (20 mm i.d.) with an LC-918 (Japan Analytical Industry Co., Ltd.).

Instrumentation. Proton nuclear magnetic resonance (^{1}H NMR), carbon nuclear magnetic resonance (^{13}C NMR), phosphorus nuclear magnetic resonance (^{31}P NMR) spectra were recorded on JEOL ECS400 (392 MHz) or BRUKER AVANCE III (600 MHz) NMR spectrometers. Proton chemical shift values are reported in parts per million (ppm, δ scale) downfield from tetramethylsilane. ^{13}C NMR spectra were recorded at 98.5 or 151 MHz: carbon chemical shift values are reported in parts per million (ppm, δ scale) downfield from tetramethylsilane and are referenced to the carbon resonance of CD_2Cl_2 (δ 53.8). ^{31}P NMR spectra were recorded at 158.6 MHz: Phosphorus chemical shift values are reported in parts per million (ppm, δ scale) and are referenced to the external standard phosphorus signal of $(PhO)_3P{=}O$ ($CDCl_3$, δ –16.4) or PPh_3 (CD_2Cl_2, δ –6.0). Data are presented as: chemical shift, multiplicity (s = singlet, d = doublet, t = triplet, q = quartet, quint = quintet, sext = sextet, sept = septet, m = multiplet and/or multiplet resonances, br = broad), coupling constant in hertz (Hz), signal area integration in natural numbers, and assignment (*italic*). IR spectra were recorded on an ATR-FTIR spectrometer (FT/IR-Spectrum One, PerkinElmer). Characteristic IR absorptions are reported in cm^{-1}. Melting points were recorded on a Yanaco MP-500D. High-resolution mass spectra (HRMS) were obtained using the electron impact (EI) method or fast atom bombardment (FAB) method with JEOL JMS-700, JMS-HX110A and JMS-SX102A. UV-visible spectra were measured by JASCO Ubest V-570. Fluorescence spectra and absolute quantum yields were recorded on a Hamamatsu Photonics C9920-02 Absolute PL Quantum Yield Measurement System. Fluorescence lifetimes were recorded on a HORIBA FluoroCube 1000-U. Cyclic voltammetry was conducted on a BAS Electrochemical Analyzer ALS 620C using a three-electrode cell with a glassy carbon working electrode, a platinum wire counter electrode, and an $Ag/AgNO_3$ reference electrode. Purity of isolated compounds

[9] Still, W. C.; Kahn, M.; Mitra, A. *J. Org. Chem.* **1978,** *43*, 2923–2925.

was determined by GC analysis on Shimadzu GC-17A instrument equipped with an FID detector and a capillary column, InertCap 1MS (GL Sciences Inc., 30 m × 0.25 mm i.d., 0.25 μm film thickness) and/or ^{1}H NMR analyses.

Solvent. Anhydrous tetrahydrofuran (THF) and toluene were purchased from Wako Pure Chemical Industries, Ltd. (Wako) and dried over Molecular Sieves 4A and degassed before use. Water content of the solvent was determined with a Karl Fischer Moisture Titrator (MKC-210, Kyoto Electronics Company) to be less than 15 ppm.

Materials. Materials were purchased from Wako, Tokyo Chemical Industry Co., Ltd., Aldrich Inc., and other commercial suppliers, and were used after appropriate purification, unless otherwise noted. Florisil® (100–200 mesh) was purchased from Wako. Arylmagnesium bromides (ArMgBr) were prepared from the corresponding aryl bromides and magnesium (turnings) using a standard method and titrated before use. Aryl halides were purified by distillation or recrystallization to be over 99.5% pure by GC analysis.

Synthesis of 1,1′-(2-iodo-1,3-phenylene)dinaphthalene (4a)

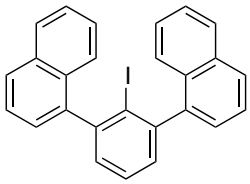

A solution of butyllithium in hexane (30.7 mL, 1.63 M, 50 mmol) was added slowly to a solution of 1,3-dichlorobenzene (7.35 g, 50 mmol) in THF (80 mL) at –78 ºC under argon. After 2 h, reaction mixture was added to a suspension of 1-naphthylmagnesium bromide in THF (100 mL, 1.00 M, 0.10 mol) at 0 ºC. After stirring at room temperature for 1 h, the reaction mixture was allowed to warm to 80 ºC and stirred for 18 h. Iodine (19.0 g, 75 mmol) was added to the reaction mixture at 0 ºC. After stirring at room temperature for 30 min, a saturated aqueous solution of Na_2SO_3 (150 mL) was added. The aqueous layer was separated and extracted with diethyl ether (100 mL, three times). The organic layers were combined and washed with a saturated aqueous solution of NaCl (200 mL). The organic layer was dried over $MgSO_4$ and condensed *in vacuo*. The resultant yellow residue was triturated with hexane by using a sonicator to give the title compound as a white-yellow solid (18.1 g, 79% yield, > 98% pure on GC analysis). IR (neat): cm^{-1} 3049 (Ar-H), 1506, 1380, 1011, 799, 775, 733, 699; mp: 205.6–206.4 ºC; ^1H NMR (CD_2Cl_2, 400 MHz) δ 7.39–7.61 (m, 13H), 7.90–7.96 (m, 4H); ^{13}C NMR (CD_2Cl_2, 98.5 MHz) δ 106.9–107.2 (two peaks derived from axial diastereomers), 125.6 (2C), 126.2, 126.3, 126.4, 126.5, 126.6, 127.3, 127.5, 128.1, 128.2, 128.4 (2C), 128.5, 128.6, 130.1 (2C), 131.9 (2C), 133.9 (2C), 143.5, 143.6, 146.8, 146.9; HRMS (FAB) *m/z* $[M]^+$ calcd for $C_{26}H_{17}I$ 456.0375; observed 456.0379.

Synthesis of 1,1′-(2-iodo-1,3-phenylene)bis(2-methylnaphthalene) (4b)

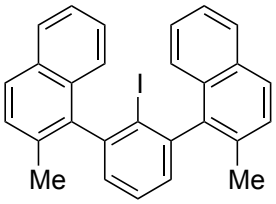

A solution of butyllithium in hexane (18.3 mL, 1.64 M, 30 mmol) was added slowly to a solution of 1,3-dichlorobenzene (4.41 g, 30 mmol) in THF (40 mL) at –78 ºC under argon. After 2 h, a solution of (2-methylnaphthalen-1-yl)magnesium bromide in THF (69.8 mL, 0.86 M, 60 mmol) was added at 0 ºC. After stirring at room temperature for 1 h, the reaction mixture stirred at 80 ºC for 14 h. Iodine (8.38 g, 33 mmol) was added to the reaction mixture at 0 ºC. After stirring at room temperature for 30 min, a saturated aqueous solution of Na_2SO_3 (100 mL) was added. The aqueous layer was separated and extracted with diethyl ether (100 mL, three times). The organic layers were combined and washed with a saturated aqueous solution of NaCl (200 mL). The organic layer was dried over $MgSO_4$ and condensed *in vacuo*. The resultant yellow residue was triturated

with hexane by using a sonicator to give the title compound as a white-yellow solid (4.65 g, 32% yield, > 98% pure on GC analysis). IR (neat): cm^{-1} 3837, 3735, 3045 (Ar-H), 1595, 1508, 1451, 1375, 1213, 1026, 1013, 866, 856, 809, 797, 781, 744, 691, 673; mp: 169.9–170.9 ºC; ^{1}H NMR (CD_2Cl_2, 392 MHz) δ 2.25–2.29 (two peaks derived from axial diastereomers, 6H, C*H*$_3$), 7.24–7.45 (m, 10H), 7.66 (t, *J* = 7.3 Hz, 1H, CCHC*H*CHC), 7.83–7.88 (m, 4H); ^{13}C NMR (CD_2Cl_2, 98.5 MHz) δ 20.5 (2C), 107.8, 125.3 (2C), 125.6, 125.7 (2C), 126.5 (2C), 128.0, 128.1 (2C), 128.2, 129.0 (2C), 129.2 (2C), 129.7 (2C), 132.4 (2C), 133.7 (2C), 141.3 (2C), 146.3 (2C); HRMS (FAB) *m*/*z* $[M]^+$ calcd for $C_{28}H_{21}I$ 484.0688; observed 484.0686.

Synthesis of 5,5′-(2-iodo-1,3-phenylene)bis(1,2-dihydroacenaphthylene) (4c)

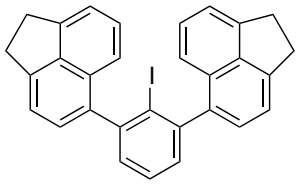

The reaction was carried out according to the synthetic procedure for **4b** described above on a 0.20 mol scale by using a solution of butyllithium in hexane (122.7 mL, 1.63 M, 0.20 mol), 1,3-dichlorobenzene (29.4 g, 0.20 mol) in THF (300 mL), a solution of (1,2-dihydroacenaphthylen-5-yl)magnesium bromide in THF (400 mL, 1.00 M, 0.40 mol) and iodine (101.5 g, 0.40 mol). Conditions: 0 ºC, 2 h then 80 ºC, 14 h. The title compound (72.6 g, 71% yield, > 99% pure on GC analysis) was obtained as a white-yellow solid after trituration with hexane, methanol and acetonitrile. IR (neat): cm^{-1} 3837, 3734, 3030 (Ar-H), 1604, 1574, 1499, 1444, 1422, 1398, 1367, 1268, 1216, 1112, 1009, 893, 838, 798, 772, 745, 731; mp: 266.7–267.6 ºC; ^{1}H NMR (CD_2Cl_2, 392 MHz) δ 3.43–3.46 (m, 8H, C*H*$_2$), 7.26–7.48 (m, 12H), 7.53 (dt, *J* = 2.8, 7.6 Hz, 1H, ICCCHC*H*); ^{13}C NMR (CD_2Cl_2, 98.5 MHz) δ 30.5 (2C), 30.9 (2C), 107.2–107.4 (two peaks derived from axial diastereomers), 119.1, 119.8 (2C), 121.2, 121.3, 128.0, 128.1, 128.3, 128.4, 129.0, 129.2, 130.0 (2C), 130.2, 130.3, 139.2 (2C), 139.5 (2C), 146.5 (2C), 146.6 (2C), 146.7, 146.8; HRMS (FAB) *m*/*z* $[M]^+$ calcd for $C_{30}H_{21}I$ 508.0688; observed 508.0680.

Synthesis of 15b-(thiophospha)naphtho[1,8-*ab*]perylene (2a)

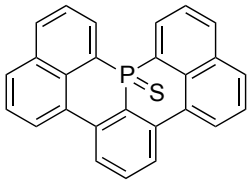

A solution of tertiary butyllithium in pentane (2.58 mL, 1.55 M, 4.0 mmol) was added slowly to a solution of **4a** (0.913 g, 2.0 mmol) in toluene (20 mL) at –78 ºC under argon. After 1 h, the solution was allowed to warm to 0 ºC and stirred for 1 h,

trichlorophosphine (0.275 g, 2.0 mmol) was added to reaction mixture at –78 ºC. After stirring at room temperature for 2 h, pentane was removed *in vacuo*, and the reaction mixture was added to a solution of aluminum trichloride (0.800 g, 6.0 mmol), sulfur powder (96.0 mg, 3.0 mmol) and NEt^iPr_2 (0.517 g, 4.0 mmol) in toluene (10 mL) at 0 ºC. After stirring at 80 ºC for 14 h, 1,4-diazabicyclo[2.2.2]octane (0.673 g, 6.0 mmol) was added. The reaction mixture was filtered with a pad of Celite® and Florisil®. After the solvent was removed *in vacuo*, the crude product was purified by chromatography on silica gel (20%, 50% dichloromethane in toluene) to obtain the title compound (0.102 g, 13% yield, > 99% pure on GC analysis) as yellow solid. IR (neat): cm^{-1} 3045 (Ar-H), 1565, 1442, 1354, 1257, 1212, 1192, 1147, 1084, 924, 831, 796, 767, 713, 649, 628, 585; mp: 348.8–349.5 ºC; ^{1}H NMR (392 MHz, CD_2Cl_2) δ 7.77–7.87 (m, 5H), 8.07 (d, *J* = 8.2 Hz, 2H, PCCHCHC*H*), 8.18 (d, *J* = 8.2 Hz, 2H, PCCHCHCHCC*H*), 8.22 (dd, *J* = 4.1, 8.2 Hz, 2H, PCCC*H*), 8.57 (d, *J* = 7.8 Hz, 2H, PCCCC*H*), 8.62 (dd, *J* = 7.3, 14.2 Hz, 2H, PCC*H*); ^{13}C NMR (CD_2Cl_2, 151 MHz) δ 123.6, 124.1, 125.8, 126.5, 126.6, 126.7, 126.8, 127.4 (2C), 127.6, 128.2, 128.6 (2C), 130.0, 130.1, 131.1 (2C), 131.8 (2C), 131.9, 132.9, 133.0, 134.3, 134.4, 137.7, 137.8; ^{31}P NMR (CD_2Cl_2, 158.6 MHz) δ –7.59; HRMS (FAB) *m/z* $[M+H]^+$ calcd for $C_{26}H_{16}PS$ 391.0710; observed 391.0712.

Synthesis of 6,10-dimethyl-15b-(thiophospha)naphtho[1,8-*ab*]perylene (2b)

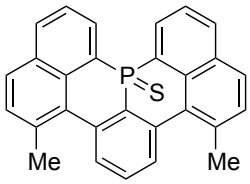

The reaction was carried out according to a procedure similar to that described for the synthesis of **2a** on a 2.0 mmol scale by using a solution of tertiary butyllithium in pentane (2.58 mL, 1.55 M, 4.0 mmol), a solution of **4b** (0.969 g, 2.0 mmol) in toluene (20 mL), trichlorophosphine (0.275 g, 2.0 mmol), a solution of aluminum trichloride (0.800 g, 6.0 mmol), sulfur powder (96.0 mg, 3.0 mmol) and NEt^iPr_2 (0.517 g, 4.0 mmol) in toluene (10 mL). Conditions: 0 ºC, 1 h; room temperature, 2 h; then 80 ºC, 12 h. The title compound (0.363 g, 43% yield, > 99% pure on GC analysis) was obtained as a white-yellow solid after silica gel chromatography (20%, 50% dichloromethane in toluene). IR (neat): cm^{-1} 3735, 3050 (Ar-H), 2943, 1593, 1572, 1499, 1443, 1360, 1328, 1227, 1147, 1134, 1075, 924, 899, 831, 815, 731, 664, 637, 580; mp: decomposes 380 ºC; ^{1}H NMR (392 MHz, CD_2Cl_2) δ 2.99 (s, 6H, CH_3), 7.57 (t, *J* = 8.2 Hz, 1H, PCCCHC*H*), 7.66 (d, *J* = 8.7 Hz, 2H, CH_3C*H*), 7.70–7.75 (m, 4H), 7.89 (d, *J* = 8.7 Hz, 2H, CH_3CHC*H*), 8.06 (d, *J* = 8.2 Hz, 2H, PCCHCHC*H*), 8.58 (dd, *J* = 7.3, 13.7 Hz, 2H, PCC*H*); ^{13}C NMR (CD_2Cl_2, 98.5 MHz) δ 24.2 (2C), 125.6, 125.8, 127.6, 128.5, 129.0 (2C), 129.7, 130.3 (2C), 130.4 (2C), 130.9 (2C), 131.0, 131.1, 131.8 (2C), 132.1 (2C), 132.2 (3C), 136.6 (2C), 138.6 (2C); ^{31}P NMR (CD_2Cl_2, 158.6 MHz) δ –8.04; HRMS (EI) *m/z* $[M]^+$ calcd for $C_{28}H_{19}PS$ 418.0945; observed 418.0946.

Synthesis of 15b-thiophospha-3,4,12,13-tetrahydroacenaphtho[5,6-*ab*]cyclopenta [*lm*]perylene (2c)

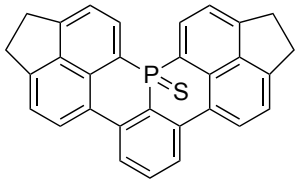

The reaction was carried out according to a procedure similar to that described for the synthesis of **2a** on a 2.0 mmol scale by using a solution of tertiary butyllithium in pentane (2.52 mL, 1.59 M, 4.0 mmol), a solution of **4c** (1.02 g, 2.0 mmol) in toluene (12 mL), trichlorophosphine (0.275 g, 2.0 mmol) and a solution of aluminum trichloride (0.800 g, 6.0 mmol), sulfur powder (96.0 mg, 3.0 mmol) and NEt^iPr_2 (0.517 g, 4.0 mmol) in toluene (10 mL). Conditions: 0 ºC, 1 h; room temperature, 2 h; then 80 ºC, 18 h. The title compound (0.097 g, 11% yield) was obtained as a yellow solid after purification by GPC (eluent: $CHCl_3$). IR (neat): cm^{-1} 3036 (Ar-H), 2914, 2827, 1598, 1559, 1442, 1412, 1366, 1304, 1252, 1205, 1190, 1091, 850, 834, 788, 708, 648, 630, 590, 570; mp: decomposes 420 ºC; ^{1}H NMR (392 MHz, CD_2Cl_2) δ 3.47–3.64 (m, 8H, C*H*$_2$), 7.59 (d, *J* = 7.4 Hz, 2H, PCCCCHC*H*), 7.68 (d, *J* = 7.8 Hz, 2H, PCCHC*H*), 7.74 (t, *J* = 8.2 Hz, 1H, CHC*H*CH), 8.26 (dd, *J* = 4.1, 8.2 Hz, 2H, C*H*CHC*H*), 8.52 (d, *J* = 7.4 Hz, 2H, PCCCC*H*), 8.61 (dd, *J* = 7.8, 13.8 Hz, 2H, PCC*H*); ^{13}C NMR (CD_2Cl_2, 151 MHz) δ 30.6 (2C), 31.5 (2C), 121.2, 121.3 (3C), 125.1 (2C), 125.6, 125.8, 126.7 (2C), 128.3 (2C), 128.5 (2C), 129.3 (2C), 130.9, 131.3, 132.6 (2C), 132.7 (2C), 133.6 (2C), 149.6, 150.2; ^{31}P NMR (CD_2Cl_2, 158.6 MHz) δ –8.07; HRMS (FAB) *m/z* $[M+H]^+$ calcd for $C_{30}H_{20}PS$ 443.1023; observed 443.1034. Anal. calcd for $C_{30}H_{19}PS$ C, 81.43; H, 4.33, found C, 81.16; H, 4.46.

Synthesis of 15b-phosphanaphtho[1,8-*ab*]perylene (1a)

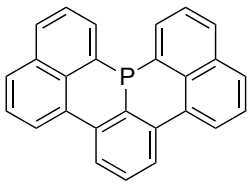

Triethylphosphine (20.0 mg, 0.17 mmol) was added to a solution of **2a** (59.0 mg, 0.15 mmol) in chlorobenzene (1.0 mL) at 0 ºC under argon. After stirring at 120 ºC for 12 h, the solution was condensed *in vacuo*, and triturated with hexane by using a sonicator to give the title compound as a yellow solid (40.0 mg, 75% yield, > 99% pure on GC analysis). IR (neat): cm^{-1} 3045 (Ar-H), 1562, 1491, 1438, 1401, 1354, 1317, 1188, 1150, 1082, 969, 822, 790, 763, 753, 697, 578; mp: 171.0–171.7 ºC; ^{1}H NMR (C_6D_6, 392 MHz) δ 7.14 (t, *J* = 8.2 Hz, 1H, PCCCHC*H*), 7.24 (dd, *J* = 6.9, 7.8 Hz, 2H, PCCHC*H*), 7.25 (dd, *J* = 8.2, 8.7 Hz, 2H, PCCCCHC*H*), 7.51 (d, J = 8.7 Hz, 2H, PCCHCHCHCC*H*), 7.55 (d, *J* = 8.2 Hz, 2H, PCCCC*H*), 7.57 (dd, *J* = 2.3, 8.2 Hz, 2H,

PCCC*H*), 7.87 (d, *J* = 7.8 Hz, 2H, PCCHCHC*H*), 7.92 (dd, *J* = 6.9, 6.9 Hz, 2H, PCC*H*); ^{13}C NMR (CD_2Cl_2, 98.5 MHz) δ 122.9, 125.9 (2C), 126.1, 126.2, 127.0, 127.2 (2C), 127.4, 128.2, 129.2, 129.6, 129.7, 129.9, 130.1, 131.0, 132.3, 133.5 (2C), 133.6, 135.0 (2C), 136.3, 136.4 (2C), 138.7; ^{31}P NMR (CD_2Cl_2, 158.6 MHz) δ –41.53 (–39.74 in $CDCl_3$); HRMS(EI) *m*/*z* $[M]^+$ calcd for $C_{26}H_{15}P$ 358.0911; observed 358.0912.

Synthesis of 6,10-dimethyl-15b-phosphanaphtho[1,8-*ab*]perylene (1b)

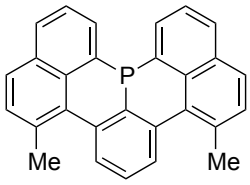

The reaction was carried out according to a procedure similar to that described for the synthesis of **1a** on a 0.40 mmol scale by using triethylphosphine (52.0 mg, 0.44 mmol), **2b** (0.167 g, 0.40 mmol) and chlorobenzene (2.0 mL). Conditions: 120 ºC, 12 h. The title compound (0.115 g, 80% yield, > 99% pure on GC analysis) was obtained as a yellow solid after triturated with hexane. IR (neat): cm^{-1} 3045 (Ar-H), 2977, 2942, 1592, 1571, 1548, 1500, 1444, 1357, 1340, 1320, 1179, 1148, 1083, 1070, 999, 878, 825, 805, 760, 746, 736, 659, 575, 541; mp: 219.1–220.0 ºC; ^{1}H NMR (CD_2Cl_2, 392 MHz) δ 2.86 (s, 6H, CH_3), 7.40 (t, *J* = 7.8 Hz, 1H, PCCCHC*H*), 7.47 (m, 2H, PCCHC*H*), 7.53–7.58 (m, 4H), 7.77 (d, *J* = 8.7 Hz, 2H, CH_3CHC*H*), 7.78 (d, *J* = 8.2 Hz, 2H, PCCHCHC*H*), 8.23 (t, *J* = 7.3 Hz, 2H, PCC*H*); ^{13}C NMR (CD_2Cl_2, 98.5 MHz) δ 23.5 (2C), 125.2, 125.3, 127.2, 127.3 (2C), 127.4, 127.8, 128.5 (2C), 129.8 (2C), 130.1, 130.5, 130.7, 131.5 (2C), 132.8 (2C), 133.5 (2C), 133.6 (2C), 134.0, 134.1, 135.4, 135.5; ^{31}P NMR (CD_2Cl_2, 158.6 MHz) δ –44.60 (–42.76 in $CDCl_3$); HRMS (EI) *m*/*z* $[M]^+$ calcd for $C_{28}H_{19}P$ 386.1224; observed 386.1222.

Synthesis of 15b-phospha-3,4,12,13-tetrahydroacenaphtho[5,6-*ab*]cyclopenta[*lm*] perylene (1c)

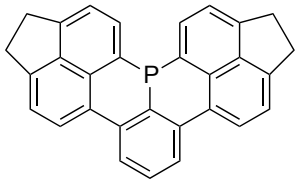

The reaction was carried out according to a procedure similar to that described for the synthesis of **1a** on a 0.10 mmol scale by using triethylphosphine (13.0 mg, 0.11 mmol), **2c** (44.3 mg, 0.10 mmol) and chlorobenzene (1.0 mL). Conditions: 120 ºC, 12 h. The title compound (31.3 mg, 76% yield) was obtained as a yellow solid after triturated with hexane. IR (neat): cm^{-1} 3036 (Ar-H), 2913, 2828, 1598, 1559, 1442, 1412, 1366, 1243, 1190, 1091, 919, 849, 833, 787, 707, 648, 630, 584; mp: decomposes 361 ºC; ^{1}H NMR (CD_2Cl_2, 392 MHz) δ 3.40–3.44 (m, 8H, CH_2), 7.37–7.40 (m, 3H), 7.43 (d, *J* = 6.9 Hz, 2H, PCCHC*H*), 7.91 (dd, *J* = 2.8, 8.2 Hz, 2H, PCCC*H*CH), 8.03 (dd, *J* = 6.9, 6.9 Hz,

2H, PCC*H*), 8.11 (d, *J* = 7.3 Hz, 2H, PCCCCHC*H*); ^{13}C NMR (CD_2Cl_2, 98.5 MHz) δ 30.6 (2C), 30.9 (2C), 120.7 (2C), 120.8 (2C), 123.4 (2C), 124.3 (2C), 128.1 (2C), 128.3 (2C), 128.6, 129.9, 134.2 (2C), 136.6 (2C), 136.7 (2C), 140.2 (2C), 146.0 (2C), 148.1 (2C); ^{31}P NMR (CD_2Cl_2, 158.6 MHz) δ –38.38; HRMS (FAB) *m/z* $[M]^+$ calcd for $C_{30}H_{19}P$ 410.1224; observed 410.1218.

Synthesis of 15b-(oxophospha)naphtho[1,8-*ab*]perylene (3a)

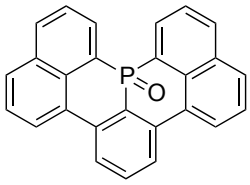

Hydrogen peroxide (30%, 1.5 mL) was added to a solution of **2a** (58.6 mg, 0.15 mmol) in dichloromethane (50 mL) at room temperature. After 6 h, the combined organic extracts were purified by silica gel column chromatography (dichloromethane, ethyl acetate) to obtain the title compound as a yellow solid (44.4 mg, 79% yield, > 99% pure on GC analysis). IR (neat): cm^{-1} 3058 (Ar-H), 1571, 1496, 1442, 1354, 1322, 1260, 1178 (P=O), 1120, 1092, 924, 831, 795, 758, 715, 654; mp: 304.1–305.0 ºC; ^{1}H NMR (CD_2Cl_2, 392 MHz) δ 7.77–7.87 (m, 5H), 8.08 (d, *J* = 8.2 Hz, 2H, PCCHCHC*H*), 8.23 (d, *J* = 8.7 Hz, 2H, PCCHCHCHCC*H*), 8.26 (dd, *J* = 4.1, 8.2 Hz, 2H, PCCC*H*), 8.60 (d, *J* = 7.8 Hz, 2H, PCCHCHCHCCHCHC*H*), 8.64 (dd, *J* = 7.3, 12.8 Hz, 2H, PCC*H*); ^{13}C NMR (CD_2Cl_2, 151 MHz) δ 123.9, 124.6, 126.0, 126.1, 126.2, 126.3 (3C), 126.7, 127.3 (2C), 129.6, 129.7, 130.1, 130.2, 131.0 (2C), 132.3, 132.4 (2C), 133.6 (2C), 134.3 (2C), 138.7, 138.8; ^{31}P NMR (CD_2Cl_2, 158.6 MHz) δ –12.24; HRMS (EI) *m/z* $[M]^+$ calcd for $C_{26}H_{15}PO$ .374.0861; observed 374.0862.

Synthesis of 6,10-dimethyl-15b-(oxophospha)naphtho[1,8-*ab*]perylene (3b)

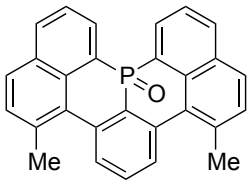

The reaction was carried out according to a procedure similar to that described for the synthesis of **3a** on a 0.20 mmol scale by using hydrogen peroxide (30%, 2.0 mL), **2b** (77.0 mg, 0.20 mmol) and dichloromethane (20 mL). Conditions: room temperature, 6 h. The title compound (57.0 mg, 71% yield, > 99% pure on GC analysis) was obtained as a yellow solid after silica gel column chromatography (dichloromethane, ethyl acetate). IR (neat): cm^{-1} 3050 (Ar-H), 1591, 1568, 1498, 1450, 1360, 1324, 1230, 1176 (P=O), 1149, 1124, 1082, 931, 851, 826, 810, 746, 715, 670, 662, 592, 557; mp: decomposes 360 ºC; ^{1}H NMR (CD_2Cl_2, 392 MHz) δ 2.99 (s, 6H, CH_3), 7.62 (t, *J* = 8.2 Hz, 1H, PCCCHC*H*), 7.66 (d, *J* = 8.7 Hz, 2H, CH_3C*H*), 7.71–7.76 (m, 4H), 7.91 (dd, *J* = 1.4, 8.7 Hz, 2H, CH_3CHC*H*), 8.12 (d, *J* = 8.2 Hz, 2H, PCCHCHC*H*), 8.64 (dd, *J* = 6.7,

12.4 Hz, 2H, PCC*H*); ^{13}C NMR (CD_2Cl_2, 98.5 MHz) δ 24.3 (2C), 125.3, 125.4, 128.9 (2C), 130.1, 130.3, 130.4 (2C), 130.8, 130.9, 131.4 (3C), 131.5, 131.6, 132.1 (2C), 132.2 (3C), 132.7 (2C), 137.0 (2C), 140.0, 140.1; ^{31}P NMR (CD_2Cl_2, 158.6 MHz) δ –10.56; HRMS (EI) *m*/*z* $[M+H]^+$ calcd for $C_{28}H_{20}PO$ 403.1252; observed 403.1245.

Synthesis of 15b-oxophospha-3,4,12,13-tetrahydroacenaphtho[5,6-*ab*]cyclopenta[*lm*]perylene (3c)

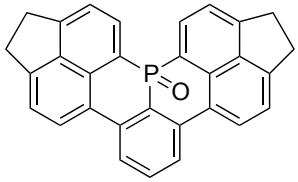

The reaction was carried out according to a procedure similar to that described for the synthesis of **3a** on a 0.22 mmol scale by using hydrogen peroxide (30%, 2.2 mL), **2c** (96.0 mg, 0.22 mmol), dichloromethane (220 mL). Conditions: room temperature, 6 h. The title compound (0.066 g, 70% yield) was obtained as a yellow solid after GPC (eluent: $CHCl_3$). IR (neat): cm^{-1} 3028 (Ar-H), 2921, 1775, 1716, 1598, 1580, 1563, 1445, 1414, 1368, 1256, 1191, 1159 (P=O), 1138, 1107, 1058, 1042, 856, 838, 791, 723, 690, 621, 594; mp: decomposes 360 ºC; ^{1}H NMR (CD_2Cl_2, 392 MHz) δ 3.52–3.62 (m, 8H, CH_2), 7.60 (d, *J* = 7.8 Hz, 2H, PCCCCHC*H*), 7.68 (d, *J* = 7.3 Hz, 2H, PCCHC*H*), 7.78 (t, *J* = 8.2 Hz, 1H, CHC*H*CH), 8.31 (dd, *J* = 4.1, 8.2 Hz, 2H, C*H*CHC*H*), 8.55 (d, *J* = 7.8 Hz, 2H, PCCCC*H*), 8.66 (dd, *J* = 7.3, 12.4 Hz, 2H, PCC*H*); ^{13}C NMR (CD_2Cl_2, 151 MHz) δ 30.6 (2C), 31.6 (2C), 120.7, 120.8, 121.2 (2C), 124.5 (2C), 126.2, 126.3, 127.0 (2C), 127.8 (2C), 127.9, 131.8, 133.2, 133.3, 138.2, 138.3, 139.5 (2C), 149.5, 151.8, 152.6, 152.7 (2C), 155.2; ^{31}P NMR (CD_2Cl_2, 158.6 MHz) δ –12.61; HRMS (EI) *m*/*z* $[M+H]^+$ calcd for $C_{30}H_{20}PO$ 427.1252; observed 427.1244.

Synthesis of chloro[6,10-dimethyl-15b-phosphanaphtho[1,8-*ab*]perylene-κP-15b]gold(I)

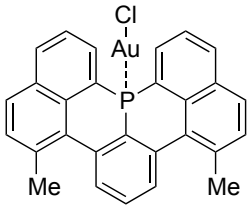

$AuCl{\cdot}SMe_2$ (29.4 mg, 0.10 mmol) was added to a suspension of **1b** (38.6 mg, 0.10 mmol) in methanol (2.0 mL) at 0 ºC under argon. After stirring at room temperature for 2 h, the solution was condensed *in vacuo*, and purified by chromatography on silica gel (dichloromethane, ethyl acetate) to obtain the title compound as a colorless solid (60.0 mg, 97% yield). IR (neat): cm^{-1} 3746, 3059 (Ar-H), 2982, 1608, 1593, 1573, 1498, 1447, 1361, 1330, 1228, 1148, 1076, 1020, 931, 895, 834, 809, 780, 742, 708, 657, 577, 545; mp: decomposes 340 ºC; ^{1}H NMR (CD_2Cl_2, 392 MHz) δ 2.96 (s, 6H, CH_3), 7.58 (t, *J* = 8.2 Hz, 1H, PCCCHC*H*), 7.63–7.74 (m, 6H), 7.90 (dd, *J* = 1.4, 8.7 Hz, 2H,

PCCHCHC*H*), 8.04 (d, *J* = 8.2 Hz, 2H, CH_3CCHCH), 8.44 (dd, *J* = 7.4, 13.8 Hz, 2H, PCC*H*); ^{13}C NMR (CD_2Cl_2, 98.5 MHz) δ 23.9 (2C), 125.4, 125.6, 129.4 (2C), 130.4 (2C), 130.5, 130.6, 130.7 (2C), 130.8, 130.9, 131.0, 131.1, 131.2 (2C), 131.6, 131.7, 132.4, 132.5 (2C), 132.6, 136.7 (2C), 137.9 (2C); ^{31}P NMR (CD_2Cl_2, 158.6 MHz) δ –28.38; HRMS (FAB) *m*/*z* $[M\text{-}Cl]^+$ calcd for $C_{28}H_{19}PAu$ 583.0890; observed 583.0887.

Synthesis of 1,1′,1′′,1′′′-(3,6-diiodobenzene-1,2,4,5-tetrayl)tetrakis(2-methyl naphthalene) (4d)

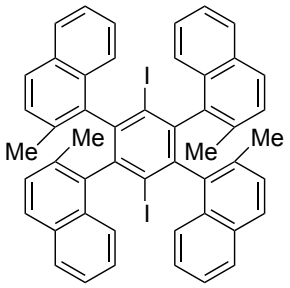

A solution of 1-(2-methylnaphthyl) magnesium bromide in THF (200 mL, 1.20 M, 240 mmol) was added to hexabromobenzene (16.5 g, 30 mmol) at 0 ºC. After stirring at room temperature for 1 h, the reaction mixture stirred at 80 ºC for 14 h. Iodine (60.9 g, 240 mmol) was added to the reaction mixture at 0 ºC. After stirring at room temperature for 30 min, a saturated aqueous solution of Na_2SO_3 (300 mL) was added. The aqueous layer was separated and extracted with dichrolomethane (100 mL, three times). The organic layer was dried over $MgSO_4$ and condensed *in vacuo*. The resultant brown residue was triturated with hexane by using a sonicator to give the title compound as a white-yellow solid (5.10 g, 19% yield). ^1H NMR (CD_2Cl_2, 392 MHz) δ 2.19–2.49 (s, 12H, seven peaks of methyl substitutes derived three stereoisomers), 6.87–7.83 (m, 24H, aromatic peaks of stereoisomers); HRMS (FAB) *m*/*z* $[M]^+$ calcd for $C_{50}H_{36}I_2$ 890.0906; observed 890.0887.

Synthesis of 3b,15b-bis(thiophospha)-9,10,21,22-tetramethyldibenzo[*de*,*op*]di phenaleno[3,2,1-*hi*:3′,2′,1′-*st*]pentacene (2d)

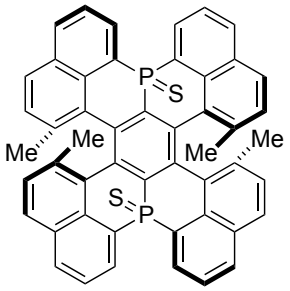

A solution of tertiary butyllithium in pentane (14.5 mL, 1.55 M, 22.5 mmol) was added slowly to a solution of **4d** (4.45 g, 5.0 mmol) in THF (50 mL) at –78 ºC under argon. After 1 h, the solution was allowed to warm to 0 ºC and stirred for 1 h, bis(diethylamino)chlorophosphine (2.95 g, 14.0 mmol) was added to reaction mixture at

–78 ºC. After stirring at room temperature for 1 h, solvent was removed *in vacuo*, The resultant yellow residue was triturated with methanol by using a sonicator to give **6d** as a yellow solid (3.50 g). Then chlorobenzene (10 mL) was poured to sulfur powder (0.280 g, 8.8 mmol) and **6d**. After stirring at room temperature for 8 h, solvent was removed *in vacuo*, The resultant yellow residue was triturated with methanol by using a sonicator to give **7d** as a yellow solid (4.10 g). A solution of **7d** in 1,2-dichlorobenzene (20 mL) was added to aluminum trichloride (3.20 g, 24.0 mmol) in 1,2-dichlorobenzene (10 mL) at 0 ºC. After stirring at room temperature for 8 h, then 150 ºC for 12 h, 1,4-diazabicyclo[2.2.2]octane (3.14 g, 28.0 mmol) was added. The reaction mixture was filtered with a pad of Celite® and Florisil®. After the solvent was removed *in vacuo*, the crude product was purified by chromatography on silica gel (50%, 100% dichloromethane in toluene) to obtain the title compound (0.387 g, 10% yield) as an orange solid. IR (neat): cm^{-1} 3052 (Ar-H), 1604, 1493, 1445, 1358, 1299, 1234, 1148, 1180, 908, 827, 785, 744, 731, 693, 660, 629, 614, 516; mp: >500 ºC; ^{1}H NMR (CD_2Cl_2, 392 MHz) δ 0.74 [s, 6H, C*H*$_3$(upper)], 1.96 [s, 6H, C*H*$_3$(downer)], 6.86 [d, *J* = 8.7 Hz, 2H, CH_3C*H*(upper)], 7.16 (d, *J* = 8.2 Hz, 2H, CH_3C*H*(downer)), 7.51 [td, *J* = 2.3, 8.2 Hz, 2H, PCCHC*H*(upper)], 7.69 [dd, *J* = 2.3, 8.7 Hz, 2H, CH_3CHC*H*(upper)], 7.76–7.81 (m, 4H), 7.86 [td, *J* = 2.3, 8.7 Hz, 2H, PCCHC*H*(downer)], 7.94 [d, *J* = 8.2 Hz, 2H, PCCHCHC*H*(upper)], 8.16 [d, *J* = 8.2 Hz, 2H, PCCHCHC*H*(downer)], 8.70 [dd, *J* = 8.7, 14.7 Hz, 2H, PCC*H*(downer)]; ^{13}C NMR (CD_2Cl_2, 151 MHz) δ 21.8 (2C), 23.4 (2C), 122.5 (2C), 123.1 (2C), 125.4 (2C), 125.6 (2C), 128.3 (2C), 128.5 (2C), 128.7 (2C), 129.2 (2C), 129.4 (2C), 129.5 (2C), 129.9 (2C), 131.1 (2C), 131.2 (2C), 131.3 (2C), 131.4 (2C), 132.7 (2C), 133.0 (2C), 133.8 (2C), 134.1 (2C), 135.2 (2C), 136.2 (2C), 137.4 (2C), 139.7 (2C); ^{31}P NMR (CD_2Cl_2, 158.6 MHz) δ –0.29; HRMS (FAB) *m*/*z* $[M]^+$ calcd for $C_{50}H_{32}P_2S_2$ 758.1421; observed 758.1422.

Crystallographic data collection and structure determination. Crystals of **2a**, **2b**, **2c**, **3b**, **AuCl(1b)**, and **2d** were mounted on a Rigaku Saturn CCD diffractometer for data collection using graphite-monochromated Mo Kα radiation (λ = 0.71070 Å). Crystal data and data statistics are summarized in Figure 8 and 9. These structures were solved by direct methods (SHELXS-97) [10] , and expanded using Fourier techniques (DIRDIF-99)[11]. The positional parameters and thermal parameters of non-hydrogen atoms were refined using a full-matrix least-squares method. Hydrogen atoms were placed at calculated positions (C–H = 0.95 Å) and kept fixed. All non-hydrogen atoms were anisotropically refined. In the subsequent refinement, the function $\sum w(F_o^2 - F_c^2)^2$ was minimized, where $|F_o|$ and $|F_c|$ are the observed and calculated structure factor amplitudes, respectively. The agreement indices are defined as $R1 = \sum(||F_o| - |F_c||)/\sum|F_o|$ and $wR2 = [\sum w(F_o^2 - F_c^2)^2 / \sum(wF_o^4)]^{1/2}$. All calculations were performed by using the Crystal Structure crystallographic software packages and illustrations were drawn by using ORTEP–3.

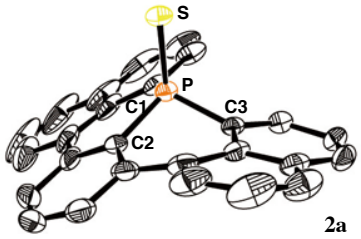

2a

Selected bond lengths		Selected angles	
P–S	1.9660(8) Å	C1–P–C2	104.94(12)°
P–C1	1.786(2) Å	C2–P–C3	100.56(11)°
P–C2	1.775(2) Å	C1–P–C3	113.31(11)°
P–C3	1.798(2) Å		

Formula	$C_{26}H_{15}PS$
Formula Weight	390.44
Temperature, K	173.1
Wavelength, Å	0.71070
Crystal System	Monoclinic
Space Group	$P\,2_1/n$ (No. 14)
a, Å	8.854(3)
b, Å	17.030(5)
c, Å	12.111(4)
α, deg	90
β, deg	96.124(5)
γ, deg	90
Volume, Å	1815.6(9)
Z	4
$Density_{calcd}$, g·cm^{-3}	1.428

Abs. Coefficient, cm^{-1}	0.275
F(000)	808.00
Crystal Size, mm^3	0.2, 0.2, 0.2
$2\theta_{min}$, $2\theta_{max}$, deg	6.0, 55.0
Index Ranges	−11≤h≤11
	−21≤k≤21
	−13≤l≤15
Reflections (unique)	4132
Reflections (I>2.0σ(I))	2381
Parameters	268
GOF on F^2	1.013
$R1$ (I>2.0σ(I))	0.0478
R, w$R2$ (all data)	0.0836, 0.0979
Largest diff peak and hole, e, Å^{-3}	0.45, −0.53

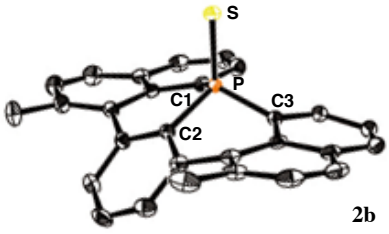

2b

Selected bond lengths		Selected angles	
P–S	1.9664(6) Å	C1–P–C2	102.70(6)°
P–C1	1.8086(13) Å	C2–P–C3	100.92(6)°
P–C2	1.7943(14) Å	C1–P–C3	114.41(6)°
P–C3	1.8047(14) Å		

Formula	$C_{28}H_{19}PS$
Formula Weight	418.49
Temperature, K	173.1
Wavelength, Å	0.71070
Crystal System	Orthorhombic
Space Group	$P\,n\,a\,2_1$ (No. 33)
a, Å	9.4741(17)
b, Å	12.370(3)
c, Å	17.179(4)
α, deg	90
β, deg	90
γ, deg	90
Volume, Å	2013.3(8)
Z	4
$Density_{calcd}$, g·cm^{-3}	1.381

Abs. Coefficient, cm^{-1}	0.253
F(000)	872.00
Crystal Size, mm^3	0.4, 0.4, 0.4
$2\theta_{min}$, $2\theta_{max}$, deg	6.4, 55.0
Index Ranges	−12≤h≤9
	−16≤k≤13
	−22≤l≤22
Reflections (unique)	4586
Reflections (I>2.0σ(I))	4240
Parameters	291
GOF on F^2	1.039
$R1$ (I>2.0σ(I))	0.0233
R, w$R2$ (all data)	0.0252, 0.0550
Largest diff peak and hole, e, Å^{-3}	0.59, −0.32

Figure 8. X-ray crystal structures of **2a** and **2b** (left), and crystal data and structure refinement (right). Thermal ellipsoids are shown at 50% probability and H atoms have been omitted for clarity.

[10] Sheldrick, G. M. Program for the Solution of Crystal Structures; University of Göttingen, Germany, 1997.

[11] Beurskens, P. T.; Beuskens, G.; de Gelder, R.; Garcîa-Grana, S.; Gould, R. O.; Israel, R.; Smits, J. M. M. The DIRDIF-99 Program System; Technical Report of the Crystallography Laboratory; University of Nijmegen, Nijmegen, The Netherlands, 1999.

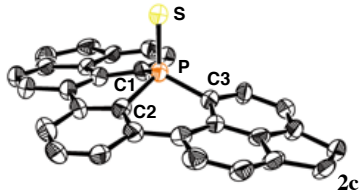

2c

Selected bond lengths		Selected angles	
P–S	1.965(3) Å	C1–P–C2	110.7(2)°
P–C1	1.776(8) Å	C2–P–C3	103.4(3)°
P–C2	1.799(7) Å	C1–P–C3	114.1(3)°
P–C3	1.809(7) Å		

Formula	$C_{30}H_{19}PS$
Formula Weight	442.48
Temperature, K	103(2)
Wavelength, Å	0.71075
Crystal System	Triclinic
Space Group	*P*–1 (No. 2)
a, Å	8.1709(8)
b, Å	11.9296(8)
c, Å	20.3704(18)
α, deg	90.222(3)
β, deg	93.980(5)
γ, deg	91.528(8)
Volume, Å	1980.1(3)
Z	4
$Density_{calcd}$, g·cm^{-3}	1.484

Abs. Coefficient, cm^{-1}	0.262
F(000)	920
Crystal Size, mm^3	0.10, 0.10, 0.05
$2\theta_{min}$, $2\theta_{max}$, deg	4.0, 50.0
Index Ranges	–9≤h≤9
	–14≤k≤14
	–24≤l≤24
Reflections (unique)	6854
Reflections (I>2.0σ(I))	3896
Parameters	577
GOF on F^2	1.078
$R1$ (I>2.0σ(I))	0.0937
R, w$R2$ (all data)	0.1658, 0.2419
Largest diff peak and hole, e, Å^{-3}	0.77, –0.34

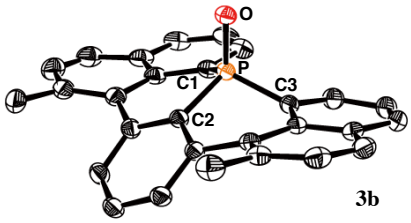

3b

Selected bond lengths		Selected angles	
P–O	1.4911(11) Å	C1–P–C2	103.46(7)°
P–C1	1.7961(15) Å	C2–P–C3	100.73(7)°
P–C2	1.7789(14) Å	C1–P–C3	115.08(7)°
P–C3	1.8055(19) Å		

Formula	$C_{28}H_{19}PO$
Formula Weight	402.42
Temperature, K	173.1
Wavelength, Å	0.71070
Crystal System	Monoclinic
Space Group	*P* $2_1/n$ (No. 14)
a, Å	7.2044(15)
b, Å	20.622(4)
c, Å	13.225(3)
α, deg	90
β, deg	102.745(3)
γ, deg	90
Volume, Å	1916.4(7)
Z	4
$Density_{calcd}$, g·cm^{-3}	1.395

Abs. Coefficient, cm^{-1}	0.169
F(000)	872.00
Crystal Size, mm^3	0.5, 0.5, 0.5
$2\theta_{min}$, $2\theta_{max}$, deg	6.6, 55.0
Index Ranges	–9≤h≤9
	–22≤k≤26
	–17≤l≤15
Reflections (unique)	4321
Reflections (I>2.0σ(I))	3580
Parameters	290
GOF on F^2	1.006
$R1$ (I>2.0σ(I))	0.0473
R, w$R2$ (all data)	0.0559, 0.1429
Largest diff peak and hole, e, Å^{-3}	0.77, –0.34

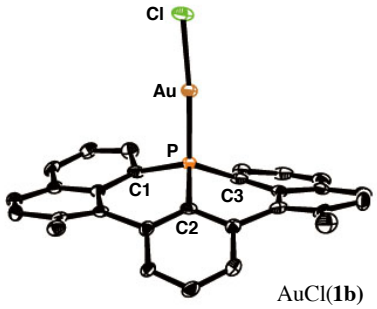

AuCl(**1b**)

Selected bond lengths		Selected angles	
P–Au	2.2343(12) Å	C1–P–C2	103.0(2)°
P–C1	1.805(6) Å	C2–P–C3	101.4(2)°
P–C2	1.786(5) Å	C1–P–C3	114.4(2)°
P–C3	1.815(6) Å	Cl–Au–P	175.13(6)°
Au–Cl	2.2945(12) Å		

Formula	$C_{28}H_{19}AuClP$
Formula Weight	618.85
Temperature, K	173.1
Wavelength, Å	0.71070
Crystal System	Monoclinic
Space Group	*P* $2_1/c$ (No. 14)
a, Å	9.705(4)
b, Å	23.070(9)
c, Å	10.283(4)
α, deg	90
β, deg	113.342(4)
γ, deg	90
Volume, Å	2114.1(14)
Z	4
$Density_{calcd}$, g·cm^{-3}	1.994

Abs. Coefficient, cm^{-1}	7.199
F(000)	1192.00
Crystal Size, mm^3	0.2, 0.2, 0.2
$2\theta_{min}$, $2\theta_{max}$, deg	6.0, 55.0
Index Ranges	–8≤h≤12
	–19≤k≤29
	–13≤l≤13
Reflections (unique)	4789
Reflections (I>2.0σ(I))	3432
Parameters	281
GOF on F^2	0.997
$R1$ (I>2.0σ(I))	0.0341
R, w$R2$ (all data)	0.0471, 0.0711
Largest diff peak and hole, e, Å^{-3}	2.49, –1.95

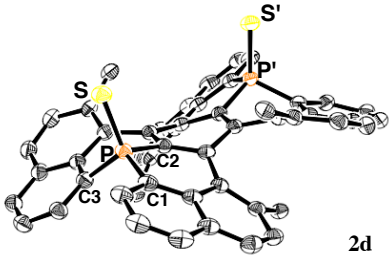

2d

Selected bond lengths		Selected angles	
P–S	1.9691(13) Å	C1–P–C2	105.12(17)°
P–C1	1.777(4) Å	C2–P–C3	100.24(16)°
P–C2	1.777(4) Å	C1–P–C3	112.63(17)°
P–C3	1.796(4) Å		

Formula	$C_{50}H_{32}P_2S_2$, $2H_2O$, C_7H_8
Formula Weight	882.95
Temperature, K	173
Wavelength, Å	0.71070
Crystal System	Tetragonal
Space Group	*I* $4_1/a$ (No. 88)
a, Å	16.5125(5)
b, Å	16.5125(5)
c, Å	33.4968(12)
α, deg	90
β, deg	90
γ, deg	90
Volume, Å	9133.3(5)
Z	8
$Density_{calcd}$, g·cm^{-3}	1.994

Abs. Coefficient, cm^{-1}	0.230
F(000)	3680
Crystal Size, mm^3	0.2, 0.2, 0.2
$2\theta_{min}$, $2\theta_{max}$, deg	4.3, 51.0
Index Ranges	–19≤h≤19
	–20≤k≤20
	–40≤l≤40
Reflections (unique)	4253
Reflections (I>2.0σ(I))	2877
Parameters	281
GOF on F^2	0.997
$R1$ (I>2.0σ(I))	0.0694
R, w$R2$ (all data)	0.1012, 0.2420
Largest diff peak and hole, e, Å^{-3}	0.654, –0.519

Figure 9. X-ray crystal structures of **2c**, **3b**, AuCl(**1b**), **2d** (left), and crystal data and structure refinement (right). Thermal ellipsoids are shown at 50% probability and H atoms have been omitted for clarity.

Synchrotron X-ray powder diffraction measurement and structure determination. Synchrotron X-ray powder diffraction data were recorded for **1b** at 80 K on beamline BL19B2 at SPring-8 (Debye-Scherer camera equipped with a curved Imaging Plate detector) with wavelength 1.30 Å (0.3 mm diameter borosilicate glass capillary, with sample spinning during measurement; data collection time 60 min). The diffraction patterns were indexed by using DICVOL91[12] to obtain lattice parameters that were subsequently refined in a Pawley fit[13]. Z-Matrixes describing the molecular topology of the fragments in the compound were generated automatically by DASH[14]. Ten runs with 10^7 simulated annealing (SA) moves per run were performed for structure solution. A final Rietveld refinement was performed by using the RIETAN-FP[15] program.

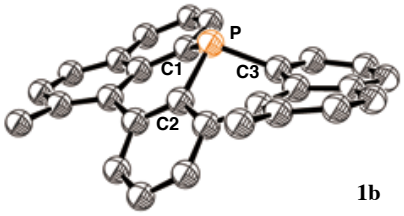

1b

Selected bond lengths		Selected angles	
P–C1	1.777 Å	C1–P–C2	101.73°
P–C2	1.864 Å	C2–P–C3	94.71°
P–C3	1.889 Å	C1–P–C3	111.64°

Formula	$C_{28}H_{19}P$
Formula Weight	386.42
Temperature, K	80.0
Wavelength, Å	1.30000
Crystal System	Monoclinic
Space Group	$P\,2_1/a$ (No. 14)
a, Å	11.8709(17)
b, Å	18.0107(17)
c, Å	9.9332(15)
α, deg	90
β, deg	117.3494(87)
γ, deg	90

Volume, Å	1886.4(85)
Z	4
$\text{Density}_{\text{calcd}}$, g·cm^{-3}	1.361
F(000)	808.00
Crystal Size, mm^3	powder
$2\theta_{\text{min}}$, $2\theta_{\text{max}}$, deg	3.01, 70.0
S	1.287
R_e	0.0559
R_p, R_{wp}	0.0571, 0.0720

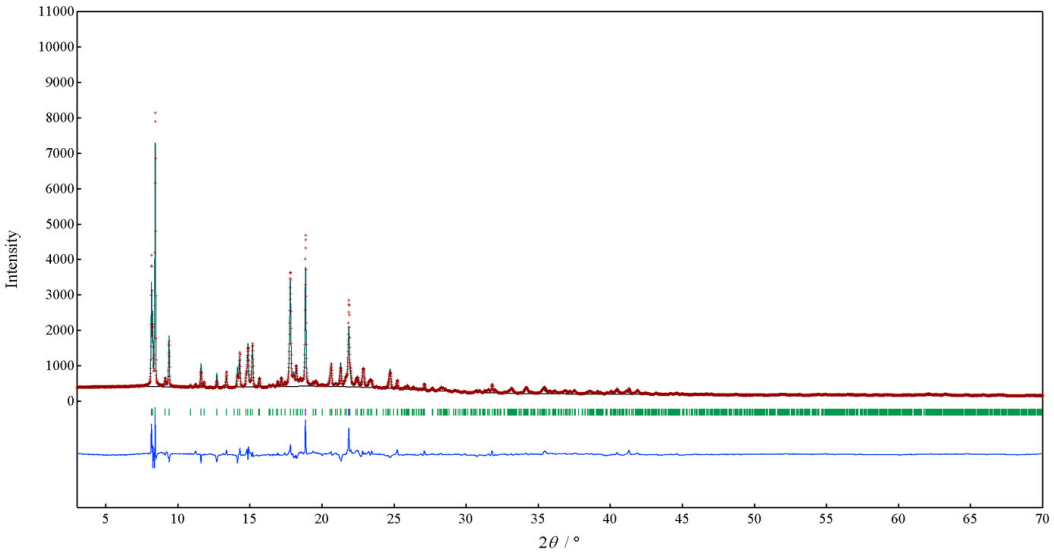

Figure 10. Structural data and result of Rietveld refinement of **1b**. H atoms have been omitted for clarity.

[12] Boultif, A.; Lour, D. *J. Appl. Crystallogr.* **1991,** *24*, 987–993.
[13] Pawley, G. S. *J. Appl. Crystallogr.* **1981,** *14*, 357–361.
[14] DASH (3.01), David, W. I. F.; Shankland, K. Cambridge Crystallographic Data Centre, Cambridge, 2004.
[15] (a) Izumi, F.; Ikeda, T. *Mater. Sci. Forum* **2000,** *198*, 321–324. (b) Izumi, F.; Momma, K. *Solid State Phenom.* **2007,** *130*, 15–20.

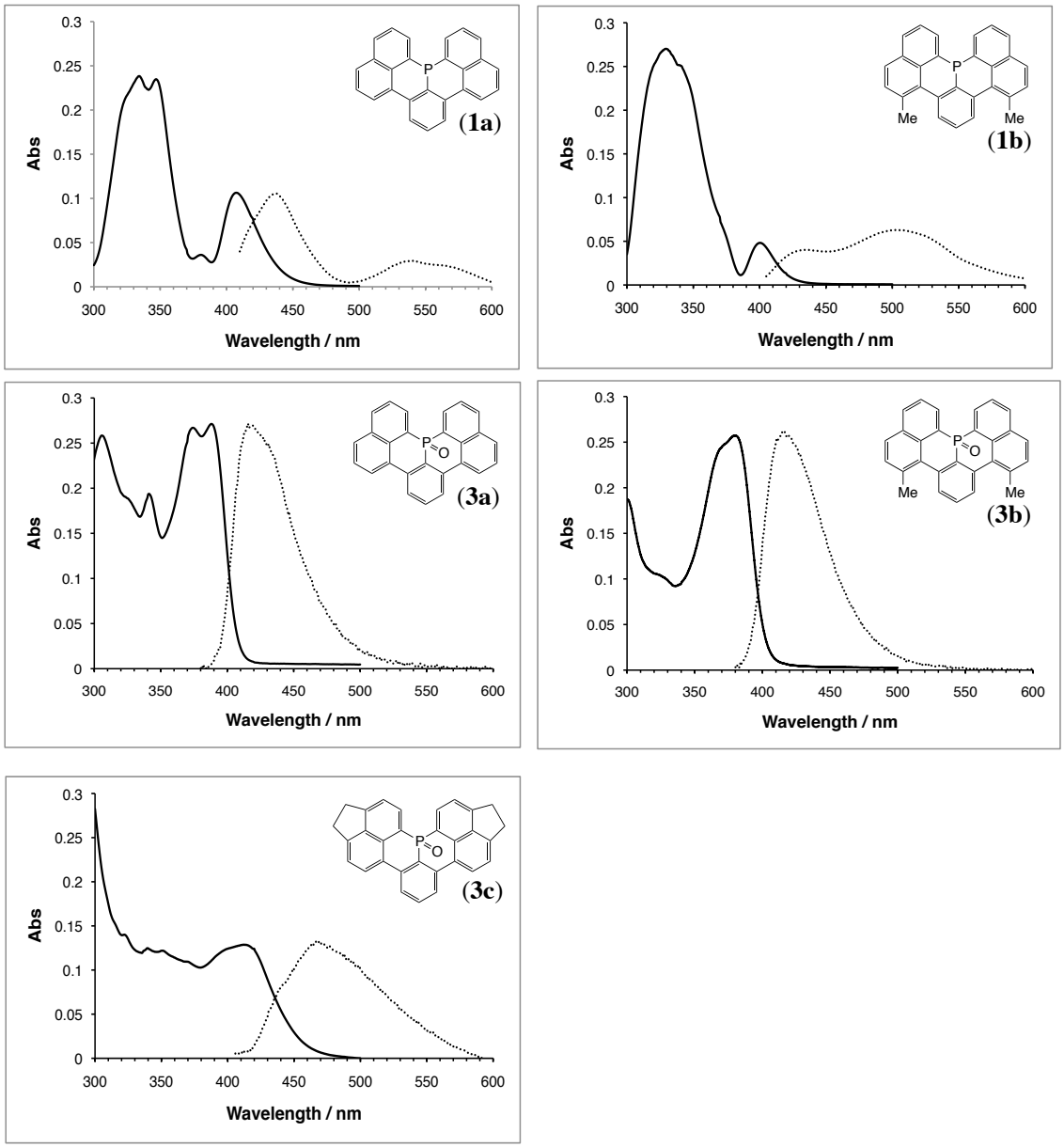

Figure 11. UV-visible (solid line, 0.02 mM in CH_2Cl_2) and fluorescence (dotted line, 0.01 mM in CH_2Cl_2) spectra of **1a**, **1b**, **3a**, **3b**, and **3c**.

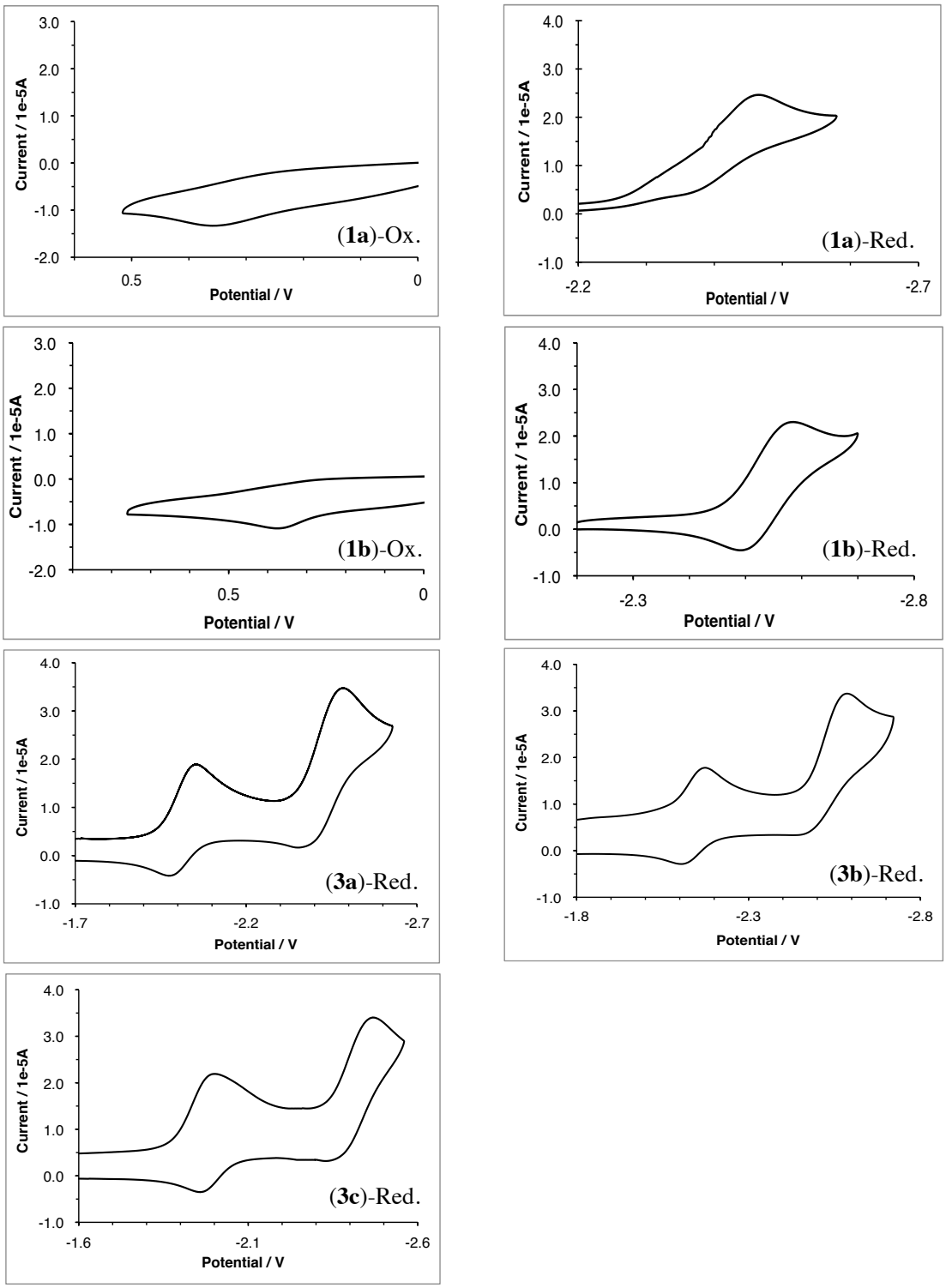

Figure 12. Cyclic voltammograms of **1a**, **1b**, **3a**, **3b**, and **3c** in MeCN with 0.10 M *n*-$Bu_4N^+PF_6^-$. Redox potentials are given in V *vs*. Fc/Fc^+ couple.

Computational studies. All calculations were performed with Gaussian 03[16] packages. The DFT method was employed using the B3LYP hybrid functional.[17] Structures were optimized with the SDD basis set consisting of the Stuttgart/Dresden effective core potential (ECP) for Au[18] and 6-31G(d) for the rest (denoted as 631SDD).[19] Each stationary point was adequately characterized by normal coordinate analysis (no imaginary frequencies for an equilibrium structure and one imaginary frequency for a transition structure) using the same method as for the geometry optimization. Intrinsic reaction coordinate (IRC) analyses[20] were carried out throughout the reaction pathways to confirm that all stationary points are smoothly connected to each other using the same method as for the geometry optimization. The time-dependent density functional theory (TD-DFT) calculation[21] was conducted at the B3LYP/6-311+G (d, p) level after the geometry optimization at the B3LYP/6-31G (d) level.

---

[16] Gaussian 03, Revision E.01, Frisch, M. J.; Trucks, G. W.; Schlegel, H. B.; Scuseria, G. E.; Robb, M. A.; Cheeseman, J. R.; Montgomery, Jr., J. A.; Vreven, T.; Kudin, K. N.; Burant, J. C.; Millam, J. M.; Iyengar, S. S.; Tomasi, J.; Barone, V.; Mennucci, B.; Cossi, M.; Scalmani, G.; Rega, N.; Petersson, G. A.; Nakatsuji, H.; Hada, M.; Ehara, M.; Toyota, K.; Fukuda, R.; Hasegawa, J.; Ishida, M.; Nakajima, T.; Honda, Y.; Kitao, O.; Nakai, H.; Klene, M.; Li, X.; Knox, J. E.; Hratchian, H. P.; Cross, J. B.; Bakken, V.; Adamo, C.; Jaramillo, J.; Gomperts, R.; Stratmann, R. E.; Yazyev, O.; Austin, A. J.; Cammi, R.; Pomelli, C.; Ochterski, J.W.; Ayala, P. Y.; Morokuma, K.; Voth, G. A.; Salvador, P.; Dannenberg, J. J.; Zakrzewski, V. G.; Dapprich, S.; Daniels, A. D.; Strain, M. C.; Farkas, O.; Malick, D. K.; Rabuck, A. D.; Raghavachari, K.; Foresman, J. B.; Ortiz, J. V.; Cui, Q.; Baboul, A. G.; Clifford, S.; Cioslowski, J.; Stefanov, B. B.; Liu, G.; Liashenko, A.; Piskorz, P.; Komaromi, I.; Martin, R. L.; Fox, D. J.; Keith, T.; Al-Laham, M. A.; Peng, C. Y.; Nanayakkara, A.; Challacombe, M.; Gill, P. M. W.; Johnson, B.; Chen, W.; Wong, M. W.; Gonzalez, C. and Pople, J. A. Gaussian, Inc., Wallingford CT, 2004.

[17] (a) Becke, A. D. *J. Chem. Phys.* **1993,** *98*, 5648–5652. (b) Lee, C.; Yang, W.; Parr, R. G. *Phys. Rev. B* **1988,** *37*, 785–789.

[18] Dolg, M.; Wedig, U.; Stoll, H.; Preuss, H. *J. Chem. Phys.* **1987,** *86*, 866–872.

[19] Hehre, W. J.; Radom, L.; Schleyer, P. v. R.; Pople, J. A. *Ab Initio Molecular Orbital Theory*; John Wiley & Sons: New York, **1986** and references cited therein.

[20] (a) Fukui, K. *Acc. Chem. Res.* **1981,** *14*, 363–368. (b) Gonzalez, C.; Schlegel, H. B. *J. Chem. Phys.* **1989,** *90*, 2154–2161. (c) Gonzalez, C.; Schlegel, H. B. *J. Phys. Chem.* **1990,** *94*, 5523–5527.

[21] (a) Casida, M. E.; Jamorski, C.; Casida, K. C.; Salahub, D. R. *J. Chem. Phys.* **1998,** *108*, 4439–4449. (b) Stratmann, R. E.; Scuseria, G. E.; Frisch, M. J. *J. Chem. Phys.* **1998,** *109*, 8218–8224.

Table 2. The lowest-energy transition of **1a–b**, **3a–c** calculated by the TD-DFT method at the B3LYP/6-311+G(d, p) level and UV-visible absorption in CH_2Cl_2 (0.02 mM).

	calculation				experiment	
Compd	λ_{ex} (nm)	energy gap (eV)	ocillator strength *f*	HOMO–LUMO coefficient	λ_{ab} (nm)	log ε ($M^{-1}cm^{-1}$)
1a	417	2.97	0.1621	0.67366	407	3.63
1b	397	3.12	0.1564	0.67167	400	3.20
3a	392	3.16	0.2443	0.66917	388	4.13
3b	387	3.21	0.2624	0.67265	379	4.11
3c	410	3.03	0.2708	0.67246	412	3.90

Cartesian Coordinates

*The isomerization barrier calculation of **2a***

(*P*)-**2a**

E(RB3LYP) = –1739.37542252 hartree

Center Number	Atomic Number	Atomic Type	Coordinates X	Y	Z
1	6	0	1.265046	1.831054	0.012242
2	6	0	1.284657	3.192877	-0.324305
3	6	0	0.098675	3.883460	-0.548828
4	6	0	-1.124172	3.228735	-0.483020
5	6	0	-1.206417	1.867047	-0.133097
6	6	0	0.006711	1.193149	0.129794
7	15	0	0.015255	-0.527115	0.670209
8	6	0	1.442671	-1.152969	-0.288972
9	6	0	-1.572897	-1.165640	0.058898
10	6	0	1.533829	-2.440910	-0.784887
11	6	0	2.775521	-2.978485	-1.191410
12	6	0	3.925920	-2.243073	-1.029546
13	6	0	3.876593	-0.909267	-0.542930
14	6	0	2.605839	-0.317451	-0.244394
15	6	0	5.064043	-0.158843	-0.343232
16	6	0	4.995950	1.132372	0.125795
17	6	0	3.743098	1.750844	0.313041
18	6	0	2.547684	1.080794	0.085311
19	6	0	-2.657545	-0.258876	-0.171875
20	6	0	-3.962224	-0.831091	-0.380426
21	6	0	-4.119695	-2.240265	-0.434772
22	6	0	-3.055782	-3.082218	-0.215901
23	6	0	-1.790403	-2.535423	0.072778
24	6	0	-2.526908	1.177399	-0.141021
25	6	0	-3.692874	1.935135	-0.178342
26	6	0	-4.969064	1.367048	-0.352479
27	6	0	-5.100533	0.007421	-0.489229
28	1	0	-5.840371	2.014716	-0.386548
29	1	0	-3.637066	3.011270	-0.068898
30	1	0	-3.189648	-4.159928	-0.224114
31	1	0	-6.074294	-0.448899	-0.647097
32	1	0	-5.113473	-2.641483	-0.617526
33	1	0	2.817996	-3.989620	-1.585933
34	1	0	0.652223	-3.067449	-0.846972
35	1	0	5.903430	1.697235	0.318928
36	1	0	3.722890	2.787940	0.630949
37	1	0	0.130863	4.932614	-0.829484
38	1	0	6.022665	-0.627339	-0.551041
39	1	0	4.894801	-2.671091	-1.274718
40	1	0	-0.989555	-3.205517	0.365866
41	1	0	-2.015642	3.780232	-0.754290
42	1	0	2.229275	3.702973	-0.474441
43	16	0	0.245671	-0.825367	2.611064

TS-**2a**

E(RB3LYP) = –1739.37437237 hartree

Center Number	Atomic Number	Atomic Type	Coordinates X	Y	Z
1	6	0	1.234461	1.836267	-0.107667
2	6	0	1.205045	3.191391	-0.480638
3	6	0	-0.000107	3.861180	-0.648157
4	6	0	-1.205237	3.191230	-0.480752
5	6	0	-1.234481	1.836191	-0.107608
6	6	0	0.000026	1.172078	0.075218
7	15	0	0.000018	-0.555564	0.610517
8	6	0	1.539663	-1.181097	-0.164318
9	6	0	-1.539674	-1.181101	-0.164192
10	6	0	1.734584	-2.530474	-0.409871
11	6	0	3.007559	-3.052907	-0.718164
12	6	0	4.104905	-2.227437	-0.693488
13	6	0	3.966646	-0.843901	-0.410851
14	6	0	2.658731	-0.283512	-0.207308
15	6	0	5.117478	-0.021812	-0.302528
16	6	0	4.989502	1.308651	0.015317

17	6	0	3.708106	1.878388	0.141183
18	6	0	2.542632	1.138017	-0.022057
19	6	0	-2.658761	-0.283589	-0.207343
20	6	0	-3.966664	-0.843960	-0.410879
21	6	0	-4.104900	-2.227519	-0.693329
22	6	0	-3.007524	-3.052983	-0.717868
23	6	0	-1.734557	-2.530528	-0.409635
24	6	0	-2.542641	1.137932	-0.021986
25	6	0	-3.708068	1.878382	0.141212
26	6	0	-4.989483	1.308673	0.015172
27	6	0	-5.117472	-0.021788	-0.302625
28	1	0	-5.867796	1.933894	0.147254
29	1	0	-3.640680	2.936138	0.369292
30	1	0	-3.115673	-4.113511	-0.925606
31	1	0	-6.096537	-0.470949	-0.448188
32	1	0	-5.101505	-2.624220	-0.870279
33	1	0	3.115675	-4.113381	-0.926187
34	1	0	0.914194	-3.229433	-0.322760
35	1	0	5.867815	1.933813	0.147663
36	1	0	3.640828	2.936130	0.369330
37	1	0	-0.000147	4.903129	-0.956070
38	1	0	6.096537	-0.471013	-0.448009
39	1	0	5.101534	-2.624057	-0.870489
40	1	0	-0.914116	-3.229457	-0.322591
41	1	0	-2.128915	3.714572	-0.696851
42	1	0	2.128614	3.714937	-0.696691
43	16	0	0.000081	-0.849860	2.565712

(*M*)-**2a**

E(RB3LYP) = –1739.37542252 hartree

Center Number	Atomic Number	Atomic Type	Coordinates X	Y	Z
1	6	0	1.206486	1.866905	-0.133265
2	6	0	1.124386	3.228470	-0.483639
3	6	0	-0.098423	3.883252	-0.549722
4	6	0	-1.284446	3.192799	-0.324986
5	6	0	-1.264937	1.831049	0.011898
6	6	0	-0.006664	1.193067	0.129598
7	15	0	-0.015218	-0.527248	0.669920
8	6	0	1.572828	-1.165739	0.058166
9	6	0	-1.442973	-1.152979	-0.288877
10	6	0	1.790296	-2.535533	0.071397
11	6	0	3.055735	-3.082232	-0.217258
12	6	0	4.119760	-2.240227	-0.435349
13	6	0	3.962330	-0.831069	-0.380343
14	6	0	2.657597	-0.258939	-0.171976
15	6	0	5.100681	0.007497	-0.488306
16	6	0	4.969176	1.367072	-0.350937
17	6	0	3.692912	1.935094	-0.177130
18	6	0	2.526965	1.177303	-0.140695
19	6	0	-2.606030	-0.317313	-0.244196
20	6	0	-3.876934	-0.909020	-0.542336
21	6	0	-3.926554	-2.242911	-1.028676
22	6	0	-2.776288	-2.978507	-1.190638
23	6	0	-1.534434	-2.441018	-0.784502
24	6	0	-2.547646	1.080975	0.085257
25	6	0	-3.742919	1.751243	0.313091
26	6	0	-4.995889	1.132903	0.126214
27	6	0	-5.064244	-0.158399	-0.342532
28	1	0	-5.903257	1.697928	0.319404
29	1	0	-3.722495	2.788399	0.630794
30	1	0	-2.818974	-3.989714	-1.584951
31	1	0	-6.022972	-0.626810	-0.550043
32	1	0	-4.895547	-2.670841	-1.273552
33	1	0	3.189535	-4.159947	-0.225994
34	1	0	0.989399	-3.205761	0.364015
35	1	0	5.840512	2.014738	-0.384299
36	1	0	3.636970	3.011182	-0.067232
37	1	0	-0.130554	4.932312	-0.830732
38	1	0	6.074501	-0.448751	-0.646020
39	1	0	5.113583	-2.641388	-0.617993
40	1	0	-0.652963	-3.067707	-0.846681
41	1	0	-2.229043	3.702912	-0.475225
42	1	0	2.015958	3.779739	-0.755066
43	16	0	-0.245063	-0.825625	2.610827

Cartesian coordinates at stationary points

1a

E(RB3LYP) = –1341.164016 hartree

Center Number	Atomic Number	Atomic Type	Coordinates X	Y	Z
1	6	0	1.181407	1.793614	-0.025739
2	6	0	1.096527	3.123904	-0.480430
3	6	0	-0.127290	3.770050	-0.600367
4	6	0	-1.308624	3.093689	-0.315831
5	6	0	-1.281270	1.762257	0.127392
6	6	0	-0.025644	1.129162	0.279691
7	15	0	-0.033225	-0.554962	0.953098
8	6	0	1.549087	-1.218498	0.320342
9	6	0	-1.460183	-1.229854	0.000768
10	6	0	1.775548	-2.587691	0.371772
11	6	0	3.042932	-3.140535	0.099296
12	6	0	4.109197	-2.308282	-0.140190
13	6	0	3.947937	-0.897943	-0.126554
14	6	0	2.640369	-0.323382	0.059502
15	6	0	5.084315	-0.057261	-0.248880

16	6	0	4.947915	1.305541	-0.154453
17	6	0	3.668454	1.876956	-0.016886
18	6	0	2.506514	1.113890	0.030967
19	6	0	-2.626655	-0.394832	0.023379
20	6	0	-3.905221	-0.995033	-0.228640
21	6	0	-3.966940	-2.349930	-0.652265
22	6	0	-2.817593	-3.089893	-0.796456
23	6	0	-1.566945	-2.538695	-0.434565
24	6	0	-2.561766	1.019834	0.284934
25	6	0	-3.749706	1.704459	0.509815
26	6	0	-5.006242	1.079407	0.376750
27	6	0	-5.085598	-0.230790	-0.035524
28	1	0	-5.909956	1.653067	0.563172
29	1	0	-3.718670	2.757378	0.770908
30	1	0	-2.865487	-4.117757	-1.145975
31	1	0	-6.049700	-0.705171	-0.201380
32	1	0	-4.940197	-2.788524	-0.857943
33	1	0	3.175111	-4.218779	0.118567
34	1	0	0.974771	-3.256925	0.668844
35	1	0	5.819051	1.953381	-0.197998
36	1	0	3.603680	2.956566	0.048531
37	1	0	-0.163139	4.793292	-0.963933
38	1	0	6.061671	-0.514916	-0.379234
39	1	0	5.103977	-2.714044	-0.306469
40	1	0	-0.687492	-3.170011	-0.490072
41	1	0	-2.258059	3.585099	-0.497012
42	1	0	1.989650	3.650897	-0.793431

2a

E(RB3LYP) = –1739.375423 hartree

Center Number	Atomic Number	Atomic Type	Coordinates X	Y	Z
1	6	0	1.206497	1.866928	-0.133277
2	6	0	1.124373	3.228521	-0.483554
3	6	0	-0.098445	3.883285	-0.549677
4	6	0	-1.284466	3.192818	-0.325036
5	6	0	-1.264953	1.831063	0.011826
6	6	0	-0.006683	1.193087	0.129524
7	15	0	-0.015218	-0.527214	0.669868
8	6	0	1.572825	-1.165751	0.058177
9	6	0	-1.442956	-1.152993	-0.288904
10	6	0	1.790287	-2.535543	0.071460
11	6	0	3.055729	-3.082254	-0.217124
12	6	0	4.119764	-2.240259	-0.435228
13	6	0	3.962330	-0.831103	-0.380295
14	6	0	2.657595	-0.258956	-0.171969
15	6	0	5.100698	0.007439	-0.488298
16	6	0	4.969208	1.367014	-0.351021
17	6	0	3.692947	1.935060	-0.177236
18	6	0	2.526975	1.177301	-0.140731
19	6	0	-2.606028	-0.317339	-0.244193
20	6	0	-3.876932	-0.909070	-0.542291
21	6	0	-3.926545	-2.242959	-1.028633
22	6	0	-2.776271	-2.978532	-1.190654
23	6	0	-1.534420	-2.441024	-0.784546
24	6	0	-2.547655	1.080965	0.085208
25	6	0	-3.742937	1.751208	0.313057
26	6	0	-4.995905	1.132844	0.126248
27	6	0	-5.064251	-0.158470	-0.342464
28	1	0	-5.903273	1.697857	0.319472
29	1	0	-3.722522	2.788371	0.630731
30	1	0	-2.818959	-3.989736	-1.584974
31	1	0	-6.022971	-0.626917	-0.549929
32	1	0	-4.895539	-2.670916	-1.273463
33	1	0	3.189534	-4.159968	-0.225820
34	1	0	0.989380	-3.205775	0.364048
35	1	0	5.840543	2.014679	-0.384429
36	1	0	3.637059	3.011154	-0.067421
37	1	0	-0.130560	4.932358	-0.830644
38	1	0	6.074511	-0.448838	-0.645971
39	1	0	5.113588	-2.641439	-0.617816
40	1	0	-0.652926	-3.067702	-0.846745
41	1	0	-2.229058	3.702918	-0.475325
42	1	0	2.015925	3.779875	-0.754863
43	16	0	-0.245072	-0.825462	2.610808

3a

E(RB3LYP) = –1416.41048 hartree

Center Number	Atomic Number	Atomic Type	Coordinates X	Y	Z
1	6	0	1.192939	1.832465	-0.081706
2	6	0	1.106990	3.184748	-0.465420
3	6	0	-0.117961	3.835652	-0.537337
4	6	0	-1.301832	3.151312	-0.283583
5	6	0	-1.276457	1.797880	0.085429
6	6	0	-0.016885	1.161965	0.207909
7	15	0	-0.026663	-0.539434	0.785425
8	6	0	1.560797	-1.191100	0.206782
9	6	0	-1.449743	-1.193156	-0.146552
10	6	0	1.782609	-2.558850	0.282426
11	6	0	3.053053	-3.115787	0.036490
12	6	0	4.116885	-2.281480	-0.210040
13	6	0	3.956354	-0.871368	-0.221400
14	6	0	2.649050	-0.294341	-0.046990
15	6	0	5.093515	-0.036527	-0.364007
16	6	0	4.957733	1.327676	-0.292466
17	6	0	3.679857	1.899882	-0.145665
18	6	0	2.514829	1.142701	-0.074857
19	6	0	-2.617507	-0.362419	-0.099267
20	6	0	-3.892634	-0.964266	-0.356956

21	6	0	-3.947181	-2.310880	-0.806198
22	6	0	-2.798029	-3.047755	-0.971401
23	6	0	-1.550050	-2.494413	-0.607047
24	6	0	-2.557157	1.045827	0.190384
25	6	0	-3.750647	1.719607	0.417914
26	6	0	-5.005242	1.093904	0.270187
27	6	0	-5.078547	-0.211227	-0.157714
28	1	0	-5.910544	1.662941	0.461556
29	1	0	-3.727934	2.765570	0.705337
30	1	0	-2.846143	-4.069215	-1.337927
31	1	0	-6.039645	-0.687584	-0.334197
32	1	0	-4.919453	-2.747299	-1.021826
33	1	0	3.189906	-4.192453	0.077555
34	1	0	0.975559	-3.218763	0.582894
35	1	0	5.827306	1.975595	-0.355356
36	1	0	3.622892	2.979713	-0.083686
37	1	0	-0.153637	4.877193	-0.845056
38	1	0	6.069138	-0.496935	-0.496866
39	1	0	5.112993	-2.687999	-0.367242
40	1	0	-0.666363	-3.118338	-0.675894
41	1	0	-2.247730	3.658492	-0.436241
42	1	0	1.994613	3.732246	-0.756974
43	8	0	-0.213681	-0.737743	2.266133

1b

E(RB3LYP) = –1419.782625 hartree

Center Number	Atomic Number	Atomic Type	Coordinates X	Y	Z
1	6	0	1.200196	-1.476548	0.236917
2	6	0	1.128435	-2.663973	0.989390
3	6	0	-0.092242	-3.260954	1.282078
4	6	0	-1.277169	-2.682814	0.840301
5	6	0	-1.262716	-1.480312	0.114204
6	6	0	-0.015564	-0.869401	-0.142059
7	15	0	-0.038227	0.774131	-0.916764
8	6	0	1.535463	1.469925	-0.279843
9	6	0	-1.476847	1.465697	0.017194
10	6	0	1.742730	2.842716	-0.335557
11	6	0	3.005696	3.415690	-0.086899
12	6	0	4.092775	2.598333	0.110421
13	6	0	3.949212	1.187904	0.082926
14	6	0	2.648428	0.593390	-0.044432
15	6	0	5.094055	0.351175	0.107539
16	6	0	4.959874	-0.999339	-0.072777
17	6	0	3.687024	-1.624778	-0.148630
18	6	0	2.527656	-0.848620	-0.015575
19	6	0	-2.638575	0.623686	0.016133
20	6	0	-3.919816	1.229076	0.216659
21	6	0	-3.998771	2.593175	0.600584
22	6	0	-2.854887	3.343315	0.741552
23	6	0	-1.598773	2.788587	0.407267
24	6	0	-2.554273	-0.801493	-0.194497
25	6	0	-3.717629	-1.512616	-0.502682
26	6	0	-4.973856	-0.853769	-0.422171
27	6	0	-5.083960	0.449252	-0.006964
28	1	0	5.870333	-1.422511	-0.659062
29	1	0	2.911870	4.380956	1.059288
30	1	0	-6.060216	0.911747	0.117156
31	1	0	-4.978346	3.032541	0.772464
32	1	0	3.119407	4.496091	-0.102722
33	1	0	0.930406	3.500596	-0.624843
34	1	0	5.845918	-1.625757	-0.147905
35	1	0	-0.121406	-4.165539	1.883392
36	1	0	6.076973	0.806068	0.202232
37	1	0	5.087815	3.016741	0.240613
38	1	0	-0.726449	3.429953	0.447028
39	1	0	-2.223446	-3.131497	1.118698
40	1	0	2.033855	-3.096821	1.394979
41	6	0	-3.735899	-2.961480	-0.946415
42	1	0	-4.082617	-3.638225	-0.153814
43	1	0	-2.754835	-3.309901	-1.275367
44	1	0	-4.435406	-3.075871	-1.783286
45	6	0	3.705223	-3.115561	-0.430811
46	1	0	2.758271	-3.479354	-0.834045
47	1	0	3.940443	-3.714232	0.459383
48	1	0	4.490498	-3.328526	-1.165860

2b

E(RB3LYP) = –1817.993829 hartree

Center Number	Atomic Number	Atomic Type	Coordinates X	Y	Z
1	6	0	1.224890	1.566131	-0.344350
2	6	0	1.156839	2.798684	-1.020670
3	6	0	-0.062002	3.417555	-1.270160
4	6	0	-1.251766	2.819197	-0.870323
5	6	0	-1.246008	1.571116	-0.226463
6	6	0	0.002795	0.949826	0.002501
7	15	0	-0.021646	-0.741608	0.629106
8	6	0	1.556884	-1.409568	0.008851
9	6	0	-1.465849	-1.377122	-0.308531
10	6	0	1.752582	-2.783381	0.015024
11	6	0	3.014264	-3.350695	-0.247804
12	6	0	4.102233	-2.525551	-0.407948
13	6	0	3.965261	-1.117044	-0.326017
14	6	0	2.667300	-0.522118	-0.181051
15	6	0	5.114118	-0.286820	-0.318901
16	6	0	4.985380	1.055371	-0.082579
17	6	0	3.715023	1.680831	0.026615
18	6	0	2.550341	0.918291	-0.141975
19	6	0	-2.624275	-0.533338	-0.270269

20	6	0	-3.900812	-1.131519	-0.508149
21	6	0	-3.972043	-2.474230	-0.961979
22	6	0	-2.828711	-3.218884	-1.135757
23	6	0	-1.577302	-2.678815	-0.765661
24	6	0	-2.542747	0.876693	0.012958
25	6	0	-3.711675	1.568507	0.344214
26	6	0	-4.966451	0.914648	0.213890
27	6	0	-5.070143	-0.366969	-0.263595
28	1	0	-5.865486	1.470697	0.469168
29	1	0	-2.884195	-4.239239	-1.504002
30	1	0	-6.043601	-0.824129	-0.422796
31	1	0	-4.949760	-2.903275	-1.167483
32	1	0	3.127431	-4.430577	-0.269901
33	1	0	0.937408	-3.443690	0.288514
34	1	0	5.873330	1.674882	0.018402
35	1	0	-0.086978	4.357730	-1.814447
36	1	0	6.094558	-0.741316	-0.436619
37	1	0	5.096483	-2.941128	-0.552694
38	1	0	-0.703757	-3.315943	-0.823768
39	1	0	-2.193999	3.288357	-1.126290
40	1	0	2.061712	3.251440	-1.403960
41	6	0	-3.739522	2.986021	0.878740
42	1	0	-4.081916	3.709639	0.126761
43	1	0	-2.764951	3.315364	1.243491
44	1	0	-4.448663	3.042030	1.712976
45	6	0	3.744672	3.153324	0.392079
46	1	0	2.802947	3.501623	0.819627
47	1	0	3.983942	3.797194	-0.464739
48	1	0	4.533494	3.317044	1.135381
49	16	0	-0.232686	-0.985214	2.579977

3b

E(RB3LYP) = –1495.028499 hartree

Center Number	Atomic Number	Atomic Type	Coordinates X	Y	Z
1	6	0	1.212626	1.520985	-0.290496
2	6	0	1.140764	2.732888	-1.002725
3	6	0	-0.080590	3.343286	-1.262253
4	6	0	-1.268062	2.758044	-0.836336
5	6	0	-1.256331	1.528449	-0.157888
6	6	0	-0.006421	0.912385	0.083408
7	15	0	-0.032173	-0.761157	0.741689
8	6	0	1.545478	-1.440717	0.151422
9	6	0	-1.472185	-1.420509	-0.170975
10	6	0	1.745058	-2.813284	0.212885
11	6	0	3.011043	-3.389684	-0.008703
12	6	0	4.099222	-2.569518	-0.190229
13	6	0	3.959926	-1.158762	-0.166234
14	6	0	2.659857	-0.561343	-0.056098
15	6	0	5.107924	-0.327881	-0.185212
16	6	0	4.975661	1.022632	-0.004943
17	6	0	3.703887	1.649918	0.073988
18	6	0	2.540033	0.880384	-0.070669
19	6	0	-2.634690	-0.580520	-0.130410
20	6	0	-3.914899	-1.186000	-0.327413
21	6	0	-3.991953	-2.540672	-0.743330
22	6	0	-2.850797	-3.288030	-0.919999
23	6	0	-1.593394	-2.734305	-0.592107
24	6	0	-2.550830	0.838380	0.110977
25	6	0	-3.716040	1.538258	0.439240
26	6	0	-4.971892	0.879596	0.349632
27	6	0	-5.081459	-0.416614	-0.085151
28	1	0	-5.867497	1.442532	0.602045
29	1	0	-2.912070	-4.317894	-1.260036
30	1	0	-6.056747	-0.879748	-0.213298
31	1	0	-4.972707	-2.976033	-0.919556
32	1	0	3.126237	-4.469447	0.012832
33	1	0	0.923936	-3.464942	0.490663
34	1	0	5.862176	1.647252	0.075597
35	1	0	-0.109531	4.266363	-1.835080
36	1	0	6.089829	-0.785046	-0.278217
37	1	0	5.095419	-2.988621	-0.309992
38	1	0	-0.718450	-3.369837	-0.657095
39	1	0	-2.211590	3.220937	-1.099333
40	1	0	2.042307	3.175409	-1.405528
41	6	0	-3.738939	2.971770	0.930042
42	1	0	-4.092790	3.671008	0.160502
43	1	0	-2.759931	3.313987	1.270250
44	1	0	-4.436683	3.053355	1.771800
45	6	0	3.732496	3.134974	0.385454
46	1	0	2.791023	3.497818	0.801265
47	1	0	3.969586	3.747555	-0.494566
48	1	0	4.522391	3.326726	1.120893
49	8	0	-0.204409	-0.924834	2.228282

1c

E(RB3LYP) = –1496.009792 hartree

Center Number	Atomic Number	Atomic Type	Coordinates X	Y	Z
1	15	0	0.025307	-0.284952	1.040064
2	6	0	1.478062	-0.992513	0.166273
3	6	0	0.016706	1.396207	0.319905
4	6	0	-1.535108	-0.981425	0.395310
5	6	0	2.599582	-0.105659	0.115023
6	6	0	3.863017	-0.692070	-0.115024
7	6	0	4.051266	-2.062118	-0.401975
8	6	0	2.945383	-2.880418	-0.446997
9	6	0	1.670778	-2.336188	-0.132501
10	6	0	2.556772	1.320109	0.281635
11	6	0	3.775470	1.993391	0.385305

12	6	0	5.035747	1.362708	0.238091
13	6	0	5.080710	0.017662	-0.057383
14	6	0	-1.199234	2.060874	0.023804
15	6	0	-1.131383	3.401410	-0.399861
16	6	0	0.083710	4.062671	-0.517835
17	6	0	1.272165	3.389074	-0.264352
18	6	0	1.266354	2.049821	0.157943
19	6	0	-1.803812	-2.347286	0.450269
20	6	0	-3.084664	-2.895755	0.190638
21	6	0	-4.131140	-2.039795	-0.065325
22	6	0	-3.882127	-0.649249	-0.078480
23	6	0	-2.603088	-0.071600	0.113008
24	6	0	-5.068168	0.096402	-0.251484
25	6	0	-4.982191	1.468757	-0.212404
26	6	0	-3.711008	2.073646	-0.064617
27	6	0	-2.514507	1.362976	0.053057
28	6	0	5.534316	-2.323900	-0.601408
29	6	0	6.226405	-0.943982	-0.318560
30	6	0	-5.609211	-2.285080	-0.311404
31	6	0	-6.242183	-0.853766	-0.399267
32	1	0	-3.686350	3.157123	-0.043335
33	1	0	-6.767717	-0.702750	-1.350082
34	1	0	-6.985037	-0.696824	0.392585
35	1	0	-5.862681	2.100932	-0.297554
36	1	0	0.106654	5.095302	-0.855317
37	1	0	2.213315	3.894253	-0.449045
38	1	0	-6.061285	-2.877894	0.492702
39	1	0	-5.769610	-2.848623	-1.239029
40	1	0	-3.222904	-3.973260	0.235576
41	1	0	-1.015340	-3.032685	0.744816
42	1	0	6.897164	-1.007040	0.547396
43	1	0	6.844379	-0.620808	-1.164996
44	1	0	5.940568	1.957628	0.335754
45	1	0	3.771233	3.062262	0.573394
46	1	0	5.743692	-2.669418	-1.621550
47	1	0	5.904699	-3.106043	0.071995
48	1	0	3.026183	-3.939413	-0.680378
49	1	0	-2.033629	3.927734	-0.686715
50	1	0	0.825343	-3.015619	-0.115475

2c

E(RB3LYP) = –1894.223518 hartree

Center Number	Atomic Number	Atomic Type	Coordinates X	Y	Z
1	15	0	0.012760	-0.269875	0.804630
2	16	0	0.185166	-0.415441	2.771605
3	6	0	1.464180	-0.958978	-0.054837
4	6	0	0.006465	1.430899	0.160957
5	6	0	-1.552919	-0.953557	0.198770
6	6	0	2.583236	-0.072162	-0.105553
7	6	0	3.839122	-0.662774	-0.359765
8	6	0	4.014492	-2.029282	-0.668518
9	6	0	2.905863	-2.846417	-0.712972
10	6	0	1.641235	-2.299981	-0.374739
11	6	0	2.548515	1.348391	0.085380
12	6	0	3.774035	2.012619	0.170994
13	6	0	5.028384	1.380847	-0.010300
14	6	0	5.062047	0.038216	-0.318730
15	6	0	-1.213774	2.100652	-0.112552
16	6	0	-1.145500	3.463954	-0.455114
17	6	0	0.069893	4.130359	-0.527739
18	6	0	1.261321	3.447193	-0.318413
19	6	0	1.260166	2.086013	0.024179
20	6	0	-1.816173	-2.319106	0.262588
21	6	0	-3.092381	-2.868753	-0.003896
22	6	0	-4.134036	-2.009435	-0.276058
23	6	0	-3.886812	-0.619265	-0.294719
24	6	0	-2.611049	-0.038846	-0.090913
25	6	0	-5.071000	0.121390	-0.494251
26	6	0	-4.986635	1.494498	-0.465514
27	6	0	-3.720206	2.099711	-0.290480
28	6	0	-2.523057	1.394677	-0.141451
29	6	0	5.491625	-2.297967	-0.893098
30	6	0	6.196624	-0.924752	-0.615480
31	6	0	-5.607839	-2.258933	-0.536807
32	6	0	-6.239515	-0.830867	-0.661197
33	1	0	-3.702357	3.182858	-0.269171
34	1	0	-6.737624	-0.693004	-1.628593
35	1	0	-7.003844	-0.663100	0.107250
36	1	0	-5.864547	2.125975	-0.575060
37	1	0	0.091236	5.181979	-0.800484
38	1	0	2.198488	3.967620	-0.477096
39	1	0	-6.066576	-2.834836	0.275556
40	1	0	-5.755459	-2.843669	-1.453098
41	1	0	-3.234771	-3.944817	0.049826
42	1	0	-1.030507	-2.995787	0.581813
43	1	0	6.887269	-0.997391	0.233575
44	1	0	6.794687	-0.596583	-1.474115
45	1	0	5.936471	1.972046	0.075490
46	1	0	3.782031	3.076955	0.381106
47	1	0	5.681095	-2.643052	-1.917062
48	1	0	5.863687	-3.085339	-0.227058
49	1	0	2.981287	-3.902038	-0.960557
50	1	0	-2.044726	4.010877	-0.709473
51	1	0	0.792262	-2.973550	-0.346600

3c

E(RB3LYP) = –1571.258542 hartree

Center Number	Atomic Number	Atomic Type	Coordinates X	Y	Z

1	15	0	0.021910	-0.275694	0.894781
2	8	0	0.167601	-0.375104	2.391084
3	6	0	1.467104	-0.974790	0.047339
4	6	0	0.012550	1.414102	0.241196
5	6	0	-1.544091	-0.963610	0.313350
6	6	0	2.591013	-0.091628	0.009865
7	6	0	3.850967	-0.683870	-0.219932
8	6	0	4.029763	-2.052620	-0.516445
9	6	0	2.921334	-2.869370	-0.572941
10	6	0	1.651637	-2.318198	-0.261616
11	6	0	2.554158	1.331796	0.187358
12	6	0	3.779090	1.996172	0.282318
13	6	0	5.035875	1.362820	0.124259
14	6	0	5.073659	0.016876	-0.168810
15	6	0	-1.205501	2.085865	-0.040898
16	6	0	-1.136027	3.448644	-0.38547
17	6	0	0.080700	4.113800	-0.453113
18	6	0	1.271376	3.432294	-0.233549
19	6	0	1.266617	2.071610	0.111530
20	6	0	-1.812453	-2.326827	0.412103
21	6	0	-3.093156	-2.880459	0.174970
22	6	0	-4.134598	-2.025349	-0.110560
23	6	0	-3.884662	-0.636410	-0.166046
24	6	0	-2.606090	-0.054988	0.015648
25	6	0	-5.068008	0.100811	-0.381855
26	6	0	-4.979580	1.473912	-0.393844
27	6	0	-3.711412	2.080434	-0.236351
28	6	0	-2.515121	1.377883	-0.067724
29	6	0	5.509740	-2.323639	-0.719285
30	6	0	6.211846	-0.949044	-0.441178
31	6	0	-5.610265	-2.278291	-0.357893
32	6	0	-6.239269	-0.852762	-0.519272
33	1	0	-3.692320	3.163699	-0.245277
34	1	0	-6.739853	-0.740290	-1.488684
35	1	0	-7.001137	-0.662410	0.246393
36	1	0	-5.855735	2.104540	-0.521363
37	1	0	0.103704	5.164790	-0.728606
38	1	0	2.208961	3.954259	-0.385354
39	1	0	-6.066828	-2.830335	0.472123
40	1	0	-5.763363	-2.887876	-1.256911
41	1	0	-3.238062	-3.954576	0.255811
42	1	0	-1.021558	-2.999571	0.728195
43	1	0	6.889555	-1.016179	0.418768
44	1	0	6.823369	-0.627869	-1.292959
45	1	0	5.942712	1.955261	0.215185
46	1	0	3.785041	3.062654	0.481585
47	1	0	5.712596	-2.675114	-1.738518
48	1	0	5.872516	-3.107172	-0.043625
49	1	0	3.000463	-3.926600	-0.812800
50	1	0	-2.032941	3.998102	-0.642828
51	1	0	0.800231	-2.990048	-0.250455

AuCl(**1b**)

E(RB3LYP) = –2015.854408 hartree

Center Number	Atomic Number	Atomic Type	Coordinates X	Y	Z
1	79	0	0.434231	-1.778698	-1.001731
2	17	0	0.977455	-3.414824	-2.566870
3	15	0	-0.092829	-0.157140	0.534044
4	6	0	-1.532592	2.088353	-0.306365
5	6	0	-1.580001	3.464911	-0.594963
6	6	0	-0.416556	4.206738	-0.764961
7	6	0	0.830533	3.605812	-0.633774
8	6	0	0.937585	2.244761	-0.304680
9	6	0	-0.257199	1.516486	-0.118082
10	6	0	-1.695697	-0.433725	1.351810
11	6	0	1.278309	0.110795	1.721833
12	6	0	-1.826423	-1.495589	2.236300
13	6	0	-3.081360	-1.874418	2.750365
14	6	0	-4.214086	-1.248718	2.286046
15	6	0	-4.132669	-0.221563	1.312449
16	6	0	-2.855204	0.257992	0.867307
17	6	0	-5.312064	0.292428	0.716388
18	6	0	-5.222312	1.165293	-0.333779
19	6	0	-3.976924	1.689706	-0.772424
20	6	0	-2.800640	1.334238	-0.098103
21	6	0	2.394790	0.821872	1.172869
22	6	0	3.669132	0.653393	1.799226
23	6	0	3.755989	-0.039417	3.034869
24	6	0	2.635092	-0.585289	3.616471
25	6	0	1.399572	-0.547410	2.932325
26	6	0	2.277571	1.673645	0.015625
27	6	0	3.439855	2.072580	-0.651141
28	6	0	4.704838	1.785065	-0.070806
29	6	0	4.820707	1.163861	1.146908
30	1	0	5.598534	2.107215	-0.599615
31	1	0	2.701587	-1.095715	4.572734
32	1	0	5.795421	1.018682	1.605600
33	1	0	4.728804	-0.135869	3.510341
34	1	0	-3.148439	-2.688380	3.465838
35	1	0	-0.959050	-2.089086	2.504320
36	1	0	-6.123912	1.483092	-0.851613
37	1	0	-0.483297	5.271512	-0.970343
38	1	0	-6.277486	-0.069512	1.060202
39	1	0	-5.198137	-1.565237	2.622457
40	1	0	0.552058	-1.066405	3.363384
41	1	0	1.725166	4.210616	-0.719208
42	1	0	-2.535100	3.971317	-0.640034
43	6	0	3.449696	2.783228	-1.988682
44	1	0	3.692917	3.849790	-1.891992
45	1	0	2.496450	2.700865	-2.514207
46	1	0	4.224322	2.340807	-2.625489
47	6	0	-4.038750	2.567449	-2.008225
48	1	0	-3.078396	2.644481	-2.521040

49	1	0	-4.385302	3.585574	-1.786557
50	1	0	-4.761853	2.137628	-2.710721

2d

E(RB3LYP) = –3403.707541 hartree

Center Number	Atomic Number	Atomic Type	Coordinates X	Y	Z
1	15	0	-3.045627	-0.063865	0.846082
2	15	0	3.045619	0.063858	0.846078
3	16	0	-3.255263	0.042288	2.808958
4	16	0	3.255251	-0.042338	2.808954
5	6	0	-0.690309	-1.220419	-0.058274
6	6	0	0.690301	1.220415	-0.058276
7	6	0	1.343833	0.009402	0.270782
8	6	0	0.697922	-1.242446	0.287995
9	6	0	-0.697932	1.242440	0.287995
10	6	0	-1.343843	-0.009406	0.270782
11	6	0	-1.421770	-2.286416	-0.792720
12	6	0	-1.464969	2.495217	0.536460
13	6	0	1.421765	2.286423	-0.792709
14	6	0	1.464968	-2.495223	0.536441
15	6	0	-2.846034	-2.489156	-0.599406
16	6	0	-3.488887	-3.627283	-1.195531
17	6	0	-2.748988	-4.464056	-2.068172
18	6	0	-1.460298	-4.137040	-2.390159
19	6	0	-0.780833	-3.043354	-1.789206
20	6	0	0.780839	3.043346	-1.789214
21	6	0	1.460318	4.137011	-2.390192
22	6	0	2.749002	4.464038	-2.068189
23	6	0	3.488886	3.627287	-1.195515
24	6	0	2.846027	2.489164	-0.599386
25	6	0	-0.866747	3.643694	1.071101
26	6	0	-1.545202	4.889940	0.971423
27	6	0	-2.773591	5.009108	0.373647
28	6	0	-3.483698	3.844426	-0.019343
29	6	0	-2.861543	2.569478	0.154729
30	6	0	2.861539	-2.569473	0.154698
31	6	0	3.483706	-3.844417	-0.019358
32	6	0	2.773628	-5.009097	0.373692
33	6	0	1.545254	-4.889926	0.971500
34	6	0	0.866772	-3.643691	1.071131
35	6	0	-3.683776	-1.605655	0.150392
36	6	0	-5.019550	-1.903484	0.385389
37	6	0	-5.613727	-3.060491	-0.150789
38	6	0	-4.858064	-3.894178	-0.943068
39	6	0	-4.804924	3.918743	-0.534275
40	6	0	-5.528306	2.778681	-0.805292
41	6	0	-4.980821	1.517401	-0.487110
42	6	0	-3.689668	1.410920	-0.001620
43	6	0	4.858057	3.894191	-0.943029
44	6	0	5.613712	3.060514	-0.150731
45	6	0	5.019535	1.903501	0.385437
46	6	0	3.683765	1.605666	0.150420
47	6	0	3.689656	-1.410910	-0.001657
48	6	0	4.980804	-1.517382	-0.487166
49	6	0	5.528291	-2.778661	-0.805353
50	6	0	4.804924	-3.918728	-0.534311
51	6	0	-0.587341	2.754385	-2.368170
52	6	0	0.455311	3.661304	1.803880
53	6	0	0.587337	-2.754389	-2.368186
54	1	0	6.536051	-2.845690	-1.204890
55	1	0	5.593902	-0.627388	-0.593275
56	1	0	6.658869	3.277706	0.048560
57	1	0	5.608524	1.239063	1.011295
58	1	0	-6.536071	2.845716	-1.204816
59	1	0	-5.593925	0.627410	-0.593213
60	1	0	-6.658889	-3.277675	0.048487
61	1	0	-5.608544	-1.239044	1.011241
62	1	0	1.047017	-5.773853	1.362172
63	1	0	5.243386	-4.900918	-0.694088
64	1	0	3.242355	-5.982545	0.252026
65	1	0	-0.921367	-4.726925	-3.127592
66	1	0	-5.301598	-4.776774	-1.397628
67	1	0	-3.236299	-5.327276	-2.514182
68	1	0	-1.046937	5.773873	1.362045
69	1	0	0.921402	4.726874	-3.127652
70	1	0	-5.243377	4.900937	-0.694058
71	1	0	-3.242304	5.982560	0.251953
72	1	0	5.301594	4.776787	-1.397586
73	1	0	3.236318	5.327247	-2.514213
74	6	0	-0.455296	-3.661287	1.803892
75	1	0	-0.775532	-2.668738	2.125618
76	1	0	-1.258607	-4.097463	1.198980
77	1	0	-0.352910	-4.285640	2.699385
78	1	0	-0.932333	1.740807	-2.164363
79	1	0	-1.349061	3.447581	-1.996213
80	1	0	-0.541474	2.882557	-3.456295
81	1	0	0.775782	2.668718	2.125245
82	1	0	1.258520	4.097909	1.199138
83	1	0	0.352760	4.285293	2.699609
84	1	0	1.349011	-3.447755	-1.996450
85	1	0	0.541373	-2.882300	-3.456339
86	1	0	0.932448	-1.740895	-2.164171

Chapter 5

Mechanistic Study on Bora-Friedel–Crafts Reaction and Its Application to Other Heteroatoms

Mechanism

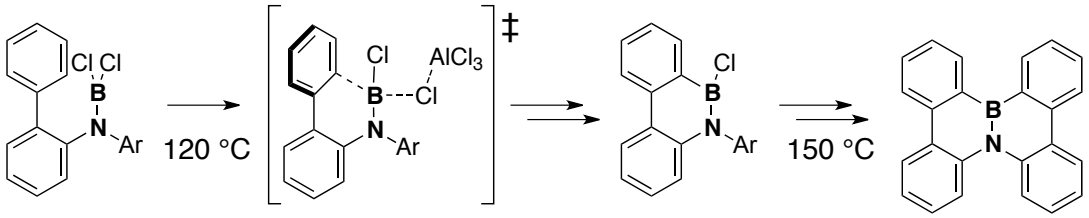

$\Delta G^{\ddagger}$ = +27.1 kcal/mol

Scope and Limitations

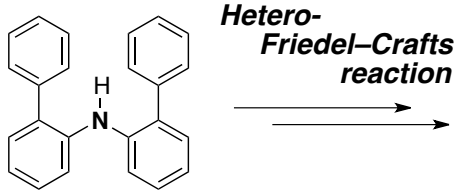

Aza**hetero-**dibenzo[*g*,*p*]chrysenes

X	yield
P=S	61%
Si–Ph	20%
Ge–Ph	42%
Al	ND
Ga	ND
Sn–Ph	ND

Abstract: In situ NMR measurements and DFT calculations of the reaction pathway were performed as the basis of a mechanistic study of the bora-Friedel–Crafts reaction. The ^{1}H NMR spectra clearly indicate that the first cyclization takes place at 120 °C and the second cyclization takes place at 150 °C. The ^{11}B NMR spectra suggest that three-fold coordinated boron species are major intermediates during the reaction rather than four-fold coordinated species. DFT calculations suggest that the mechanism proceeds *via* a relatively stable aluminate intermediate. The activation energy calculated for the first cyclization step is 27.1 kcal/mol ($\Delta G^{\ddagger}$), which is good agreement with the experimental results. Next, to establish further applications of the hetero-Friedel–Crafts reaction, 4b-aza-hetero-dibenzo[*g*,*p*]chrysene derivatives have been synthesized *via* phospha-, sila-, and germa-Friedel–Crafts reactions. The development of these reactions has led to insights into a wide variety of molecular structures of azadibenzochrysene derivatives with heteroatom junctions and into the suitable ranges of electronegativity and atomic radius of the heteroatoms for the reactions.

Chapter 5

5-1. Introduction

Replacement of the C–C units in dibenzo[*g*,*p*]chrysene with isoelectronic B–N units affords novel hetero-π-conjugated molecules that are structurally similar to their all-carbon analogs but exhibit substantially different optical and electronic properties (see Chapter 1). Changes in the heteroatom junctions perturb the π-conjugated framework, which makes modifying the heteroatom junction a promising way to modulate the physical properties and explore the novel characters of these molecules.[1,2] This makes the development of a facile synthetic method for introducing various heteroatoms especially desirable. First, this author investigated the reaction mechanism of the bora-Friedel–Crafts reaction in detail. From this framework, the development of various hetero-Friedel–Crafts reactions was envisioned based on these theoretical insights (Scheme 1).

Scheme 1. Tandem hetero-Friedel–Crafts reaction producing a π-conjugated framework with a heteroatom junction

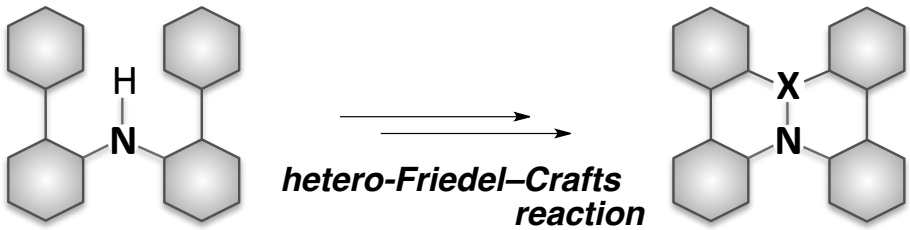

In this chapter, both NMR and theoretical studies on the mechanism of the bora-Friedel–Crafts reactions for the synthesis of **1** are described. In addition, novel phospha-, sila-, and germa-Friedel–Crafts reactions have been developed based on the obtained mechanistic understanding, and the syntheses of other 4b-azadibenzo[*g*,*p*]chrysene derivatives (**2**, **3**, and **4**) are described.

Chart 1. 4b-Azadibenzo[*g*,*p*]chrysene derivatives

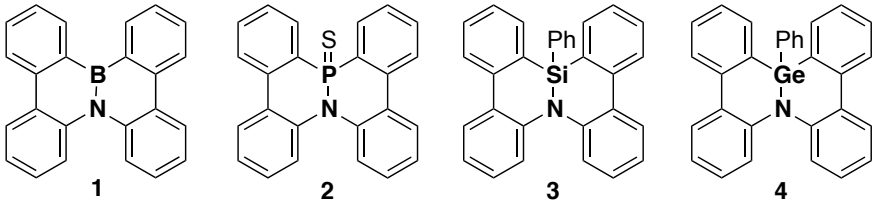

[1] Reviews: (a) Liu, Z.; Marder, T. B. *Angew. Chem., Int. Ed.* **2008,** *47*, 242–244. (b) Bosdet, M. J. D.; Piers, W. E. *Can. J. Chem.* **2009,** *87*, 8–29. (c) Ashe, A. J., III *Organometallics* **2009,** *28*, 4236–4248. (d) Fukazawa, A.; Yamaguchi, S. *Chem. Asian J.* **2009,** *4*, 1386–1400.

[2] Recent examples: (a) Saito, S.; Matsuo, K.; Yamaguchi, S. *J. Am. Chem. Soc.* **2012,** *134*, 9130–9133. (b) Chen, L.; Puniredd, S. R.; Tan, Y.-Z.; Baumgarten, M.; Zschieschang, U.; Enkelmann, V.; Pisula, W.; Feng, X.; Klauk, H.; Müllen, K. *J. Am. Chem. Soc.* **2012,** *134*, 17869–17872. (c) Dou, C.; Saito, S.; Matsuo, K.; Hisaki, I.; Yamaguchi, S. *Angew. Chem., Int. Ed.* **2012,** *51*, 12206–12210.

5-2. Results and Discussion

5-2-1. NMR and theoretical studies on the bora-Friedel–Crafts reaction

To gain mechanistic insight into the bora-Friedel–Crafts reaction, ^{1}H and ^{11}B NMR studies were carried out during the course of the reaction (Figures 1 and 2). Figure 1a shows the ^{1}H NMR spectrum of **5**; all peaks were observed in the range of 5.9 ppm to 7.3 ppm. Figure 1b shows the ^{1}H NMR spectrum of the reaction mixture including **6**, which was obtained by treating **5** with 4 equivalents of $AlCl_3$ and 1.5 equivalents of 2,2,6,6-tetramethylpiperidine for 12 h at 120 ºC. The peaks derived from **5**, such as the H^a and H^b peaks, disappeared completely, and a new set of characteristic peaks was observed in the range of 7.5 ppm to 8.6 ppm. In particular, the peaks at 8.6 ppm and around 8.2 ppm could be assigned the proton at the position *ortho* to the boron atom (H^c) and protons on the uncyclized phenyl ring, respectively. These results suggest the complete conversion of boron dichloride **5** to the monochloride **6**. When the reaction mixture was further heated at 150 ºC for 12 h, the peaks assigned to **6** became minor, and the peaks of **1** were observed as a major component of the reaction mixture (Figure 1c). The peaks corresponding to the position *ortho* to the boron atom have been slightly shifted to a lower field by the cyclization (H^c *vs*. H^d). These results clearly indicate that the first cyclization takes place at 120 °C, whereas the second cyclization is much slower and takes place at 150 °C.

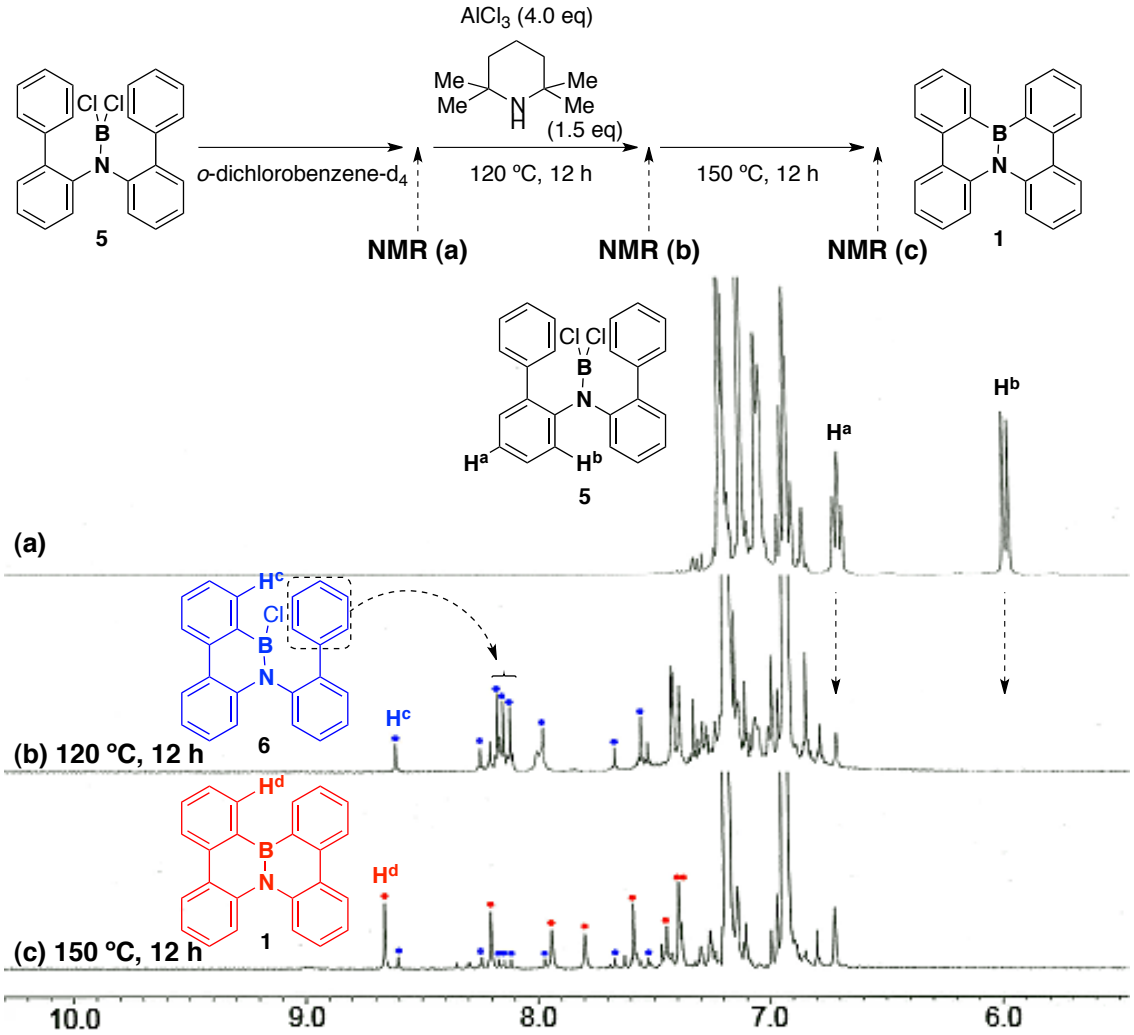

Figure 1. ^{1}H NMR spectra of (a) aminoboron dichloride **5** and the reaction mixture after treatments at (b) 120 ºC for 12 h and (c) 150 ºC for a further 12 h (392 MHz, *o*-dichlorobenzene-d_4).

To obtain detailed insight into the boron intermediates in this reaction, ^{11}B NMR spectra were also measured and analyzed (Figure 2). Figures 2a and 2b show the ^{11}B NMR spectra of boron trichloride (46 ppm) and **5** (31 ppm), respectively. After the treatment at 120 ºC for 12 h, the peak derived from **5** disappeared, and a new broad peak (35 ppm) appeared (Figure 2c). This peak did not show any notable change upon further heating at 150 ºC for 12 h (Figure 2d–e). However, the ^{1}H NMR results confirm that **1** would be generated at 150 ºC. It is possible that the peaks could not be separated because **1** and **6** have close ^{11}B NMR shifts. Furthermore, ^{11}B NMR spectra of four-fold and symmetric three-fold coordinated boron species generally tend to have a sharper singlet peak than those of asymmetric three-fold coordinated boron species, because of the quadrupolar relaxation.[3] These results suggest that three-fold coordinated boron

[3] Odom, J. D. *Comprehensive Organometallic Chemistry*, Wilkinson, G.; Stone, F. G. A.; Abel, E.

species are major intermediates during the reaction, rather than four-fold species such as boron-amine complexes.[4]

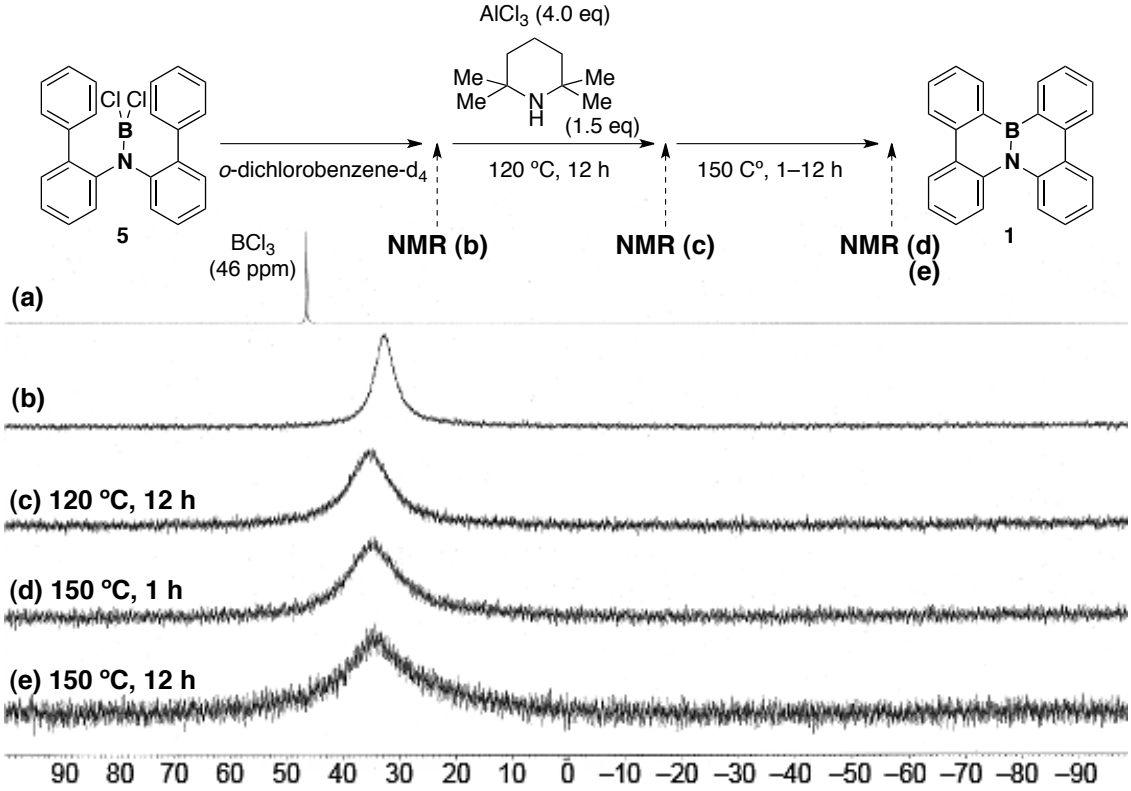

Figure 2. ^{11}B NMR Spectra of (a) BCl_3, (b) aminoboron dichloride **5**, and the reaction mixture after treatments at (c) 120 °C for 12 h, (d) 150 °C for a further 1 h, and (e) 150 °C for a further 12 h (98 MHz, *o*-dichlorobenzene-d_4).

To further investigate the reaction pathway of the bora-Friedel–Crafts reaction, DFT calculations were performed at the B3LYP/6-31G(d) level. Figures 3 and 5 show sections of energy profile (all Gibbs free energy, ΔG) for the reaction pathway of the first cyclization reaction to form **6**. In Figure 3, aluminum chloride dimer (Al_2Cl_6) dissociates into monomer ($AlCl_3$) with $\Delta\Delta G$ = +5.0 kcal/mol. Aminoboron chloride **5** interacts with $AlCl_3$ to form complex **CP1**, which is 3.4 kcal/mol higher in energy than the sum of **5** and $AlCl_3$. The cyclization of **CP1** *via* **TS1** and **CP2** requires an activation energy of $\Delta G^{\ddagger}$ = +18.7 kcal/mol to form an aluminate complex, **CP3**. This transformation is exothermic, with $\Delta\Delta G$ = –3.9 kcal/mol. Normally, an arenium ion intermediate **CP2** is found in the intrinsic reaction coordinate calculations. However, this state could not be observed for this reaction, because the following **CP3** has been stabilized. The existence of this intermediate could potentially become a driving force for this cyclization reaction. In addition, the calculated structures, along with key bond

W. Eds.; Pergamon: Oxford, **1982,** Vol. 1, p. 253.

[4] Grosso, A. D.; Singleton, P. J.; Muryn, C. A.; Ingleson, M. J. *Angew. Chem., Int. Ed.* **2011,** *50*, 2102–2106.

distances, are depicted in Figure 4 for **TS**, **CP1**, and **CP3**. During the transformation from **TS1** to **CP3**, the C1–H distance increases from 1.089 to 1.159 Å. This result suggests that **CP3** would be likely susceptible to the following deprotonation reaction.

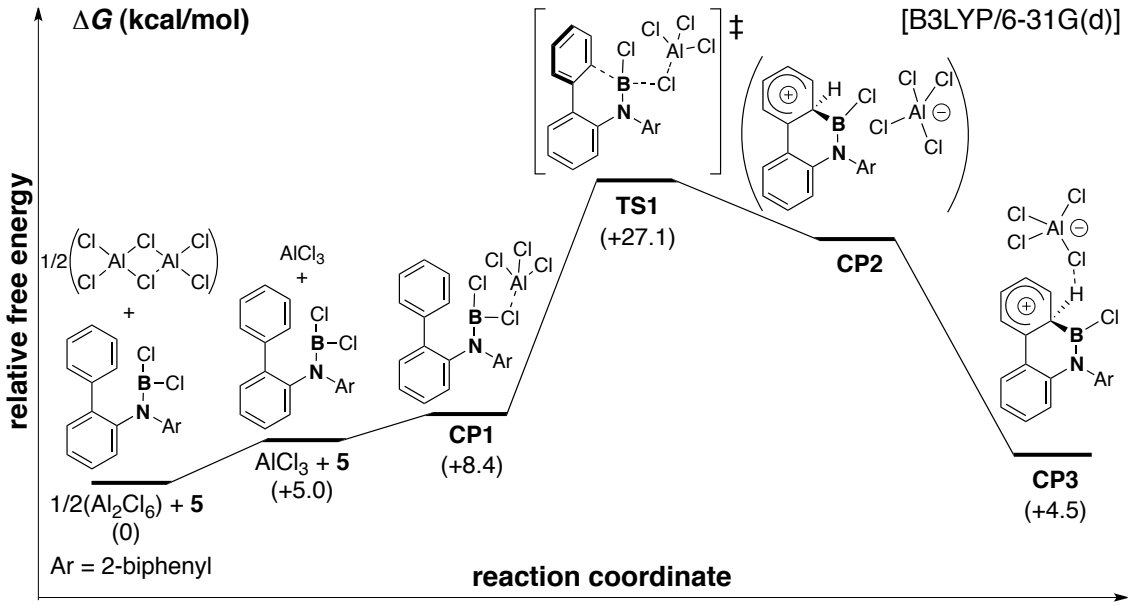

Figure 3. Gibbs free energy profiles for the early part of the bora-Friedel–Crafts reaction mechanism based on DFT calculations at the B3LYP/6-31G(d) level.

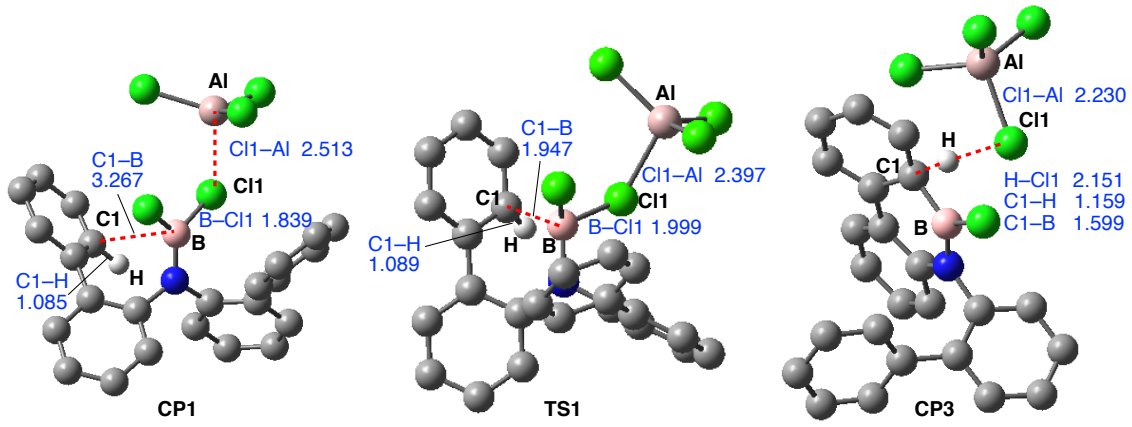

Figure 4. Calculated structures of the transition state **TS1** and intermediates **CP1** and **CP3**. H atoms are not shown, except that bonded to the C1 atom. Key bond distances (Å) are indicated.

Next, the elimination of hydrogen chloride from **CP3** takes place *via* **TS2** with a very small activation energy of $\Delta\Delta G^{\ddagger}$ = +1.5 kcal/mol to form the monocyclized product **PD1** and $AlCl_3$·HCl (Figure 5, left). 2,2,6,6-Tetramethylpiperidine and $AlCl_3$·HCl form an ion pair of tetrachloroaluminate and tetramethylpiperidinium to make the whole process exothermic, with a stabilization energy of 40.5 kcal/mol (Figure 5, right). Because this large exothermicity inhibits the progress of the reverse reaction, 2,2,6,6-tetramethylpiperidine could play an important role in enhancing the

product yield. The pathway of the second cyclization reaction could not be found at present; however, it has been assumed that the mechanism proceeds *via* a similar aluminate intermediate.

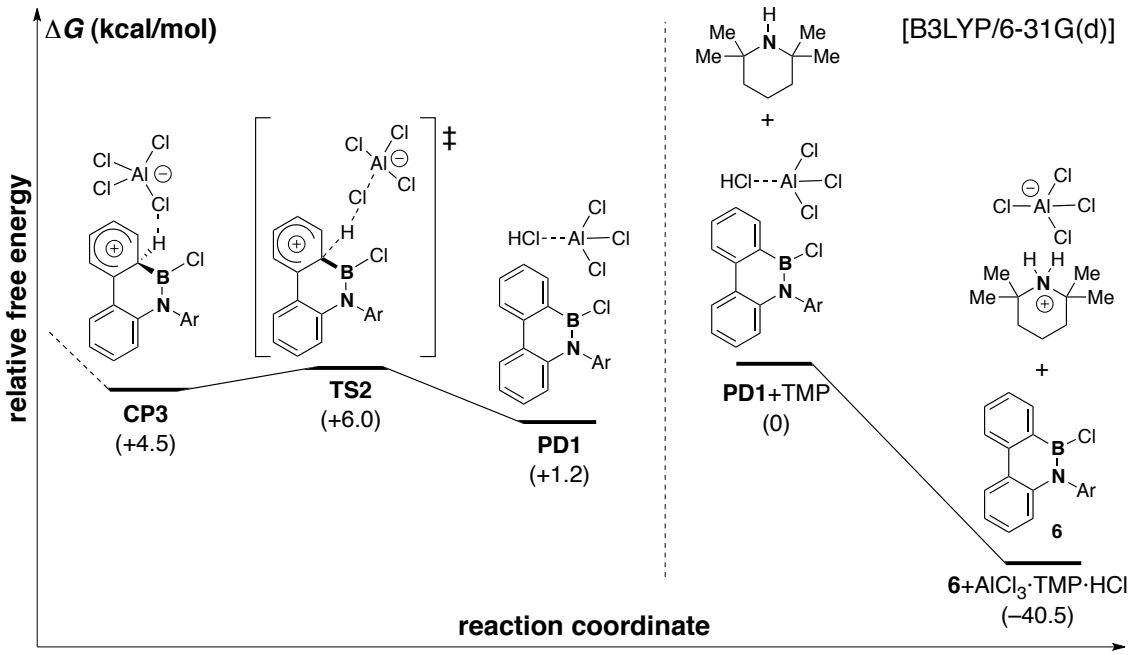

Figure 5. Gibbs free energy profiles for the early part of the bora-Friedel–Crafts reaction mechanism based on DFT calculations at the B3LYP/6-31G(d) level.

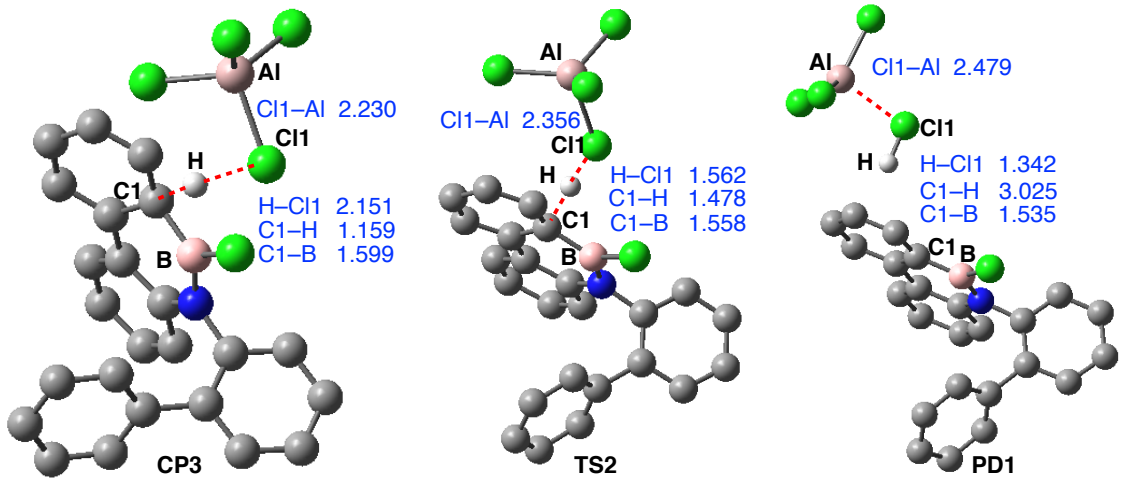

Figure 6. Calculated structures of **TS2**, **CP3**, and **PD1**. H atoms are not shown, except that the bonded to the C1 or Cl1 atom. Key bond distances (Å) are indicated.

5-2-2. Synthesis of azaphosphadibenzochrysene derivatives

To obtain a comprehensive understanding of the hetero-Friedel–Crafts reaction and the physical properties of heterodibenzochrysenes, the syntheses of azadibenzo[*g*,*p*]chrysene derivatives possessing heteroatoms other than boron were also investigated. The phospha-Friedel–Crafts reaction was examined first (Scheme 2). In this reaction, phosphination of diarylamine **7** through sequential treatments with BuLi

and PCl_3 gave diarylaminodichlorophosphine **8**. Sulfurization of **8** with sulfur and the subsequent tandem phospha-Friedel–Crafts reaction with $AlCl_3$ at 120 ºC afforded compound **2** in 61% yield. The reaction did not proceed at all without sulfurization of **8**. One reason for this might be that the electrophilicity of phosphine dichloride is smaller than that of thiophosphine dichloride. When teraryldichlorophosphines were used, the phospha-Friedel–Crafts reaction gave several byproducts in the absence of NEt^iPr_2 (see Chapter 4). However, the addition of amine is not indispensable in this reaction of **8**. This might be because the aminothiophosphine **8** is more stabilized to treatment with acidity by the nitrogen atom than the arylthiophosphines.

Scheme 2. Synthesis of **2** *via* the phospha-Friedel–Crafts reaction

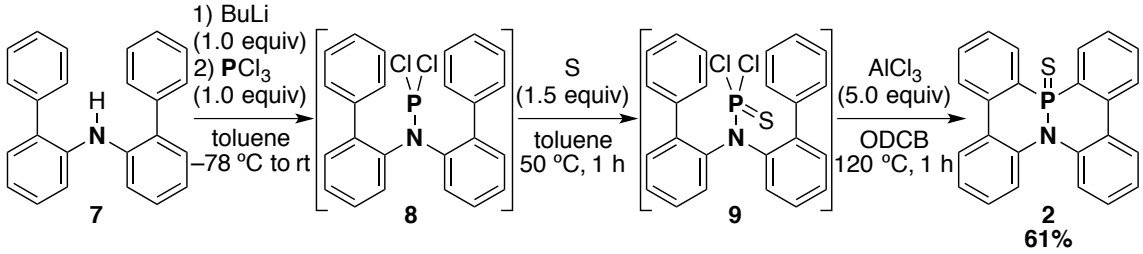

The molecular structure of **2** has been determined by performing X-ray crystallography (Figure 7). The P–N bond length [1.6901(15) Å] was found to be longer than the B–N bond length in azaboradibenzochrysene **1** [1.426(3) Å], which is consistent with the covalent radii of the P and B atoms (P 1.11 *vs*. B 0.85 Å).[5] The phosphorus center adopts a distorted tetrahedral geometry with C1–P–N, N–P–C2, and C2–P–C1 bond angles of 99.09(8)°, 102.66(8)°, and 110.20(9)°, respectively. Because of the tetrahedral geometry of the phosphorus centers as well as the steric repulsion between the hydrogen atoms at the positions *ortho* to the phosphorus atom (C5–C7–C6–C8 dihedral angle = 66.82°), **2** adopts a twisted conformation. In particular, the rigid tetrahedral geometry of the phosphorus center caused the biphenyl moieties of **2** to be highly twisted compared to those in **1** (Figure 7b). In the crystal, the *P*-helix (shown in blue) and *M*-helix (shown in pink) enantiomers are packed alternately. However, the intermolecular π-π distances of **2** are longer than those of **1** because of the presence of sulfur atoms (4.3–5.0 *vs*. 3.3–3.6 Å).

[5] Pyykkö, P.; Atsumi, M. *Chem. Eur. J.* **2009,** *15*, 186–197.

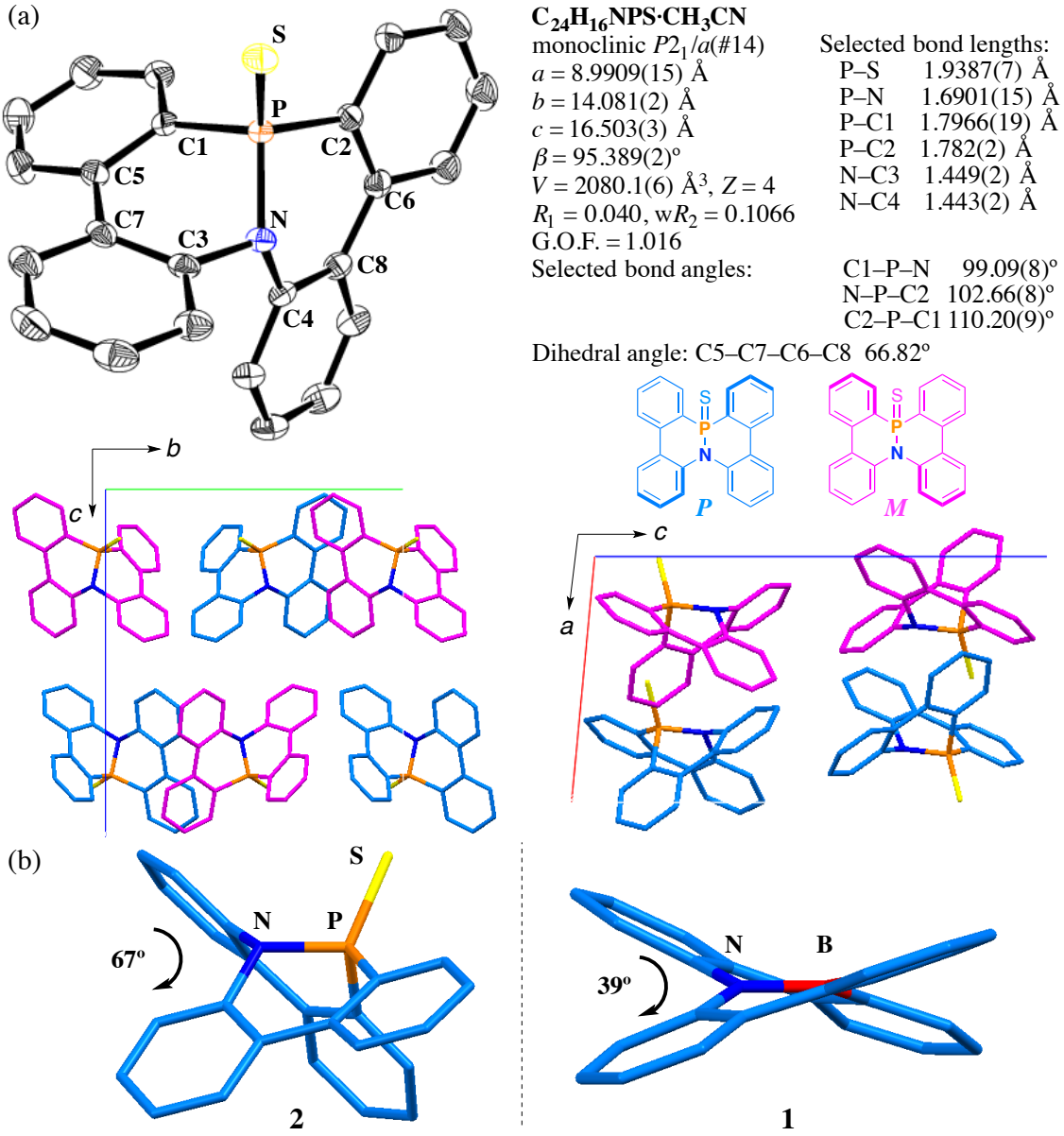

Figure 7. (a) ORTEP drawing and packing structures of **2**. Thermal ellipsoids are shown at 50% probability, and H atoms have been omitted for clarity. (b) Comparison of dihedral angles in **2** with those in **1**. The *P*-enantiomer is shown in blue, and the *M*-enantiomer is shown in pink.

Compound **2** had broader ^{1}H NMR peaks because of the molecular inversion motion between the *P*- and *M*-isomers. In variable-temperature NMR (VT-NMR) measurements, the peaks sharpened as the temperature dropped because molecular motion was suppressed (Figure 8, left). This result indicates that the isomers of **2** exchange configurations slowly around room temperature. The isomerization barrier between the *P*- and *M*-enantiomers of **2** was estimated from DFT calculations to be +13.1 kcal/mol (Figure 8, right). On the other hand, azaboradibenzochrysene **1** had sharp peaks in its ^{1}H NMR spectra at 20 ºC because of the smooth inversion between *P*- and *M*-isomers (Figure 9).

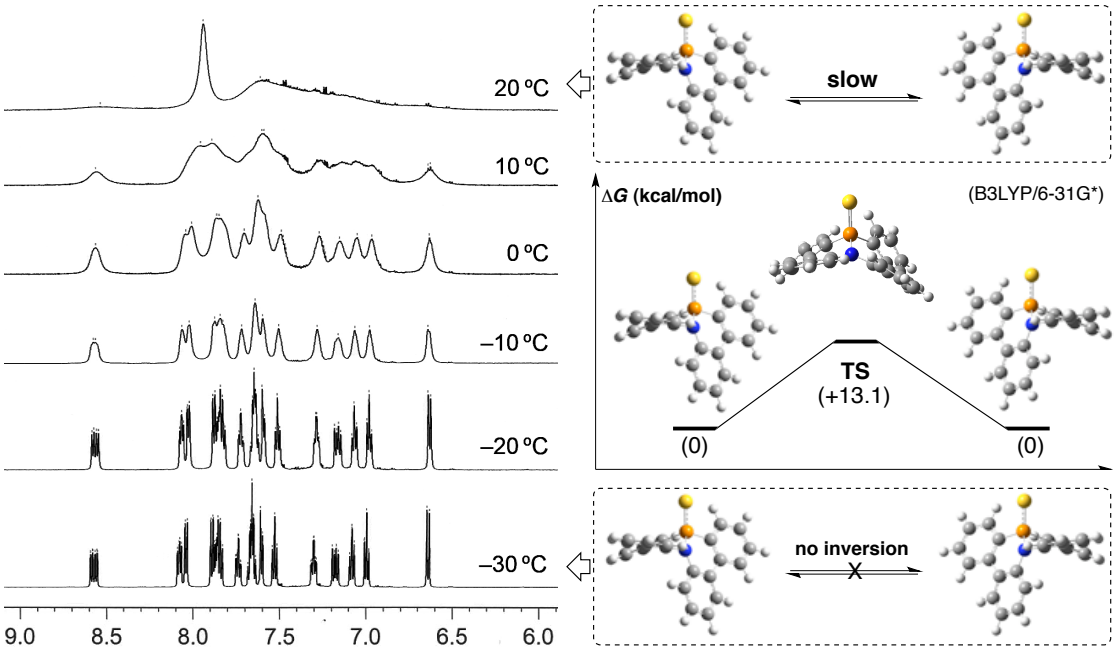

Figure 8. VT-^{1}H NMR analysis in $CDCl_3$ and calculated inversion barrier for **2**.

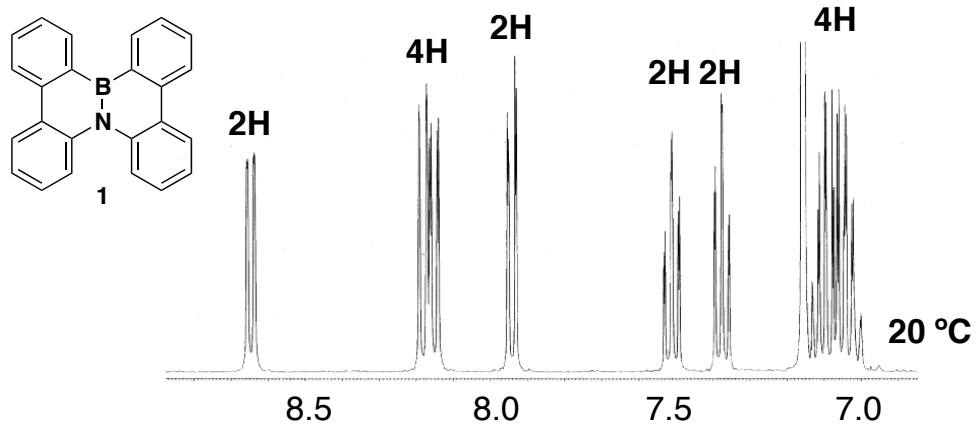

Figure 9. ^{1}H NMR analysis of **1** in $CDCl_3$ at 20 ºC.

5-2-3. Synthesis of azasiladibenzochrysene and azagermadibenzochrysene derivatives

To apply the present synthetic strategy to the introduction of group 14 elements, the corresponding sila- and germa-Friedel–Crafts reactions were used to synthesize the SiN- and GeN-fused polycyclic aromatic compounds **3** and **4** (Scheme 3). Introduction of silicon or germanium to diarylamine **7** was achieved by treating it with BuLi and $PhXCl_3$ (X = Si or Ge), and the subsequent tandem hetero-Friedel–Crafts reactions in the presence of $AlCl_3$ and 2,2,6,6-tetramethylpiperidine were found to afford compounds **3** and **4** in 20% and 42% yields, respectively. Although synthesis of the corresponding SnN-fused polycyclic aromatic compound using $PhSnCl_3$ in the same manner described above was also attempted, no cyclized product was obtained. This may be because the compound is thermodynamically unstable because of the large radius of the tin atom (Si 1.16 *vs*. Ge 1.24 *vs*. Sn 1.40 Å),[5] which requires significant distortion of the expected cyclized product.

Scheme 3. Sila- and germa-Friedel–Crafts reactions

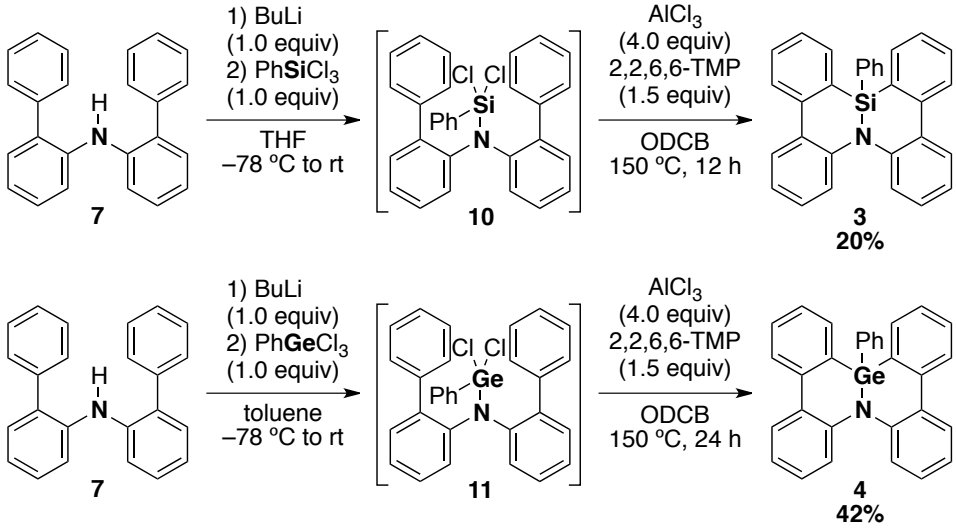

The molecular structures of **3** and **4** have been determined by performing X-ray crystallography (Figure 10, 11). The Si–N and Ge–N bond lengths [1.7260(19) and 1.8512(16) Å] were found to be longer than the P–N bond length in **2** [1.6901(15) Å], which is consistent with their covalent radii (Si 1.16 and Ge 1.24 *vs*. P 1.11). In the structure of **3**, the silicon center adopts a distorted tetrahedral geometry with C1–Si–N, N–Si–C2, and C2–Si–C1 bond angles of 101.68(10)°, 102.34(10)°, and 118.97(10)°, respectively. Likewise, in the case of **4**, the germanium center also adopts a similar geometry with C1–Ge–N, N–Ge–C2, and C2–Ge–C1 bond angles of 101.68(10)°, 102.34(10)°, and 118.97(10)°, respectively. Because of the tetrahedral geometries of the silicon and germanium centers, the biphenyl moieties of **3** and **4** were highly twisted, as was the case for **2**, because these atoms have similar atomic radii (Figure 11b). On the

other hand, the *P*- and *M*-isomers of **3** are arranged in an offset packing in a monoclinic crystal system, whereas the molecules of **4** are packed in a triclinic system. This change might be induced by many factors, such as the difference between the dipole moments of **3** and **4** (Si 1.244 D *vs*. Ge 1.688 D). Molecules of **3** adopt a similar packing to that found for **2**, but the molecular orientations alternate along the *b* axis. This is because the phenyl group in **3** is more bulky than the sulfur in **2**, which makes these alternating orientations necessary for void filling in the crystal.

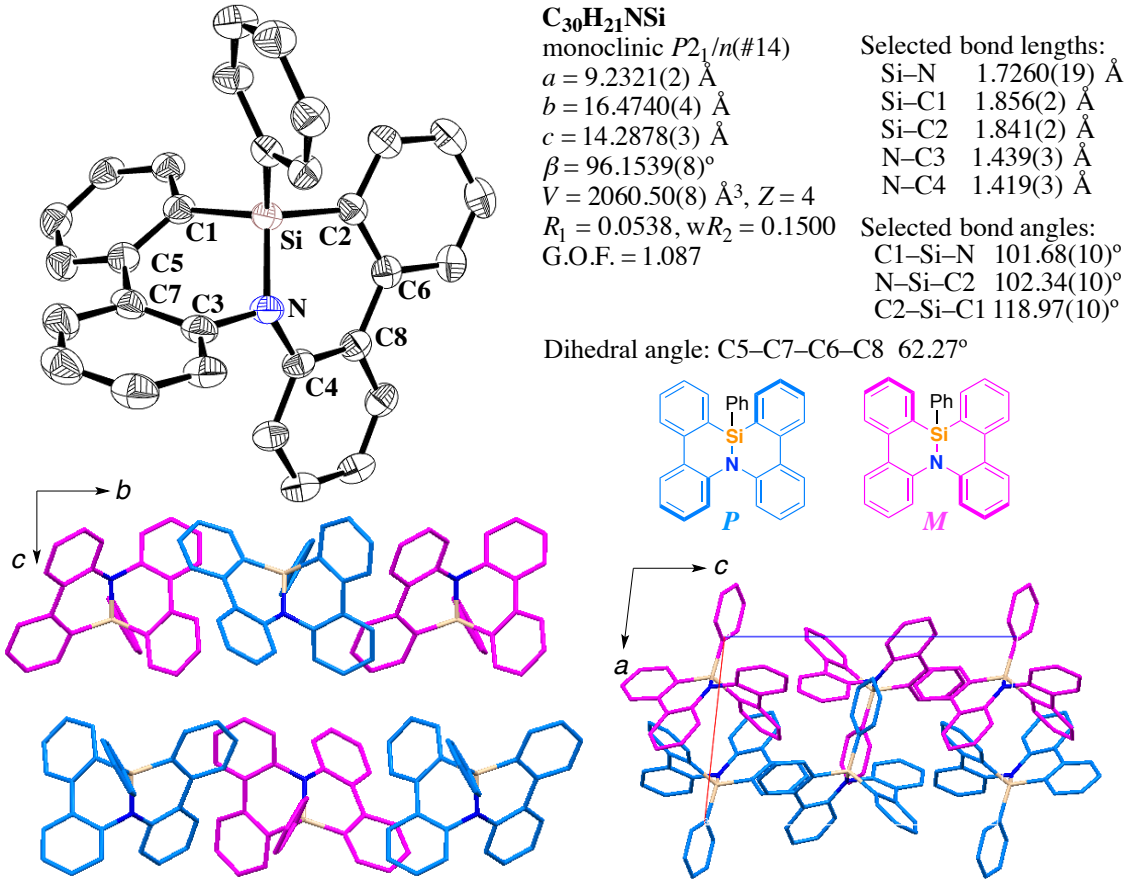

$C_{30}H_{21}NSi$
monoclinic $P2_1/n$(#14)
a = 9.2321(2) Å
b = 16.4740(4) Å
c = 14.2878(3) Å
β = 96.1539(8)°
V = 2060.50(8) Å^3, Z = 4
R_1 = 0.0538, wR_2 = 0.1500
G.O.F. = 1.087

Selected bond lengths:

Si–N	1.7260(19) Å
Si–C1	1.856(2) Å
Si–C2	1.841(2) Å
N–C3	1.439(3) Å
N–C4	1.419(3) Å

Selected bond angles:

C1–Si–N	101.68(10)°
N–Si–C2	102.34(10)°
C2–Si–C1	118.97(10)°

Dihedral angle: C5–C7–C6–C8 62.27°

Figure 10. ORTEP drawing and packing structures of **3**. Thermal ellipsoids are shown at 50% probability, and H atoms have been omitted for clarity. The *P*-enantiomer is shown in blue, and the *M*-enantiomer is shown in pink.

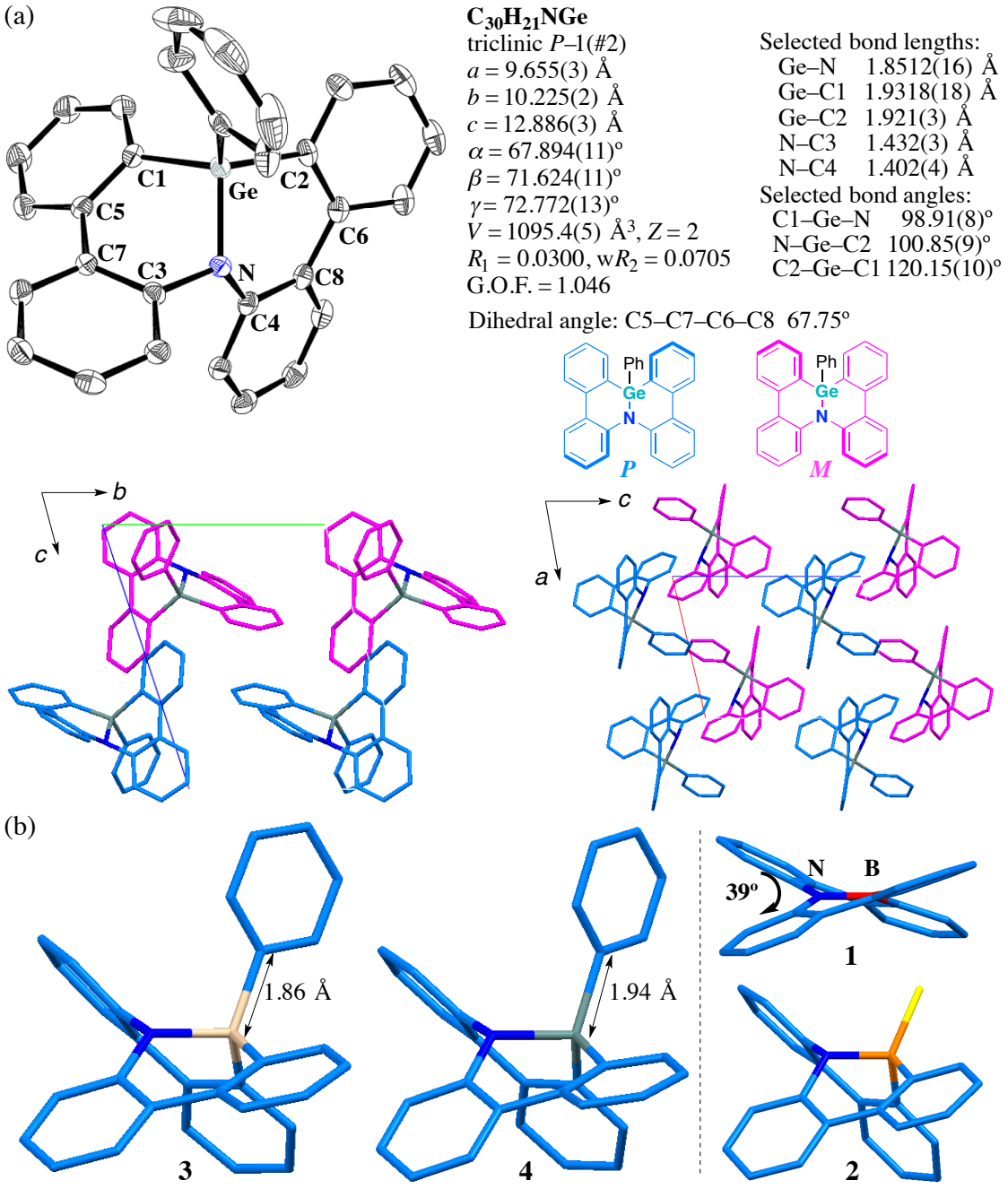

Figure 11. (a) ORTEP drawing and packing structures of **4**. Thermal ellipsoids are shown at 50% probability, and H atoms have been omitted for clarity. (b) Comparison of structures **1**–**4**. The *P*-enantiomer is shown in blue, and the *M*-enantiomer is shown in pink.

5-2-4. Range of applicability of hetero-Friedel–Crafts reactions

The hetero-Friedel–Crafts reactions for the other group 13 elements, theoretically producing AlN- and GaN-fused polycyclic aromatic compounds, were also investigated, but no cyclized products were obtained. Figure 12 shows the electronegativities (Pauling's scale)[6] and covalent radii[3] of the group 13, 14, and 15 elements. Considering the successful syntheses of the azadibenzochrysenes possessing boron, phosphorus, silicon, and germanium atoms and the failures of the syntheses of aluminum, gallium, and tin derivatives, heteroatoms with electronegativities ≥1.90 and covalent radii ≤1.24 would be suitable for the present hetero-Friedel–Crafts protocol. It is conceivable that mono- or bis-cyclized products with electropositive heteroatoms may not be stable under the reaction conditions, and the reverse reaction or undesirable side reactions may occur. On the other hand, the formation of six-membered rings including heteroatoms with large radii would be kinetically unfavorable. From this point of view, the development of the arsa-Friedel–Crafts reaction, for example, remains a matter for future investigation. As for larger atoms, changes in the aromatic framework to adjust the heteroatom-carbon bond lengths of the product would be necessary, such as the introduction of a five-membered ring into the starting material or a seven-membered ring into the product. These insights into strategies for accommodating large atoms would be helpful for introducing transition metals such as iridium, platinum, and so on.

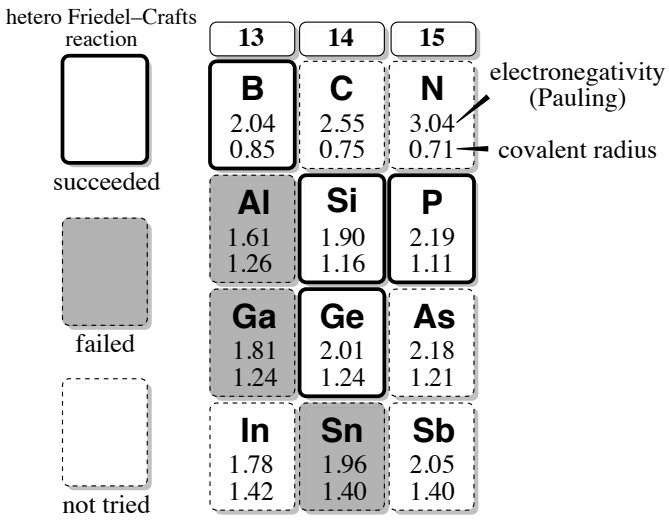

Figure 12. Electronegativities and covalent radii of group 13, 14, and 15 elements.

[6] Pauling, L. *The Nature of the Chemical Bond*, 3rd ed.; Cornell University Press: Ithaca, New York, **1960**.

5-3. Conclusions

Mechanistic studies on the bora-Friedel–Crafts reaction using in situ NMR measurements and DFT calculations of the reaction pathway have been conducted. The ^{1}H NMR spectra clearly indicate that the first cyclization takes place at 120 °C, and the second cyclization takes place at 150 °C. The ^{11}B NMR spectra also suggest that the cyclization reaction occurs at 120 ºC. However, the mono- and bis-cyclized compounds could not be distinguished, probably because these peaks appear at similar shifts (one broad peak at 35 ppm). These results suggest that three-fold coordinated boron species are major intermediates during the reaction, rather than four-fold coordinated species. In addition, DFT calculations have revealed the reaction pathway of the first cyclization. The second cyclization pathway is still unclear, but it is supposed that the mechanism proceeds *via* a relatively stabilized aluminate intermediate. The activation energies correspond well with the aforementioned reaction temperatures in the actual synthesis.

Further applications of the hetero-Friedel–Crafts reactions were examined based on the information obtained from the above-mentioned mechanistic study: azathiophospha- (**2**), azaphenylsila- (**3**), and azaphenylgermadibenzochrysene (**4**) derivatives have also been synthesized. In the obtained crystals, these heteroatom centers adopted a distorted tetrahedral geometry corresponding to each covalent radius, and their twisted *P*-helix and *M*-helix enantiomers were packed alternately in a racemic cocrystal. Thus, this author has shown that azadibenzochrysene derivatives with heteroatom junctions can adopt a wide variety of molecular structures and that hetero-Friedel–Crafts reactions are suitable for particular ranges of the electronegativity and atomic radius of the heteroatom.

5-4. Experimental Section

General. All the reactions dealing with air- or moisture-sensitive compounds were carried out in a dry reaction vessel under a positive pressure of argon. Air- and moisture-sensitive liquids and solutions were transferred via a syringe or a stainless steel cannula. Organic solutions were concentrated by rotary evaporation at *ca*. 30–400 mmHg. Gel permeation chromatography was performed on a JAIGEL-1H and 2H (20 mm i.d.) with an LC-9204 (Japan Analytical Industry Co., Ltd.).

Instrumentation. Proton nuclear magnetic resonance (^{1}H NMR) and carbon nuclear magnetic resonance (^{13}C NMR) spectra were recorded on JEOL ECS400 (392 MHz) NMR spectrometers. Proton chemical shift values are reported in parts per million (ppm, δ scale) downfield from tetramethylsilane, and are referenced to the tetramethylsilane (δ 0). ^{13}C NMR spectra were recorded at 98.5 MHz: carbon chemical shift values are reported in parts per million (ppm, δ scale) downfield from tetramethylsilane, and are referenced to the carbon resonance of CD_2Cl_2 (δ 54.2), C_6D_6 (δ 128.0), and tetramethylsilane (δ 0). ^{11}B NMR spectra were recorded at 131 MHz: boron chemical shift values are reported in parts per million (ppm, δ scale) and are referenced to the external standard boron signal of $BF_3{\cdot}Et_2O$ (δ 0). Data are presented as: chemical shift, multiplicity (s = singlet, d = doublet, t = triplet, q = quartet, quint = quintet, sext = sextet, sept = septet, m = multiplet and/or multiplet resonances, br = broad), coupling constant in hertz (Hz), signal area integration in natural numbers, and assignment (*italic*). IR spectra were recorded on an ATR-FTIR spectrometer (FT/IR-Spectrum One, PerkinElmer). Characteristic IR absorptions are reported in cm^{-1}. Melting points were recorded on a Yanaco MP-500V. High-resolution mass spectra (HRMS) were obtained using the electron impact (EI) method with JEOL JMS-700, JMS-SX102A or the fast atom bombardment (FAB) method with JEOL JMS-HX110A or the matrix assisted laser desorption/ionization (MALDI) method with Thermo Fisher Scientific orbitrapXL. Purity of isolated compounds was determined by GC analysis on Shimadzu GC-2010 Plus instrument equipped with an FID detector and a capillary column, ZB-1MS (Phenomenex, 10 m × 0.10 mm i.d., 0.10 μm film thickness) and/or ^{1}H NMR analyses.

Solvent. *o*-Dichlorobenzene and anhydrous toluene were purchased from Wako Pure Chemical Industries, Ltd. (Wako) and dried over Molecular Sieves 4A and degassed before use. Water content of the solvent was determined with a Karl Fischer Moisture Titrator (MKC-610, Kyoto Electronics Company) to be less than 15 ppm.

Materials. Materials were purchased from Wako, Tokyo Chemical Industry Co., Ltd., Aldrich Inc., Hokko Chemical Industry Co., Ltd., and other commercial suppliers, and were used after appropriate purification, unless otherwise noted. Florisil® (100–200

mesh) and Celite® were purchased from Wako. Aryl halides and aryl amines were purified by distillation or recrystallization to be over 99.5% pure by GC analysis.

Synthesis of 4b-aza-12b-thiophosphadibenzo[*g*, *p*]chrysene (2)

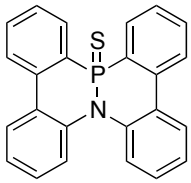

A solution of butyllithium in hexane (1.23 mL, 1.63 M, 2.0 mmol) was added slowly to a solution of **7** (0.642 g, 2.0 mmol) in toluene (10 mL) at –78 ºC under argon. After 1 h, the reaction mixture stirred at 0 ºC for 1 h. A solution of phosphorus trichloride (0.275 g, 2.0 mmol) was added at –78 ºC. After stirring at room temperature for 1 h, sulfur (0.096 g, 3.0 mmol) was added at 0 ºC and stirred at 50 ºC for 1 h. Then solvent was removed *in vacuo*, and the reaction mixture was added to a solution of aluminum trichloride (1.33 g, 10 mmol) in 1,2-dichlorobenzene (10 mL) at 0 ºC. After stirring at 120 ºC for 1 h, 1,4-diazabicyclo[2.2.2]octane (1.12 g, 10 mmol) was added. The reaction mixture was filtered with a pad of Celite®. After the solvent was removed *in vacuo*, the crude product was purified by GPC (eluent: toluene) to obtain the title compound (0.465 g, 61% yield) as white-yellow powder. IR (neat): cm^{-1} 3054 (Ar-H), 1578, 1474, 1445, 1428, 1269, 1242, 1192, 1067, 966, 894, 867, 783, 749, 730, 715, 700, 652, 610, 545, 516, 486, 462; mp: >450 ºC; ^{1}H NMR (CD_2Cl_2 at –40 ºC, 600 MHz) δ 6.65 (d, 1H, *J* = 8.4 Hz), 7.01 (t, 1H, *J* = 7.2 Hz), 7.09 (t, 1H, *J* = 7.8 Hz), 7.19 (dd, 1H, *J* = 7.8, 13.8 Hz), 7.31 (td, 1H, *J* = 3.0, 7.8 Hz), 7.54 (t, 1H, *J* = 7.8 Hz), 7.62 (d, 1H, *J* = 7.2 Hz), 7.65–7.69 (m, 2H), 7.75 (td, 1H, *J* = 3.0, 7.8 Hz), 7.84–7.91 (m, 3H), 8.05 (d, 2H, *J* = 7.2 Hz), 8.09 (t, 1H, *J* = 7.2 Hz), 8.58 (dd, 1H, *J* = 7.8, 15.6 Hz); ^{13}C NMR (CD_2Cl_2 at –40 ºC, 151 MHz) δ 118.1, 120.8, 121.2, 122.3, 124.4, 126.5, 128.1, 128.5, 128.6, 128.7, 128.9, 129.3, 130.2 (2C), 131.6, 132.1, 132.8, 132.9, 134.4, 134.5, 135.2, 135.3, 136.2, 141.5; HRMS (EI) *m*/*z* $[M]^+$ calcd for $C_{24}H_{16}NB$ 381.0741; observed 381.0746.

Synthesis of 4b-aza-12b-siladibenzo[*g*, *p*]chrysene (3)

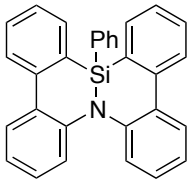

A solution of butyllithium in hexane (0.62 mL, 1.60 M, 1.0 mmol) was added slowly to a solution of **7** (0.321 g, 1.0 mmol) in THF (5 mL) at –78 ºC under argon. After 1 h, trichlorophenylsilane (0.212 g, 1.0 mmol) was added at –78 ºC. After stirring at room temperature for 12 h, solvent was removed *in vacuo*, and the reaction mixture was added to a solution of aluminum trichloride (0.533 g, 4.0 mmol) and 2,2,6,6-tetramethylpiperidine (0.233 g, 1.50 mmol) in 1,2-dichlorobenzene (10 mL) at 0

ºC. After stirring at 150 ºC for 24 h, 1,4-diazabicyclo[2.2.2]octane (1.12 g, 4.0 mmol) was added. The reaction mixture was filtered with a pad of Celite®. After the solvent was removed *in vacuo*, the crude product was purified by GPC (eluent: toluene) to obtain the title compound (0.085 g, 20% yield) as colorless powder. IR (neat): cm^{-1} 3046 (Ar-H), 1591, 1568, 1475, 1428, 1270, 1205, 1114, 1066, 998, 973, 889, 782, 746, 730, 711, 699, 617, 553, 522, 510; mp: 235.0–235.9 ºC; ^{1}H NMR (CD_2Cl_2, 392 MHz) δ 7.01–7.17 (m, 6H), 7.22 (td, 2H, *J* = 0.9, 6.7 Hz), 7.28–7.34 (m, 3H), 7.39 (td, 2H, *J* = 0.9, 7.2 Hz), 7.57–7.64 (m, 4H), 7.80 (dd, 2H, *J* = 1.3, 7.6 Hz), 7.96 (d, 2H, *J* = 8.1 Hz); ^{13}C NMR (CD_2Cl_2, 98.5 MHz) δ 122.9 (2C), 125.6, 125.7 (2C), 127.1 (2C), 128.0 (2C), 128.4 (2C), 128.5 (2C), 128.8 (2C), 129.3, 130.6 (2C), 131.5 (2C), 133.9 (2C), 134.3 (2C), 135.5 (2C), 141.7 (2C), 142.6 (2C); HRMS (FAB) *m/z* $[M]^+$ calcd for $C_{30}H_{21}NSi$ 423.1443; observed 423.1426.

Synthesis of 4b-aza-12b-germadibenzo[*g*, *p*]chrysene (4)

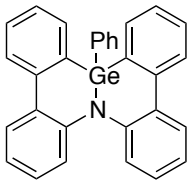

A solution of butyllithium in hexane (1.25 mL, 1.60 M, 2.0 mmol) was added slowly to a solution of **7** (0.643 g, 2.0 mmol) in toluene (20 mL) at –78 ºC under argon. After 1 h, the reaction mixture stirred at 0 ºC for 1 h. A solution of phenylgermanium trichloride (0.512 g, 2.0 mmol) was added at –78 ºC. After stirring at room temperature for 12 h, solvent was removed *in vacuo*, and the reaction mixture was added to a solution of aluminum trichloride (1.07 g, 8.0 mmol) and 2,2,6,6-tetramethylpiperidine (0.466 g, 3.00) in 1,2-dichlorobenzene (10 mL) at 0 ºC. After stirring at 150 ºC for 24 h, 1,4-diazabicyclo[2.2.2]octane (1.12 g, 10 mmol) was added. The reaction mixture was filtered with a pad of Celite®. After the solvent was removed *in vacuo*, the crude product was purified by GPC (eluent: toluene) to obtain the title compound (0.389 g, 42% yield) as colorless powder. IR (neat): cm^{-1} 3061 (Ar–H), 1591, 1568, 1472, 1425, 1300, 1274, 1201, 1159, 1119, 1106, 1092, 1062, 999, 943, 917, 889, 871, 777, 733, 721, 698, 673, 615, 562, 530, 512, 494, 464; mp: 232.3–233.1 ºC; ^{1}H NMR (CD_2Cl_2, 392 MHz) δ 7.01–7.17 (m, 6H), 7.22 (td, 2H, *J* = 0.9, 6.7 Hz), 7.28–7.34 (m, 3H), 7.39 (td, 2H, *J* = 0.9, 7.2 Hz), 7.57–7.64 (m, 4H), 7.80 (dd, 2H, *J* = 1.3, 7.6 Hz), 7.96 (d, 2H, *J* = 8.1 Hz); ^{13}C NMR (CD_2Cl_2, 98.5 MHz) δ 122.7 (2C), 124.3 (2C), 127.4 (2C), 127.8 (3C), 129.0 (2C), 129.5 (2C), 130.1 (2C), 130.5, 130.9 (2C), 131.8 (2C), 134.5 (2C), 134.8 (2C), 135.2 (2C), 143.0 (2C), 145.1 (2C); HRMS (MALDI) *m/z* $[M+H]^+$ calcd for $C_{30}H_{21}NGe$ 470.0964; observed 470.0980.

Crystallographic data collection and structure determination. Crystals of **2**, **3** and **4** were mounted on a Rigaku Saturn CCD diffractometer for data collection using graphite-monochromated Mo Kα radiation (λ = 0.71070 Å). Crystal data and data statistics are summarized in Figure 13. The structures were solved by direct methods with (SIR2008)[7] and refined by full-matrix least-squares techniques against F^2 (SHELXL-97)[8]. The non-hydrogen atoms were refined anisotropically. Hydrogen atoms were placed at calculated positions (C–H = 0.95 Å) and kept fixed. In the subsequent refinement, the function $\sum w(F_o^2 - F_c^2)^2$ was minimized, where $|F_o|$ and $|F_c|$ are the observed and calculated structure factor amplitudes, respectively. The agreement indices are defined as $R1 = \sum(||F_o| - |F_c||)/\sum|F_o|$ and $wR2 = [\sum w(F_o^2 - F_c^2)^2 / \sum(wF_o^4)]^{1/2}$. All calculations were performed by using Crystal Structure 4.0, and illustrations were drawn by using ORTEP–3.

[7] Burla, M. C.; Caliandro, R.; Camalli, M.; Carrozzini, B.; Cascarano, G. L.; de Caro, L.; Giacovazzo, C.; Polidori, G.; Siliqi, D.; Spagna, R. *J. Appl. Cryst.* **2007,** *40*, 609-613.

[8] Sheldrick, G. M. Program for the Solution of Crystal Structures; University of Göttingen, Germany, 1997.

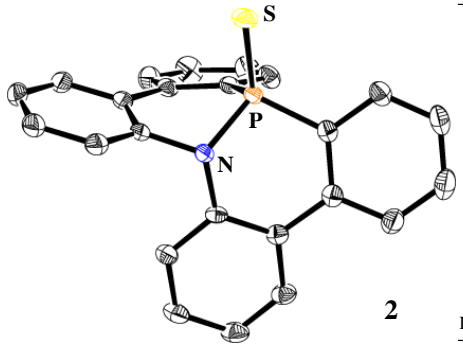

2

Formula	$C_{24}H_{16}NPS{\cdot}CH_3CN$	Abs. Coefficient, cm^{-1}	0.248
Formula Weight	422.48	F(000)	888.00
Temperature, K	173	Crystal Size, mm^3	0.20, 0.20, 0.20
Wavelength, Å	0.71070	$2\theta_{min}$, $2\theta_{max}$, deg	6.2, 55.0
Crystal System	Monoclinic	Index Ranges	$-9 \le h \le 11$
Space Group	$P\,2_1/a$ (No. 14)		$-18 \le k \le 16$
a, Å	8.9909(15)		$-21 \le l \le 21$
b, Å	14.081(2)	Reflections (unique)	4778
c, Å	16.503(3)	Reflections ($I>2.0\sigma(I)$)	3333
α, deg	90	Parameters	347
β, deg	95.389(2)	GOF on F^2	1.016
γ, deg	90	R_1 ($I>2.0\sigma(I)$)	0.0440
Volume, Å	2080.1(6)	*R*, wR_2 (all data)	0.0593, 0.1066
Z	4	Largest diff peak and hole, e, $Å^{-3}$	0.380, –0.510
$Density_{calcd}$, $g{\cdot}cm^{-3}$	1.349		

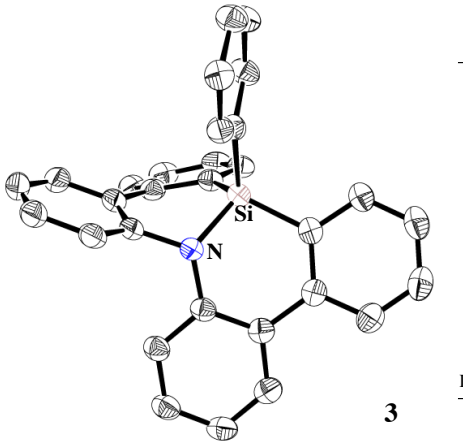

3

Formula	$C_{30}H_{21}NSi$	Abs. Coefficient, cm^{-1}	0.127
Formula Weight	423.57	F(000)	888.00
Temperature, K	100(2)	Crystal Size, mm^3	0.05, 0.02, 0.01
Wavelength, Å	0.71069	$2\theta_{min}$, $2\theta_{max}$, deg	3.78, 51.0
Crystal System	Monoclinic	Index Ranges	$-10 \le h \le 11$
Space Group	$P\,2_1/n$ (No. 14)		$-18 \le k \le 19$
a, Å	9.2321(2)		$-17 \le l \le 17$
b, Å	16.4740(4)	Reflections (unique)	3878
c, Å	14.2878(3)	Reflections ($I>2.0\sigma(I)$)	3371
α, deg	90	Parameters	289
β, deg	96.1539(8)	GOF on F^2	1.087
γ, deg	90	R_1 ($I>2.0\sigma(I)$)	0.0538
Volume, Å	2160.50(8)	*R*, wR_2 (all data)	0.0632, 0.1500
Z	4	Largest diff peak and hole, e, $Å^{-3}$	0.560, –0.494
$Density_{calcd}$, $g{\cdot}cm^{-3}$	1.302		

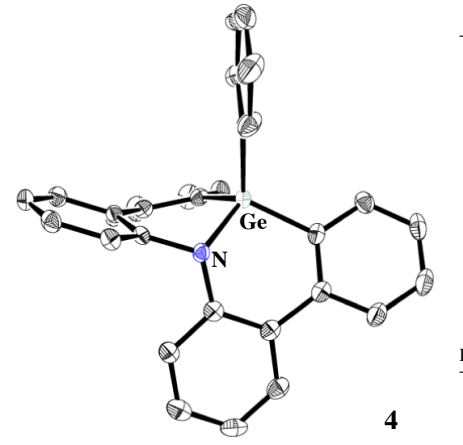

4

Formula	$C_{30}H_{21}NGe$	Abs. Coefficient, cm^{-1}	1.416
Formula Weight	468.09	F(000)	480.00
Temperature, K	173	Crystal Size, mm^3	0.2, 0.2, 0.2
Wavelength, Å	0.71070	$2\theta_{min}$, $2\theta_{max}$, deg	6.3, 54.9
Crystal System	Triclinic	Index Ranges	$-11 \le h \le 11$
Space Group	*P*–1 (No. 2)		$-12 \le k \le 12$
a, Å	9.655(3)		$-15 \le l \le 15$
b, Å	10.225(2)	Reflections (unique)	4293
c, Å	12.886(3)	Reflections ($I>2.0\sigma(I)$)	3856
α, deg	67.894(11)	Parameters	289
β, deg	71.624(11)	GOF on F^2	1.046
γ, deg	72.722(13)	R_1 ($I>2.0\sigma(I)$)	0.0300
Volume, Å	1095.4(5)	*R*, wR_2 (all data)	0.0347, 0.0705
Z	2	Largest diff peak and hole, e, $Å^{-3}$	0.440, –0.290
$Density_{calcd}$, $g{\cdot}cm^{-3}$	1.419		

Figure 13. X-ray crystal structures of **2**, **3** and **4** (left), and crystal data and structure refinement (right). Thermal ellipsoids are shown at 50% probability and H atoms have been omitted for clarity.

Computational studies. The calculations for the reaction pathway of bora-Friedel–Crafts reaction (Figures 3–6) and inversion barrier of **2** (Figure 8) were performed with Gaussian 03[9] and 09[10] packages. The DFT method was employed using the B3LYP hybrid functional.[11] Structures were optimized with the 6-31G(d) basis set.[12] Each stationary point was adequately characterized by normal coordinate analysis (no imaginary frequencies for an equilibrium structure and one imaginary frequency for a transition structure) using the same method as for the geometry optimization. Intrinsic reaction coordinate (IRC) analyses[13] were carried out throughout the reaction pathways to confirm that all stationary points are smoothly connected to each other using the same method as for the geometry optimization.

---

[9] Gaussian 03, Revision E.01, Frisch, M. J.; Trucks, G. W.; Schlegel, H. B.; Scuseria, G. E.; Robb, M. A.; Cheeseman, J. R.; Montgomery, Jr., J. A.; Vreven, T.; Kudin, K. N.; Burant, J. C.; Millam, J. M.; Iyengar, S. S.; Tomasi, J.; Barone, V.; Mennucci, B.; Cossi, M.; Scalmani, G.; Rega, N.; Petersson, G. A.; Nakatsuji, H.; Hada, M.; Ehara, M.; Toyota, K.; Fukuda, R.; Hasegawa, J.; Ishida, M.; Nakajima, T.; Honda, Y.; Kitao, O.; Nakai, H.; Klene, M.; Li, X.; Knox, J. E.; Hratchian, H. P.; Cross, J. B.; Bakken, V.; Adamo, C.; Jaramillo, J.; Gomperts, R.; Stratmann, R. E.; Yazyev, O.; Austin, A. J.; Cammi, R.; Pomelli, C.; Ochterski, J. W.; Ayala, P. Y.; Morokuma, K.; Voth, G. A.; Salvador, P.; Dannenberg, J. J.; Zakrzewski, V. G.; Dapprich, S.; Daniels, A. D.; Strain, M. C.; Farkas, O.; Malick, D. K.; Rabuck, A. D.; Raghavachari, K.; Foresman, J. B.; Ortiz, J. V.; Cui, Q.; Baboul, A. G.; Clifford, S.; Cioslowski, J.; Stefanov, B. B.; Liu, G.; Liashenko, A.; Piskorz, P.; Komaromi, I.; Martin, R. L.; Fox, D. J.; Keith, T.; Al-Laham, M. A.; Peng, C. Y.; Nanayakkara, A.; Challacombe, M.; Gill, P. M. W.; Johnson, B.; Chen, W.; Wong, M. W.; Gonzalez, C. and Pople, J. A. Gaussian, Inc., Wallingford CT, 2004.

[10] Gaussian 09, Revision B.01, Frisch, M. J.; Trucks, G. W.; Schlegel, H. B.; Scuseria, G. E.; Robb, M. A.; Cheeseman, J. R.; Scalmani, G.; Barone, V.; Mennucci, B.; Petersson, G. A.; Nakatsuji, H.; Caricato, M.; Li, X.; Hratchian, H. P.; Izmaylov, A. F.; Bloino, J.; Zheng, G.; Sonnenberg, J. L.; Hada, M.; Ehara, M.; Toyota, K.; Fukuda, R.; Hasegawa, J.; Ishida, M.; Nakajima, T.; Honda, Y.; Kitao, O.; Nakai, H.; Vreven, T.; Montgomery, Jr., J. A.; Peralta, J. E.; Ogliaro, F.; Bearpark, M.; Heyd, J. J.; Brothers, E.; Kudin, K. N.; Staroverov, V. N.; Kobayashi, R.; Normand, J.; Raghavachari, K.; Rendell, A.; Burant, J. C.; Iyengar, S. S.; Tomasi, J.; Cossi, M.; Rega, N.; Millam, N. J.; Klene, M.; Knox, J. E.; Cross, J. B.; Bakken, V.; Adamo, C.; Jaramillo, J.; Gomperts, R.; Stratmann, R. E.; Yazyev, O.; Austin, A. J.; Cammi, R.; Pomelli, C.; Ochterski, J. W.; Martin, R. L.; Morokuma, K.; Zakrzewski, V. G.; Voth, G. A.; Salvador, P.; Dannenberg, J. J.; Dapprich, S.; Daniels, A. D.; Farkas, Ö.; Foresman, J. B.; Ortiz, J. V.; Cioslowski, J.; Fox, D. J. Gaussian, Inc., Wallingford CT, 2009.

[11] (a) Becke, A. D. *J. Chem. Phys.* **1993,** *98*, 5648–5652. (b) Lee, C.; Yang, W.; Parr, R. G. *Phys. Rev. B* **1988,** *37*, 785–789.

[12] Hehre, W. J.; Radom, L.; Schleyer, P. v. R.; Pople, J. A. *Ab Initio Molecular Orbital Theory*; John Wiley & Sons: New York, **1986** and references cited therein.

[13] (a) Fukui, K. *Acc. Chem. Res.* **1981,** *14*, 363–368. (b) Gonzalez, C.; Schlegel, H. B. *J. Chem. Phys.* **1989,** *90*, 2154–2161. (c) Gonzalez, C.; Schlegel, H. B. *J. Phys. Chem.* **1990,** *94*, 5523–5527.

Cartesian coordinates

The reaction pathway of bora-Friedel–Crafts reaction (Figures 3–6)

Al_2Cl_6

E(RB3LYP) = –3246.4814253 hartree

Center Number	Atomic Number	Atomic Type	Coordinates X	Y	Z
1	13	0	1.618559	0.000029	0.000061
2	13	0	-1.618533	0.000062	-0.000009
3	17	0	-2.640290	-1.826549	-0.000003
4	17	0	-2.638563	1.827627	-0.000035
5	17	0	2.639849	-1.826856	0.000058
6	17	0	2.639049	1.827308	-0.000192
7	17	0	0.000019	-0.000641	1.627352
8	17	0	-0.000083	-0.000958	-1.627220

$AlCl_3$

E(RB3LYP) = –1623.2220743 hartree

Center Number	Atomic Number	Atomic Type	Coordinates X	Y	Z
1	13	0	0.000060	-0.000003	0.000154
2	17	0	-0.966681	1.850385	-0.000039
3	17	0	-1.119182	-1.762338	-0.000039
4	17	0	2.085817	-0.088045	-0.000039

5

E(RB3LYP) = –1925.4932848 hartree

Center Number	Atomic Number	Atomic Type	Coordinates X	Y	Z
1	7	0	0.000015	0.300315	-0.000023
2	5	0	0.000004	-1.117499	-0.000098
3	17	0	-0.657494	-2.042887	-1.366334
4	17	0	0.657515	-2.043091	1.365983
5	6	0	-3.074702	1.693880	-1.655457
6	6	0	-2.512911	2.648799	-2.497633
7	6	0	-1.130620	2.835119	-2.497628
8	6	0	-0.334570	2.051849	-1.667734
9	6	0	-0.892757	1.075575	-0.831269
10	6	0	-2.295917	0.895174	-0.797005
11	6	0	0.892711	1.075578	0.831274
12	6	0	2.295873	0.895133	0.797165
13	6	0	3.074602	1.693806	1.655695
14	6	0	2.512770	2.648773	2.497790
15	6	0	1.130493	2.835188	2.497588
16	6	0	0.334493	2.051943	1.667621
17	1	0	-4.153639	1.573916	-1.626997
18	1	0	-3.152069	3.253040	-3.135185
19	1	0	-0.671436	3.582580	-3.138302
20	1	0	0.740170	2.199586	-1.654997
21	1	0	4.153536	1.573790	1.627348
22	1	0	3.151886	3.252989	3.135406
23	1	0	0.671272	3.582713	3.138162
24	1	0	-0.740230	2.199773	1.654743
25	6	0	-3.011150	-0.076836	0.082152
26	6	0	-4.494545	-1.853186	1.697217
27	6	0	-4.004039	-0.903675	-0.472096
28	6	0	-2.777481	-0.161196	1.464873
29	6	0	-3.511317	-1.040103	2.262376
30	6	0	-4.737730	-1.781417	0.324394
31	1	0	-4.183016	-0.870791	-1.542981
32	1	0	-2.024772	0.467430	1.927325
33	1	0	-3.313808	-1.084338	3.329995
34	1	0	-5.493889	-2.415673	-0.130544
35	1	0	-5.062863	-2.538713	2.319844
36	6	0	3.011174	-0.076810	-0.082009
37	6	0	4.494672	-1.852992	-1.697160
38	6	0	4.004021	-0.903707	0.472221
39	6	0	2.777603	-0.161019	-1.464756
40	6	0	3.511486	-1.039845	-2.262303
41	6	0	4.737765	-1.781366	-0.324313
42	1	0	4.182920	-0.870939	1.543123
43	1	0	2.024927	0.467666	-1.927184
44	1	0	3.314054	-1.083966	-3.329941
45	1	0	5.493892	-2.415671	0.130608
46	1	0	5.063030	-2.538456	-2.319819

CP1

E(RB3LYP) = –3548.7293998 hartree

Center Number	Atomic Number	Atomic Type	Coordinates X	Y	Z
1	13	0	-3.241845	1.441067	0.078698
2	17	0	-3.850999	0.460688	-1.690662
3	17	0	-2.502858	3.412574	-0.103040
4	17	0	-4.339159	0.997688	1.837639
5	5	0	0.207869	0.070776	-0.341459

6	17	0	0.046739	0.911969	-1.866247
7	17	0	-1.217801	0.148685	0.818161
8	7	0	1.339054	-0.646125	0.075731
9	6	0	4.479981	1.035429	-1.122648
10	6	0	5.165586	-0.044679	-1.670589
11	6	0	4.596959	-1.317649	-1.622578
12	6	0	3.343689	-1.486052	-1.041971
13	6	0	2.643368	-0.397289	-0.507161
14	6	0	3.216268	0.895373	-0.518933
15	6	0	1.294432	-1.682699	1.087371
16	6	0	0.408842	-2.781350	0.988568
17	6	0	0.433454	-3.725516	2.032330
18	6	0	1.302371	-3.615460	3.113715
19	6	0	2.190008	-2.541008	3.177936
20	6	0	2.181402	-1.584945	2.167337
21	1	0	4.938037	2.019876	-1.127737
22	1	0	6.144478	0.105201	-2.116847
23	1	0	5.121231	-2.175334	-2.033732
24	1	0	2.899978	-2.474662	-0.990614
25	1	0	-0.232255	-4.580438	1.963689
26	1	0	1.296727	-4.372990	3.892074
27	1	0	2.883986	-2.443682	4.007619
28	1	0	2.876105	-0.752570	2.204080
29	6	0	2.577688	2.116080	0.055967
30	6	0	1.472267	4.489396	1.104162
31	6	0	2.524636	3.291141	-0.713809
32	6	0	2.069450	2.157631	1.365389
33	6	0	1.522601	3.332427	1.882980
34	6	0	1.977677	4.464452	-0.196742
35	1	0	2.894560	3.273745	-1.735078
36	1	0	2.111195	1.273508	1.992440
37	1	0	1.138126	3.342041	2.899076
38	1	0	1.936388	5.356519	-0.815523
39	1	0	1.038238	5.400348	1.505933
40	6	0	-0.547749	-3.007498	-0.135316
41	6	0	-2.389628	-3.551760	-2.200406
42	6	0	-1.886423	-3.326875	0.154451
43	6	0	-0.151757	-2.969559	-1.483058
44	6	0	-1.063937	-3.239735	-2.503740
45	6	0	-2.797931	-3.594254	-0.865970
46	1	0	-2.217652	-3.341944	1.189010
47	1	0	0.876244	-2.739458	-1.740752
48	1	0	-0.734040	-3.207165	-3.538393
49	1	0	-3.829911	-3.825316	-0.617723
50	1	0	-3.100366	-3.753441	-2.996594

TS1

E(RB3LYP) = –3548.7007230 hartree

Center Number	Atomic Number	Atomic Type	Coordinates X	Y	Z
1	13	0	3.676051	-0.071841	-0.088595
2	17	0	3.417209	-1.764977	1.161732
3	17	0	4.012814	1.787407	0.905269
4	17	0	4.884110	-0.373181	-1.813692
5	5	0	-0.055870	0.674435	-0.202559
6	17	0	0.282678	0.516958	1.555406
7	17	0	1.594472	0.228919	-1.238416
8	7	0	-1.210497	0.014420	-0.842471
9	6	0	-3.893695	2.611256	-0.872254
10	6	0	-4.955260	1.925567	-1.456953
11	6	0	-4.754887	0.605117	-1.859666
12	6	0	-3.524722	-0.026677	-1.676312
13	6	0	-2.443096	0.652047	-1.087997
14	6	0	-2.644938	2.002281	-0.695345
15	6	0	-1.076485	-1.375605	-1.239074
16	6	0	-1.220614	-2.447273	-0.330806
17	6	0	-1.002482	-3.748938	-0.822752
18	6	0	-0.682165	-3.993644	-2.154431
19	6	0	-0.571254	-2.926386	-3.046949
20	6	0	-0.763475	-1.629201	-2.582037
21	1	0	-4.014196	3.649195	-0.573077
22	1	0	-5.914166	2.413277	-1.599787
23	1	0	-5.565609	0.047186	-2.320339
24	1	0	-3.405690	-1.058842	-1.981405
25	1	0	-1.110248	-4.581083	-0.133381
26	1	0	-0.526614	-5.013538	-2.494746
27	1	0	-0.324302	-3.098871	-4.090410
28	1	0	-0.658147	-0.784998	-3.256837
29	6	0	-1.518616	2.740299	-0.116052
30	6	0	0.753705	4.067283	0.942789
31	6	0	-1.635739	3.540598	1.023646
32	6	0	-0.221129	2.550851	-0.695769
33	6	0	0.891600	3.285847	-0.186139
34	6	0	-0.513251	4.185806	1.542599
35	1	0	-2.597832	3.636393	1.516629
36	1	0	-0.189574	2.281768	-1.750431
37	1	0	1.857017	3.189975	-0.670919
38	1	0	-0.621395	4.793288	2.437601
39	1	0	1.609477	4.583421	1.364440
40	6	0	-1.588078	-2.301795	1.107250
41	6	0	-2.287412	-2.159972	3.829545
42	6	0	-0.774595	-2.890161	2.089622
43	6	0	-2.763303	-1.650077	1.510943
44	6	0	-3.108888	-1.580760	2.860795
45	6	0	-1.118270	-2.815717	3.438821

46	1	0	0.148280	-3.380011	1.792373
47	1	0	-3.420906	-1.213062	0.766440
48	1	0	-4.026820	-1.077847	3.154399
49	1	0	-0.467775	-3.264653	4.184514
50	1	0	-2.556859	-2.102389	4.880845

CP3

E(RB3LYP) = –3548.7330564 hartree

Center Number	Atomic Number	Atomic Type	Coordinates X	Y	Z
1	13	0	4.332941	0.519563	0.184915
2	17	0	4.518353	0.282867	-1.960647
3	17	0	4.032970	-1.423397	1.102383
4	17	0	5.930551	1.628603	1.063723
5	5	0	-0.522814	0.356244	-1.107397
6	17	0	-0.694864	1.264965	-2.613549
7	17	0	2.416933	1.619176	0.495735
8	7	0	-1.333825	0.607425	0.018713
9	6	0	-0.146138	-1.902366	2.534809
10	6	0	-0.781694	-1.459907	3.680833
11	6	0	-1.603354	-0.328044	3.611181
12	6	0	-1.780532	0.351379	2.412575
13	6	0	-1.136221	-0.079755	1.243286
14	6	0	-0.302410	-1.235020	1.299094
15	6	0	-2.366060	1.628696	-0.022370
16	6	0	-3.722027	1.280119	-0.176040
17	6	0	-4.663990	2.322157	-0.149920
18	6	0	-4.277944	3.652702	0.005840
19	6	0	-2.927711	3.975672	0.146392
20	6	0	-1.973542	2.959532	0.138079
21	1	0	0.533052	-2.745546	2.593052
22	1	0	-0.627265	-1.972724	4.624525
23	1	0	-2.102225	0.037703	4.503980
24	1	0	-2.410852	1.230497	2.382362
25	1	0	-5.713829	2.073414	-0.275334
26	1	0	-5.031174	4.435395	0.011197
27	1	0	-2.615461	5.008721	0.265779
28	1	0	-0.918787	3.185969	0.263507
29	6	0	0.382307	-1.702091	0.112989
30	6	0	1.748191	-2.506247	-2.264207
31	6	0	0.824128	-3.021413	-0.048057
32	6	0	0.625568	-0.740307	-0.965891
33	6	0	1.326488	-1.209191	-2.156527
34	6	0	1.488665	-3.406088	-1.204930
35	1	0	0.636572	-3.757826	0.724517
36	1	0	1.308976	0.071641	-0.504691
37	1	0	1.534659	-0.489945	-2.940397
38	1	0	1.823734	-4.435954	-1.295964
39	1	0	2.291693	-2.841842	-3.140584
40	6	0	-4.192044	-0.125907	-0.341440
41	6	0	-5.162251	-2.749389	-0.657025
42	6	0	-3.785191	-0.914122	-1.429955
43	6	0	-5.101287	-0.670859	0.578976
44	6	0	-5.580433	-1.972323	0.424549
45	6	0	-4.266478	-2.214466	-1.585361
46	1	0	-3.117638	-0.494142	-2.176515
47	1	0	-5.425135	-0.071185	1.425483
48	1	0	-6.279995	-2.378169	1.150297
49	1	0	-3.950200	-2.805829	-2.440577
50	1	0	-5.536766	-3.761902	-0.779795

TS2

E(RB3LYP) = –3548.7267282 hartree

Center Number	Atomic Number	Atomic Type	Coordinates X	Y	Z
1	13	0	3.676051	-0.071841	-0.088595
2	17	0	3.417209	-1.764977	1.161732
3	17	0	4.012814	1.787407	0.905269
4	17	0	4.884110	-0.373181	-1.813692
5	5	0	-0.055870	0.674435	-0.202559
6	17	0	0.282678	0.516958	1.555406
7	17	0	1.594472	0.228919	-1.238416
8	7	0	-1.210497	0.014420	-0.842471
9	6	0	-3.893695	2.611256	-0.872254
10	6	0	-4.955260	1.925567	-1.456953
11	6	0	-4.754887	0.605117	-1.859666
12	6	0	-3.524722	-0.026677	-1.676312
13	6	0	-2.443096	0.652047	-1.087997
14	6	0	-2.644938	2.002281	-0.695345
15	6	0	-1.076485	-1.375605	-1.239074
16	6	0	-1.220614	-2.447273	-0.330806
17	6	0	-1.002482	-3.748938	-0.822752
18	6	0	-0.682165	-3.993644	-2.154431
19	6	0	-0.571254	-2.926386	-3.046949
20	6	0	-0.763475	-1.629201	-2.582037
21	1	0	-4.014196	3.649195	-0.573077
22	1	0	-5.914166	2.413277	-1.599787
23	1	0	-5.565609	0.047186	-2.320339
24	1	0	-3.405690	-1.058842	-1.981405
25	1	0	-1.110248	-4.581083	-0.133381
26	1	0	-0.526614	-5.013538	-2.494746
27	1	0	-0.324302	-3.098871	-4.090410

28	1	0	-0.658147	-0.784998	-3.256837
29	6	0	-1.518616	2.740299	-0.116052
30	6	0	0.753705	4.067283	0.942789
31	6	0	-1.635739	3.540598	1.023646
32	6	0	-0.221129	2.550851	-0.695769
33	6	0	0.891600	3.285847	-0.186139
34	6	0	-0.513251	4.185806	1.542599
35	1	0	-2.597832	3.636393	1.516629
36	1	0	-0.189574	2.281768	-1.750431
37	1	0	1.857017	3.189975	-0.670919
38	1	0	-0.621395	4.793288	2.437601
39	1	0	1.609477	4.583421	1.364440
40	6	0	-1.588078	-2.301795	1.107250
41	6	0	-2.287412	-2.159972	3.829545
42	6	0	-0.774595	-2.890161	2.089622
43	6	0	-2.763303	-1.650077	1.510943
44	6	0	-3.108888	-1.580760	2.860795
45	6	0	-1.118270	-2.815717	3.438821
46	1	0	0.148280	-3.380011	1.792373
47	1	0	-3.420906	-1.213062	0.766440
48	1	0	-4.026820	-1.077847	3.154399
49	1	0	-0.467775	-3.264653	4.184514
50	1	0	-2.556859	-2.102389	4.880845

PD1

E(RB3LYP) = –3548.7337284 hartree

Center Number	Atomic Number	Atomic Type	Coordinates X	Y	Z
1	13	0	-5.974533	0.194508	-0.018198
2	17	0	-5.964698	0.536477	2.075446
3	17	0	-5.808101	-1.835254	-0.604092
4	17	0	-7.128473	1.476173	-1.234347
5	5	0	1.167083	0.871959	0.431377
6	17	0	1.270937	2.415161	1.340360
7	17	0	-3.730882	1.066598	-0.609570
8	7	0	2.193565	0.518381	-0.479678
9	6	0	0.999877	-2.728324	-1.886692
10	6	0	1.987039	-3.003735	-2.817951
11	6	0	3.046692	-2.105283	-2.976100
12	6	0	3.105147	-0.955619	-2.203685
13	6	0	2.111179	-0.668742	-1.248772
14	6	0	1.021719	-1.570338	-1.079486
15	6	0	3.345352	1.375270	-0.682987
16	6	0	4.573707	1.110120	-0.044669
17	6	0	5.652715	1.963621	-0.330990
18	6	0	5.521720	3.044357	-1.201330
19	6	0	4.295514	3.294905	-1.817654
20	6	0	3.214044	2.454558	-1.559864
21	1	0	0.180235	-3.429940	-1.788289
22	1	0	1.930650	-3.905664	-3.419776
23	1	0	3.827853	-2.298063	-3.705981
24	1	0	3.925103	-0.263385	-2.342277
25	1	0	6.603551	1.775089	0.159256
26	1	0	6.373876	3.690576	-1.392320
27	1	0	4.178988	4.135195	-2.495809
28	1	0	2.255100	2.623991	-2.040223
29	6	0	-0.046143	-1.293668	-0.109857
30	6	0	-2.109410	-0.702884	1.742504
31	6	0	-1.119340	-2.192763	0.105130
32	6	0	-0.015727	-0.085433	0.635965
33	6	0	-1.051514	0.185165	1.554689
34	6	0	-2.126055	-1.909142	1.011636
35	1	0	-1.171477	-3.128974	-0.437215
36	1	0	-2.977929	0.428632	0.299234
37	1	0	-1.015278	1.107301	2.127326
38	1	0	-2.938474	-2.615539	1.153697
39	1	0	-2.882134	-0.497204	2.478974
40	6	0	4.786100	-0.040206	0.881770
41	6	0	5.277419	-2.186928	2.634588
42	6	0	4.062977	-0.167326	2.078219
43	6	0	5.766781	-1.000219	0.584772
44	6	0	6.008701	-2.066341	1.451741
45	6	0	4.306992	-1.232308	2.945828
46	1	0	3.328690	0.586717	2.343255
47	1	0	6.333101	-0.913817	-0.338819
48	1	0	6.767211	-2.803099	1.200936
49	1	0	3.742304	-1.310613	3.871013
50	1	0	5.464966	-3.016345	3.311068

2,2,6,6-tetramethylpiperidine(TMP)

E(RB3LYP) = –409.15252616 hartree

Center Number	Atomic Number	Atomic Type	Coordinates X	Y	Z
1	7	0	-0.000034	-0.855527	-0.441549
2	1	0	-0.000017	-1.847991	-0.211635
3	6	0	1.257593	1.241706	-0.424783
4	6	0	-0.000015	1.954106	0.088528
5	6	0	-1.257540	1.241694	-0.424901
6	6	0	-1.293104	-0.256575	-0.051476
7	6	0	1.293033	-0.256609	-0.051544
8	1	0	-2.164075	1.730307	-0.045576
9	1	0	-0.000068	1.989865	1.185852

10	1	0	0.000003	2.998238	-0.249337
11	1	0	1.282523	1.323779	-1.519811
12	1	0	2.164064	1.730192	-0.045141
13	1	0	-1.282186	1.323530	-1.519954
14	6	0	1.673659	-0.443078	1.439910
15	1	0	1.588068	-1.498356	1.728086
16	1	0	2.712470	-0.135447	1.613579
17	1	0	1.042338	0.138225	2.116553
18	6	0	2.363610	-0.966476	-0.902175
19	1	0	3.354598	-0.527647	-0.735717
20	1	0	2.425634	-2.032085	-0.643816
21	1	0	2.115810	-0.890268	-1.965294
22	6	0	-1.673506	-0.443054	1.439945
23	1	0	-2.712057	-0.134706	1.613954
24	1	0	-1.588705	-1.498486	1.727857
25	1	0	-1.041537	0.137551	2.116541
26	6	0	-2.363741	-0.966413	-0.902002
27	1	0	-2.425413	-2.032143	-0.644043
28	1	0	-3.354802	-0.527916	-0.735078
29	1	0	-2.116351	-0.889755	-1.965188

6

E(RB3LYP) = –1464.6972066 hartree

Center Number	Atomic Number	Atomic Type	Coordinates X	Y	Z
1	5	0	0.900940	-1.407076	0.056883
2	17	0	0.320113	-2.985622	0.695555
3	7	0	-0.004849	-0.562965	-0.637140
4	6	0	2.130759	2.338253	-1.609089
5	6	0	1.238379	3.106917	-2.339197
6	6	0	-0.073792	2.655871	-2.506897
7	6	0	-0.470235	1.452589	-1.942814
8	6	0	0.427319	0.667405	-1.194372
9	6	0	1.768855	1.109366	-1.017728
10	6	0	-1.385580	-0.947380	-0.843331
11	6	0	-2.417121	-0.451581	-0.019980
12	6	0	-3.733855	-0.842288	-0.318104
13	6	0	-4.022842	-1.698767	-1.378896
14	6	0	-2.988682	-2.183942	-2.179620
15	6	0	-1.676153	-1.800715	-1.910862
16	1	0	3.146702	2.698809	-1.499721
17	1	0	1.561800	4.046486	-2.777610
18	1	0	-0.789228	3.238914	-3.080190
19	1	0	-1.486159	1.108269	-2.085939
20	1	0	-4.536770	-0.473265	0.313796
21	1	0	-5.051451	-1.988729	-1.574870
22	1	0	-3.198775	-2.853628	-3.008647
23	1	0	-0.858165	-2.156052	-2.530251
24	6	0	2.741754	0.305774	-0.260931
25	6	0	4.588081	-1.290377	1.173262
26	6	0	4.067870	0.740121	-0.041328
27	6	0	2.349202	-0.953677	0.265541
28	6	0	3.289244	-1.731038	0.973865
29	6	0	4.971687	-0.042665	0.661494
30	1	0	4.404287	1.699918	-0.415971
31	1	0	2.977944	-2.692974	1.369627
32	1	0	5.985222	0.319423	0.814769
33	1	0	5.300223	-1.900903	1.721506
34	6	0	-2.183119	0.486715	1.116067
35	6	0	-1.836326	2.266683	3.269058
36	6	0	-1.369596	0.141123	2.206589
37	6	0	-2.828264	1.733978	1.128989
38	6	0	-2.654847	2.617945	2.194354
39	6	0	-1.198028	1.024791	3.272469
40	1	0	-0.893420	-0.833576	2.232122
41	1	0	-3.458621	2.014880	0.289300
42	1	0	-3.156847	3.581844	2.181945
43	1	0	-0.568488	0.737649	4.110492
44	1	0	-1.699178	2.954043	4.099538

$AlCl_3$·TMP·HCl

E(RB3LYP) = –2493.2654859 hartree

Center Number	Atomic Number	Atomic Type	Coordinates X	Y	Z
1	7	0	1.900579	-0.000045	-0.862833
2	1	0	2.197787	-0.000041	-1.844848
3	6	0	2.035556	1.263572	1.276639
4	6	0	2.595575	0.000010	1.943911
5	6	0	2.035785	-1.263682	1.276667
6	6	0	2.325779	-1.350446	-0.233282
7	6	0	2.325652	1.350358	-0.233263
8	1	0	2.450030	-2.165141	1.742901
9	1	0	3.692945	0.000124	1.927810
10	1	0	2.306625	-0.000007	3.000172
11	1	0	0.950274	1.304062	1.430431
12	1	0	2.449510	2.165131	1.742945
13	1	0	0.950527	-1.304402	1.430529
14	6	0	3.802332	1.634902	-0.543781
15	1	0	4.021035	1.520414	-1.612555
16	1	0	4.009944	2.676817	-0.282215
17	1	0	4.497573	1.012485	0.020448
18	6	0	1.452488	2.421384	-0.904038

19	1	0	1.707826	3.397537	-0.480072
20	1	0	1.633999	2.470415	-1.984932
21	1	0	0.386717	2.250376	-0.732530
22	6	0	3.802424	-1.634962	-0.543911
23	1	0	4.010040	-2.676930	-0.282561
24	1	0	4.021104	-1.520260	-1.612669
25	1	0	4.497691	-1.012661	0.020425
26	6	0	1.452505	-2.421474	-0.903924
27	1	0	1.633863	-2.470593	-1.984842
28	1	0	1.707856	-3.397603	-0.479915
29	1	0	0.386750	-2.250432	-0.732294
30	1	0	0.860417	-0.000244	-0.923887
31	13	0	-2.461312	0.000133	0.045963
32	17	0	-1.222501	0.000327	-1.805409
33	17	0	-1.850001	1.766832	1.148110
34	17	0	-1.849739	-1.766548	1.148101
35	17	0	-4.527646	-0.000520	-0.474927

*The isomerization barrier calculation of **2** (Figure 8)*

(*P*)-**2**

E(RB3LYP) = –1718.5076967 hartree

Center Number	Atomic Number	Atomic Type	Coordinates X	Y	Z
1	6	0	-1.835302	-1.007152	1.001142
2	6	0	-2.499142	-0.119061	0.012939
3	6	0	-2.478658	-1.399593	2.185302
4	6	0	-0.525254	-1.492582	0.766596
5	6	0	-3.896809	-0.102241	-0.131601
6	6	0	-1.741144	0.715554	-0.841495
7	6	0	-1.856818	-2.257310	3.091727
8	15	0	0.264587	-0.935097	-0.778913
9	6	0	2.046184	-0.717637	-0.556666
10	7	0	-0.302039	0.700287	-0.749171
11	6	0	2.880599	-1.775386	-0.947318
12	6	0	4.263795	-1.650536	-0.874872
13	6	0	-4.519102	0.723689	-1.063707
14	6	0	-0.569681	-2.737299	2.841713
15	6	0	0.095808	-2.348310	1.679167
16	6	0	-3.753474	1.545211	-1.894741
17	6	0	2.583216	0.502855	-0.089789
18	6	0	-2.364221	1.529492	-1.788092
19	16	0	-0.234586	-1.980212	-2.357585
20	6	0	1.722992	1.620037	0.359331
21	6	0	2.269884	2.641706	1.159368
22	6	0	0.343202	1.703504	0.028355
23	6	0	4.813013	-0.437762	-0.452428
24	6	0	1.529853	3.732863	1.594112
25	6	0	3.988673	0.619100	-0.082557
26	6	0	0.185202	3.818040	1.235428
27	6	0	-0.398574	2.813125	0.473323
28	1	0	-3.467218	-1.011695	2.411705
29	1	0	-4.501266	-0.769616	0.474827
30	1	0	-2.376686	-2.542624	4.002199
31	1	0	2.431497	-2.682615	-1.339660
32	1	0	4.904074	-2.475045	-1.173999
33	1	0	-5.601445	0.710431	-1.156053
34	1	0	-0.084303	-3.402053	3.550620
35	1	0	1.102620	-2.706347	1.482020
36	1	0	-4.233138	2.176222	-2.637356
37	1	0	-1.744083	2.138674	-2.438064
38	1	0	3.303771	2.560805	1.475161
39	1	0	5.891464	-0.305832	-0.428316
40	1	0	1.993015	4.495874	2.212317
41	1	0	4.448090	1.561623	0.192124
42	1	0	-0.423174	4.656393	1.563736
43	1	0	-1.449823	2.881816	0.226554

TS-**2**

E(RB3LYP) = –1718.4879754 hartree

Center Number	Atomic Number	Atomic Type	Coordinates X	Y	Z
1	6	0	2.106626	-1.105892	-0.604721
2	6	0	2.512109	0.294898	-0.382069
3	6	0	2.847940	-1.946620	-1.460487
4	6	0	0.999152	-1.657152	0.066672
5	6	0	3.867517	0.629179	-0.558962
6	6	0	1.603046	1.305139	0.044833
7	6	0	2.551761	-3.297776	-1.583846
8	15	0	-0.077265	-0.557792	1.056012
9	6	0	-1.730805	-0.986973	0.428355
10	7	0	0.221506	0.957074	0.253025
11	6	0	-2.287607	-2.210484	0.828564
12	6	0	-3.407652	-2.725977	0.183400
13	6	0	4.348020	1.918425	-0.383225
14	6	0	1.495971	-3.850323	-0.854220
15	6	0	0.720109	-3.027235	-0.045885
16	6	0	3.455799	2.908430	0.014763
17	6	0	-2.377961	-0.191368	-0.541187
18	6	0	2.118509	2.597998	0.243769
19	16	0	0.170017	-0.632376	2.998148

20	6	0	-2.062884	1.252224	-0.636245
21	6	0	-3.059729	2.129880	-1.097566
22	6	0	-0.889690	1.810363	-0.051963
23	6	0	-3.963876	-2.017083	-0.884832
24	6	0	-2.965475	3.509561	-0.959026
25	6	0	-3.467022	-0.764497	-1.227794
26	6	0	-1.891491	4.034449	-0.248215
27	6	0	-0.888949	3.188449	0.220275
28	1	0	3.656228	-1.528264	-2.050240
29	1	0	4.565888	-0.158881	-0.816959
30	1	0	3.141730	-3.919620	-2.251586
31	1	0	-1.841174	-2.749925	1.658907
32	1	0	-3.832640	-3.674144	0.499284
33	1	0	5.401476	2.137373	-0.529596
34	1	0	1.266369	-4.909230	-0.929934
35	1	0	-0.114829	-3.456924	0.493147
36	1	0	3.795351	3.926233	0.185294
37	1	0	1.492704	3.395675	0.594969
38	1	0	-3.965725	1.717340	-1.525665
39	1	0	-4.807914	-2.426724	-1.432899
40	1	0	-3.755760	4.151729	-1.336108
41	1	0	-3.945408	-0.215867	-2.031808
42	1	0	-1.835981	5.096573	-0.027225
43	1	0	-0.132658	3.614326	0.856358

(*M*)-**2**

E(RB3LYP) = –1718.5076968 hartree

Center Number	Atomic Number	Atomic Type	Coordinates X	Y	Z
1	6	0	-2.584030	0.501158	-0.088399
2	6	0	-1.725652	1.619413	0.361667
3	6	0	-3.989733	0.614910	-0.080541
4	6	0	-2.045174	-0.718063	-0.556512
5	6	0	-2.274647	2.640221	1.161414
6	6	0	-0.345559	1.704718	0.032345
7	6	0	-4.812443	-0.443065	-0.450756
8	15	0	-0.263507	-0.932826	-0.780577
9	6	0	0.527542	-1.496028	0.762243
10	7	0	0.301973	0.702669	-0.744483
11	6	0	-0.092429	-2.356003	1.671583
12	6	0	0.573942	-2.749333	2.832148
13	6	0	-1.536472	3.732063	1.597521
14	6	0	-4.261372	-1.654652	-0.874207
15	6	0	-2.878024	-1.776993	-0.947459
16	6	0	-0.191420	3.818844	1.240722
17	6	0	1.837335	-1.010609	0.998150
18	6	0	0.394424	2.814925	0.478944
19	16	0	0.235656	-1.971152	-2.363746
20	6	0	2.499940	-0.117786	0.013427
21	6	0	3.897556	-0.099173	-0.131563
22	6	0	1.740909	0.719858	-0.837125
23	6	0	1.860872	-2.269467	3.083491
24	6	0	4.518847	0.731252	-1.060300
25	6	0	2.481602	-1.407522	2.180336
26	6	0	3.752221	1.555677	-1.887552
27	6	0	2.363045	1.538311	-1.780514
28	1	0	-4.450755	1.556379	0.195015
29	1	0	-3.308790	2.558081	1.475985
30	1	0	-5.891102	-0.312951	-0.426093
31	1	0	-1.099082	-2.713951	1.473486
32	1	0	0.089416	-3.417388	3.538532
33	1	0	-2.001329	4.494293	2.215413
34	1	0	-4.900371	-2.480068	-1.173567
35	1	0	-2.427623	-2.683152	-1.340784
36	1	0	0.415634	4.657672	1.570263
37	1	0	1.445967	2.884798	0.233791
38	1	0	4.502774	-0.768674	0.471749
39	1	0	2.381430	-2.558211	3.992486
40	1	0	5.601165	0.719269	-1.153100
41	1	0	3.469983	-1.019828	2.407858
42	1	0	4.231074	2.190232	-2.627665
43	1	0	1.742229	2.149701	-2.427763

List of Publications

The present thesis is composed of the following papers.

Chapter 1:

(1) Synthesis of BN-fused Polycyclic Aromatics via Tandem Intramolecular Electrophilic Arene Borylation

Hatakeyama, T.; Hashimoto, S.; Seki, S.; Nakamura, M.

J. Am. Chem. Soc. **2011**, *133*, 18614–10617. Highlighted in *SYNFACTS*, **2012,** 0159.

Chapter 2:

(2) Azaboradibenzo[6]helicene: Carrier Inversion Induced by Helical Homochirality

Hatakeyama, T.; Hashimoto, S.; Oba, T.; Nakamura, M.

J. Am. Chem. Soc. **2012**, *134*, 19600–19603. Highlighted in *JACS Spotlights*, **2013,** *135*, 1. Highlighted in *SYNFACTS*, **2013,** 0157.

Chapter 3:

(3) Synthesis of BN-fused Polycyclic Aromatic Compounds Containing Five-membered Heterocyclic Ring

Hashimoto, S.; Hatakeyama, T.; Nakamura, M.

In preparation. (A patent application has been filed for the results described in this chapter: PCT/JP2012/056206.)

Chapter 4:

(4) Tandem Phospha-Friedel–Crafts Reaction Toward Curved π-Conjugated Frameworks with a Phosphorus Ring Junction

Hatakeyama, T.; Hashimoto, S.; Nakamura, M.

Org. Lett. **2011,** *13*, 2130–2133.

Chapter 5:

(5) Mechanistic Study on Bora-Friedel–Crafts Reaction and Its Application to Other Heteroatoms

Hashimoto, S.; Hatakeyama T.; Nakamura, M.

In preparation.

List of Publications

The following publication is not included in this Thesis

(6) Highly Selective Biaryl Cross-Coupling Reactions between Aryl Halides and Aryl Grignard Reagents: A New Catalyst Combination of *N*-Heterocyclic Carbenes and Iron, Cobalt, and Nickel Fluorides

Hatakeyama, T.; Hashimoto, S.; Ishizuka, K.; Nakamura, M.

J. Am. Chem. Soc. **2009**, *131*, 11949–11963.

Patent

(1) 「多環芳香族化合物」

畠山琢次，中村正治，橋本士雄磨

PCT/JP2010/053818，WO 2010/104047 A1

(2) 「多環芳香族化合物」

畠山琢次，中村正治，橋本士雄磨

PCT/JP2012/056206

Review

(1) 「鉄及び鉄族元素触媒による高選択的ビアリールクロスカップリング」

畠山琢次，橋本士雄磨，中村正治

ペトロテック, **2013,** *36*, 17–21.

Book

(1) 「34. Williamson エーテル合成」

橋本士雄磨，清家弘史，中村正治

トップドラッグから学ぶ創薬化学　第Ⅱ部

有機合成化学協会編，東京化学同人 2012 年

Acknowledgments

The study described in this thesis has been carried out under the direction of Professor Masaharu Nakamura from April 2007 to March 2013 at the International Research Center for Elements Science, Institute for Chemical Research, Kyoto University.

I would like to express my sincerest gratitude to Professor Masaharu Nakamura for his kind guidance, helpful suggestions, and hearty encouragement throughout this study. I wish to appreciate to Associate Professor Hikaru Takaya and Assistant Professor Takuji Hatakeyama for their guidance and helpful discussions during for the course of this study. They provided insight and direction-right up to my goal. I am grateful to Dr. Kentaro Ishizuka, Dr. Katsuhiro Isozaki, and Dr. Hirofumi Seike for their helpful discussions, technical assistance and kind encouragement. I also acknowledge the contribution of Tsuyoshi Oba and Yuma Aoki for their helpful experiments in the study. I am obliged to Saori Takami for kindly supporting my daily work. I appreciate to all present members and alumni of Professor Nakamura's group for their kind supports and encouragement.

I acknowledge my appreciation to Professor Kouichi Ohe and Professor Yasujiro Murata for careful reviewing of this thesis and fruitful comments. I wish to thank Professor Shuhei Seki (Osaka university) for TRMC measurements, and Toshiaki Ikuta and Jingping Ni (JNC Petrochemical Corporation) for TOF and IP measurements. Powder X-ray diffraction and micro-crystallography measured at SPring-8 (BL19B2, BL38B1, BL40XU), I would like to appreciate to the beam-line staffs. I thank all members of Professor Tokitoh's group, Ozawa's group, Murata's group, Kawabata's group, Yamago's group, and Kaji's group.

I am indebted to the staff at Institute for Chemical Research and Graduate School of Engineering, Kyoto University, for the provision of services. Especially, I would like to thank Toshiko Hirano for elemental analysis and precision weighing, Kyoko Ohmine for high resolution NMR analysis, and Tomoko Terada, Akiko Fujihashi, Mayumi Inutsuka, Keiko Kuwata, Sakiko Goto for Mass spectrometry.

I appreciate the financial support of Research Fellowships for Young Scientists of Japan Society for the Promotion of Science (JSPS).

Of course no acknowledgments would be complete without giving thanks to my father, Masaru Hashimoto and my brother Mahito Hashimoto. Their love provided my inspiration and was my driving force. I would like to thank my wife Nayoung Kim for her personal support and great patience at all times.

Finally, I would like to dedicate this work to my lost mother, Yoshiko Hashimoto, who left us too soon. I hope that this work makes you proud.

March, 2013

Sigma Hashimoto